2014

Identification of a Microrna Network that Regulates Melanoma Metastasis and Angiogenesis by Targeting Apoe

Nora Pencheva

IDENTIFICATION OF A MICRORNA NETWORK THAT REGULATES MELANOMA METASTASIS AND ANGIOGENESIS BY TARGETING APOE

A Thesis Presented to the Faculty of

The Rockefeller University

in Partial Fulfillment of the Requirements for

the degree of Doctor of Philosophy

by

Nora Pencheva

June 2014

IDENTIFICATION OF A MICRORNA NETWORK THAT REGULATES MELANOMA METASTASIS AND ANGIOGENESIS BY TARGETING APOE

Nora Pencheva, Ph.D.
The Rockefeller University 2014

Metastatic melanoma, a prevalent and deadly form of skin cancer, remains an aggressive clinical outcome that lacks effective preventative and/or curative therapeutics. Patients diagnosed with advanced metastatic melanoma face a dreaded 10-year survival rate of less than 10%. By performing *in vivo* selection for highly metastatic melanoma cells, we systematically identified three microRNAs (miRNAs) that promoted metastasis across multiple mutationally diverse human melanoma subtypes. These miRNAs were found to promote metastasis by enhancing the invasive capacity of melanoma cells and also by allowing melanoma cells to recruit endothelial cells into the metastatic niche, leading to enhanced metastatic angiogenesis. Importantly, the expression levels of these miRNAs served as prognostic biomarkers in stratifying melanoma patients at high risk from those at low risk for metastatic relapse. Notably, therapeutic delivery of specific locked nucleic acids (LNAs) antisense to the three miRNAs synergistically suppressed metastasis in pre-clinical models, attesting to the therapeutic potential of combinatorial miRNA silencing for the prevention of melanoma metastasis.

Through systematic transcriptomic analyses and mutagenesis studies, I found that the three miRNAs silenced a common set of target genes: the heat-shock factor *DNAJA4* and the metabolic protein apolipoprotein E (*ApoE*). Interestingly, this work also revealed that DNAJA4 positively regulated *ApoE* expression, establishing *ApoE* as the central molecule in

this convergent network. Consistent with these findings, treatment of multiple melanoma lines with ApoE blocked their metastatic capacity, while ApoE expression in patients' tumors was significantly prognostic of melanoma progression outcomes. Systematic loss-of-function experiments revealed that melanoma-derived extracellular ApoE exerted dual cell-intrinsic/ cell-extrinsic effects on metastasis: ApoE acting on melanoma cell LRP1 receptors inhibited melanoma invasiveness, while ApoE acting on endothelial cell LRP8 receptors suppressed metastatic endothelial recruitment (MER).

In light of ApoE's key metastasis-suppressive role, we next investigated therapeutic approaches to chronically activate ApoE in metastatic melanoma. We identified the nuclear hormone liver-X receptor (LXRβ), a known transcriptional trans-activator of *ApoE*, as an ideal target given its ubiquitous expression across all normal tissues as well as melanoma subtypes. Oral delivery of LXR agonists strongly suppressed melanoma tumor progression and metastasis across multiple mutationally diverse and genetically initiated pre-clinical melanoma models, consistent with broad-spectrum *in vivo* efficacy of LXRβ activation therapy in melanoma. Importantly, combining LXR agonist treatment with approved melanoma drugs elicited additive melanoma-suppressive responses, revealing therapeutic cooperativty between LXR activation and modern frontline agents. Complementary molecular and genetic approaches revealed that LXRβ agonism mediated melanoma suppression through the coordinate transcriptional induction of *ApoE* in both melanoma cells as well as stromal tissues. Collectively, this thesis provides molecular, genetic, and pharmacologic lines of evidence that establish ApoE as a robust metastasis suppressor in melanoma.

За моите първи учители, моите безценни родители…

ACKNOWLEDGEMENTS

I would like to genuinely thank my advisor Sohail Tavazoie for being an exemplary mentor and a role model during the past five years. Sohail's extreme enthusiasm for science, strong dedication, and unparalleled insightfulness struck me as unusual when I first met him and inspired me on my quest to becoming a molecular biologist. The heavy focus in his lab on the use of systematic and multi-disciplinary techniques has given me the skills and stamina to fearlessly approach molecularly complex questions. I thank him for this rare opportunity. I am also grateful to my committee members, Charles Rice and Fred Cross, for all of their support, guidance, and constructive criticism during the course of the project. Their thoughtful comments during the annual committee meetings proved essential in making me more rigorous in my experiments and greatly improved my ability to think critically about experimental data. I would also like to express gratitude to Filippo Giancotti for agreeing to serve as an external examiner at my thesis defense and providing valuable input on my research.

Special thanks go to past and current members of the Tavazoie lab for all of their help and support. I thank Hien Tran, a former clinical fellow, who initiated the early phases of the project and served as a mentor during my first couple of months in the lab. I am most appreciative of Colin Buss, a gifted former technician in the lab, who worked rigorously side by side with me for two years and contributed to many of the experiments discussed in this work. I especially thank Nils Halberg and Claudio Alacrón, senior post-docs in the lab, for all of their intellectual contribution, support, and countless discussions. I am also grateful to

Jessica Posada, a medical student, who has been working with me for the past year and has greatly assisted with mouse work.

I would like to tremendously thank my family and friends for always being there for me and making me believe in myself throughout my life. I thank my mother Darina for teaching me early on that big dreams always come with hard work, my father George for passing on his gift and passion for math and sciences, and my brother Yasen for showing me what it takes to be creative. I also thank all my good friends in New York for making the past five years in this city feel like a home that I will most certainly miss.

Finally, I sincerely thank Sid, Emily, Marta, Cris, and the entire Dean's office for their support during the past five years and especially for their assistance with the preparation and formatting of this thesis.

TABLE OF CONTENTS

Dedication……iii

Acknowledgements……iv

Table of Contents……vi

List of Figures……xii

List of Tables……xviii

List of Abbreviations……xix

Chapter I: Introduction……1

Molecular Determinants of Malignant Melanoma……1

Immunomodulatory Therapy in Melanoma……4

The Metastatic Cascade……6

Discovery, Biogenesis, and Function of miRNAs……9

Deregulated miRNA Expression as a Hallmark of Human Cancers……14

Regulation of Metastatic Progression by miRNAs……15

miRNAs as Suppressors of Breast Cancer Metastasis……15

miRNAs as Promoters of Breast Cancer Metastasis……20

Metastasis Regulatory miRNAs with Pleiotropic Roles in Cancer Progression……23

Search for Metastasis Regulatory miRNAs in Melanoma……26

Overview and Biological Significance……28

Chapter II: Identification, Functional Characterization, and Clinical Validation of miRNAs that Promote Melanoma Metastasis……30

In Vivo Enrichment for Highly Metastatic Melanoma Sub-Populations of Cells……30

Identification of Metastasis-Promoting miRNAs in Human Melanoma……31

Cellular Phenotypes Conferred by Metastasis-Promoting miRNAs……39

Clinical Association of miR-199a-3p, miR-199a-5p, and miR-1908 Expression with Human Melanoma Metastasis……45

Therapeutic Targeting of Metastasis-Promoting miRNAs in Melanoma……48

Mechanisms Upstream of miRNA Overexpression in Melanoma Metastasis……..53
Deregulated Transcriptional Control of miR-199a and miR-1908…….....53
Deregulated Post-Transcriptional Processing of miR-199a and miR-1908…….....59
Summary of Findings from Chapter II……..61

Chapter III: Identification, Functional Characterization, and Clinical Validation of miRNA Effector Genes in Melanoma Metastasis…….…..62
Systematic Identification of Genes Repressed by miR-199a-3p, miR-199a-5p, and miR-1908 in Melanoma……...….62
Validation of *ApoE* and *DNAJA4* as Direct Target Genes of miR-199a and miR-1908……...64
Functional Validation of ApoE and DNAJA4 as Suppressors of Melanoma Progression Phenotypes……...……..67
Mechanisms of Action by DNAJA4 in Melanoma…….....…….....72
DNAJA4 Positively Regulates *ApoE*'s Expression……..……..72
Identification of Putative DNAJA4 Binding Partners in Melanoma Cells…..……74
Clinical Association of ApoE and DNAJA4 Expression with Melanoma Progression.....78
Summary of Findings from Chapter III……...…….83

Chapter IV: Cell-Autonomous and Non-Cell-Autonomous Regulation of Melanoma Progression Phenotypes by Extracellular ApoE……...……...…..85
Extracellular ApoE Suppresses Melanoma Invasion and Endothelial Recruitment…..….85
Enhancement of Extracellular ApoE Levels Robustly Suppresses Melanoma Metastasis……..…….88
ApoE Targeting of Melanoma LRP1 Receptors Suppresses Melanoma Cell Invasion.....91
ApoE Targeting of Endothelial LRP8 Receptors Suppresses Endothelial Cell Migration……...93
ApoE/LRP8-Dependent Regulation of Endothelial VEGFR2 Activity…….....98
Summary of Findings from Chapter IV……...101

Chapter V: Therapeutic Activation of *ApoE* in Metastatic Melanoma Through Nuclear Hormone Receptor Targeting…….....103

Identification of LXRβ as a Novel Therapeutic Target in Melanoma……..……...103

Oral Delivery of LXR Agonists Inhibits Melanoma Tumor Progression……...…....111

LXR Agonist Therapy Suppresses Melanoma Metastatic Progression…….....117

LXRβ Agonism Suppresses *In Vitro* Melanoma Progression Phenotypes by Transcriptionally Activating *ApoE* in Melanoma Cells…….…….121

LXRβ Agonism Suppresses *In Vivo* Melanoma Progression through the Engagement of both Melanoma-Derived and Stromal *ApoE*…….……..128

LXRβ Therapy Inhibits Melanoma Progression in a Genetically-Initiated Melanoma Model…….…..……137

ApoE Activation Therapy Inhibits Melanomas Resistant to Mainstay Therapeutics Dacarbazine and Vemurafenib…….....142

Cooperativity between LXRβ Activation Therapy and Mainstay Melanoma Therapeutics……....…147

Summary of Findings from Chapter V……...…152

Chapter VI: Discussion……..…153

Overview of Major Findings…….....……153

Role of Metastasis Regulatory miRNAs in Development……..……157

Convergent versus Divergent Target Regulation by miRNAs……....159

Therapeutic Potential of miRNA Targeting……...…161

Mechanisms Underlying miRNA Deregulation in Metastasis……....163

Implications for the *ApoE* Variants (*ApoE2*, *ApoE3*, *ApoE4*) in Melanoma Progression……..……....166

LRP1/LRP8 Targeting by Extracellular ApoE……..…..168

Implications for LRP8 Receptor Targeting to Tumor Angiogenesis…….....169

Potential Mechanisms Downstream of ApoE/LRP1 Targeting in Melanoma Cells...171

Metastatic Endothelial Recruitment…….....173

Metastasis Suppression by DNAJA4……...174

The LXRβ Receptor as a Novel Therapeutic Target in Metastatic Melanoma…….....178

Potential Roles of LXR Targeting in Other Epithelial Cancer Types…….....182
Clinical Implications for LXRβ Activation Therapy in Melanoma……..…...…183
Potential Solutions to Emergence of Clinical Resistance to LXR Activation Therapy...186
Conclusions……...……...189

Materials and Methods…….……..190
Cell Culture……..190
Mouse Experiments…….……...……190
In Vivo Selection for Highly Metastatic Melanoma Derivatives..……....……...191
Experimental Metastasis Assays…….……...…...……..192
In Vivo Selection Validation…….……..…...193
Functional Testing of Metastasis Promoter miRNAs……...193
LNA Pre-Treatment Experiments…….……....193
In Vivo LNA Therapy……..…....194
Epistasis Experiments……...……..…..194
ApoE Pre-Treatment Experiments…….…..194
Effects of LXR Agonists on Metastasis……...195
Orthotopic Metastasis Assay…….…..196
Primary Tumor Growth Assays…….…197
Effects of miR-199a and miR-1908 on Tumor Growth……...197
Effects of LXR Agonist Therapy on Tumor Growth……...197
Genetically Initiated Model of Melanoma Progression…….....199
Generation of DTIC-Resistant Melanoma Cells..……..200
Generation of Vemurafenib-Resistant Melanoma Cells…….……...201
miRNA Microarray Hybridization…….....202
Microarray-Based Target Gene Prediction for miR-199a and miR-1908……...202
Analysis of miRNA and mRNA Expression in Cell Lines……..203
Analysis of miRNA Copy Number……...…..204
Analysis of Nuclear Hormone Receptor Expression in the NCI60 Series……...204
Analysis of LXR and RXR Isoform Expression in Primary Human Melanoma Lines...205
Transcriptomic Analysis of Secreted Gene Products in Melanoma Cells Treated with

GW3965…….206
Lentiviral miRNA Inhibition and mRNA Knockdown Studies…….....206
Retroviral miRNA and Protein Overexpression Studies…….....207
siRNA-Based Gene Knockdown…….....207
LNA-Based miRNA Inhibition……..208
Therapeutic LNA-Based *In Vivo* Targeting of miRNAs ……..……...208
Luciferase Reporter Assays……..……...209
Validation of Direct miRNA Target Genes……...……....209
ApoE Promoter Activity Assay…….…….....211
Western Blotting…….....212
ApoE ELISA……....213
DNAJA4 Immunoprecipitation and MS-Based Analysis of Interacting Partners……..213
LXRβ ChIP……..214
Phenotypic Assays……....…..215
In Vitro Cell Proliferation Assay…….215
Endothelial Adhesion Assay…….216
Colony Formation Assay……..216
Serum Starvation Assay……...….216
Anoikis Assay……...217
Matrigel Invasion…….217
Endothelial Recruitment…….….218
Endothelial Migration Assay…….....219
ApoE Gradient Migration Assay…….219
In Vivo Matrigel Plug Assay…….....219
Histochemistry……..220
Macroscopic Lung Nodule Visualization…….220
Endothelial Cell Content Analyses……...220
Metastatic Nodule Angiogenic Perfusion Analysis……....…..221
Histochemical Analyses of LXR agonist-treated tumors…… 222
Analysis of miRNA Expression in Human Melanoma Skin Lesions……..…..….223
Analysis of ApoE and DNAJA4 Protein Levels in Primary Melanoma Lesions……..224

Analysis of ApoE, DNAJA4, and LXRβ Protein Expression in TMA Melanoma Progression Sets……225
Statistical Analyses……227
Appendix A—List of Cell Lines……....228
Appendix B—List of Primer Sequences……....229
Appendix C—List of miR-Zip and shRNA Sequences……..231

Publications……..232

Bibliography……233

LIST OF FIGURES

Chapter I:

Figure 1.1. The Multiple Steps of the Metastatic Cascade……...……...8
Figure 1.2. The Basic Steps of Mammalian miRNA Biogenesis…….....13
Figure 1.3. miRNA Regulatory Networks that Suppress Breast Cancer Metastasis…...…..18
Figure 1.4. miRNA Regulatory Networks that Promote Breast Cancer Metastasis…….....21
Figure 1.5. Pleiotropic Control of Metastasis by miR-200s.....24
Figure 1.6. miRNA Regulatory Networks that Promote Melanoma Metastasis.....27

Chapter II:

Figure 2.1. Lung Metastatic Colonization by *In Vivo*-Selected Metastatic Melanoma Derivatives and Their Parental Populations.....31
Figure 2.2. Identification of Deregulated miRNAs in Metastatic Melanoma Cells.....32
Figure 2.3. Identification of miR-199a and miR-1908 as Promoters of Melanoma Metastasis to the Lung..... 34
Figure 2.4. Endogenous miR-199a-3p, miR-199a-5p, and miR-1908 Promote Lung Colonization and Metastatic Initiation.....35
Figure 2.5. Endogenous miR-199a-3p, miR-199-5p, and miR-1908 Promote Metastasis by an Independent Melanoma Cell Line.....36
Figure 2.6. *In Vivo* Selection for Metastatic Melanoma Derivatives of Primary Human Melanoma Cell Populations…….37
Figure 2.7. Pervasive Upregulation of miR-199a-3p, miR-199a-5p, and miR-1908 across Melanoma Metastatic Derivatives.....38
Figure 2.8. Effects of miR-199a and miR-1908 on *In Vitro* Melanoma Cell Proliferation and *In Vivo* Melanoma Tumor Growth.....39
Figure 2.9. Effects of miR-199a and miR-1908 on Pro-Metastatic *In Vitro* Phenotypes.....40
Figure 2.10. Overexpression of miR-199a or miR-1908 Enhances Matrigel Invasion and Endothelial Recruitment Phenotypes.....41
Figure 2.11. Endogenous miR-199a-3p, miR-199a-5p, and miR-1908 Promote Matrigel Invasion and Endothelial Recruitment by Highly Metastatic Melanoma Cells.....42

Figure 2.12. Endogenous miR-199a-3p, miR-199a-5p, and miR-1908 Enhance Metastatic Endothelial Recruitment *In Vivo*.....44
Figure 2.13. Endogenous miR-199a-3p, miR-199a-5p, and miR-1908 Enhance Angiogenic Metastatic Perfusion.....45
Figure 2.14. miR-199a-3p, miR-199a-5p, and miR-1908 are Upregulated in Primary Melanoma Lesions with Metastatic Propensity.....46
Figure 2.15. Prognostic Capacity of miR-199a-3p, mR-199a-5p, and miR-1908 in Metastatic Melanoma.....47
Figure 2.16. LNA-Mediated Silencing of miR-199a-3p, miR-199a-5p, and miR-1908 Cooperatively Suppresses Melanoma Metastasis.....49
Figure 2.17. Broad Suppression of Melanoma Metastasis by Combinatorial miRNA Targeting.....50
Figure 2.18. LNA-Mediated Combinatorial miRNA Targeting Suppresses Systemic Melanoma Metastasis to Multiple Organs.....51
Figure 2.19. Therapeutic Delivery of LNAs Targeting miR-199a-3p, miR-199a-5p, and miR-1908 Suppresses Melanoma Metastasis.....52
Figure 2.20. Efficiency of Therapeutically Delivered LNAs in Silencing Target miRNAs *In Vivo*.....53
Figure 2.21. Genomic Copy Number of miR-199a-1, miR-199a-2, and miR-1908 in Highly Metastatic Melanoma Cells and Their Respective Parental Populations.....54
Figure 2.22. Transcriptional Induction of miR-199a and miR-1908 in Highly Metastatic Melanoma Cells.....55
Figure 2.23. Schematic of CREB Binding Motifs Found within the Putative Promoter Regions of miR-199a-1, miR-199a-2, and miR-1908.....56
Figure 2.24. Endogenous CREB Promotes miR-199a-3p, miR-199a-5p, and miR-1908 Expression in Metastatic Melanoma Cells.....57
Figure 2.25. CREB Activation is Enhanced in Metastatic Melanoma Cells.....58
Figure 2.26. CREB Expression is Upregulated in Clinical Melanoma Metastases.....58
Figure 2.27. Deregulated Processing of miR-199a-3p, miR-199a-5p, and miR-1908 in Metastatic Melanoma Cells.....60

Chapter III:

Figure 3.1. Identification of Putative miRNA Target Genes.....63

Figure 3.2. miR-199a and miR-1908 Repress the Expression of *ApoE* and *DNAJA4*.....63

Figure 3.3. miR-199a and miR-1908 Directly Target *ApoE* and *DNAJA4*.....65

Figure 3.4. Convergent Targeting of *ApoE* and *DNAJA4* by miR-199a-3p, miR-199a-5p, and miR-1908.....66

Figure 3.5. Anti-Correlation between the Aggregate Expression of miR-199a-3p/ miR-199a-5p/ miR-1908 and Their Target Genes.....67

Figure 3.6. Suppression of Melanoma Invasion and Endothelial Recruitment by *ApoE* and *DNAJA4*.....68

Figure 3.7. Endogenous Epistatic Interactions between miR-199a/miR-1908 and *ApoE* or *DNAJA4*.....69

Figure 3.8. Endogenous *ApoE* and *DNAJA4* Suppress miRNA-Dependent Metastatic Endothelial Recruitment *In Vivo*.....70

Figure 3.9. miR-199a/miR-1908-Mediated Effects on Melanoma Progression Phenotypes are Occluded by Concurrent Overexpression of ApoE or DNAJA4.....71

Figure 3.10. Regulation of *ApoE* Expression by DNAJA4.....73

Figure 3.11. DNAJA4-Mediated Metastatic Phenotypes are Dependent on ApoE.....74

Figure 3.12. Isoform-Specific Regulation of *DNAJA4* Expression in Metastatic Melanoma Cells and Suppression of Melanoma Invasion by DNAJA4.3.....75

Figure 3.13. Identification of Putative Binding Partners for DNAJA4.2 and DNAJA4.3 in Melanoma Cells.....77

Figure 3.14. Clinical Correlation of ApoE and DNAJA4 Expression with Melanoma Progression Outcomes.....79

Figure 3.15. Prognostic Capacity of ApoE and DNAJA4 Expression in Metastatic Melanoma.....81

Figure 3.16. Prognostic Capacity of Combined ApoE/DNAJA4 and Combined ApoE/DNAJA4/3 miRNAs Expression Signatures in Melanoma.....82

Chapter IV:

Figure 4.1. Endogenous miR-199a-5p and miR-1908 Repress Extracellular ApoE Levels...86

Figure 4.2. Extracellular ApoE Suppresses Melanoma Invasion and Endothelial Recruitment……..87

Figure 4.3. ApoE Pre-Treatment Suppresses Metastatic Colonization by Melanoma Cells…….....89

Figure 4.4. Genetic Inactivation of ApoE Accelerates Melanoma Lung Colonization……..90

Figure 4.5. Identification of LRP1 as the ApoE Receptor on Melanoma Cells Mediating ApoE's Effects on Invasion Suppression……...92

Figure 4.6. Melanoma Cell LRP1 Mediates miRNA-Dependent Metastatic Colonization...93

Figure 4.7. Endothelial Cell LRP8 Mediates miRNA/ApoE-Dependent Endothelial Recruitment……...…..94

Figure 4.8. ApoE/LRP8 Targeting Suppresses Endothelial Cell Migration in a Cancer Cell-Free System**…**……...…..96

Figure 4.9. ApoE Inhibits *In Vivo* Endothelial Cell Recruitment and Angiogenesis…….....97

Figure 4.10. ApoE Inhibits VEGFR2 Activation in an LRP8-Dependent Manner…….100

Chapter V:

Figure 5.1. Analysis of Nuclear Hormone Receptor Expression in Melanoma……....105

Figure 5.2. Effects of LXR or RXR Agonists on *In Vitro* Melanoma Cell Invasion and Endothelial Recruitment…….…….…..106

Figure 5.3. Effects of LXR or RXR Agonists on *In Vitro* Melanoma Cell Proliferation and Survival…..……...107

Figure 5.4. LXRβ Mediates Invasion and Endothelial Recruitment Suppression by LXR Agonists……109

Figure 5.5. Expression of LXRβ during Melanoma Progression……110

Figure 5.6. Therapeutic Delivery of LXR Agonists Suppresses Melanoma Tumor Growth……...112

Figure 5.7. Therapeutic Delivery of LXR Agonists Suppresses the Growth of Large Melanoma Tumors, Inhibits Long-Term Tumor Progression, and Extends Animal Survival……..114

Figure 5.8. LXR Agonist Treatment Suppresses Tumor Angiogenesis……...……116
Figure 5.9. Therapeutic LXR Activation Inhibits Lung Metastatic Colonization by Melanoma Cells……118
Figure 5.10. LXR Agonist Treatment Suppresses Melanoma Metastasis to the Brain…...119
Figure 5.11. LXR Activation Therapy Suppresses Colonization by Disseminated Melanoma Cells and Halts the Progression of Established Metastases……...120
Figure 5.12. Pharmacologic LXR Activation Enhances *ApoE* Transcript Levels……...122
Figure 5.13. LXR Agonism Transcriptionally Activates Melanoma Cell *ApoE* Expression……..123
Figure 5.14. ApoE is the Downstream Determinant of LXRβ-Dependent Suppression of Melanoma Invasion and Endothelial Recruitment……...…...125
Figure 5.15. LXRβ is Required for LXR Agonist-Mediated Transcriptional *ApoE* Induction……127
Figure 5.16. LXR Agonist Therapy Activates Melanoma-Derived and Stromal *ApoE* Expression.....130
Figure 5.17. Activation of Stromal LXRβ Inhibits Melanoma Tumor Growth through Induction of Stromal *ApoE*……...……..134
Figure 5.18. Identification of Stromal Cells in the Tumor Microenvironment that Upregulate ApoE upon LXR Agonist Treatment……...….135
Figure 5.19. LXRβ Therapy Engages both Melanoma-Intrinsic and Stromal *ApoE* in Metastasis Suppression…….……136
Figure 5.20. LXR Agonist Treatment Inhibits Melanoma Progression in a *B-Raf*^{V600E}/*Pten*-Null Genetically Driven Model……...…….……139
Figure 5.21. LXR Agonist Therapy Suppresses Melanoma Progression in a *B-Raf*^{V600E}/ *Pten*-Null/ *CDKN2A*-Null Genetic Model……..……..…….……141
Figure 5.22. LXR Agonist Treatment Suppresses Melanomas Resistant to the Chemotherapeutic Dacarbazine…….....144
Figure 5.23. LXR Agonist Treatment Suppresses Melanomas Resistant to Vemurafenib...146
Figure 5.24. LXR Agonist Treatment Cooperates with Dacarbazine and Vemurafenib in Suppressing Melanoma Tumor Growth…….....149

Figure 5.25. Cooperativity between LXRβ Activation and Vemurafenib in Suppressing Melanoma Metastasis……....……150
Figure 5.26. Additive Effects of LXRβ Activation and Immunotherapy in Melanoma…….……151

Chapter VI:

Figure 6.1. Convergent Regulation of Melanoma Metastasis by Multiple miRNAs……...154
Figure 6.2. Suppression of Melanoma Progression by LXR/*ApoE* Activation Therapy.....156

LIST OF TABLES

Chapter II:

Table 2.1. Conserved Transcription Factor Binding Sites Present in the Putative Promoter Regions of miR-199a-1, miR-199a-2, and miR-1908.....56

Chapter V:

Table 5.1. List of Secreted Factors Significantly Upregulated in MeWo Cells in Response to GW3965 Treatment.....122

LIST OF ABBREVIATIONS

Ab	-	Antibody
ABCA1	-	ATP-binding cassette, sub-family A, member 1
AF-2	-	Activation function 2
Ago	-	Argonaute
ApoE	-	Apolipoprotein E
ARF	-	Alternative reading frame
ATCC	-	American type culture collection
ATP	-	Adenosine triphosphate
BACH1	-	BTB and CNC homology 1
BAF53a	-	BRG1-associated factor (BAF) 53 kDa subunit
bp	-	Base pair
BSA	-	Bovine serum albumin
CDK	-	Cyclin-dependent kinase
CDKN2A	-	Cyclin-dependent kinase inhibitor 2A
CDS	-	Coding sequence
ChIP	-	Chromatin immunoprecipitation
COPII	-	Coat protein complex II
CREB	-	cAMP response element-binding protein
CreER	-	Cre recombinase fused to estrogen receptor (ER)
CTLA-4	-	Cytotoxic T lymphocyte antigen 4
DAPI	-	4', 6-diamidino-2-phenylindole
DGCR8	-	DiGeorge Syndrome Critical Region Gene 8
DMSO	-	Dimethyl sulfoxide
DNAJA4	-	DnaJ (Hsp40) homolog, subfamily A, member 4
DTIC	-	Dacarbazine
EC_{50}	-	Half maximum effective concentration
EGFR	-	Epidermal growth factor receptor
ELISA	-	Enzyme-linked immunosorbent assay
EMT	-	Epithelial to mesenchymal transition
FBS	-	Fetal bovine serum
FDA	-	Food and Drug Administration
FLG	-	Flaggrin
FOXO3	-	Forkhead box O3
GALNT1/7	-	Galactosaminyltransferase 1/7
GAPDH	-	Glyceraldehyde 3-phosphate dehydrogenase
GW	-	GW3965, LXR agonist
HCV	-	Hepatitis C virus
HMGA2	-	High-mobility group AT-hook 2
HNRNPF	-	Heterogeneous nuclear ribonucleoprotein F
HOXD10	-	Homeobox D10
HSP	-	Heat-shock protein
HUVEC	-	Human umbilical vein endothelial cells
H&E	-	Hematoxylin and eosin
IGFBP	-	Insulin-like growth factor binding protein

IgG	-	Immunoglobulin G
ICD	-	Intracellular domain
IHC	-	Immunohistochemistry
IL-10	-	Interleukin 10
IP	-	Immunoprecipitation
ITGA3, ITGA5	-	Integrin alpha 3, integrin alpha 5
KD	-	Knockdown
LBD	-	Ligand-binding domain
LDLR	-	Low-density lipoprotein receptor
LIFR	-	Leukemia inhibitory factor receptor
LM2	-	2nd generation lung metastatic derivatives
LM3	-	3rd generation lung metastatic derivatives
LNA	-	Locked nucleic acid
LRP1, LRP8	-	Low-density lipoprotein receptor-related protein 1, 8
LXR, LXRE	-	Liver X receptor, liver X receptor response element
MAP	-	Mitogen activated protein
MDM2	-	Murine double minute 2
ME.1, ME.2	-	Multi-enhancer element 1, 2
MECA-32	-	Mouse endothelial cell antigen 32
MEK	-	Mitogen-activated protein kinase kinase
MER	-	Metastatic endothelial recruitment
MERTK	-	C-mer proto-oncogene tyorsine kinase
MITF	-	Microphthalmia associated transcription factor
miRNA	-	microRNA
MS	-	Mass Spectrometry
MSKCC	-	Memorial Sloan-Kettering Cancer Center
NCI	-	National Cancer Institute
NIH	-	National Institute of Health
PBS	-	Phosphate buffered saline
PDGF	-	Platelet derived growth factor
PDGFR	-	Platelet derived growth factor receptor
PD-1	-	Programmed death 1
PITPNC1	-	Phosphatidylinositol transfer protein
PFKFB3	-	6-phosphofructo-2-kinase/fructose-2,6-biphosphatase 3
PSMD11	-	Proteasome 26S subunit, non-ATPase 11
PTEN	-	Phosphatase and tensin homolog
qRT-PCR	-	Quantitative reverse transcriptase polymerase chain reaction
Rho	-	Ras homolog gene family
RDX	-	Radixin
RISC	-	RNA-induced silencing complex
RNAi	-	RNA interference
RXR	-	Retinoid X receptor
SAGE	-	Serial analysis of gene expression
SDS-PAGE	-	Sodium dodecyl sulfate polyacrylamide gel electrophoresis

SEM	-	Standard error of the mean
siRNA, shRNA	-	Short interfering RNA, short hairpin RNA
SMCs	-	Smooth muscle cells
SOX4	-	SRY (sex determining region Y) box 4
SWI/SNF	-	SWItch/ sucrose non-fermentable
TARBP2	-	TAR (HIV-1) RNA binding protein
TFAP2C	-	Transcription factor AP (activating protein) 2 gamma
TINAGL1	-	Tubulointerstitial nephritis antigen-like 1
TPM4	-	Tropomyosin 4
Tyr	-	Tyrosinase
T09	-	T0901317, LXR agonist
UV	-	Ultraviolet
VEGF	-	Vascular endothelial growth factor
VEGFR2	-	Vascular endothelial growth factor receptor 2
VLDLR	-	Very low-density lipoprotein receptor
YAP	-	Yes-associated protein
ZEB1, ZEB2	-	Zinc finger E-box binding homeobox 1, 2
3'-UTR	-	3 prime untranslated region
3p, 5p	-	3 prime, 5 prime
4-HT	-	4-hydroxytamoxifen

CHAPTER I: INTRODUCTION

Molecular Determinants of Malignant Melanoma

Malignant melanoma, the most aggressive form of skin cancer, incurs ~48,000 deaths each year globally (Lucas et al., 2006). Recently, melanoma has exhibited a steep incidence rate progression with a greater than 60% increase over the past 20 years, making it the fifth most common cancer in men and the sixth most common one in women (Garbe and Leiter, 2009; Jemal et al., 2010). Even though localized primary "stage I" melanomas are completely curable in nearly all cases, multiple distant organ spread of disseminated melanoma cells incurs a 10-year survival rate of less than 10% for advanced "stage IV" melanoma patients and a feared median survival time in the range of 8 to 18 months (Chin et al., 2006; Bhatia et al., 2009). Presently, the sole path to providing lasting cure for metastatic melanoma patients remains prevention of metastatic relapse in the adjuvant setting. However, interferon alpha, the only Food and Drug Administration (FDA)-approved melanoma adjuvant therapy, offers a meager 5-year survival benefit of ~1-3% (Garbe et al., 2011), underscoring the clinical need for the development and implementation of effective metastasis prevention therapies in melanoma. Systematic experimental approaches aimed at identifying molecules with functional and clinical relevance to melanoma metastatic progression will likely have important implications for decreasing mortality rates from this dreaded disease.

Cutaneous melanomas typically originate following the malignant transformation of skin epidermal melanocytes. The strongest risk factor for melanoma is environmental ultraviolet (UV) light exposure, which leads to accumulation of DNA damage and UV light-induced mutational inactivation of tumor suppressor genes and/or activation of oncogenes (Gilchrest et al., 1999; Pleasance et al., 2009). Interestingly, people with fair/white skin

complexion are nearly 70 times more likely to develop melanoma than those with dark/black pigmentation (Halder and Bang, 1988). Based on this observation, it was proposed that eumelanin, the type of melanin that gives rise to black/brown pigment, could serve as a physical shield against UV light by scattering UV radiation and reducing its penetration through the epidermis, thereby protecting melanocytes from UV-induced DNA damage and generation of mutations linked to melanoma initiation (Kobayashi et l., 1995; Cao et al., 2013).

In addition to UV light exposure, familial history of melanoma can also increase one's likelihood to develop melanoma by more than two-fold (Ford et al., 1995; Gandini et al., 2005), suggesting a genetic contribution to the disease's onset. To that end, genetic studies have identified inactivating germline mutations in the *CDKN2A* gene on chromosome 9p21 in 25-40% of familial melanoma tumors (Hussussian et al., 1994; Kamb et al., 1994). *CDKN2A* encodes two alternative splice variants: $p16^{INK4A}$ (also known as *MTS-1*) and $p14^{ARF}$. Both of the *CDKN2A* gene products exert a common tumor-suppressive function by halting cell cycle progression. Whereas $p16^{INK4A}$ acts by inhibiting the cyclin-dependent kinase 4 (CDK4) and thus suppressing G1 phase progression, $p14^{ARF}$ interacts with MDM2 and sequesters it away from degrading its target protein, the tumor suppressor p53 (Hollstein et al., 1991). Interestingly, somatic inactivating mutations in *CDKN2A* have also been found in a small subset (~4-20%) of sporadic melanoma tumors (Chin et al., 2006; Hodis et al., 2012)

While familial melanomas only account for about 8-12% of melanoma cases (Chin et al., 2006), the majority of melanoma tumors develop sporadically and are driven by a wide range of somatically acquired mutations following exposure to UV light and/or other environmental factors. The most frequently occurring somatic mutations found in melanoma

tumors are activating mutations in the MAP kinase signaling effectors *N-Ras* and *B-Raf*, with mutational frequencies ranging between 15-33% (Demunter et al., 2001; Goel et al., 2006) and 40-60% (Davies et al., 2002; Hodis et al., 2012), respectively. Strikingly, a single amino acid substitution (V600E) in the *B-Raf* kinase activation domain, which causes kinase hyperactivation, accounts for more than 90% of all *B-Raf* mutations found in melanoma tumors (Davies et al., 2002). The abundance of activating mutations in the *B-Raf* oncogene harbored by roughly half of melanoma patients inspired pre-clinical and clinical efforts to pharmacologically inhibit the hyperactive B-Raf mutant protein in melanoma (Yang et al., 2010; Bollag et al., 2010). This led to the FDA approval in 2011 of vemurafenib, a small molecule inhibitor of the hyperactive mutant B-Raf kinase variant, for the treatment of metastatic melanoma (Chapman et al., 2011). Despite the unprecedented success of vemurafenib in eliciting tumor-suppressive responses in over 80% of all treated advanced *B-Raf*-mutated melanoma patients and extending their respective median survival times by 6-10 months (Sosman et al., 2012), vemurafenib responses are short-lived, with nearly all patients eventually succumbing to therapeutic resistance and subsequently experiencing lethal progression of their melanoma tumors (Nazarian et al., 2010).

In addition to B-Raf inhibitors, small molecules targeting MAP kinase signaling effectors downstream of B-Raf have also been developed. Accordingly, in 2013 the FDA approved trametinib, a small molecule inhibitor of the MEK1 and MEK2 kinases, for the treatment of metastatic melanoma based on its demonstrated activity in extending progression-free survival in *B-Raf*-mutated melanoma patients (Kim et al., 2013). While the overall survival benefits of trametinib are still unclear, this targeted therapy, which acts on the same pathway as vemurafenib, is similarly undermined by emergence of clinical

resistance. Moreover, trametinib shows limited activity in patients with melanomas that have progressed on vemurafenib, rendering it ineffective in melanoma tumors with previously acquired resistance to B-Raf inhibition (Kim et al., 2013).

Besides activating mutations in *B-Raf* and *N-Ras*, a number of additional molecular alterations have been implicated in melanoma progression including hyperactivation of certain cyclin-dependent kinases such as CDK2, abnormal activation of receptor tyrosine kinase signaling (EGFR, PDGFR, c-MET, and c-KIT), mutational inactivation of PTEN and/or hyperactivation of PI3 kinase-AKT signaling, aberrant transcriptional regulation by the major melanocyte transcription factor MITF, as well as increased activation of global regulators of protein homeostasis such as HSP90 (as reviewed in Chin *et al*., 2006). However, the majority of these genetic and molecular deregulations have been functionally linked to melanoma progression by studies mainly looking at *in vitro* cell proliferation and/or *in vivo* primary tumor growth. Future studies should provide important insights into the contribution of these factors to the more advanced stages of melanoma progression involving melanoma metastatic dissemination, which is the primary cause of melanoma-related deaths.

Immunomodulatory Therapy in Melanoma

Immunotherapy, which harnesses a patient's own immune system to combat the tumor, has shown great therapeutic promise for the management of metastatic melanoma. In 2011, alongside the approval of the B-Raf inhibitor vemurafenib, the FDA also approved the immunomodulatory antibody ipilimumab for the treatment of advanced metastatic melanoma (van Elsas et al., 1999; Hodi et al., 2010). Ipilimumab acts by antagonizing cytotoxic T lymphocyte antigen 4 (CTLA-4), a T cell-expressed receptor that competes with the T cell

stimulatory CD28 receptor to inhibit ligand activation and T cell function. Thus, by blocking CTLA-4 function, ipilimumab activates the body's endogenous T cell response, leading to the immune-based suppression of melanoma tumor progression. Even though ipilimumab elicits responses in a small subset of advanced melanoma patients (10-20%), the majority of these responses, unlike for vemurafenib, are remarkably durable and can last more than two years in many cases (Page et al., 2013).

The therapeutic success of the anti-CTLA-4 antibody was followed by continuous clinical efforts to target additional regulators of T cell function. This led to the development of immunomodulatory antibodies blocking the programmed cell death (PD-1) receptor and its ligand PDL-1, whose roles are to inhibit the immune response by activating a pro-apoptotic cell program (Freeman et al., 2000; Dong et al., 2002). Therapeutic strategies targeting PD-1 signaling have shown promising results in early clinical trials (Topalian et al., 2012). Interestingly, whereas CTLA-4 serves to inhibit early T cell function and is acutely expressed during the onset of T cell activation, PD-1 shows sustained expression during chronic T cell activation and broadly inhibits T cell responses in peripheral tissues (Page et al., 2013). The distinct regulatory roles played by CTLA-4 and PD-1 in modulating T cell function have been exploited clinically in yielding additive tumor-suppressive effects upon combination regimens targeting both CTLA-4 and PD-1. Early phase I clinical testing with advanced stage melanoma patients demonstrated that combined anti-CTLA-4 and anti-PD-1 antibody treatment elicited improved response rates (up to 53% in the first trial done) compared to what was previously observed with each single agent (Wolchok et al., 2013). These findings suggest that melanoma patients may experience greater therapeutic benefit from drug combinations targeting multiple molecular determinants of immune cell function.

The development and clinical implementation of vemurafenib and ipilimumab have been deemed by physicians to be revolutionary for the clinical management of metastatic melanoma, as all other approved agents had previously failed in extending the overall survival of advanced melanoma patients in large randomized clinical trials. Nevertheless, the current median survival time of melanoma patients, even with approved therapeutics, remains less than two years and there is a large number of patients that do not respond to approved therapeutics and/or their melanomas develop resistance to targeted agents, underscoring the clinical need for the development of novel effective approaches.

The Metastatic Cascade

Nearly 100% of all deaths incurred by melanoma tumors are the consequence of melanoma metastases, which arise through the dissemination of melanoma cells from a primary lesion to multiple distal organ sites. The spread of cancer cells to distant organs is assisted by vascular flow that by necessity reaches all cell types in the body. Upon extravasating, or leaving the vasculature, cancer cells initiate colonies that expand and destroy the anatomic and functional architecture of host organs—giving rise to organ dysfunction, organ failure, and ultimately death of the organism (Gupta and Massagué, 2006; Hanahan and Weinberg, 2011; Talmadge and Fidler, 2010).

From a molecular standpoint, metastasis constitutes a fascinating process, consisting of multiple sequential and molecularly complex steps, each of which could prove rate-limiting to the ability of a cancer cell to reach and colonize distant target organs. The metastatic cascade begins with the formation of a primary tumor at an orthotopic site, such as the skin for melanoma tumors. The growth of the primary tumor is fueled by the proliferation

of cancer cells and vascularization of the tumor. The phenotypic and molecular heterogeneity present at the primary tumor stage allows for a few selected cells to eventually acquire phenotypic traits that favor their tumor detachment, stromal invasion, and ultimate entry into the blood stream. Once in the circulation, cancer cells are faced with the challenge to survive in the absence of anchorage as they migrate to peripheral sites. Eventually, the disseminated cells reach and arrest at a distant target organ, extravasate from the circulation, invade through the surrounding stroma, give rise to micrometastatic colonies, recruit endothelial cells, and initiate metastatic angiogenesis, which ultimately fuels macrometastatic formation and progressive organ colonization (Fidler, 2013; Figure 1.1).

The rate-limiting nature of each sequential step in the metastatic cascade renders this process highly inefficient, with less than 0.01% of all disseminated cells ultimately being successful in initiating metastatic colonies (Talmadge and Fidler, 2010). Additionally, disseminated cells can enter into a dormant state upon reaching their target organ site, allowing a patient to remain in remission for years (Giancotti, 2013). Unfortunately, this seemingly cancer-free state is often interrupted by an unexpected metastatic relapse as the cancer cells exit dormancy and resume colonization. Recent investigations into metastatic dormancy and re-activation mechanisms have shed light into some of the cell-intrinsic signals and cell-extrinsic cues within the metastatic niche that govern these clinically daunting processes (Zhnag et al., 2009; Gao et al., 2012).

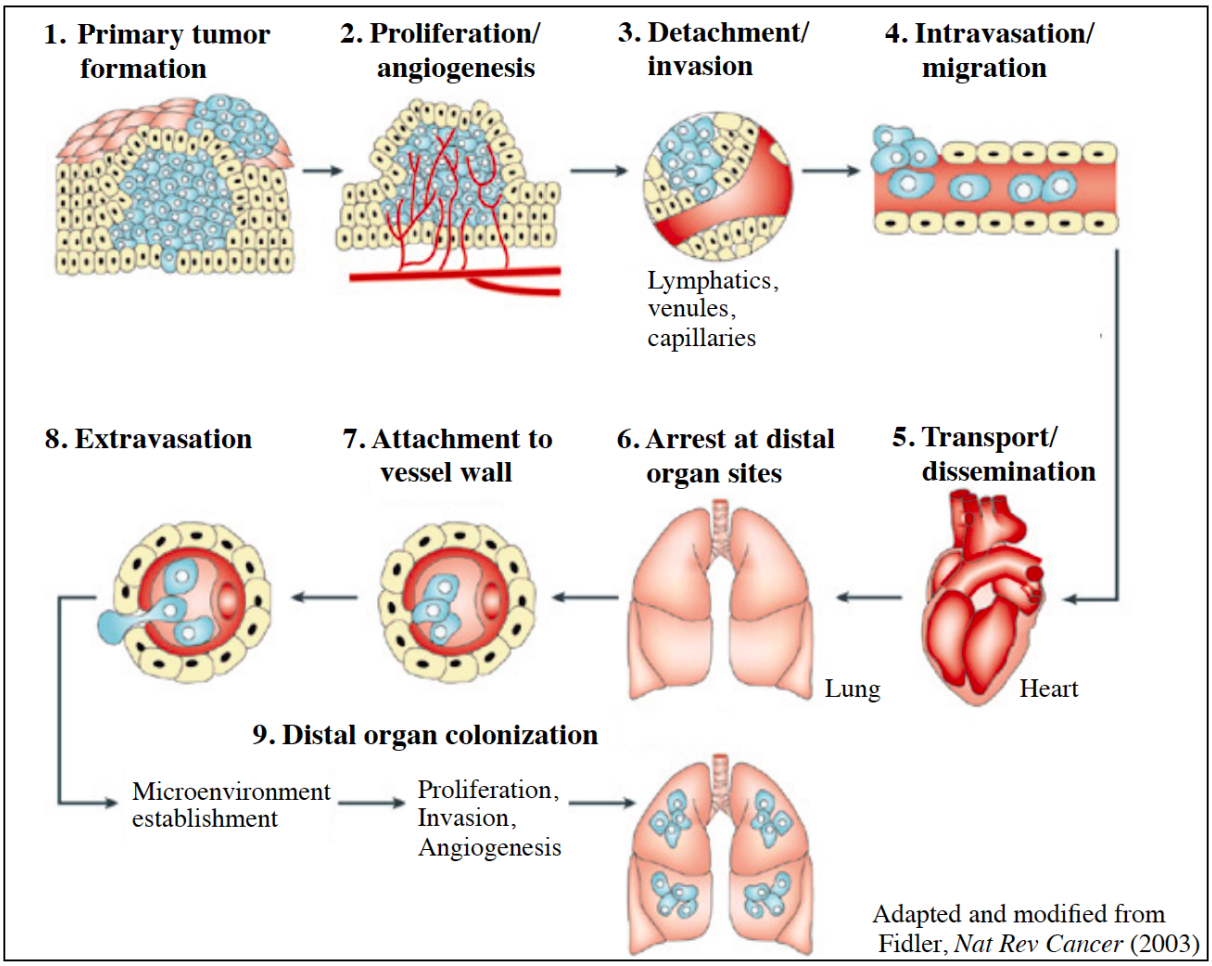

Figure 1.1. The Multiple Steps of the Metastatic Cascade. Metastatic dissemination occurs through a series of sequential events. First, the formation and growth of a primary tumor leads to the emergence of a few selected cancer cells that detach from the tumor and are able to invade through the surrounding stroma. A few of these cells eventually intravasate into the blood stream where their migration and dissemination are assisted by vascular flow. Eventually, the disseminated cancer cells arrive at a distal organ site where they arrest and extravaste into the organ stroma. Guided by both cell-intrinsic and cell-extrinsic cues, the cancer cells then initiate micrometastatic colonies, recruit blood vessels, and ultimately give rise to full organ colonization.

Given the molecular complexity of the metastatic cascade, the cellular and molecular pathways regulating this fascinating process have remained unclear until recently. During the last decade, however, advances in transcriptomic profiling approaches, RNA interference tools, and the establishment of large clinical tumor specimen collections have facilitated our molecular and conceptual understanding of the metastatic process. Multiple interdisciplinary studies by independent investigators have identified a number of coding and non-coding genes as important regulators of the metastatic process (Kang et al., 2003; Minn et al., 2005; Ma et a., 2007; Tavazoie et al., 2008; Gao et al., 2012; Png et al., 2012). A recurrent theme that emerged from these collective efforts was that metastatic colonization requires the concerted actions of many gene products. Consistent with this, transcriptomic studies of human breast cancers have revealed large sets of transcripts to be recurrently overexpressed in primary tumors that metastasize (Wang et al., 2005). This observation triggered rigorous investigations into the molecular mechanisms that govern such coordinated gene expression programs during cancer progression. In recent years, it has become increasingly clear that post-transcriptional control represents a robust mechanism by which levels of multiple transcripts are deregulated in metastasis. The post-transcriptional regulators with the most pervasive activity shown up-to-date in conferring such concerted gene expression states in metastasis are a class of small non-coding RNAs known as microRNAs or miRNAs (Bartel, 2004; He and Hannon, 2004; Lujambio and Lowe, 2012).

Discovery, Biogenesis, and Function of miRNAs

miRNAs were originally discovered in *C. elegans* in the early 1990s when elegant work by Victor Ambros, Gary Ruvkun, and colleagues showed that the protein abundance *of*

LIN-14, a gene essential for post-embryonic *C. elegans* development, is post-transcriptionally controlled by a short non-coding RNA transcript (lin-4) that negatively regulates the expression of *LIN-14* during development (Lee et al., 1993; Wightman et al., 1993). Two different lin-4 transcripts were detected of approximately 22 base pairs (bp) and 61 bp in length and were later shown to correspond to the mature lin-4 miRNA and its precursor pre-miRNA form, respectively. The lin-4 short transcripts were found to exhibit sequence complementarity to a region in the 3' untranslated region (3'-UTR) of the *LIN-14* mRNA. Based on this observation, it was proposed that lin-4 represses its target *LIN-14* through direct anti-sense RNA-RNA interactions (Lee et al., 1993; Wightman et al., 1993). This remarkable hypothesis, albeit controversial at first, has stood the test of time and ultimately shaped our current understanding of miRNA function.

It was not until seven years after the discovery of lin-4 that a second miRNA, let-7, was cloned in *C. elegans* (Reinhart et al., 2000). Remarkably, let-7 was subsequently shown to exhibit wide conservation across a large number of animal species, including humans (Pasquinelli et al., 2000). The decade that followed was marked by a great surge in miRNA discoveries. Complimentary sequencing and computational efforts led to the identification of numerous unique miRNAs across multiple species, establishing these tiny RNAs as pervasive post-transcriptional regulators of gene expression. Presently, there are over 1,800 unique annotated human miRNAs (miRBase, v. 20.0), and their number is constantly increasing as new sequences are being discovered.

While the majority of human miRNAs reside in intergenic regions or within the introns of protein-coding or non-coding genes, miRNAs located in the exons of non-coding transcripts have also been reported (UI Hussain, 2012). Intergenic miRNAs possess their own

transcriptional start sites. Intronic and exonic miRNAs are usually transcribed from the same promoter as their host gene. However, in certain cases, these miRNAs can also possess their own transcriptional initiation sites, which allow for their decoding from the anti-sense strand (UI Hussain, 2012). Single or multiple concatenated miRNA-coding sequences (known as polycistrons) are primarily transcribed by RNA polymerase II, giving rise to a primary miRNA transcript known as the pri-miRNA. In a few rare cases, pri-miRNA transcription can also be mediated by RNA polymerase III (Kim, 2005).

The processing of mammalian pri-miRNAs to mature miRNAs involves a series of cleavage events (Figure 1.2) (Kim, 2005; Winter et al., 2009). The first cleavage step is initiated when the RNA-binding protein DGCR8 detects and binds to a double-stranded hairpin embedded within the pri-miRNA. This binding allows its partner, the ribonuclease Drosha (Lee et al., 2003), to cleave the pri-miRNA at the hairpin junction site, giving rise to a roughly 60-70-bp long stem-loop product known as the pre-miRNA. The pre-miRNA is then bound by Exportin-5 and its co-factor Ran-GTP, which mediate its export across the nuclear membrane and into the cytoplasm. In the cytosol, the endonuclease Dicer (Bernstein et al., 2001) along with its co-factor, the RNA-binding protein TARBP2, recognize and bind the pre-miRNA hairpin, triggering its cleavage at two sites adjacent to the hairpin loop. Ultimately, this final cleavage event yields the mature miRNA product, a 21-26-bp long duplex structure composed of the 5 prime (5p) and 3p strands of the pre-miRNA stem (Figure 1.2).

The mature miRNA duplex is then loaded onto the RNA-induced silencing complex (RISC) (Gregory et al., 2005). The guide miRNA strand, which is typically located at the 5p end of the pre-miRNA loop owing to its higher thermodynamic stability, is preferentially

retained in the complex. The 3p arm, which is often known as the passenger strand and also designated as the star (*) form, is typically released and degraded, except for certain cases in which both the 3p (*) and 5p strands of the same pre-miRNA can mediate silencing. At the core of RISC, a member of the Argonaut (Ago) family of proteins (Liu et al., 2004) directly binds to the retained mature miRNA strand and uses it as a guide to recognize and bind mRNA transcripts bearing sequences complementary to the miRNA seed sequence—a 6-8-bp long region found within the 5p miRNA end (Meister et al., 2004; Czech and Hannon, 2011). While the majority of validated miRNA regulatory sites lie within the 3'UTRs of transcripts, certain miRNAs have also been reported to repress their targets by directly interacting with the coding sequences of transcripts (Duursma et al., 2008; Forman et al., 2008). The binding of Ago to target mRNA transcripts results in the recruitment of a set of silencing effector proteins such as GW182 (Ding and Han, 2007). The molecular interaction of multiple RISC-associated proteins with the target transcript ultimately triggers mRNA deadenylation and decay and/or translational repression (Filipowicz et al., 2008).

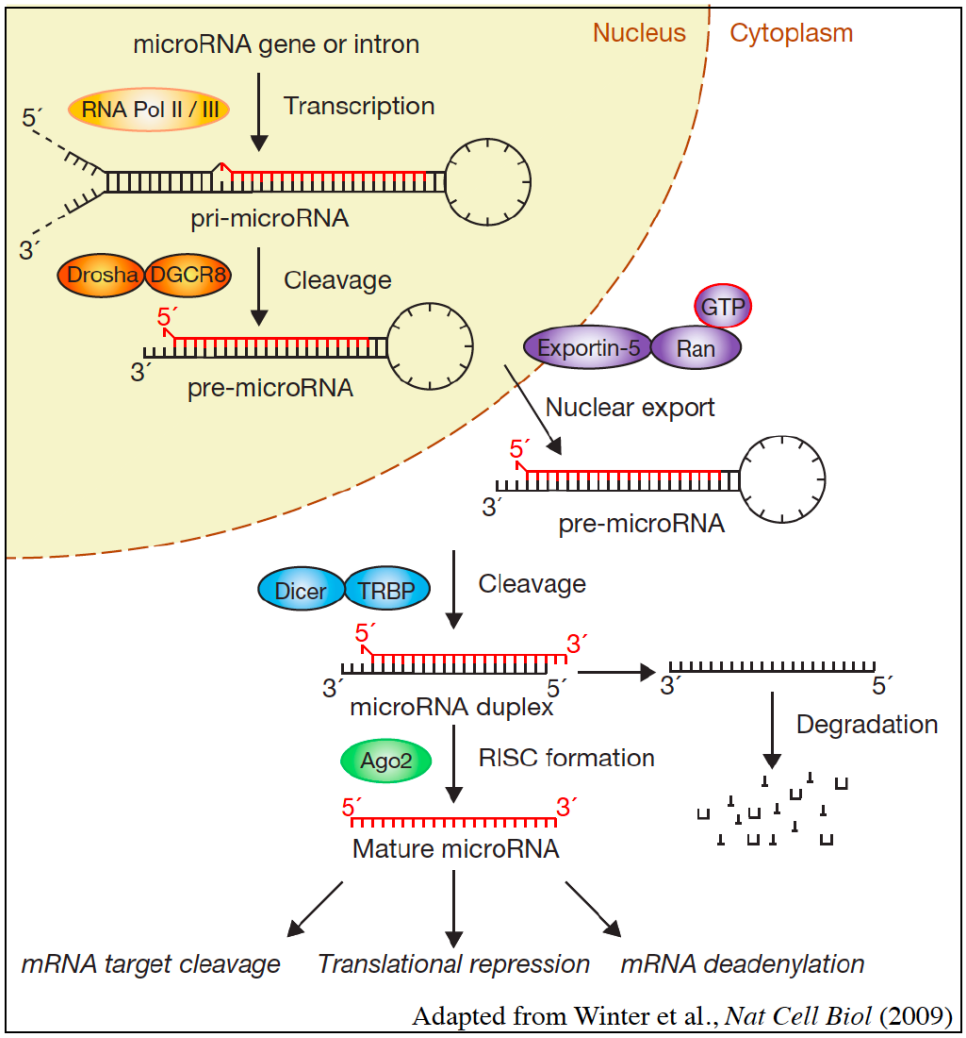

Figure 1.2. The Basic Steps of Mammalian miRNA Biogenesis. Mature miRNA sequences are encoded within pri-miRNA transcripts located within genes, between genes, or within introns. Pri-miRNAs are transcribed by RNA Pol II (or less frequently by PoI III) and processed into mature miRNAs through a series of cleavage events. First, Drosha in complex with DGCR8 recognizes and cleaves the pri-miRNA transcript, giving rise to the pre-miRNA stem-loop "hairpin". The pre-miRNA is then exported into the cytoplasm via its interaction with Exportin-5 and its associated co-factors. In the cytosol, the pre-miRNA is bound and cleaved by Dicer, generating the mature miRNA duplex structure. In this final cleavage event, Dicer is assisted by its co-factor, TARBP2. The thermodynamically more stable miRNA strand (typically at the 5p end) is then loaded into the RISC complex and bound by an Ago protein. Ago then directs the bound miRNA to complementary seed sequences on target mRNAs, leading to mRNA cleavage, deadenylation, and/or translational repression.

Deregulated miRNA Expression as a Hallmark of Human Cancers

Prior to the discovery of miRNAs as functional determinants of cancer progression, it had become clear that aberrant miRNA expression is a pervasive phenomenon across many tumor types (Calin and Croce, 2006; Garzon et al., 2009). The development of whole-genome transcriptomic approaches allowed for the global analyses of miRNA expression in various tumor types. Calin, Croce, and colleagues were the first to report abnormal miRNA expression in cancer by examining the miRNA expression signature of B cell chronic lymphocytic leukemia. This study found two clustered miRNAs, miR-15a and miR-16, to be deleted or downregulated in the majority (> 60%) of tumors tested (Calin et al., 2002). Subsequently, many more miRNAs were found to exhibit deregulated expression across diverse cancer types: For instance, let-7 was found to be silenced in lung cancers (Takamizawa et al., 2004; Yanaihara et al., 2006), while colon (Michael et al., 2003) and breast (Iorio et al., 2005) carcinomas displayed reduced miR-145 levels relative to normal tissues. Conversely, multiple groups observed overexpression of miR-155, miR-21, and the miR-17-92 cluster in breast and lung cancers (Iorio et al., 2005; Hayashita et al., 2005) as well as in B cell's and Hodgkin's lymphomas (Eis et al., 2005; Kluiver et al., 2005). The pervasive upregulation of miR-155, miR-21, and miR-17-92 observed across diverse types of cancer implicated these miRNAs as general oncogenically acting miRNAs, often referred to as "oncomiRs".

Despite individual studies reporting upregulation of a subset of specific miRNAs, findings by multiple groups, which performed transcriptomic analyses of large collections of human tumors, implicated global downregulation of miRNA expression and processing as a general phenomenon during tumorigenesis (Lu et al., 2005; Kumar et al., 2007; Yan et al.,

2012). Importantly, these early miRNA profiling studies raised the intriguing possibility that distinct miRNA expression signatures could be used to classify distinct tumor types as well as to predict the clinical prognosis of these malignancies (Calin et al., 2004; Yanaihara et al., 2006; Roldo et al., 2006).

Regulation of Metastatic Progression by miRNAs

miRNAs as Suppressors of Breast Cancer Metastasis

Given that early studies pointed to pervasive downregulation of miRNAs in human cancers, a popular hypothesis that emerged in the field was that silencing of miRNAs could modulate metastasis by de-repressing the expression of pro-metastatic genes. The initial quest for miRNAs that possess endogenous metastasis regulatory activity originally focused on breast cancer. Using an *in vivo* selection-based mouse model of human breast cancer metastasis, Tavazoie and colleagues performed small RNA profiling of highly metastatic breast cancer cell derivatives and their poorly metastatic parental populations (Tavazoie et al., 2008). These analyses revealed a subset of miRNAs to be strongly downregulated in highly metastatic cells, hinting to a putative metastasis-suppressive role for these miRNAs. In agreement with this, overexpression of three miRNAs—miR-335, miR-206, or miR-126— in highly metastatic cell variants strongly inhibited metastatic colonization. Conversely, silencing of miR-335 and miR-126 in poorly metastatic breast cancer cells led to enhanced metastatic capacity (Tavazoie et al., 2008; Png et al., 2012), consistent with endogenous activity of these miRNAs in suppressing metastasis. Importantly, the expression levels of each of these miRNAs in primary breast tumors correlated with the likelihood of metastatic relapse in breast cancer patients (Tavazoie et al., 2008), supporting a role for these small

RNAs in human metastatic progression. Silenced expression of these specific metastasis suppressor miRNAs, originally identified in breast cancer, has also been observed across numerous additional human cancers including adrenal (Schmitz et al., 2011), liver (Dohi et al., 2013), renal (White et al., 2011), lung (Donnem et al., 2011), gastric (Xu et al., 2012), and rhabdomyosarcoma (Missiaglia et al., 2010; Taulli et al., 2009) malignancies.

What was the mechanism by which these miRNAs inhibited metastasis? Both miR-335 and miR-126 were found to silence the expression of distinct sets of pro-metastatic genes, attesting to the ability of miRNAs to modulate metastatic gene expression programs (Tavazoie et al., 2008; Png et al., 2012). Importantly, the expression levels of the target genes of each of these miRNAs were also found to significantly correlate with metastatic outcomes in breast cancer patients. Systematic functional analyses demonstrated that while miR-335 directly targeted *SOX4* and *tenascin-C* to limit breast cancer cell invasion and migration (Tavazoie et al., 2008; Figure 1.3a), miR-126 acted by silencing *PITPNC1*, *MERTK*, and *IGFBP2* to limit cell-extrinsic endothelial recruitment capacity by breast cancer cells (Png et al., 2012; Figure 1.3b). Therefore, these two miRNAs were found to suppress breast cancer metastasis by divergently silencing unique sets of target genes that modulating distinct cell-intrinsic and cell-extrinsic phenotypes.

Figure 1.3. miRNA Regulatory Networks that Suppress Breast Cancer Metastasis. **a.** miR-335 inhibits metastatic progression by targeting *SOX4* and *tenascin-C*—genes that in turn promote cancer cell migration and invasion. Silencing of miR-335 in breast cancer metastatic cells is attained through both epigenetic mechanisms and copy number loss. **b.** miR-126 suppresses metastasis by targeting *PITPNC1*, *IGFBP2*, and *MERTK*. Each of these genes drives metastasis by enhancing endothelial recruitment and metastatic angiogenesis. **c.** let-7 inhibits metastasis by targeting *BACH1* and *HMGA2*. The let-7 target genes act by inducing a pro-invasive gene expression program, leading to enhanced cancer cell invasion and metastasis. **d.** Metastasis suppression by miR-31 is conferred by miRNA-mediated repression of *ITGA5*, *Rdx*, and *RhoA*—genes that promote metastatic colonization by enhancing anoikis resistance, migration, and invasion by breast cancer cells.

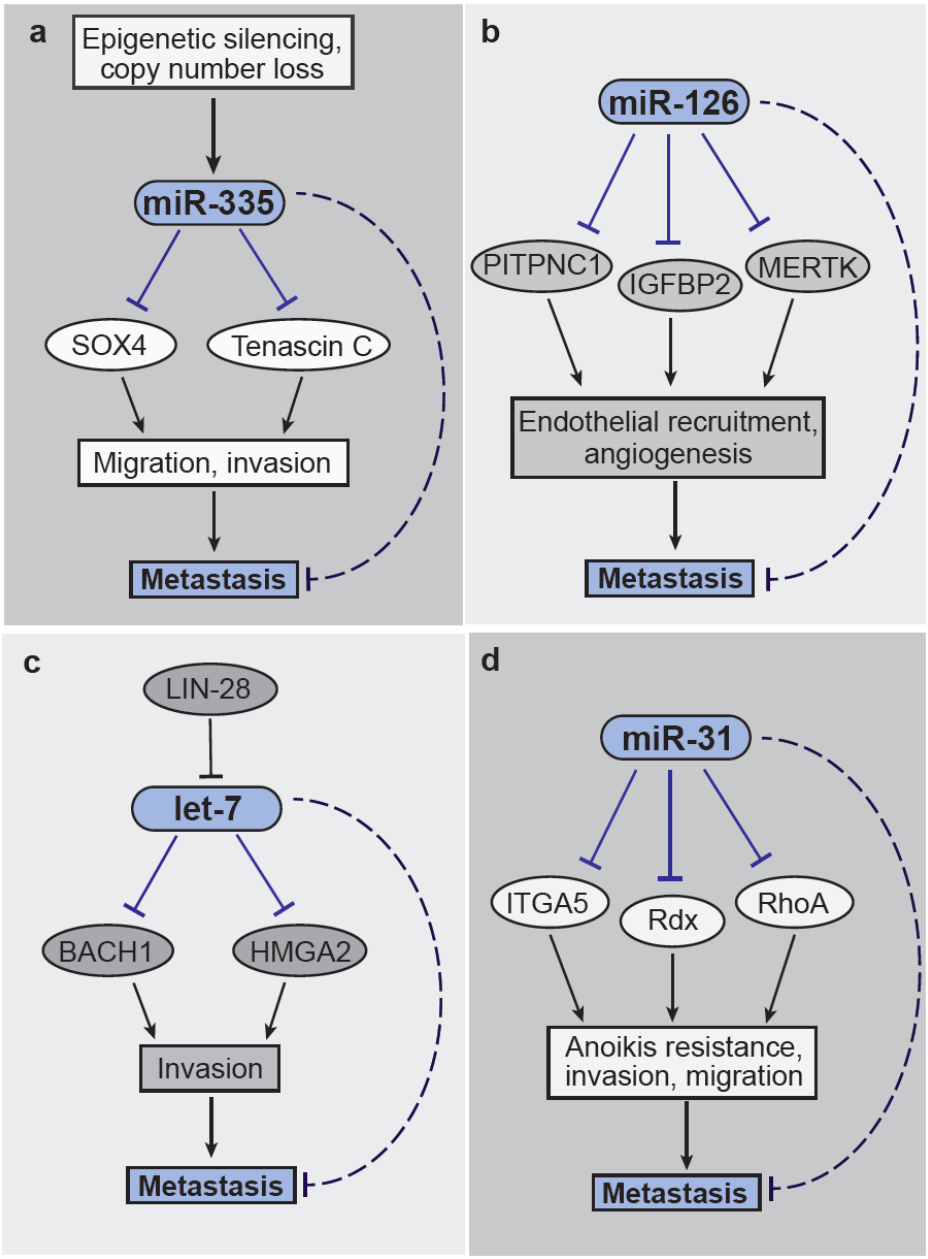

Modified from Pencheva and Tavazoie, *Nat Cell Biol*, 2013

Figure 1.3. miRNA Regulatory Networks that Suppress Breast Cancer Metastasis

Being the first miRNA to be discovered in humans (Pasquinelli et al., 2000), let-7 was also among the first miRNAs to be implicated in human breast cancer metastasis. Initially, overexpression of let-7 in human breast cancer cells was found to decrease the frequency of metastatic events to the liver and lung (Yu et al., 2007). Subsequent studies by an independent group confirmed the metastasis-suppressive role of let-7 and further demonstrated that let-7 suppressed breast cancer invasiveness and metastasis to the bone through the direct targeting of the transcription factor *BACH1* and the chromatin remodeler *HMGA2* (Figure 1.3c). Both BACH1 and HMGA2 were found to promote the transcription of multiple pro-invasive genes, thereby allowing for the broad activation of a pro-metastatic gene expression program in response to let-7 silencing (Dangi-Garimella et al., 2009; Yun et al., 2011).

The miR-31 pathway represents another prominent example of a metastasis-suppressive miRNA. This miRNA was initially implicated in breast cancer progression based on its observed downregulation in human breast cancer cells relative to mammary epithelial cells (Valastyan et al., 2009b). Subsequent functional studies demonstrated that miR-31 robustly suppressed metastasis in both loss- and gain-of-function mouse experiments. Mechanistically, miR-31 was found to inhibit metastatic progression through the coordinate repression of three genes (*ITGA5*, *RDX*, and *RhoA*), each of which was shown to promote anoikis resistance, migration, invasion, and metastasis by breast cancer cells (Valastyan et al., 2009a; Valastyan et al., 2009b) (Figure 1.3d). Importantly, consistent with these functional findings, the expression levels of each miR-31 and its target gene signature were found to segregate breast cancer patients into low and high risk of metastatic relapse (Valastyan et al., 2009b), underscoring the clinical relevance of this miRNA regulatory network to human

cancer progression. Additional studies have reported reduced expression of miR-31 in multiple other cancer types, suggesting that the metastasis-suppressive role of miR-31 may not be limited to breast cancer (Wszolek et al., 2011; Schaefer et al., 2010; Creighton et al., 2010; Zhang et al., 2010).

Taken together, the findings on miR-335, miR-126, miR-31, and let-7 collectively illustrate that breast cancer cells can attain metastatic capacity through the silencing of specific metastasis suppressor miRNAs, allowing for the de-repression of key pro-invasive and pro-metastatic genes (Figure 1.3). The identification of these miRNAs as suppressors of breast cancer metastasis has led to the discovery of multiple miRNA target genes as novel promoters of metastasis and new promising therapeutic targets in breast cancer progression.

miRNAs as Promoters of Breast Cancer Metastasis

While early studies looking into the global expression profiles of miRNAs in human malignancies hinted to a suppressive role for these regulators in tumor progression, an outstanding question in the field was whether a miRNA could, on the contrary, drive metastasis by silencing metastasis-suppressive factors. Indeed, at roughly the same time as the discovery of the first metastasis suppressor miRNAs, the first breast cancer metastasis promoter miRNA was also identified (Ma et al., 2007). Upregulation of miR-10b in breast cancer cells relative to normal epithelia initially implicated an oncogenic role for this miRNA in cancer progression. As predicted from these expression-based studies, ectopic expression of miR-10b was found to drive metastasis by human breast cancer cells (Ma et al., 2007), while subsequent studies demonstrated that silencing of endogenous miR-10b inhibited metastasis (Ma et al., 2010a). This miRNA was shown to increase metastasis by directly

targeting a gene known as *homeobox D10* (*HOXD10*). HOXD10 was found to act by inhibiting the expression of *RhoC* , a gene with a previously known metastasis-promoting function (Ma et al., 2007; Hakem et al., 2005). De-repression of *RhoC* in response to miR-10b overexpression ultimately enhanced breast cancer cell migration, invasion, and metastasis (Figure 1.4a).

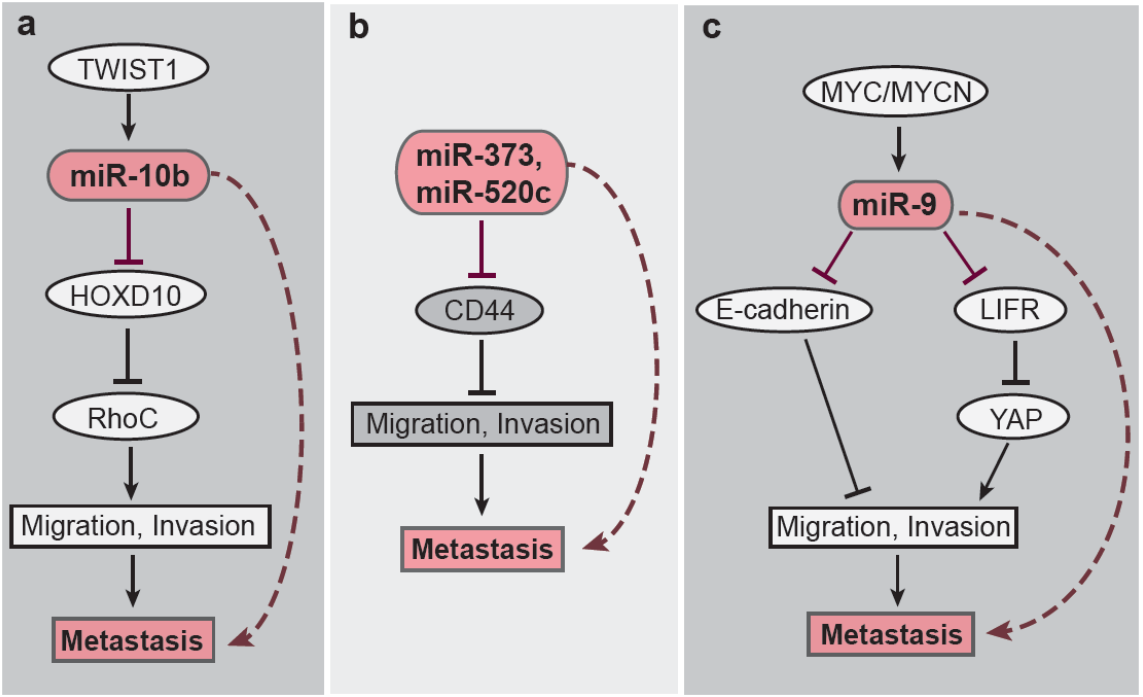

Modified from Pencheva and Tavazoie, *Nat Cell Biol*, 2013

Figure 1.4. miRNA Regulatory Networks that Promote Breast Cancer Metastasis. **a.** miR-10b promotes metastasis by directly targeting *HOXD10*. HOXD10 in turn represses *RhoC*—a promoter of cancer cell migration and invasion. miR-10b becomes upregulated in breast cancer cells through transcriptional activation by TWIST-1. **b.** miR-373 and miR-520c, which belong to the same family of miRNAs, enhance cancer cell migration, invasion, and metastasis by targeting of *CD44*. **c.** miR-9, which is transcriptionally activated by MYC/MYCN, promotes metastasis via two distinct pathways. In *E-cadherin*-positive breast cancer cells, miR-9 targeting of *E-cadherin* enhances cancer cell migration and invasion. In breast cancer cells that do not express *E-cadherin*, miR-9-mediated repression of *LIFR* drives YAP-depended migration and invasion.

Parallel to the identification of miR-10b, an independent systematic analysis employing a forward genetic screen identified two additional miRNAs as promoters of breast cancer metastasis. In this study, human breast cancer cells were transduced with a miRNA-expression library and assessed for their migration capacity. Cells that showed an enhancement in migratory ability were subsequently profiled for miRNA expression, leading to the identification of miR-373 and miR-520c as miRNAs that were preferentially enriched in highly migratory breast cancer cells *in vitro* (Huang et al., 2008). These miRNAs, which are members of the same miRNA family and share common seed sequences, were found to repress a common target gene, *CD44,* in promoting both cell migration and invasion (Figure 1.4b). Importantly, non-metastatic cells engineered to overexpress each miR-373 or mR-520c exhibited a greatly enhanced metastatic capacity, providing important *in vivo* evidence for the metastasis promoting function of these miRNAs (Huang et al., 2008).

Shortly after the discovery of the first metastasis-promoting miRNAs, miR-9 was also found to drive invasion and metastasis by breast cancer cells through directly repressing *E-cadherin* (Ma et al., 2010b) (Figure 1.4c). Interestingly, follow-up work demonstrated a metastasis-promoting role for miR-9 that is independent of *E-cadherin* targeting (Chen et al., 2012). Overexpression of miR-9 in *E-cadherin*-negative human breast cancer cells was sufficient to enhance metastasis, revealing miR-9 to act by repressing alternative target genes. Leukemia inhibitory factor receptor (*LIFR*) was identified as a direct miR-9 target in the absence of *E-cadherin* and was shown to act as a suppressor of invasion, migration, and metastasis through destabilization of YAP, a signaling effector in the Hippo pathway with a previously known oncogenic function (Chen et al., 2012) (Figure 1.4c).

In addition to the cell-intrinsic role of miR-9 in promoting breast cancer metastasis (Ma et al., 2010b, Chen et al., 2012), a recent study has implicated an independent cell-extrinsic role for miR-9 in regulating the tumor microenvironment. Work by Ferrara and colleagues demonstrated that cancer cell-expressed miR-9, which is secreted by cancer cells within microvesicles known as exosomes, gets transported into endothelial cells where it regulates endothelial cell migration by directly targeting gene expression programs within endothelial cells (Zhuang et al., 2012). While miR-9 represents the first example of a cancer cell-secreted miRNA acting directly on endothelial cell-signaling pathways, the relevance of such cell-extrinsic alterations by miRNA-containing vesicles to metastasis remains to be demonstrated.

Metastasis Regulatory miRNAs with Pleiotropic Roles in Cancer Progression

The phenotypically diverse control exerted by miRNAs on cancer progression is further nuanced by pleiotropically acting miRNAs that can simultaneously suppress and promote discrete stages of the metastatic process. The miR-200s family of miRNAs (miRs-200a/b/c, miR-429, and miR-141) represents one of the best-studied examples of miRNAs with such dual metastasis regulatory roles. At roughly the same time, several independent groups showed that the tumor cell epithelial phenotype is in large part maintained by the miR-200s family (Gregory et al., 2008; Korpal et al., 2008; Park et al., 2008; Burk et al., 2008). miR-200s were shown to block the epithelial-to-mesenchymal transition (EMT) exhibited by disseminating tumor cells, a molecular process that is thought to be a key determinant of human breast cancer metastasis (Yu et al., 2013). Consistent with this, it was demonstrated that overexpression of miR-200s can inhibit metastatic dissemination from an

orthotopic site in a syngeneic model of murine breast cancer (Gibbons et al., 2009). The miR-200s family members were found to suppress cell migration and EMT by targeting a set of transcription factors (*ZEB1* and *ZEB2*) that had previously been shown to transcriptionally repress the epithelial marker *E-cadherin* (Park et al., 2008; Korpal et al., 2008) (Figure 1.5).

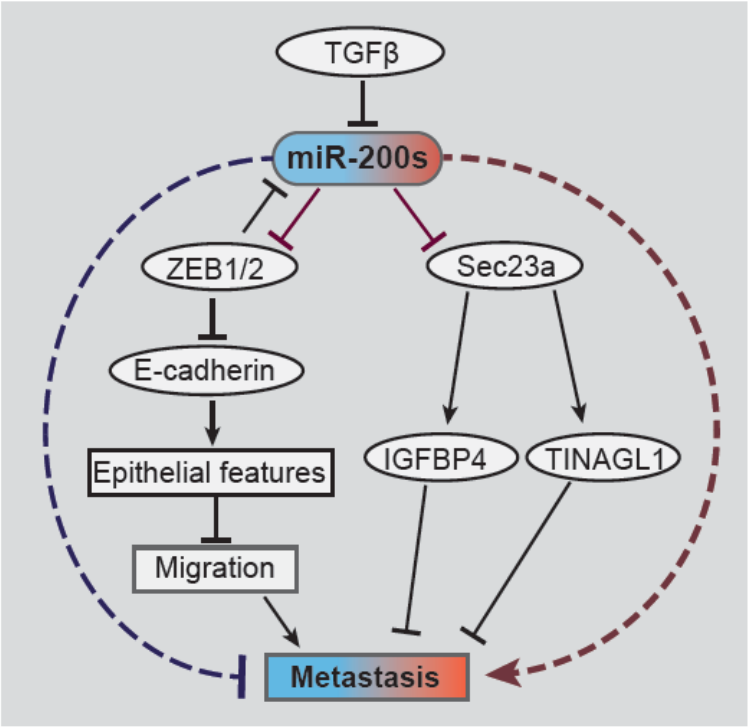

Modified from Pencheva and Tavazoie, *Nat Cell Biol*, 2013

Figure 1.5. Pleiotropic Control of Metastasis by miR-200s. The miR-200s family exerts dual metastasis-suppressive/promoting effects on metastasis. At the primary tumor stage, miR-200s-mediated targeting of *ZEB1/2* leads to de-repression of *E-cadherin*, which in turn inhibits cancer cell migration and metastatic dissemination. Conversely, at a distal metastatic site, miR-200s promote colonization by directly targeting *Sec23a*—a COPII vesicle component that enhances secretion of the metastasis-suppressive factors IGFBP4 and TNAGL1.

These early reports on the role of miR-200s in inhibiting EMT suggested that the miR-200s family suppressed metastasis by limiting local tumor invasion and dissemination. However, recent findings have contrasted that notion by implicating a metastasis-promoting role for miR-200s through targeting of *Sec23a*, a COPII vesicle component, which was shown to decrease secretion of the metastasis-suppressive factors IGFBP4 and TINAGL1 (Korpal et al., 2011) (Figure 1.5). Both overexpression of miR-200s as well as knockdown of each IGFBP4 and TINAGL1 were found to enhance lung colonization by murine breast cancer cells. Importantly, high expression levels of miR-200s correlated with shorter metastasis-free survival times in human breast cancer patients, further arguing in favor of a pro-metastatic role for this miRNA family in breast cancer (Korpal et al., 2011).

Even though the metastasis regulatory role of miR-200s remains to be extended to human breast cancer cells and validated in loss-of-function studies testing endogenous activity of miR-200s, the present findings implicate the miR-200s family members as potential pleiotropically acting miRNAs with dual metastasis-suppressing/metastasis-promoting roles in the control of metastatic progression phenotypes. How could one explain these seemingly opposing functions of miR-200s in metastasis? Considering the multifaceted nature of metastasis, expression of miR-200s at the primary tumor level may inhibit metastasis by blocking ZEB1/2-dependent EMT and early orthotropic tumor cell dissemination, whereas upregulation of miR-200s at a metastatic site may drive metastasis through targeting of *Sec23* and inhibiting secretion of factors that suppress colonization in a distal organ site such as the lung.

Search for Metastasis Regulatory miRNAs in Melanoma

Inspired by early work in breast cancer that revealed robust metastasis control by specific metastasis suppressor and promoter miRNAs, subsequent studies investigated metastasis regulatory miRNAs in multiple additional human cancers, including melanoma. Several studies have examined the distinct miRNA expression signature associated with melanoma progression. Notably, high miR-191 levels but low miR-193b levels were associated with longer post-metastasis survival in cutaneous melanoma patients (Caramuta et al., 2010), while high let-7 and miR-199a-5p levels were found to correlate with uveal melanoma progression (Worley et al., 2008). However, the correlative nature of these findings has precluded conclusions about the functional roles of these miRNAs in metastasis.

One of the first experimental attempts to functionally characterize the role of a particular miRNA in melanoma metastasis focused on a single miRNA: miR-182 (Segura et al., 2009). This miRNA initially captured the researchers' interest given its genomic location—miR-182 is flanked by the *c-Met* and *B-Raf* oncogenes in a genomic region on chromosome 7 that is frequently amplified in human melanomas. Functional studies showed that overexpression of miR-182 was sufficient in promoting lung colonization by murine melanoma cells and implicated the major melanocyte-specific transcription factor *MITF* as a direct downstream target of miR-182 (Segura et al. 2009; Figure 1.6a). More recently, miR-214 and miR-30b/30d were also reported to promote melanoma metastasis. While miR-214 was found to directly target *ITGA3* and *TFAP2C* in driving invasion, extravasation, and colonization by melanoma cells (Penna et al., 2011; Figure 1.6b), overexpression of miR-30b/30d enhanced micrometastasis formation through targeting of *GALNT1* and *GALNT7* (Gaziel-Sovran et al., 2011; Figure 1.6c). The miR-30b/30d target genes were found to

inhibit cell invasion, and *GALNT7* was also implicated in immune cell activation by downregulating the immunosuppressive cytokine IL-10. Therefore, it was speculated that by indirectly activating the expression of IL-10, miR-30b/30d triggers immune cell suppression, which ultimately enhances melanoma metastatic progression. Importantly, the expression levels of miR-30b/30d in primary melanoma tumors were shown to correlate with metastatic outcomes of melanoma patients (Gaziel-Sovran et al., 2011), supporting previous findings that specific miRNAs may act as potential biomarkers in melanoma progression (Worley et al., 208; Caramuta et al., 2010).

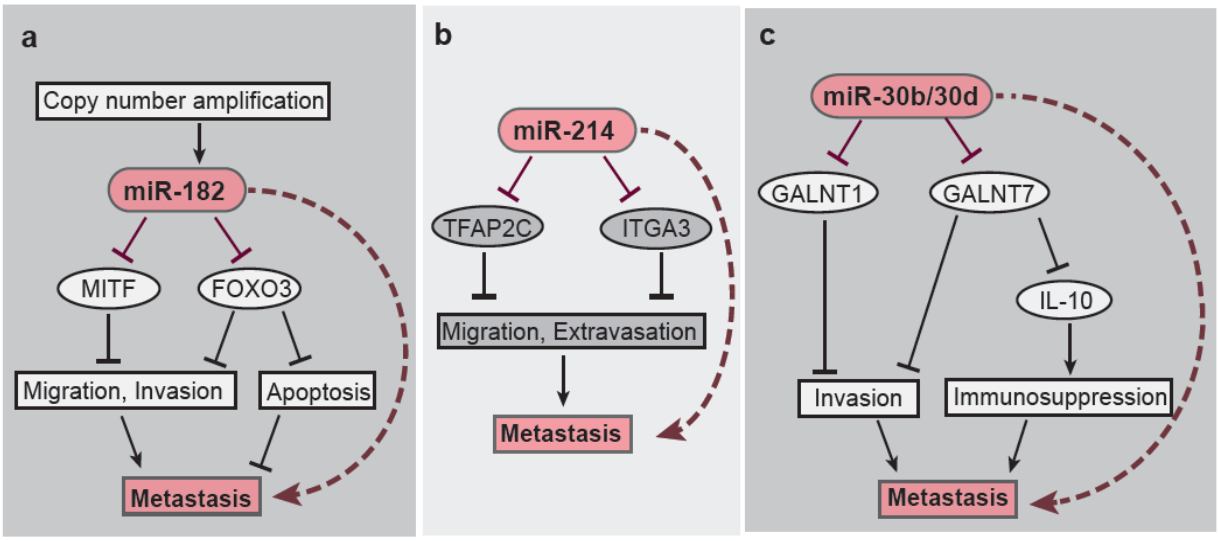

Modified from Pencheva and Tavazoie, *Nat Cell Biol*, 2013

Figure 1.6. miRNA Regulatory Networks that Promote Melanoma Metastasis.
a. Overexpression of miR-182 promotes mouse melanoma metastasis by targeting *MITF* and *FOXO3*—genes that suppress cell migration and invasion. In addition, *FOXO3* was also shown to suppress cell apoptosis. **b.** miR-214 enhances melanoma cell migration, extravasation, and metastasis through targeting of *TFAP2C* and *ITGA3*. **c.** miR-30b/30d directly targets the galactosaminyltransferases *GALNT1* and *GALNT7*, which in turn act as suppressors of melanoma invasion and metastasis. Additionally, GALNT7 also suppresses the secretion of the immunosuppressive cytokine IL-10.

Overview and Biological Significance

Recent work by multiple independent groups has led to the emergence of miRNAs as robust regulators of metastatic progression (Pencheva and Tavazoie, 2013). Whereas the majority of early studies provided strong evidence for endogenous miRNA activity in the control of breast cancer metastasis through the use of loss-of-function mouse studies and clinicopathologic analyses, the role of endogenous miRNAs in other metastatic epithelial cancers is less well established. Melanoma, a highly prevalent malignancy with steadily increasing incidence, remains clinically intractable following metastasis of the primary tumor (Garbe et al., 2011). The molecular underpinnings of melanoma metastasis are still poorly understood, which has hindered the development and clinical implementation of effective therapeutic approaches to prevent and/or treat metastasis. Despite several studies reporting deregulated miRNA expression in melanoma and showing that overexpression of certain miRNAs can drive melanoma metastasis, no systematic analyses had been performed, prior to this work, to identify miRNAs with robust endogenous activity in melanoma metastatic progression. The discovery of endogenous miRNA as regulators of melanoma metastasis would further support the pervasive metastasis control exerted by these small RNAs across multiple human cancers. More importantly, these miRNAs can then be used as functionally guided probes to uncover novel molecular pathways regulating metastasis. Such mechanistic insights will not only deepen and diversify our molecular understanding of the biology underlying cancer metastasis, but also will ultimately lead to the emergence of novel molecules as potential therapeutic targets in melanoma metastasis, a poorly understood molecular process that results in a fatal outcome for more than 90% of advanced melanoma patients (Bhatia et al., 2009).

In this thesis, I describe the use of a systematic *in vivo* selection-based approach for the identification and functional characterization of miRNAs (Chapter II) and their effector genes (Chapter III) in the regulation of melanoma metastasis. Our unbiased interrogation of deregulated miRNA pathways in melanoma metastasis led to the identification of a single gene, *ApoE*, as a convergent target of multiple metastasis-promoting miRNAs in melanoma (Chapter III). The central position of ApoE in this miRNA regulatory network as well as the significant correlation of ApoE expression with melanoma progression outcomes motivated us to further investigate the molecular role of ApoE in melanoma metastasis, which is the focus of Chapter IV. Finally, in light of the robust metastasis suppression effects exerted by ApoE, I describe the development and implementation of a therapeutic approach to chronically activate *ApoE* expression in metastatic melanoma by pharmacologically targeting the liver X nuclear hormone receptor beta (LXRβ), a ubiquitously expressed transcriptional trans-activator of *ApoE* (Chapter V). In the final Chapter VI, I discuss the biological and clinical implications of these findings to melanoma metastasis and angiogenesis.

CHAPTER II: IDENTIFICATION, FUNCTIONAL CHARACTERIZATION, AND CLINICAL VALIDATION OF MIRNAS THAT PROMOTE MELANOMA METASTASIS

In Vivo Enrichment for Highly Metastatic Melanoma Sub-Populations of Cells

In order to enrich for highly metastatic cell derivatives from heterogeneous parental human melanoma cell populations, we employed an *in vivo* selection approach originally developed by Isaiah Fidler (Pollack and Fidler, 1982). Hien Tran, a former clinical fellow in the lab, carried out *in vivo* selection with two independent human melanoma cell lines: the melanotic *B-Raf* wild-type MeWo line and the amelanotic *B-Raf* mutant A375 line. In brief, parental cells were injected via the tail-vein into immunocompromised Nod SCID mice. Following formation of macroscopic metastatic nodules in the lungs, nodules were extracted and melanoma cells were dissociated, yielding a first generation of lung metastatic (LM1) derivatives that were then re-injected into mice and subjected to another round of *in vivo* selection. Ultimately, cells dissociated from the LM1-forming metastatic nodules gave rise to a second generation of lung metastatic cells designated as LM2.

I then tested whether the *in vivo* selected metastatic melanoma cells, generated using the approach described above, exhibited enhanced metastatic capacity relative to the parental population they were derived from. Indeed, *in vivo* bioluminescence imaging of luciferase-expressing melanoma cells complemented with *ex vivo* gross lung histology revealed that the MeWo-LM2 metastatic derivatives colonized the lungs to a significantly greater extent than that of the parental population (Figure 2.1a). Similar results were obtained for the independently derived A375-LM3 (third generation) metastatic derivatives (Figure 2.1b).

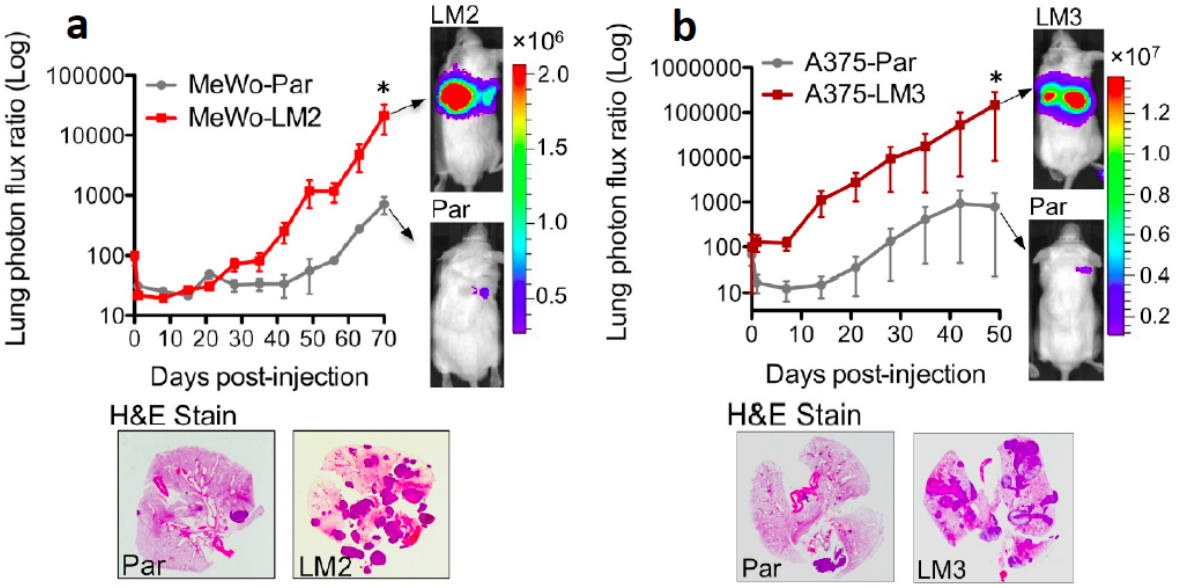

Figure 2.1. Lung Metastatic Colonization by *In Vivo-Selected* Metastatic Melanoma Derivatives and Their Parental Populations. a. Bioluminescence imaging plot of lung colonization by 4×10^4 MeWo parental (MeWo-Par) and MeWo lung metastatic derivatives (MeWo-LM2). Lungs were extracted at day 72 and H&E-stained. $n \geq 4$. **b.** Lung colonization, quantified by weekly bioluminescence imaging, by 1×10^5 A375-Par and A375-LM3 melanoma cells. H&E-stained lungs correspond to lungs extracted at the final day of imaging, day 49. $n \geq 4$. All data are represented as mean ± SEM. *$p < 0.05$. p-values based on Mann-Whitney's t-tests.

Identification of Metastasis-Promoting miRNAs in Human Melanoma

Having obtained highly metastatic derivatives from an isogenic parental population, Hien Tran and I next examined whether there exist any molecular differences between poorly metastatic and highly metastatic human melanoma cells. In these early analyses, we focused on miRNA expression given previous evidence of deregulated miRNA expression in highly metastatic breast cancer cells (Tavazoie et al., 2008). Hybridization-based small RNA profiling of 894 mature miRNAs followed by stem-loop quantitative reverse-transcriptase PCR (qRT-PCR) validation revealed four miRNAs (miR-1908, miR-214, miR-199a-5p, and

miR-199a-3p) to be upregulated greater than two-fold in multiple A375 and MeWo metastatic derivatives relative to their respective parental cells (Figures 2.2a-b). This analysis also implicated two miRNAs (miR-7 and miR-18a) that exhibited modest downregulation (up to 2-fold decrease) in only a subset of the metastatic derivatives (data not shown). In comparison, the observed upregulation of miR-1908, miR-214, miR-199a-3p, and miR-199a-5p was robust (up to 10,000-fold increase) and pervasive, as it was seen across all metastatic derivatives we examined. Therefore, we decided to focus on these miRNAs for further studies.

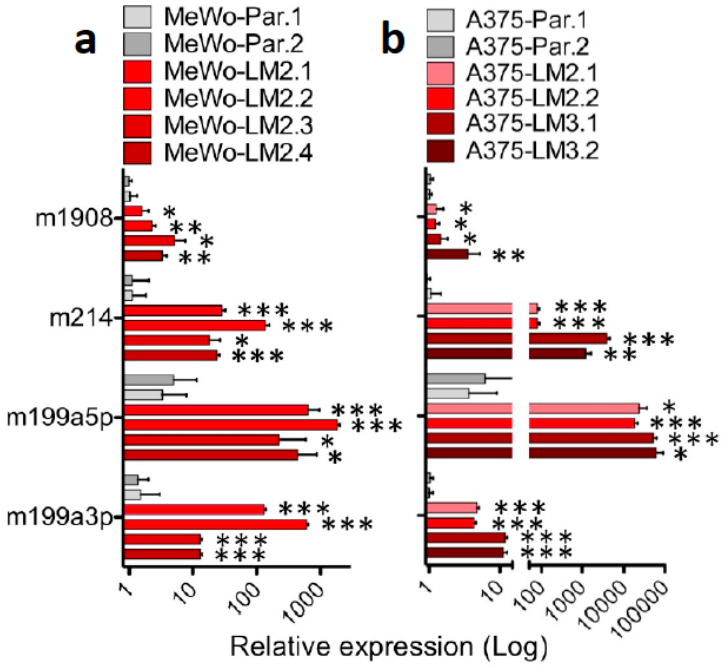

Figure 2.2. Identification of Deregulated miRNAs in Metastatic Melanoma Cells.
a-b. qRT-PCR validation of the expression levels of miR-1908, miR-214, miR-199a-5p, and miR-199a-3p in multiple lung metastatic derivatives and their respective parental populations for the MeWo (**a**) and A375 (**b**) human melanoma cell lines. The four miRNAs were chosen for qRT-PCR validation based on their greater than two-fold upregulation based on microarray analyses. n = 3. All data are represented as mean ± SEM. *p < 0.05, **p < 0.01, ***p < 0.001. p-values based on unpaired student's t-tests.

The significant induction of miR-199a-3p, miR-199a-5p, miR-214, and miR-1908 across multiple metastatic derivatives prompted us to examine whether these miRNAs exhibit a metastasis-promoting role in human melanoma. To directly test this, I employed a retroviral transduction approach to overexpress the precursors for miR-199a-3p and miR-199a-5p (overexpressed concomitantly as the miR-199a hairpin), miR-1908, or miR-214 in the poorly metastatic MeWo cells that exhibit relatively low endogenous levels of these miRNAs (Figure 2.3a). Subsequent lung colonization assays revealed that overexpression of miR-199a and miR-1908 led to a greater than 8-fold increase in lung metastatic colonization based on both bioluminescence signal quantification and gross lung histology, while miR-214 overexpression did not significantly affect metastasis (Figure 2.3b). Importantly, each miR-199a or miR-1908 individually increased the number of metastatic nodules formed (Figure 2.3c), consistent with a role for these miRNAs in metastatic initiation.

The lack of metastasis regulatory activity for miR-214 in the human MeWo line is in contrast to its previously reported role as a metastasis promoter in melanoma (Penna et al., 2011) and suggests that this miRNA acts as a passenger in the MeWo system. Consistent with this, miR-214 is located within a polycistron together with miR-199a on chromosome 1, implying that both miR-214 and miR-199a are processed together and undergo upregulation in metastatic melanoma cells through a common mechanism. In regards to the other two miRNAs (miR-182 and miR-30b/30d) that were previously reported to promote melanoma metastasis (Penna et al., 2011; Gaziel-Sovran et al., 2011), we did not observe upregulation of miR-30b/30d across the metastatic derivatives, while miR-182 was upregulated in the MeWo metastatic variants, but not in the A375-LM3 cells. However, overexpression of miR-182 in MeWo parental cells did not significantly modulate metastasis (data not shown).

We next asked if endogenous forms of miR-199a and miR-1908 promote metastasis. To test this, we silenced each of the miRNAs in the highly metastatic MeWo-LM2.3 cells (henceforth designated as MeWo-LM2) that express relatively high miRNA levels. Stable inhibition of mature miR-1908 and each of the two miRNAs arising from the miR-199a hairpin (miR-199a-3p and miR-199a-5p) through miR-Zip technology suppressed metastatic colonization in the highly metastatic MeWo-LM2 cells by more than 7-fold (Figure 2.4a) and dramatically decreased the number of metastatic nodules formed (Figure 2.4b).

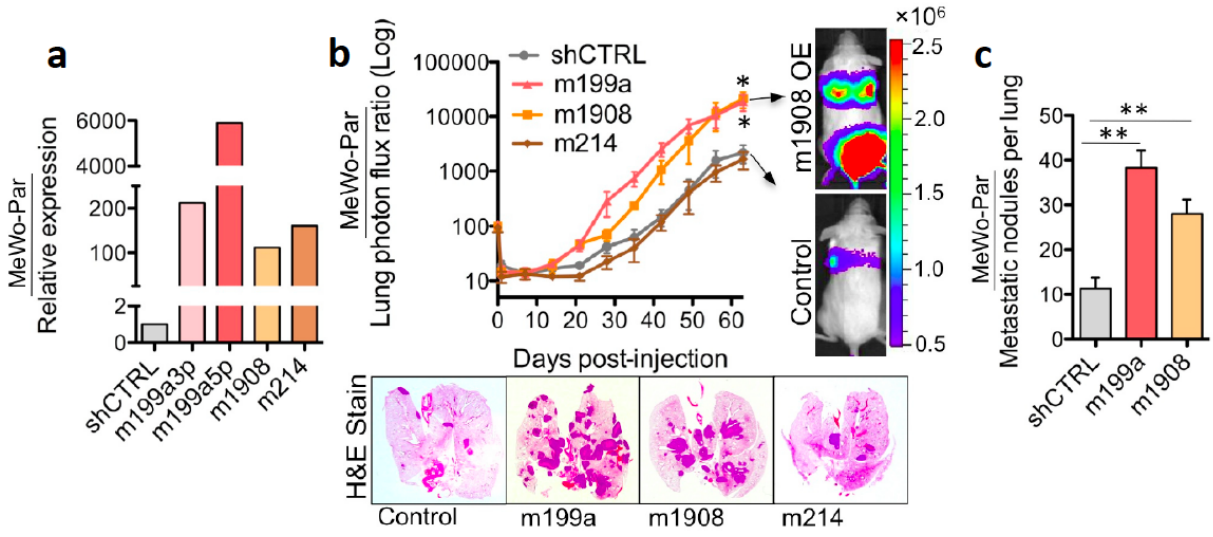

Figure 2.3. Identification of miR-199a and miR-1908 as Promoters of Melanoma Metastasis to the Lung. a. Expression levels of miR-199a-3p, miR-199a-5p, miR-1908, and miR-214 determined by qRT-PCR in MeWo parental cells that were transduced with a retrovirus expressing a control hairpin or a miRNA precursor hairpin giving rise to miR-199a (both miR-199a-3p and miR-199a-5p), miR-1908, or miR-214, respectively. **b.** Bioluminescence imaging quantification and representative H&E-stained lung images corresponding to lung colonization by 4×10^4 MeWo parental cells expressing a control hairpin or a precursor hairpin for miR-199a, miR-1908, or miR-214. $n \geq 4$. **c.** Number of macroscopic nodules formed by MeWo control cells or MeWo cells overexpressing miR-199a or miR-1908. $n = 3$. All data are represented as mean ± SEM. $^*p < 0.05$, $^{**}p < 0.01$. p-values based on Mann-Whitney's t-tests (**b**) or unpaired student's t-tests (**c**).

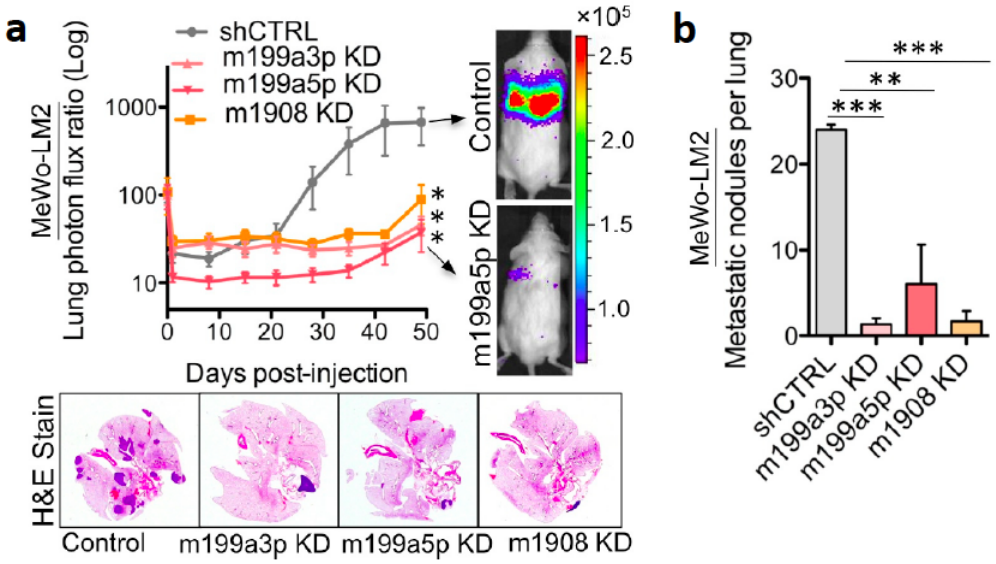

Figure 2.4. Endogenous miR-199a-3p, miR-199a-5p, and miR-1908 Promote Lung Colonization and Metastatic Initiation. a. Lung colonization, quantified by bioluminescence imaging, by 4×10^4 MeWo-LM2 cells transduced with a control hairpin (miR-Zip) or a miR-Zip targeting each mature miR-199a-3p, miR-199a-5p, or miR-1908. H&E-stained lungs correspond to the final day 49 of imaging. $n \geq 5$. **b.** Number of macroscopic lung nodules formed by MeWo-LM2 control cells or MeWo-LM2 cells with silenced expression of each miR-199a-3p, miR-199a-5p, or miR-1908. $n = 3$. All data are represented as mean ± SEM. *$p < 0.05$, **$p < 0.01$, ***$p < 0.001$. p-values based on Mann-Whitney's t-tests (**a**) or unpaired student's t-tests (**b**).

To determine whether these miRNAs also promote metastasis in an independent cell line, I silenced their expression in the A375-LM3.2 cells (henceforth designated as A375-LM3). Indeed, miR-Zip-mediated silencing of miR-1908, miR-199a-3p, or miR-199a-5p significantly reduced lung colonization by the highly metastatic A375-LM3 derivatives (Figure 2.5). Taken together, these findings establish miR-1908, miR-199a-3p, and miR-199a-5p as endogenous promoters of metastasis by human melanoma cells.

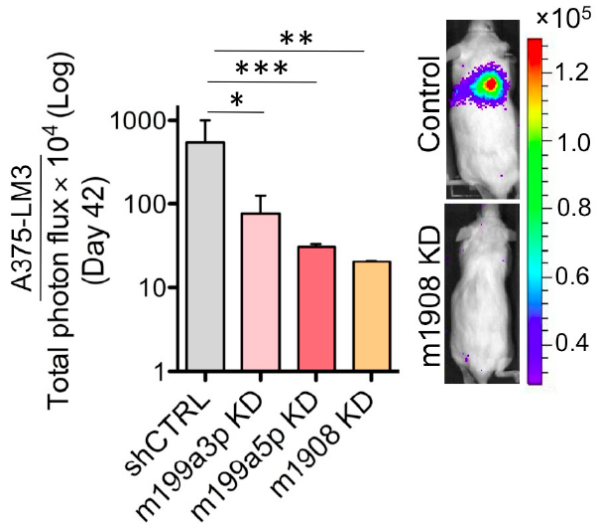

Figure 2.5. Endogenous miR-199a-3p, miR-199a-5p, and miR-1908 Promote Metastasis by an Independent Melanoma Cell Line. Lung photon flux measured by bioluminescence imaging 42 days following intravenous injection of 2 × 10^5 A375-LM3 cells expressing a control miR-Zip or a miR-Zip targeting miR-199a-3p, miR-199a-5p, or miR-1908. n ≥ 5. All data are represented as mean ± SEM. *p < 0.05, **p < 0.01, ***p < 0.001. p-values based on Mann-Whitney's t-tests.

We next wished to determine how pervasive the overexpression of miR-199a and miR-1908 is in the metastasis of different melanoma subtypes. To this end, I performed *in vivo* selection for highly metastatic derivatives of two independently derived primary human melanoma cell lines, SK-Mel-334 and SK-Mel-462 (Figure 2.6), which had had minimum expansion *in vitro* (up to passage 10) following their dissociation from patients' tumors. Remarkably, consistent with our previous findings from the MeWo and A375 *in vivo* selected metastatic melanoma sub-lines, we observed upregulation of miR-199a-3p, miR-199a-5p, and miR-1908 across the metastatic derivatives of both patients' primary melanoma lines as well as in additional metastatic derivatives of the HT-144 and WM-266-4 established melanoma lines (Figure 2.7). Our findings of pervasive deregulation of these three miRNAs

across multiple *in vivo*-selected metastatic derivatives from a total of six mutationally diverse melanoma lines isolated from different patients provide strong evidence that the observed upregulation of miR-199a-3p, miR-199a-5p, and miR-1908 during melanoma metastasis is robust and unlikely to be cell line-specific. Importantly, the induction of these miRNAs in primary melanoma metastatic derivatives indicates that this phenomenon is unlikely to be an artifact of the extensive *in vitro* passaging of established melanoma lines routinely used in the field.

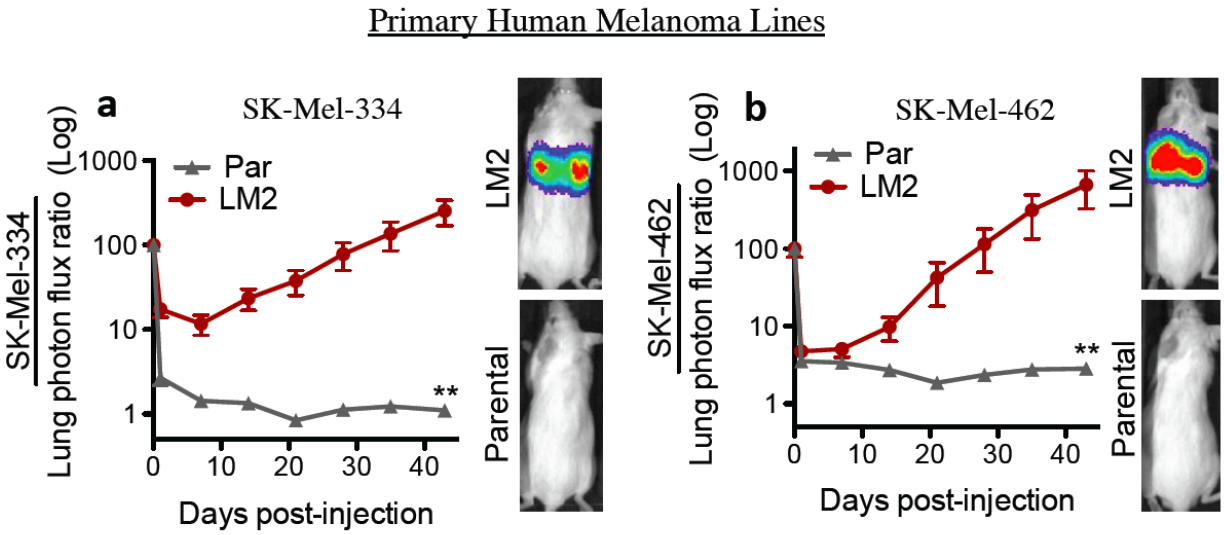

Figure 2.6. *In Vivo* Selection for Metastatic Melanoma Derivatives of Primary Human Melanoma Cell Populations. a-b. Metastatic colonization following intravenous injection of 2×10^5 parental or LM2 derivatives of the SK-Mel-334 (**a**) and SK-Mel-462 (**b**) primary melanoma lines that were derived from melanoma tumors of patients at the Memorial Sloan-Kettering Cancer Center. Lung colonization was measured by weekly bioluminescence imaging. $n \geq 5$. $^{**}p < 0.01$. p-values based on Mann-Whitney's t-tests.

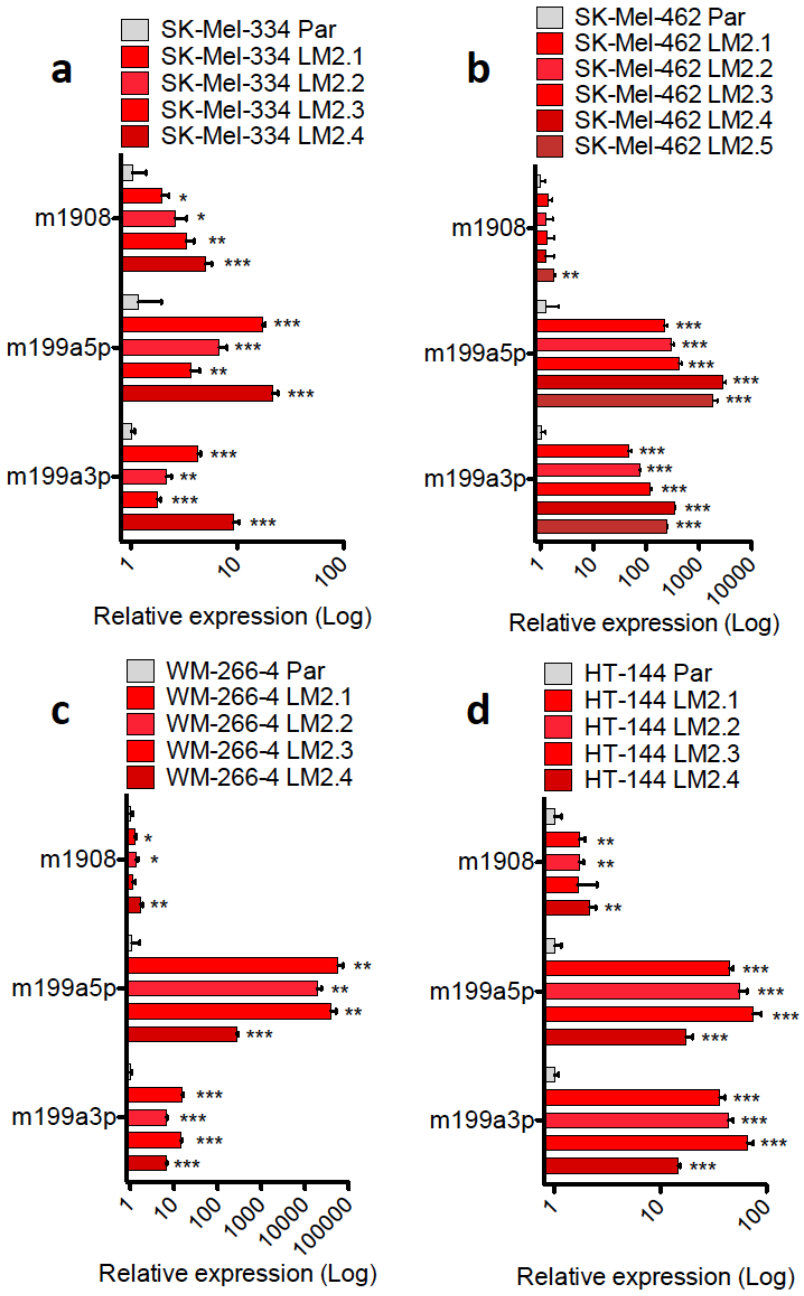

Figure 2.7. Pervasive Upregulation of miR-199a-3p, miR-199a-5p, and miR-1908 across Melanoma Metastatic Derivatives. a-d. The levels of miR-199a-3p, miR-199a-5p, and miR-1908 were analyzed by qRT-PCR in multiple metastatic derivatives attained by *in vivo* selection of the primary SK-Mel-334 (**a**) and SK-Mel-462 (**b**) human melanoma cells, as well as the established WM-266-4 (**c**) and HT-144 (**d**) human melanoma lines. All data are represented as mean ± SEM. *$p < 0.05$, **$p < 0.01$, ***$p < 0.001$. p-values based on unpaired student's t-tests.

Cellular Phenotypes Conferred by Metastasis-Promoting miRNAs

We next investigated the cellular mechanisms by which these miRNAs drive melanoma metastasis. With the help of Colin Buss, a former technician in the lab, we first tested if these miRNAs promote metastasis by enhancing proliferation/cell survival. Contrary to this, overexpression of each miRNA actually reduced cell proliferation/survival *in vitro* (Figure 2.8a). More importantly, miR-1908 overexpression did not increase primary tumor growth *in vivo*, while miR-199a overexpression led to a significant decrease (35%) in tumor volume (Figure 2.8b), indicating that the pro-metastatic effects of miR-1908 and miR-199a are not secondary to enhanced tumor growth capacity.

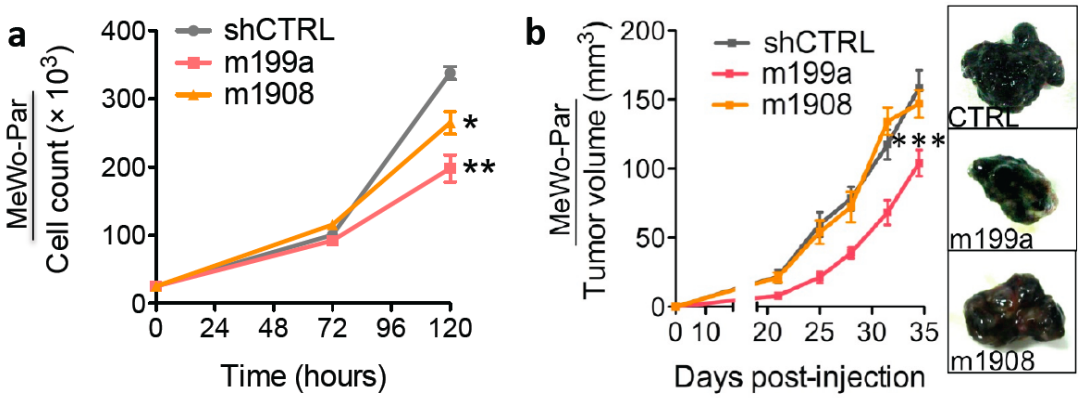

Figure 2.8. Effects of miR-199a and miR-1908 on *In Vitro* Melanoma Cell Proliferation and *In Vivo* Melanoma Tumor Growth. a. *In vitro* cell proliferation, quantified by counting the number of live cells at days 0, 3, and 5 post-seeding, by MeWo melanoma cells expressing a control hairpin or a precursor hairpin giving rise to each miR-199a or miR-1908. n = 3. **b.** Subcutaneous tumor growth by 1×10^6 MeWo cells expressing miR-199a or miR-1908 precursor hairpins or a control hairpin. n ≥ 4. All data are represented as mean ± SEM. *p < 0.05, **p < 0.01, ***p < 0.001. p-values based on unpaired student's t-tests.

Next, we systematically examined a number of additional *in vitro* phenotypes implicated with enhanced *in vivo* metastatic capacity. While overexpression of each miR-199a or miR-1908 did not affect cell survival under serum starvation, resistance to anoikis, colony formation, or adhesion to endothelial cells (Figures 2.9a-d), I found that each miRNA enhanced the ability of MeWo melanoma cells to invade through matrigel (Figure 2.10a) as well as their capacity to recruit endothelial cells in trans-well assays (Figure 2.10b). These two phenotypes were also elevated in the highly metastatic MeWo-LM2 derivatives (Figures 2.10c-d), which express higher endogenous levels of miR-199a and miR-1908 relative to the parental cells (Figure 2.2a). Importantly, silencing of each mature miRNA in the highly metastatic MeWo-LM2 cells suppressed matrigel invasion and endothelial recruitment, revealing a role for the endogenous forms of the three miRNAs in driving these *in vitro* phenotypes (Figure 2.11a-b). Endogenous miR-199a and miR-1908 were also found to promote matrigel invasion and endothelial recruitment by the independent A375-LM3 highly metastatic derivatives (Figure 2.11c-d).

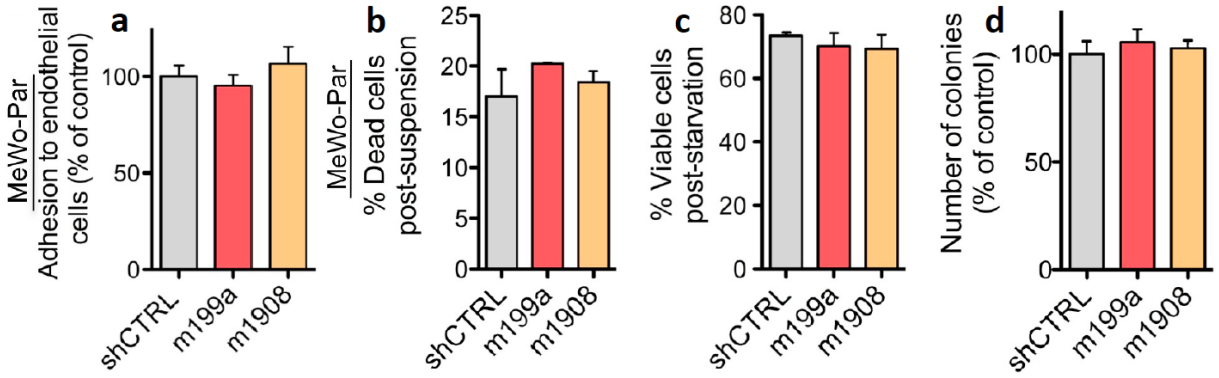

Figure 2.9. Effects of miR-199a and miR-1908 on Pro-Metastatic *In Vitro* Phenotypes. **a-d.** Parental MeWo melanoma cells overexpressing the precursors for each miR-199a or miR-1908 or cells transduced with a control hairpin were tested for their capacity to adhere to endothelial monolayers (**a**), survive in the absence of attachment (**b**), survive during serum starvation (**c**), or form colonies (**d**). n ≥ 3. All data are represented as mean ± SEM.

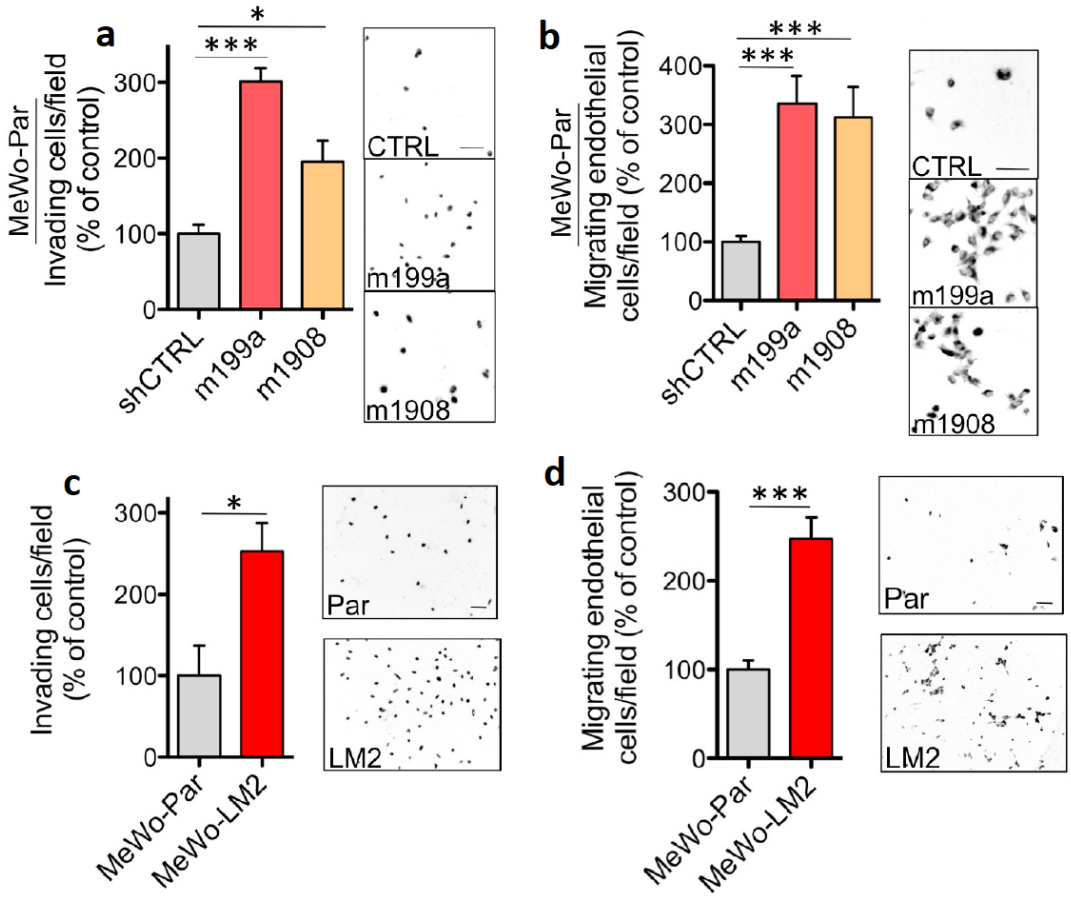

Figure 2.10. Overexpression of miR-199a or miR-1908 Enhances Matrigel Invasion and Endothelial Recruitment Phenotypes. **a.** Trans-well matrigel invasion by 1×10^5 melanoma cells expressing a control hairpin or a pre-cursor hairpin giving rise to miR-199a or miR-1908. $n \geq 3$. **b.** Trans-well endothelial recruitment by 5×10^4 melanoma MeWo cells overexpressing miR-199a or miR-1908 or control MeWo cells. $n \geq 7$. **c-d.** The highly metastatic MeWo-LM2 derivatives and their parental cells were assessed for their ability to invade through matrigel (**c**) and to recruit endothelial cells (**d**) in trans-well assays. $n \geq 3$. Thresholded images represent melanoma cells (**a, c**) or endothelial cells (**b, d**) that had successfully migrated to the basal side of trans-well inserts. All data are represented as mean ± SEM. Scale bar, 100 μm. *$p < 0.05$, ***$p < 0.001$. p-values based on unpaired student's t-tests.

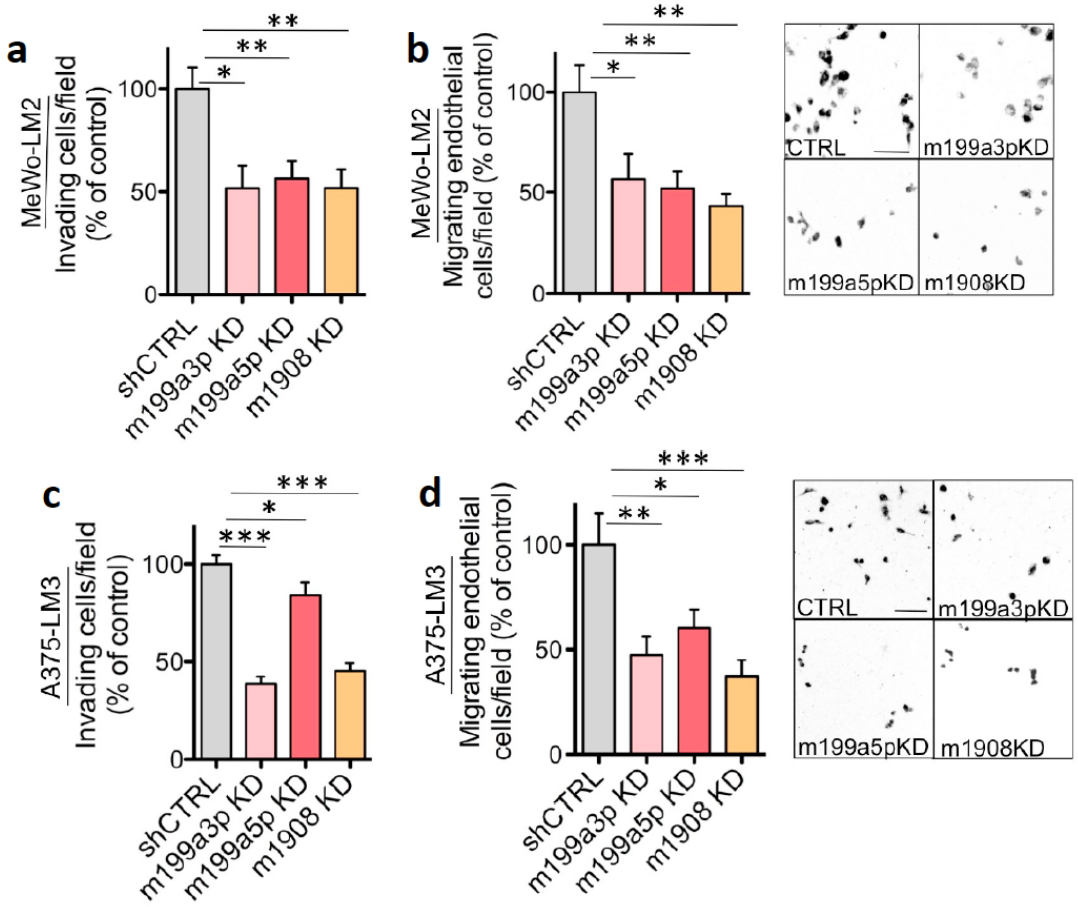

Figure 2.11. Endogenous miR-199a-3p, miR-199a-5p, and miR-1908 Promote Matrigel Invasion and Endothelial Recruitment by Highly Metastatic Melanoma Cells.

a-b. Matrigel invasion (**a**) and endothelial recruitment (**b**) capacity displayed by MeWo-LM2 cells transduced with a control hairpin or a miR-Zip hairpin targeting each miR-199a-3p, miR-199a-5p, or miR-1908. n ≥ 4. **c-d.** A375-LM3 cells expressing a control hairpin or a miR-Zip targeting miR-199a-3p, miR-199a-5p, or miR-1908 were assessed for their matrigel invasion (**c**) and endothelial recruitment (**d**) ability. n ≥ 5. All data are represented as mean ± SEM. Scale bar, 100 μm. *p < 0.05, **p < 0.01, ***p < 0.001. p-values based on unpaired student's t-tests.

The enhanced *in vitro* endothelial recruitment phenotype conferred by miR-199a-3p, miR-199a-5p, and miR-1908 prompted us to investigate whether the three miRNAs also regulate metastatic endothelial recruitment (MER) by melanoma cells *in vivo*. With the help of Colin Buss, we examined blood vessel density within lung metastatic nodules by performing co-immunostaining for human vimentin, which labels human MeWo melanoma cells, and the mouse endothelial cell antigen MECA-32, which labels mouse endothelial cells. We found that individual inhibition of miR-199a-3p, miR-199a-5p, or miR-1908 led to pronounced decreases (an average of 3-fold for miR-199a-3p and miR-199a-5p; 4.7-fold for miR-1908) in blood vessel density within metastatic nodules formed by highly metastatic MeWo-LM2 cells (Figure 2.12a). Conversely, overexpression of each miRNA in poorly metastatic melanoma cells dramatically increased metastatic blood vessel density (Figure 2.12b). Consistent with functional angiogenesis impairment, inhibition of each mature miRNA in highly metastatic melanoma cells suppressed metastatic nodule perfusion, assessed by the rate of dextran perfusion following intravenous injection of biotinylated low-molecular weight dextran (Figure 2.13). Taken together, our findings reveal endogenous miR-199a-3p, miR-199a-5p, and miR-1908 as promoters of melanoma cell invasion, endothelial recruitment, and metastatic angiogenesis.

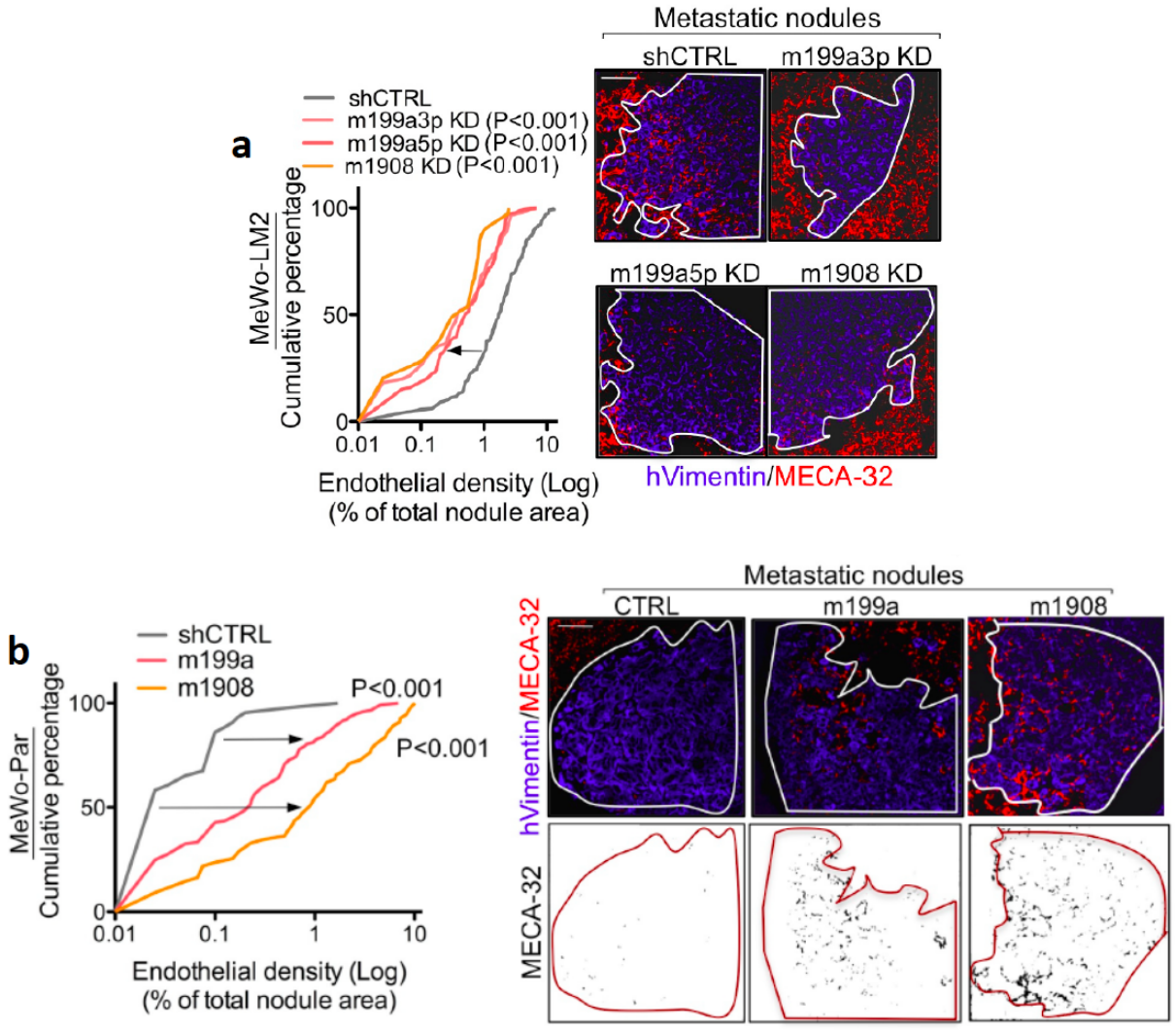

Figure 2.12. Endogenous miR-199a-3p, miR-199a-5p, and miR-1908 Enhance Metastatic Endothelial Recruitment *In Vivo*. a-b. Cumulative percentage plots depicting endothelial cell (marked by MECA-32) density within vimentin-positive lung metastatic nodules formed by MeWo-LM2 cells silenced for miR-199a-3p, miR-199a-5p, miR-1908, or a control (**a**) and MeWo parental cells transduced with a control hairpin or a pre-cursor hairpin giving rise to each miR-199a or miR-1908 (**b**). n ≥ 30 (**a**); n ≥ 43 (**b**). Scale bar, 100 μm. p-values were obtained through Kolmogorov-Smirnov tests.

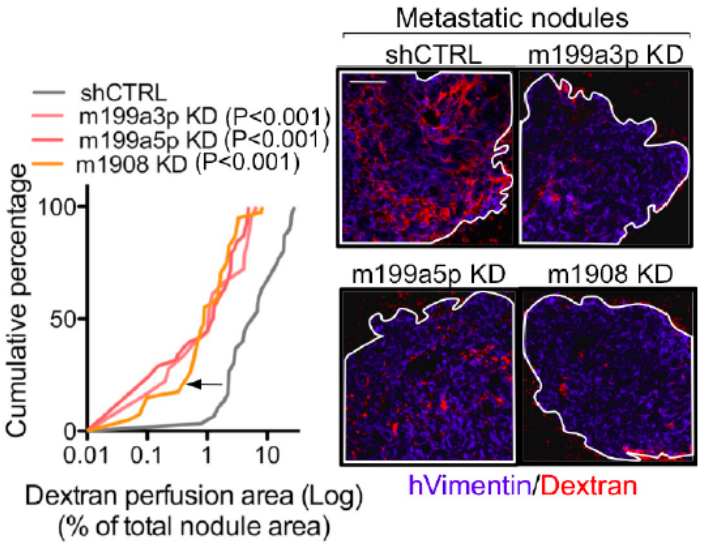

Figure 2.13. Endogenous miR-199a-3p, miR-199a-5p, and miR-1908 Enhance Angiogenic Metastatic Perfusion. Cumulative percentage plots depicting the extent of dextran perfusion, expressed as the dextran-positive area out of the total nodule area, within metastatic lung nodules formed by MeWo-LM2 cells expressing a control miR-Zip or a miR-Zip targeting each mature miR-199a-3p, miR-199a-5p, or miR-1908. Low-molecular weight (10 kDa) biotinylated dextran was introduced into the circulation and allowed to perfuse target tissues for 10 minutes, after which lungs were extracted and dextran perfusion was immunohistochemically visualized. n ≥ 18. Scale bar, 100 μm. p-values based on Kolmogorov-Smirnov tests.

Clinical Association of miR-199a-3p, miR-199a-5p, and miR-1908 Expression with Human Melanoma Metastasis

Given the robust effects exerted by miR-1908, miR-199a-3p, and miR-199a-5p in promoting melanoma metastasis in a mouse model of human cell metastasis, we next wondered whether expression levels of these miRNAs can predict the likelihood of a primary melanoma tumor to metastasize. To this end, Colin Buss and I extracted RNA from 71 primary melanoma skin lesions, resected from patients at the Memorial Sloan-Kettering Cancer Center (MSKCC). We then quantified in a blinded fashion the expression levels of

miR-199a-3p, miR-199a-5p, and miR-1908 in each primary melanoma lesion through stem-loop qRT-PCR analyses. Consistent with our findings of a metastasis-promoting function of these miRNAs in the mouse studies described above, we found that all three miRNAs were significantly upregulated in primary melanoma tumors that had metastasized relative to tumors that had not (Figure 2.13). This clinical finding suggests that induced expression of these miRNAs is an early event in melanoma metastatic dissemination.

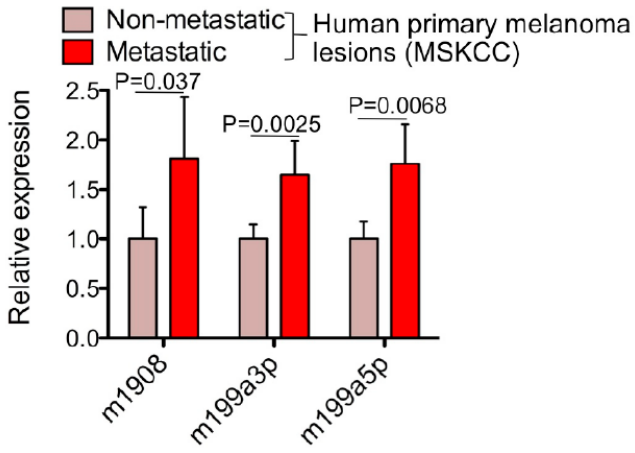

Figure 2.14. miR-199a-3p, miR-199a-5p, and miR-1908 are Upregulated in Primary Melanoma Lesions with Metastatic Propensity. Expression levels of miR-199a-3p, miR-199a-5p, and miR-1908, determined by qRT-PCR, in non-metastatic (n = 38) and metastatic (n = 33) primary melanoma skin lesions from the MSKCC melanoma patient cohort. All data are represented as mean ± SEM. p-values based on unpaired student's t-tests.

Previously documented clinical information regarding each patient's melanoma metastasis outcome allowed us to retrospectively determine the relationship between the levels of these miRNAs in primary melanoma lesions and metastatic relapse outcomes. Importantly, patients whose primary melanoma lesions expressed high (greater than the median for the population) levels of each individual miR-199a-3p, miR-199a-5p, or miR-1908 were more likely to develop distal metastases and exhibited significantly shorter

metastasis-free survival times than patients whose primary melanomas expressed low levels of each of these miRNAs (Figures 2.15a-c). Strikingly, the combined expression levels of the three miRNAs displayed the strongest power in stratifying patients at high risk from those at low risk for metastatic relapse (Figure 2.15d), indicative of prognostic cooperativity among the three miRNAs. These clinical findings suggest utility for these small RNAs as clinical biomarkers in informing melanoma metastatic outcomes. Consistent with our findings in cutaneous melanoma, miR-199a-5p expression was previously shown to also be prognostic of progression outcomes in uveal melanoma patients (Worley et al., 2008).

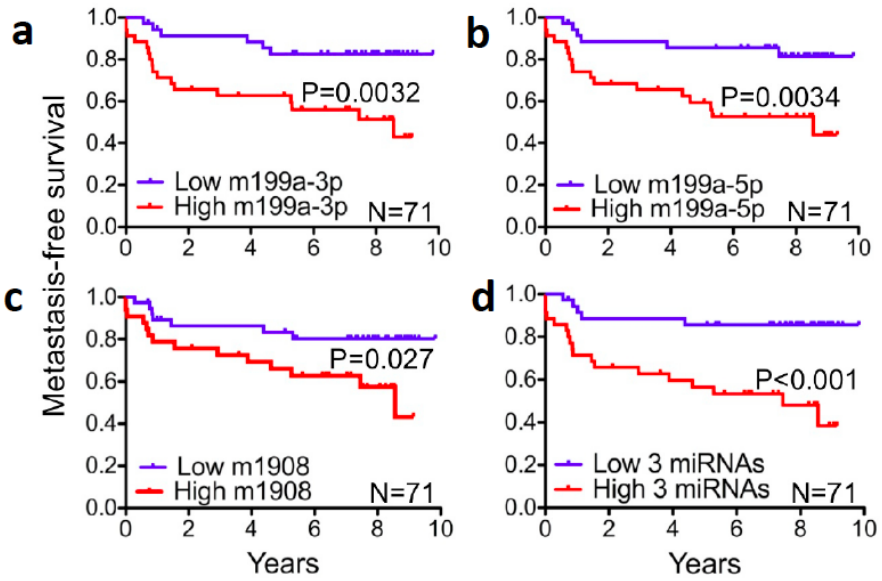

Figure 2.15. Prognostic Capacity of miR-199a-3p, miR-199a-5p, and miR-1908 in Metastatic Melanoma. Kaplan-Meier curves depicting metastasis-free survival times for patients from the MSKCC cohort (n = 71) as a function of the individual miR-199a-3p (**a**), miR-199a-5p (**b**), or miR-1908 (**c**) expression levels or the combined expression levels of the three miRNAs (**d**) determined by qRT-PCR in primary melanoma skin lesions. Patients whose melanoma tumors had miRNA expression levels below or above the median of the population were classified as miRNA negative (low, blue) or miRNA positive (high, red), respectively. p-values based on Mantel-Cox (log-rank) tests.

Therapeutic Targeting of Metastasis-Promoting miRNAs in Melanoma

In light of the current lack of effective treatment options for metastatic melanoma (Garbe et al., 2011) and the clinical relevance of miR-199a-3p, miR-199a-5p, and miR-1908 expression to melanoma metastatic progression, we next wondered whether we could therapeutically target the three miRNAs for the suppression of melanoma metastasis. We utilized locked nucleic acids (LNAs), which are modified oligonucleotides that display high specificity and stability in binding to short single-stranded RNAs (Obad et al., 2011). Given that LNAs have recently shown remarkable efficacy for the *in vivo* silencing of mature miRNAs (Elmén et al., 2008), we examined whether specific LNAs targeting miR-199a-3p, miR-199a-5p, or miR-1908 could have activity in metastasis. To this end, I first transfected highly metastatic MeWo-LM2 cells with individual LNA oligonucleotides antisense to each mature miRNA (miR-199a-3p, miR-199a-5p, or miR-1908) and injected them into mice 48 hours later. Such single LNA pre-treatment of highly metastatic melanoma cells led to a roughly four-fold decrease in metastatic activity (Figure 2.16a). In light of our clinical evidence of cooperativity among these miRNAs, I next tested the impact of concurrently silencing all three miRNAs on metastatic progression. Co-transfection of LNAs against all three miRNAs suppressed metastatic colonization by over seventy-fold, revealing synergy between endogenous miR-199a-3p, miR-199a-5p, and miR-1908 in driving melanoma metastasis (Figure 2.16a). Importantly, inhibition of these miRNAs upon triple LNA transfection did not decrease *in vitro* melanoma cell proliferation (Figure 2.16b), consistent with our previous findings that miR-199a and miR-1908 do not enhance melanoma cell proliferation (Figure 2.8) and indicating that the dramatic metastasis suppression phenotype

upon combinatorial LNA-based miRNA targeting is not secondary to impaired cell proliferation and/or survival, as measured *in vitro*.

Remarkably, we further found that combinatorial LNA-mediated miRNA inhibition robustly inhibited lung colonization by the independent and mutationally diverse SK-Mel-2 (24-fold), WM-266-4 (77-fold), HT-144 (15-fold), A2058 (17-fold), A375-LM3 (3-fold), and SK-Mel-28 (2.5-fold) human melanoma cell lines (Figure 2.17). These findings indicate that combinatorial targeting of the three miRNAs exhibits robust therapeutic potential across a variety of melanotic and amelanotic human melanoma lines representative of *B-Raf*-mutant, *N-Ras*-mutant, and *B-Raf/ N-Ras* wild-type human melanomas.

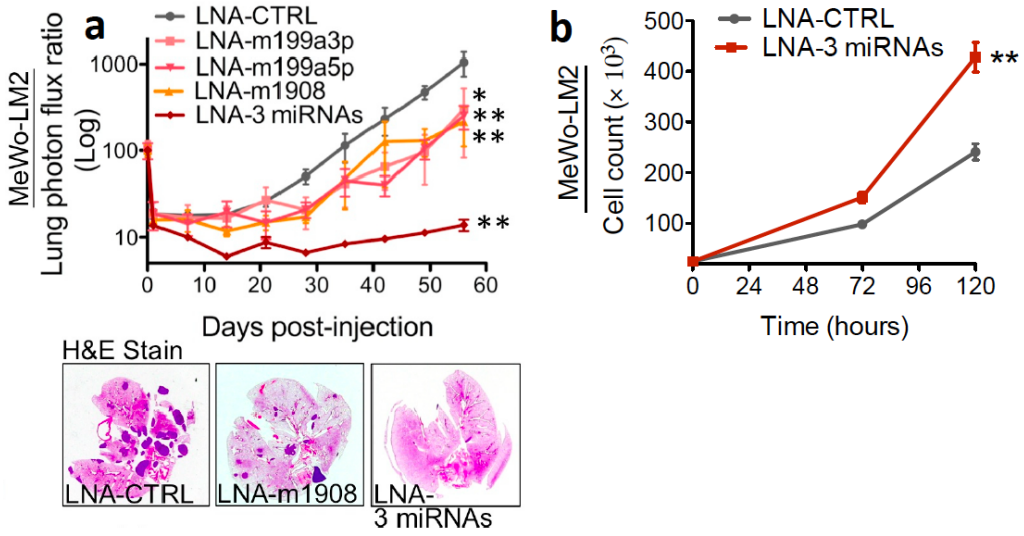

Figure 2.16. LNA-Mediated Silencing of miR-199a-3p, miR-199a-5p, and miR-1908 Cooperatively Suppresses Melanoma Metastasis. a. Lung colonization by 1×10^5 melanoma cells transfected with single LNAs individually targeting miR-199a-3p, miR-199a-5p, or miR-1908, a combination of LNAs targeting all three miRNAs (LNA-3 miRNAs), or a control LNA (LNA-CTRL) 48 hours prior to cell injection. $n \geq 5$. **b.** *In vitro* melanoma cell proliferation was determined by counting the number of live cells at days 0, 3, and 5 post-seeding of 2.5×10^4 MeWo-LM2 cells transfected with LNA-CTRL or LNA-3 miRNAs. $n = 3$. All data are represented as mean ± SEM. *$p < 0.05$, **$p < 0.01$. p-values based on Mann-Whitney's t-tests (**a**) or an unpaired student's t-test (**b**).

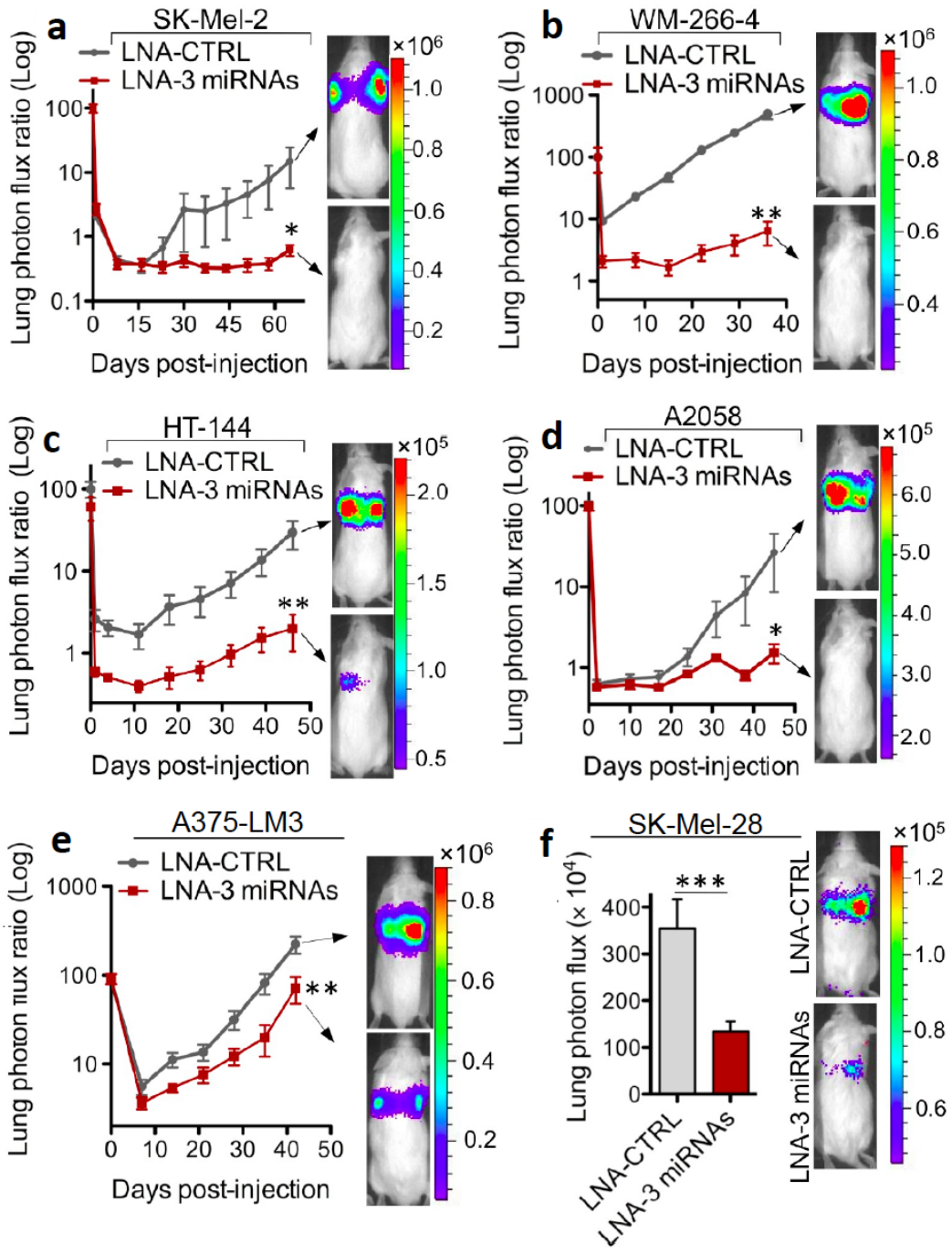

Figure 2.17. Broad Suppression of Melanoma Metastasis by Combinatorial miRNA Targeting. a-f. Following 48-hour pre-treatment with LNA-CTRL or LNA-3 miRNAs, 5 × 10^5 SK-Mel-2 (**a**), WM-266-4 (**b**), HT-144 (**c**), A2058 (**d**), A375-LM3 (**e**), or SK-Mel-28 (**f**) human melanoma cells were intravenously injected into mice and lung colonization was quantified by bioluminescence imaging. All data are represented as mean ± SEM. *p < 0.05, **p < 0.01, ***p<0.001. p-values based on Mann-Whitney's t-tests.

To determine whether the effect of miRNA inhibition is specific to the suppression of lung colonization, we tested the impact of LNA-based miRNA targeting on systemic melanoma metastasis. Consistent with a role of the three miRNAs in promoting multi-organ colonization, intracardiac injection of highly metastatic MeWo-LM2 cells pre-treated with a cocktail of LNAs targeting the three regulatory miRNAs revealed miR-199a-3p, miR-199a-5p, and miR-1908 as endogenous promoters of systemic melanoma metastasis to multiple additional distant organ sites, such as brain and bone (Figure 2.18).

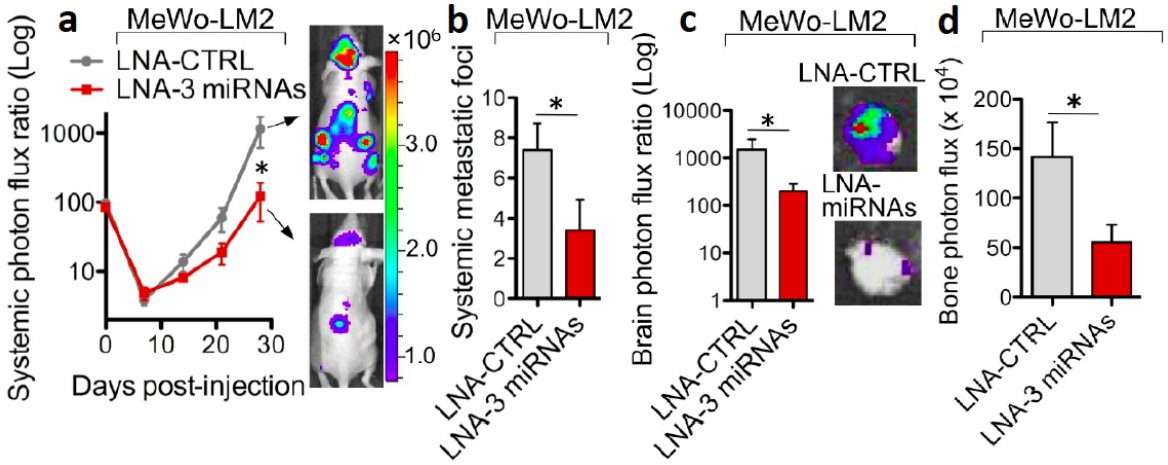

Figure 2.18. LNA-Mediated Combinatorial miRNA Targeting Suppresses Systemic Melanoma Metastasis to Multiple Organs. a-d. 1×10^5 MeWo-LM2 cells transfected with a LNA-CTRL or a cocktail of LNA-3 miRNAs were itnracardially injected into nude mice and systemic multi-organ colonization was assessed by measuring total systemic photon flux (**a**), counting the number of systemic metastatic foci (**b**), and quantifying melanoma cell colonization *ex vivo* in brain (**c**) and bone (**d**) organs by bioluminescence imaging. $n \geq 5$. All data are shown as mean ± SEM. *$p < 0.05$. p-values based on Mann-Whitney's t-tests.

Finally, we examined the therapeutic efficacy of systemically administered LNAs targeting the three miRNAs for the prevention of melanoma metastasis. To this end, I intravenously injected highly metastatic MeWo-LM2 cells into mice and the following day, I

began treating the mice by intravenous administration of a cocktail of LNAs targeting miR-199a-3p, miR-199a-5p, and miR-1908 at a low dose (12.5 mg/kg total) on a bi-weekly basis for four weeks and then once weekly for seven weeks. Notably, such combinatorial LNA treatment reduced lung colonization by greater than 10-fold (Figure 2.19a) without causing any apparent weight loss (Figure 2.19b.) Importantly, I found that these therapeutic LNAs downregulated the levels of the three miRNAs in human melanoma cells dissociated from lung metastatic nodules (Figure 2.20a) and they also silenced the mouse homologs of these miRNAs in mouse cardiac and liver tissues (Figures 2.20b-c), consistent with efficient *in vivo* miRNA targeting and LNA delivery into both melanoma tumors and stromal tissues.

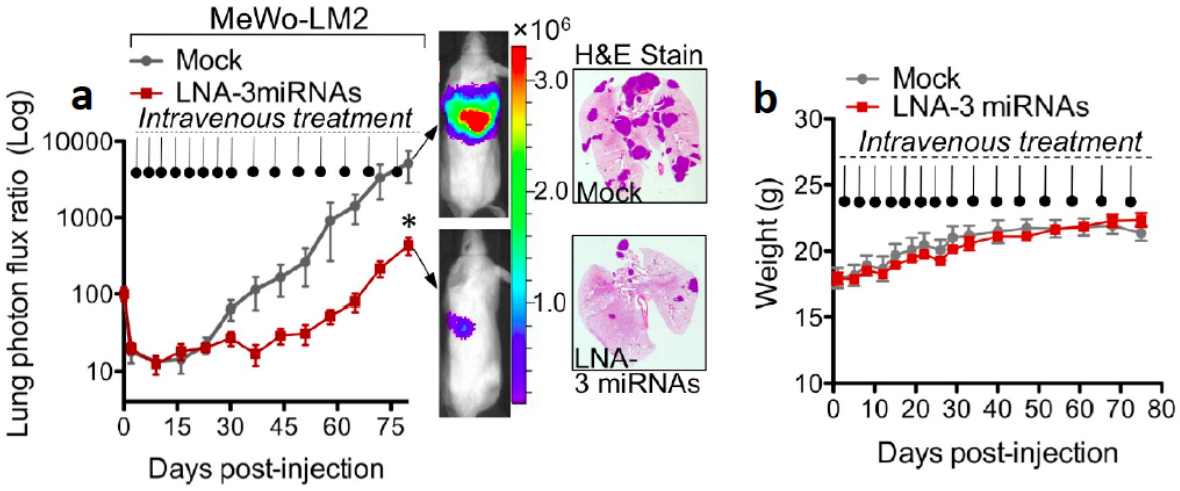

Figure 2.19. Therapeutic Delivery of LNAs Targeting miR-199a-3p, miR-199a-5p, and miR-1908 Suppresses Melanoma Metastasis. a. Following intravenous injection of 4×10^4 MeWo-LM2 cells, the next day mice were intravenously administered a cocktail of *in vivo*-optimized LNAs targeting miR-199a-3p, miR-199a-5p, and miR-1908 (12.5 mg/kg total dose) or a mock PBS control treatment, as indicated. Lung colonization was quantified by weekly bioluminescence imaging, and representative H&E-stained lungs extracted at the final day of imaging (d80) are shown. $n \geq 5$. **b.** Weight of mice intravenously treated with a cocktail of LNAs targeting the three miRNAs or a mock PBS control. All data are represented as mean ± SEM. *$p < 0.05$. p-value based on an unpaired student's t-test.

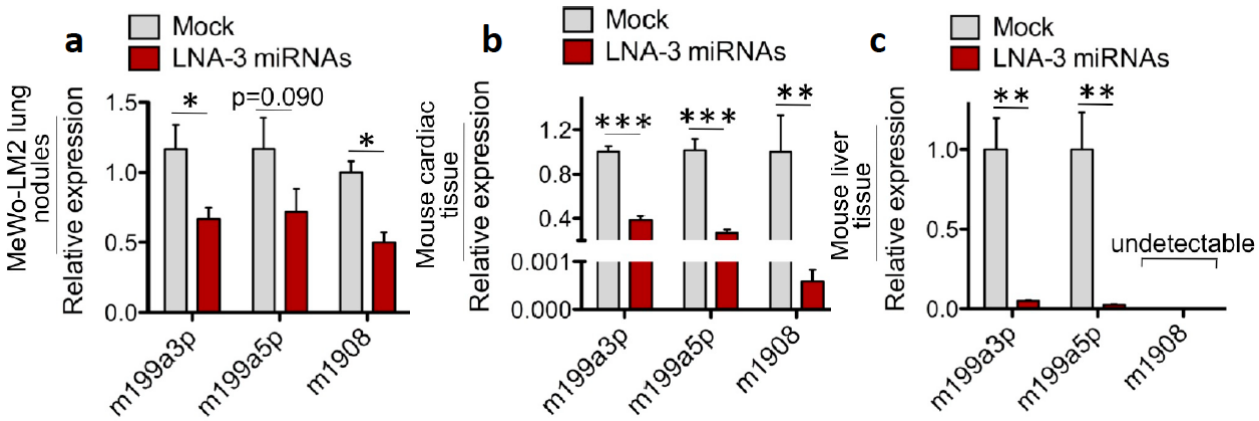

Figure 2.20. Efficiency of Therapeutically Delivered LNAs in Silencing Target miRNAs *In Vivo*. a. Expression levels of miR-199a-3p, miR-199a-5p, and miR-1908, determined by qRT-PCR, in MeWo-LM2 cells dissociated from lung metastatic nodules of mice intravenously treated with LNA-3 miRNAs (12.5 mg/kg) or a mock control. $n \geq 3$. **b**-**c**. Total RNA was extracted from cardiac (**b**) and liver (**c**) tissues harvested from mice treated with LNA-3 miRNAs (12.5 mg/kg) or a mock control, and the expression levels of miR-199a-3p, miR-199a-5p, and miR-1908 in heart (**b**) and liver (**c**) mouse tissues were analyzed by qRT-PCR. $n \geq 3$. All data are represented as mean ± SEM. $^*p < 0.05$, $^{**}p < 0.01$, $^{***}p < 0.001$. p-values based on unpaired student's t-tests.

Mechanisms Upstream of miRNA Overexpression in Melanoma Metastasis

Deregulated Transcriptional Control of miR-199a and miR-1908

In light of the broad upregulation of miR-199a and miR-1908 across multiple melanoma subtypes, we investigated the putative upstream mechanism(s) responsible for the induction of miR-199a-3p, miR-199a-5p, and miR-1908 in metastatic melanoma cells. I first examined whether upregulation of the three miRNAs is due to genomic locus amplification. Contrary to this, the genomic copy number of miR-1908 and miR-199a, which can be transcribed from two independent chromosomal loci encoding miR-199a-1 and miR-199a-2, remained unchanged in the highly metastatic derivatives of two independent melanoma lines (Figure 2.21).

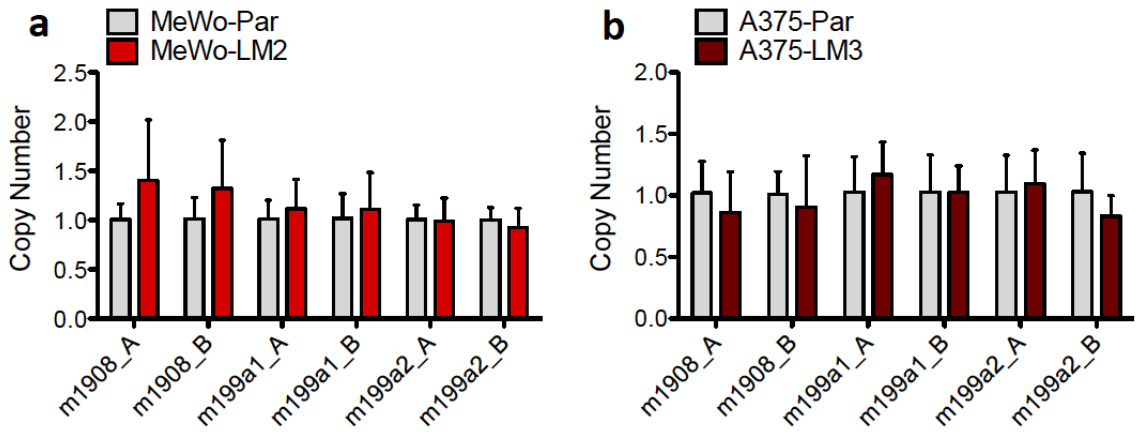

Figure 2.21. Genomic Copy Number of miR-199a-1, miR-199a-2, and miR-1908 in Highly Metastatic Melanoma Cells and Their Respective Parental Populations.
a-b. Genomic copy number levels of miR-199a-1, miR-199a-2, and miR-1908 were assessed by qRT-PCR using genomic DNA extracted from MeWo-parental cells and metastatic MeWo-LM2 derivatives (**a**) or A375-parental cells and A375-LM3 metastatic derivatives (**b**). Two independent primer pair sets (designated as A and B, respectively) were used to amplify genomic regions spanning each miRNA sequence. n = 3. All data are represented as mean ± SEM.

I next tested whether the upregulation of miR-199a and miR-1908 could be attained through transcriptional mechanisms. To this end, I examined the expression levels of the pri-miRNA transcripts, which represent the initial precursor miRNA products generated by RNA Pol II/III-mediated transcription (Figure 1.2). The pri-miRNA transcript levels for each miR-199a (encoded by either the miR-199a-1 and miR-199a-2 paralogs) and miR-1908 were elevated in a subset of highly metastatic melanoma derivatives relative to their parental cells in two independent melanoma lines (Figure 2.22), consistent with enhanced transcriptional regulation as a potential mechanism contributing to the enhanced expression levels of miR-199a and miR-1908 in metastatic melanoma.

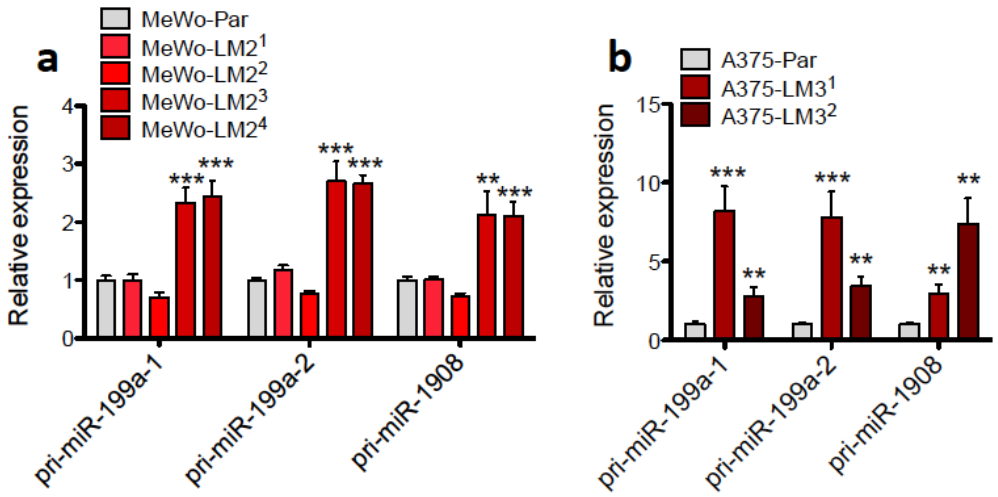

Figure 2.22. Transcriptional Induction of miR-199a and miR-1908 in Highly Metastatic Melanoma Cells. a-b. Expression levels of pri-miR-199a-1, pri-miR-199a-2, and pri-miR-1908, determined by qRT-PCR, in MeWo-LM2 metastatic derivatives and their parental cells (**a**) and A375-LM3 metastatic derivatives and their respective parental population (**b**). n = 3. All data are represented as mean ± SEM. **p < 0.01, ***p < 0.001.

In light of our findings that metastatic cells display enhanced transcriptional activation at the miR-199a-1 and miR-199a-2 paralogous loci, which encode miR-199a-5p and miR-199a-3p, as well as the miR-1908 locus, I next sought to identify transcription factors whose activity may contribute to the augmented expression of these miRNAs in metastatic melanoma cells. In light of the phenotypic commonalities displayed by miR-199a and miR-1908 with respect to their cellular and *in vivo* phenotypes (invasion, endothelial recruitment, and metastasis), we hypothesized that a common transcription factor (TF) might enhance the expression of both miR-199a and miR-1908 in metastatic melanoma cells. Indeed, promoter sequence analysis of the miR-199a-1, miR-199a-2, and miR-1908 loci using the P-Match 1.0 algorithm revealed all three miRNA promoter regions to contain common elements corresponding to the CREB (CREB1) transcription factor binding motif TGACG (Table 2.1, Figure 2.23).

Table 2.1. Conserved Transcription Factor (TF) Binding Sites Present in the Putative Promoter Regions of miR-199a-1, miR-199a-2, and miR-1908

miR-1908 promoter		miR-199a-1 promoter		miR-199a-2 promoter	
TF	Sites	TF	Sites	TF	Sites
CREB	4	BSAP	7	AREB6	2
NF-1	3	CREB	4	CDP	2
AP-4	2	AREB6	3	Evi-1	2
CDP CR3	2	COUP-TF	3	HLF	2
NF-kappaB	2	ARP-1	2	Nkx2-5	2
AREB6	1	YY1	2	NRF-2	2
ARP-1	1	CDP	1	BSAP	1
BSAP	1	E47	1	CDP CR3	1
Elk-1	1	Evi-1	1	COUP-TF	1
Evi-1	1	NF-1	1	CREB	1
HFH-1	1	NF-E2	1	E47	1
Hox-1.3	1	NF-kappaB	1	Elk-1	1
Nkx2-5	1	NRF-2	1	HFH-1	1
NRF-2	1	STATx	1	NF-kappaB	1
RREB-1	1	XFD-3	1	RORalpha	1
ZID	1	ZID	1	XBP-1	1

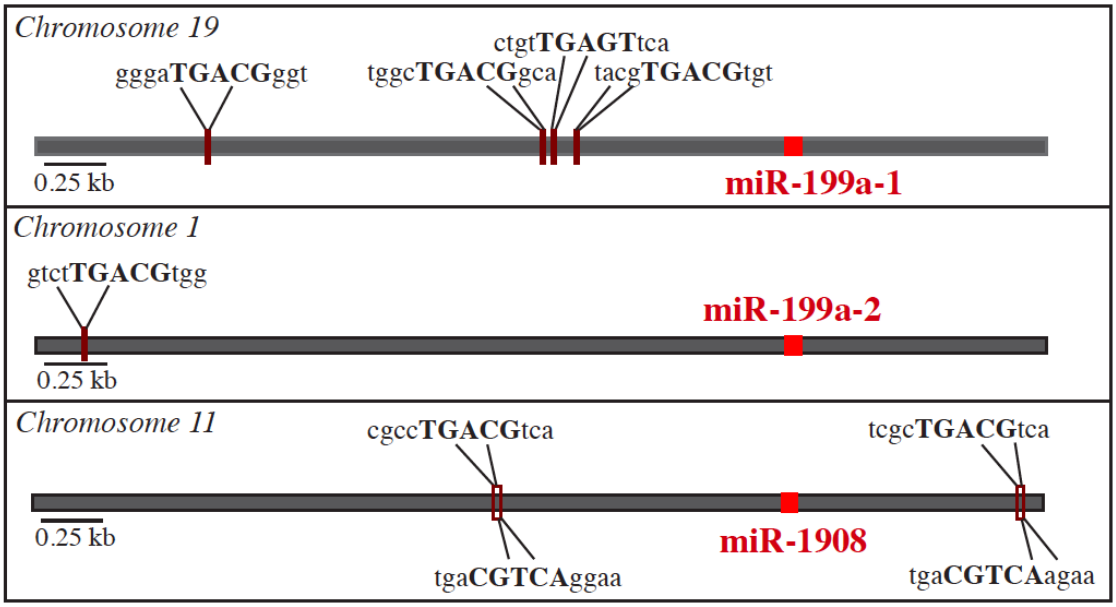

Figure 2.23. Schematic of CREB Binding Motifs Found within the Putative Promoter Regions of miR-199a-1, miR-199a-2, and miR-1908. CREB elements within the putative promoter sequences (3000 bp upstream and 1000 bp downstream) of the miR-199a-1, miR-199a-2, and miR-1908 loci were found and annotated using the P-Match 1.0 algorithm.

We next wondered whether endogenous CREB1 regulates the expression of miR-199a-3p, miR-199a-5p and miR-1908 in metastatic melanoma cells. Indeed, silencing of CREB1 with independent siRNAs in the highly metastatic MeWo-LM2 and A375-LM3 derivatives significantly reduced the expression levels of all three mature miRNAs as well as their corresponding pri-miRNA transcripts (Figure 2.24). Importantly, I further found that the levels of active (phosphorylated) CREB1 (phospho-CREB1) were upregulaed in melanoma metastatic derivatives relative to their parental cells (Figure 2.25), suggesting that enhanced CREB1 activity might account for the elevated transcriptional activation of miR-199a and miR-1908 in metastatic melanoma cells. Consistent with this, the levels of *CREB1* were upregulated in clinical melanoma metastases samples relative to primary melanoma lesions from a previously published array-based melanoma dataset (Haqq et al., 2005) (Figure 2.26).

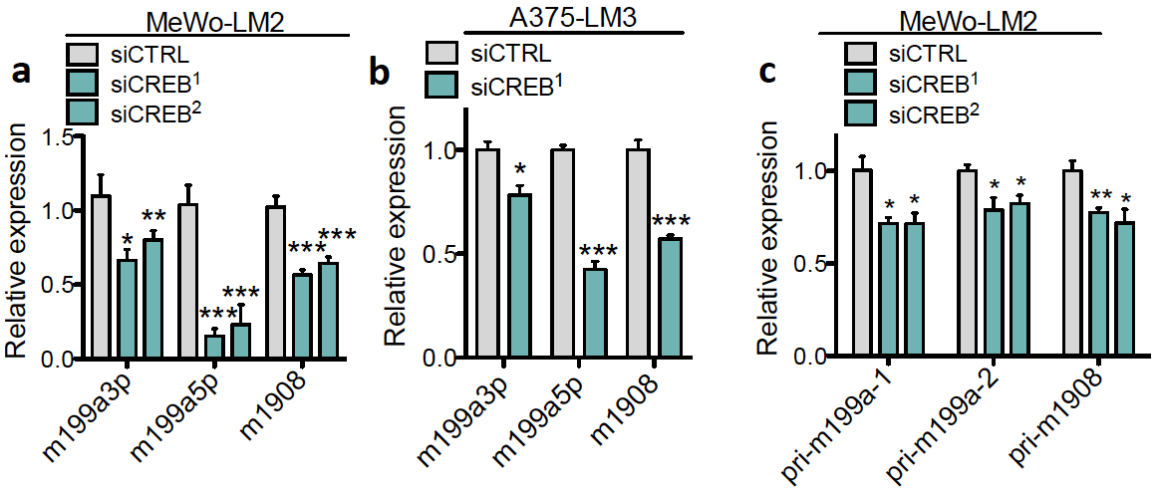

Figure 2.24. Endogenous CREB1 Promotes miR-199a-3p, miR-199a-5p, and miR-1908 Expression in Metastatic Melanoma Cells a-b. Expression levels of mature miR-199a-3p, miR-199a-5p, and miR-1908, determined by qRT-PCR, in highly metastatic MeWo-LM2 (**a**) and A375-LM3 (**b**) melanoma cells in response to siRNA-mediated CREB silencing. n = 3. **c.** Expression levels of pri-miR-199a-1, pri-miR-199a-2 and pri-miR-1908 in response to siRNA-based CREB1 knockdown in MeWo-LM2 cell. n ≥ 3. All data are represented as mean ± SEM. *p < 0.05, **p < 0.01, ***p < 0.001. p-values based on student's t-tests.

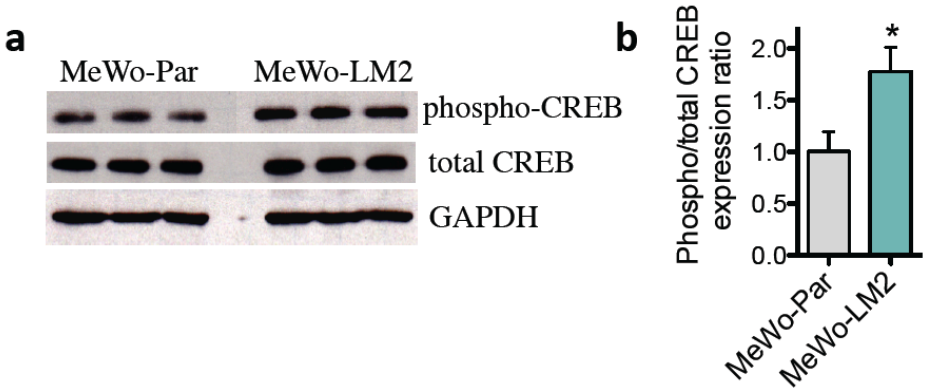

Figure 2.25. CREB Activation is Enhanced in Metastatic Melanoma Cells. a. Expression levels of total CREB and phosphorylated ("phospho") CREB, assessed by western blotting, in highly metastatic MeWo-LM2 cells and their parental MeWo cells. **b.** Quantification of active CREB levels, determined as the ratio of phosphorylated over total CREB, in MeWo-Par and MeWo-LM2 cells. n = 3. Total CREB levels were normalized to GAPDH. Data are represented as mean ± SEM. *p < 0.05. p-value based on a Student's t-test.

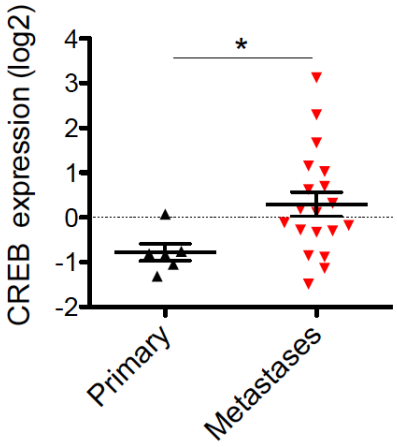

Figure 2.26. *CREB* Expression is Upregulated in Clinical Melanoma Metastases. Expression levels of *CREB* mRNA transcript, determined based on a previously published array-based clinical melanoma dataset (Haqq et al., 2005), in primary melanoma lesions and distal melanoma metastases. n = 6 (primary), 19 (metastases). Data are shown as mean ± SEM. * p <0.05. p-value based on an unpaired student's t-test.

Further chromatin immunoprecipitation (ChIP) analyses are needed to determine whether CREB directly interacts with the promoter regions of miR-199a and miR-1908. Consistent with the promoting effects of miR-199a and miR-1908 on melanoma cell invasion and metastasis, multiple previous studies have implicated CREB as a promoter of melanoma invasion and metastasis (Dobroff et al., 2009; Aucoin et al., 2004). Future work will examine whether CREB also regulates the miRNA-dependent non-cell-autonomous phenotype of endothelial recruitment. Additionally, it will be of interest to determine how much of the downstream effects of CREB activation on melanoma invasion and metastasis are potentially mediated through the transcriptional induction of the metastasis-promoting miRNAs, miR-199a-3p, miR-199a-5p, and miR-1908.

Deregulated Post-Transcriptional Processing of miR-199a and miR-1908

Interestingly, in two of the MeWo metastatic derivatives, the pri-miRNAs levels were either unchanged or actually downregulated (Figure 2.22). Furthermore, even in cases where the pri-miRNAs were elevated, the fold-changes in pri-miR-199a were more than an order of magnitude lower compared to the fold-changes in mature miR-199a-3p and miR-199a-5p (Figure 2.2), suggestive of processing deregulation of the abovementioned miRNAs in metastatic melanoma cells. Consistent with this, the ratios of mature- to pri-miR-199a-3p and mature- to pri-miR-199a-5p expression levels were elevated across all MeWo and A375 metastatic derivatives, albeit to different extents (Figure 2.27). In comparison, the ratio of mature- to pri-miR-1908 was modestly increased in the MeWo-LM2 metastatic derivatives (Figure 2.27c), but actually decreased in the A375-LM3 metastatic derivatives (Figure 2.27e), suggesting that miR-1908 overexpression in the A375-LM3 system might be primarily attained through transcriptional regulation and/or additional mechanisms.

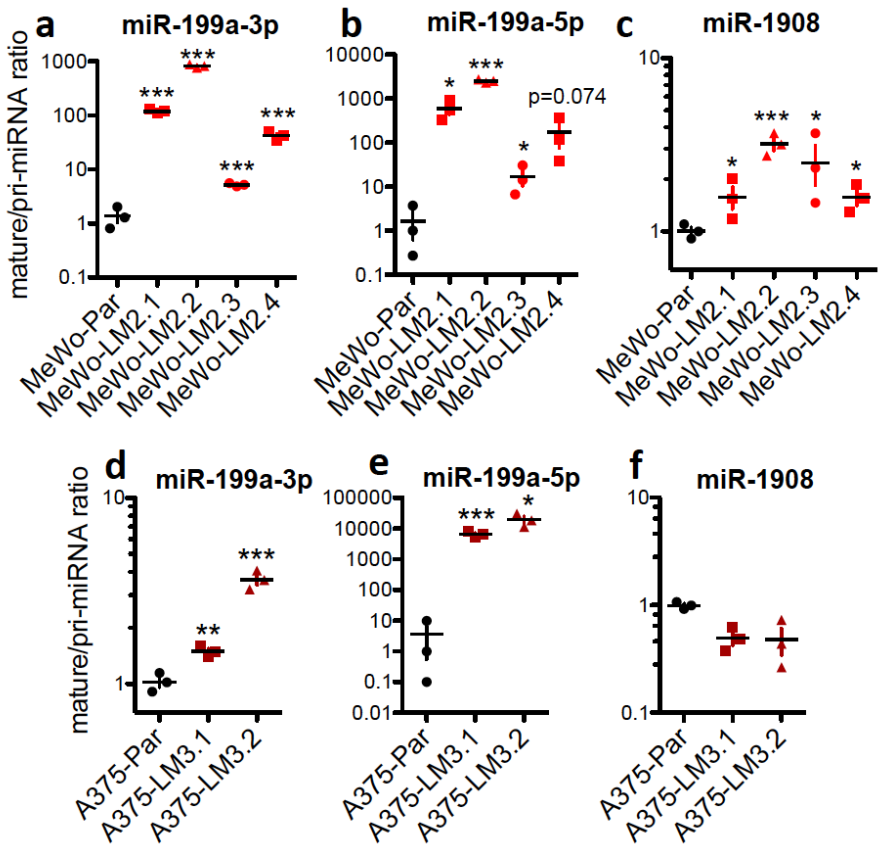

Figure 2.27. Deregulated Processing of miR-199a-3p, miR-199a-5p, and miR-1908 in Metastatic Melanoma Cells. a-f. Ratios of mature to pri-miRNA expression levels for miR-199a-3p, miR-199a-5p, and miR-1908 across multiple MeWo-LM2 (**a-c**) and A375-LM3 (**d-f**) metastatic derivatives relative to their respective parental cell lines. n = 3. *p < 0.05, **p < 0.01, ***p < 0.001. p-values based on unpaired student's t-tests.

Taken together, these findings suggest that both enhanced CREB-dependent transcription and miRNA processing alterations might contribute to miRNA induction across the various metastatic derivatives we have examined. Future work will characterize the precise molecular effectors in the miRNA processing pathway that may be deregulated in metastatic melanoma cells and ultimately investigate the extent to which transcription and miRNA processing interplay in determining miR-199a and miR-1908 overexpression in metastatic melanoma.

Summary of Findings from Chapter II

In this chapter, I describe an *in vivo*-selection based approach for the generation of highly metastatic melanoma variants from poorly metastatic parental populations isolated from the tumors of different melanoma patients. By performing small RNA profiling coupled with qRT-PCR validation, we identified four miRNAs to be robustly upregulated across multiple metastatic melanoma derivatives. Functional loss- and gain-of-function experiments revealed three of these miRNAs (miR-199a-3p, miR-199a-5p, and miR-1908) to act as endogenous promoters of melanoma metastasis. Importantly, we also found that the expression levels of these miRNAs correlated with the metastatic outcomes of melanoma patients. Consistent with clinical relevance of these miRNAs to melanoma metastatic progression, the three miRNAs exhibited robust therapeutic potential across a multitude of human melanoma lines, as evidenced by strong metastasis suppression upon combinatorial LNA-based miRNA silencing. Mechanistically, we found that the three miRNAs promoted metastasis by increasing melanoma invasion and also enhancing the ability of melanoma cells to recruit endothelial cells both *in vitro* and *in vivo*. Finally, our preliminary analyses have suggested that these miRNAs become upregulated in metastatic melanoma cells through a combination of transcriptional and post-transcriptional mechanisms. I have identified CREB as a putative transcription factor that might contribute to the transcriptional induction of the three miRNAs in metastatic melanoma. Further work is necessary to determine the molecular alteration(s) responsible for the altered processing of these metastasis-promoting miRNAs.

CHAPTER III: IDENTIFICATION, FUNCTIONAL CHARACTERIZATION, AND CLINICAL VALIDATION OF MIRNA EFFECTOR GENES IN MELANOMA METASTASIS

Systematic Identification of Genes Repressed by miR-199a-3p, miR-199a-5p, and miR-1908 in Melanoma

Mammalian miRNAs act predominantly by destabilizing target mRNA transcripts, which is reflected by reduced transcript levels and ultimately lower protein expression of target mRNAs (Guo et al., 2010). In order to identify the direct molecular effectors of miR-199a-3p, miR-199a-5p, and miR-1908, we employed a systematic and unbiased approach involving whole-genome transcriptomic profiling followed by qRT-PCR validation, reporter assays, and mutagenesis studies. Given our findings that miR-1908, miR-199a-3p, and miR-199a-5p mediate the same sets of *in vitro* and *in vivo* phenotypes (Chapter II) and the fact that miR-199a-5p and miR-199a-3p arise from the same precursor hairpin, we hypothesized that the pro-metastatic phenotypes of these miRNAs may be mediated through the convergent silencing of common target genes. To identify putative target mRNA transcripts whose expression is repressed by each miRNA, we performed transcriptomic profiling of melanoma cells in the context of both loss- and gain-of-function for each miRNA (Figure 3.1). This analysis, followed by qRT-PCR validation (performed with the help of Dowoon Huh, a former technician), revealed a set of two genes, the metabolic factor *ApoE* and the heat-shock protein *DNAJA4*, that were repressed by both exogenous and endogenous miR-199a and miR-1908 and that were also present at lower levels in the highly metastatic LM2 derivatives, which display endogenously higher levels of the three miRNAs (Figure 3.2).

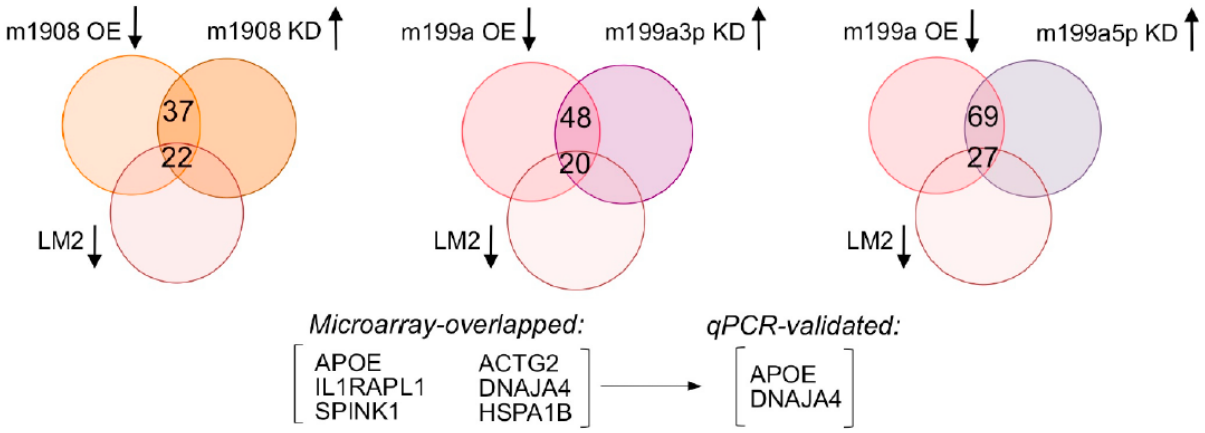

Figure 3.1. Identification of Putative miRNA Target Genes. Venn diagrams depicting the integrative experimental approach used to identify putative target genes common to miR-199a-3p, miR-199a-5p, and miR-1908. Genes downregulated by greater than 1.5-fold based on transcriptomic profiling expression data upon overexpression of each miRNA were overlapped with transcripts upregulated by greater than 1.5-fold upon miRNA silencing as well as with transcripts, for which the expression levels were downregulated by more than 1.5-fold in the highly metastatic MeWo-LM2 derivatives relative to the parental line.

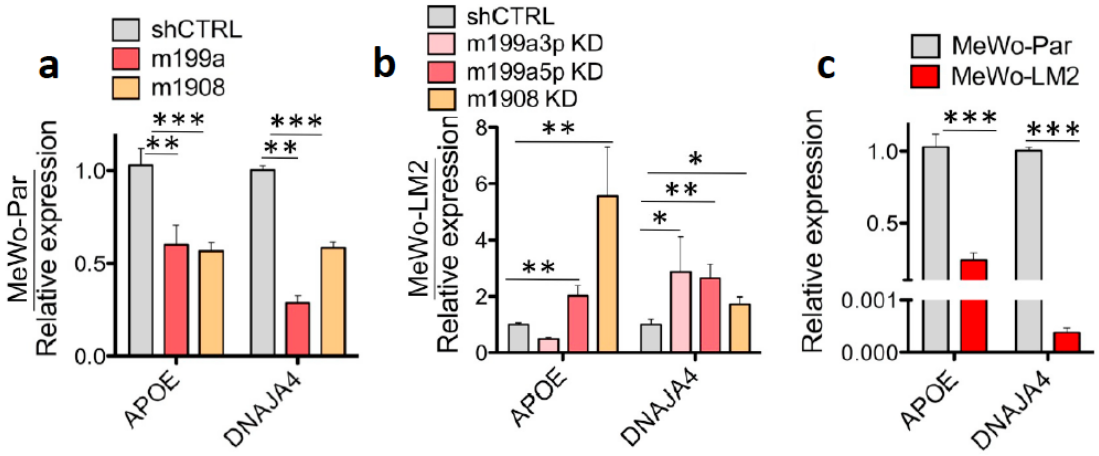

Figure 3.2. miR-199a and miR-1908 Repress the Expression of *ApoE* and *DNAJA4*. **a-c**. Expression levels of *ApoE* and *DNAJA4* in parental MeWo cells overexpressing the precursors for each miR-199a and miR-1908 (**a**), MeWo-LM2 cells with silenced expression of each miR-199a-3p, miR-199a-5p, and miR-1908 (**b**), and MeWo-LM2 relative to MeWo-parental cells (**c**). n = 3. Error bars = SEM. *p < 0.05, **p < 0.01, ***p < 0.001. p-values based on unpaired student's t-tests.

Validation of ApoE and DNAJA4 as Direct Target Genes of miR-199a and miR-1908

I next performed heterologous luciferase reporter assays to determine whether *ApoE* and *DNAJA4* are directly targeted by miR-1908, miR-199a-3p, and miR-199a-5p. In these experiments, the 3' untranslated regions (UTR) of each *ApoE* and *DNAJA4* were cloned downstream of luciferase's stop codon, whereas each gene's coding sequence (CDS) was chimerically fused to luciferase to mimic the active translation of the CDS during potential miRNA targeting, and the constructs were then transfected into human melanoma MeWo cells. The effects of each miRNA on the expression of its putative target constructs were examined by measuring luciferase activity as a read-out. I found that each miR-199a and miR-1908 individually repressed the expression levels of the 3' untranslated regions (UTR) and coding sequences (CDS) of both *ApoE* and *DNAJA4* (Figure 3.3a). Importantly, mutating the miRNA complementary sequences on each target abrogated the miRNA-mediated regulation, consistent with direct miRNA targeting of *ApoE* and *DNAJA4* (Figure 3.3a). Additionally, in a direct test of endogenous miRNA targeting, silencing of the mature forms of each miR-199a-3p, miR-199a-5p, or miR-1908 in metastatic LM2 cells led to an enhanced target-driven luciferase activity (Figure 3.3b) that was abrogated upon mutating the miRNA target sites (Figure 3.3c). These experiments revealed *ApoE* to be directly targeted by miR-1908 and miR-199a-5p and *DNAJA4* to be directly targeted by all three miRNAs (Figure 3.4a). Notably, luciferase activity driven off the CDSs and 3'UTRs of each gene was reduced in highly metastatic MeWo-LM2 cells (Figure 3.4b), which exhibit higher endogenous levels of the three regulatory miRNAs, relative to the parental MeWo cells. Collectively, these findings establish *ApoE* and *DNAJA4* as common target genes of miR-199a and miR-1908.

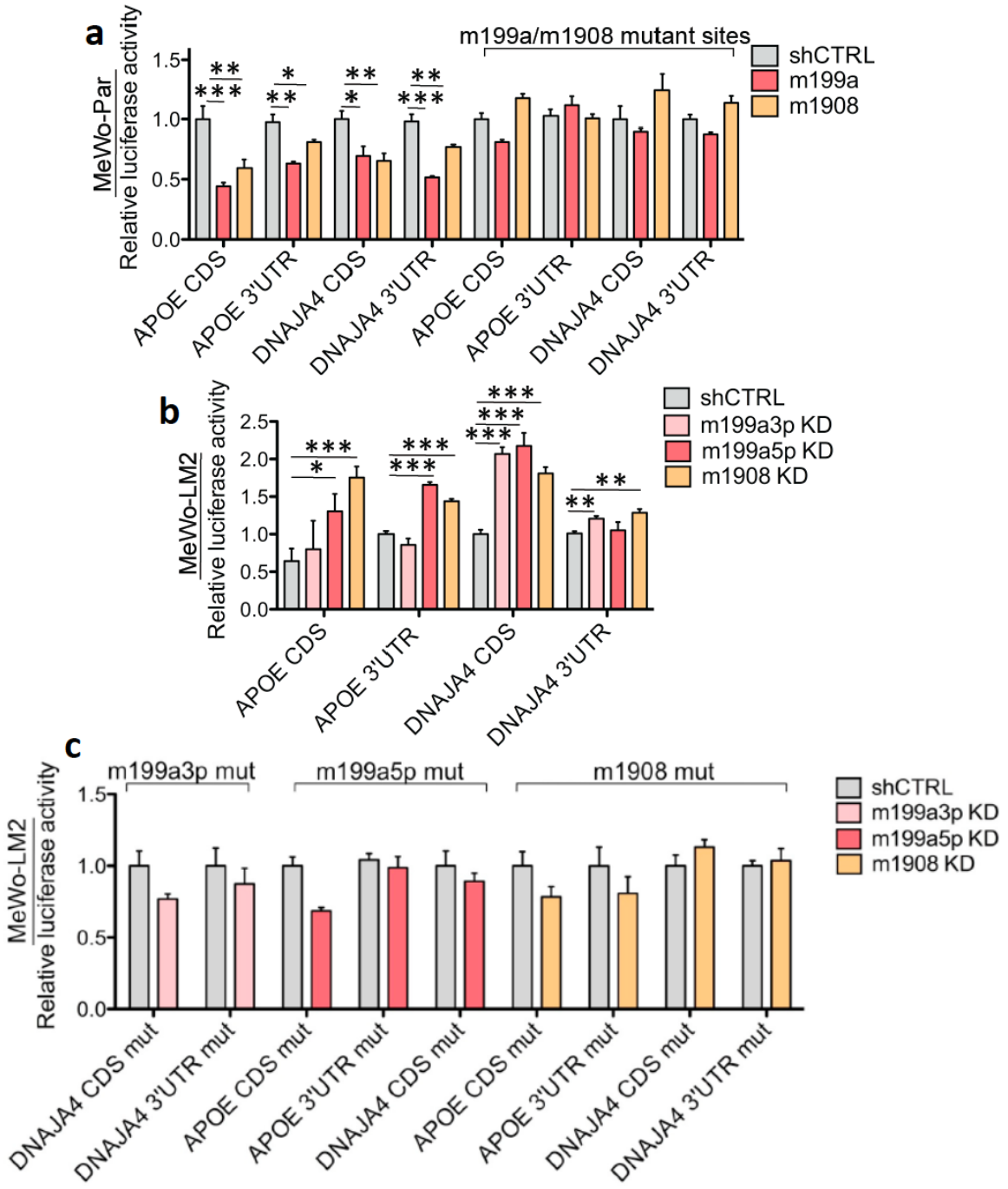

Figure 3.3. miR-199a and miR-1908 Directly Target *ApoE* and *DNAJA4*.

a-c. Heterologous reporter assays measuring luciferase activity driven off *ApoE*'s and *DNAJA4*'s wild-type or miRNA target site mutant 3'UTRs and CDSs in MeWo parental cells overexpressing miR-199a or miR-1908 (**a**) and MeWo-LM2 cells with silenced expression of miR-199a-3p, miR-199a-5p, miR-1908, or a control (**b-c**). n ≥ 3. All data are shown as mean ± SEM. *p < 0.05, **p < 0.01, ***p < 0.001. p-values based on unpaired student's t-tests.

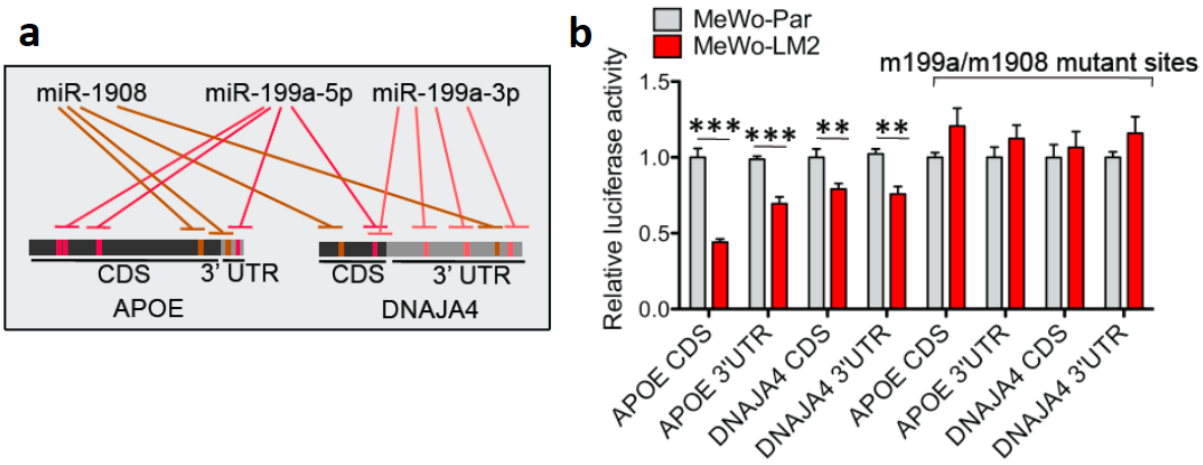

Figure 3.4. Convergent Targeting of *ApoE* and *DNAJA4* by miR-199a-3p, miR-199a-5p, and miR-1908. a. Experimentally derived model showing the convergent targeting of the CDSs and 3'UTRs of *ApoE* and *DNAJA4* by the three metastasis-promoting miRNAs. **b.** Heterologous reporter assay measuring the luciferase activity driven off the wild-type and miRNA target site mutant CDSs and 3'UTRs of each *ApoE* and *DNAJA4* in MeWo parental and MeWo-LM2 cells. All data are represented as mean ± SEM. $n \geq 3$. $^{**}p < 0.01$, $^{***}p < 0.001$. p-values based on unpaired student's t-tests.

We next wished to determine the robustness of the regulation exerted by the three miRNAs on the expression of *ApoE* and *DNAJA4* by examining the relationship between the expression levels of the three miRNAs and their target genes across a collection of parental and metastatic melanoma lines, which display varied levels of these miRNA (Figure 2.2). Consistent with direct targeting of *ApoE* and *DNAJA4* by endogenous miR-199a and miR-1908, we found a significant anti-correlation between the endogenous levels of each *ApoE* and *DNAJA4* and the aggregate (combined) expression of the three miRNAs (Figure 3.5).

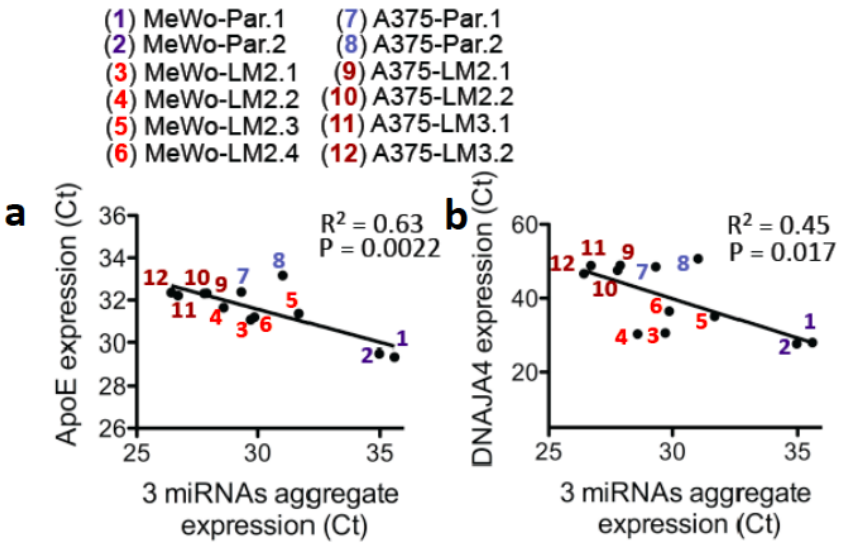

Figure 3.5. Anti-Correlation between the Aggregate Expression of miR-199a-3p/miR-199a-5p/miR-1908 and Their Target Genes. a-b. Linear regression analyses of the correlation between the combined expression of the three miRNAs (determined as the average of the individual miRNA expression values) and the expression levels of *ApoE* (**a**) or *DNAJA4* (**b**) across multiple MeWo and A375 metastatic derivatives and their respective parental lines. n = 12. R^2 values and corresponding p-values were calculated based on the Pearson correlation coefficient for each dataset.

Functional Validation of ApoE and DNAJA4 as Suppressors of Melanoma Progression Phenotypes

Given our findings that the three miRNAs convergently repress *ApoE* and *DNAJA4* expression, we next sought to determine whether these two genes mediate the miRNA-dependent effects on melanoma progression phenotypes—invasion and endothelial recruitment. I found that silencing each gene using independent shRNAs in parental MeWo melanoma cells, which express relatively high *ApoE* and *DNAJA4* levels, led to an increase in invasion and endothelial recruitment (Figure 3.6). These findings are consistent with endogenous *ApoE* and *DNAJA4* acting as suppressors of these *in vitro* melanoma progression phenotypes.

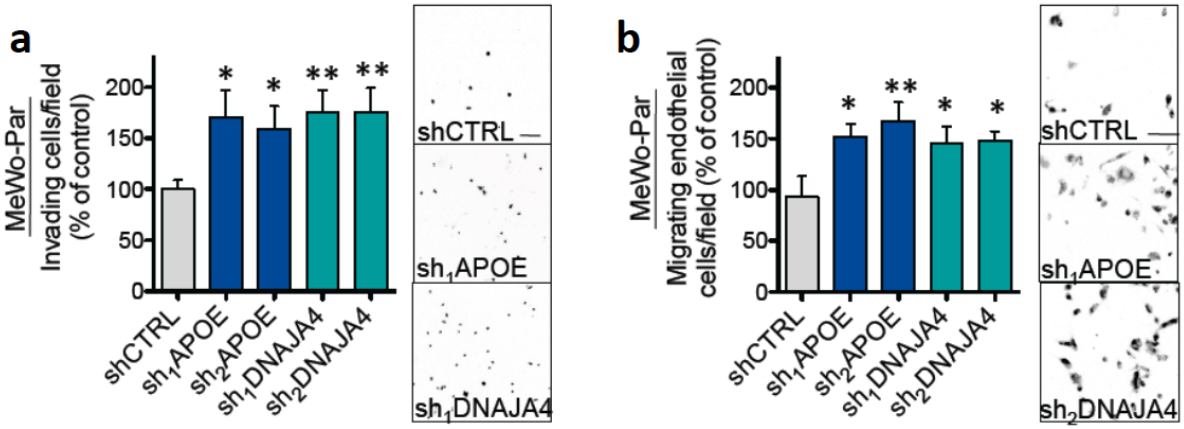

Figure 3.6. Suppression of Melanoma Invasion and Endothelial Recruitment by *ApoE* and *DNAJA4*. a-b. Trans-well matrigel invasion (**a**) and endothelial recruitment (**b**) by parental MeWo cells expressing a short hairpin (shRNA) targeting *ApoE*, *DNAJA4*, or a control sequence (shCTRL). Data are shown as mean ± SEM. Scale bar, 100 μm. $n \geq 4$. $^{*}p < 0.05$, $^{**}p < 0.01$. p-values based on unpaired student's t-tests.

We next wondered whether *ApoE* and *DNAJA4* epistatically interact with each miRNA in conferring the miRNA-dependent effects on melanoma progression phenotypes. To that end, we tested whether the suppression of melanoma phenotypes conferred upon miRNA inhibition is due to the de-repression and resulting elevated expression of *ApoE* or *DNAJA4* in the absence of each miRNA. Consistent with endogenous epistatic miRNA/target gene interactions, depletion of either *ApoE* or *DNAJA4* in the setting of miRNA inhibition significantly occluded the suppression of invasion and endothelial recruitment seen upon silencing of each miRNA (Figures 3.7a-b) and fully rescued the suppression of metastatic colonization resulting from miRNA inhibition (Figures 3.7c-e). Notably, endogenous *ApoE* and *DNAJA4* were also found to suppress metastatic endothelial recruitment *in vivo,* as metastatic nodules formed by highly metastatic melanoma cells with silenced expression of either *ApoE* or *DNAJA4* in the context of miRNA inhibition exhibited enhanced endothelial cell content (Figure 3.8).

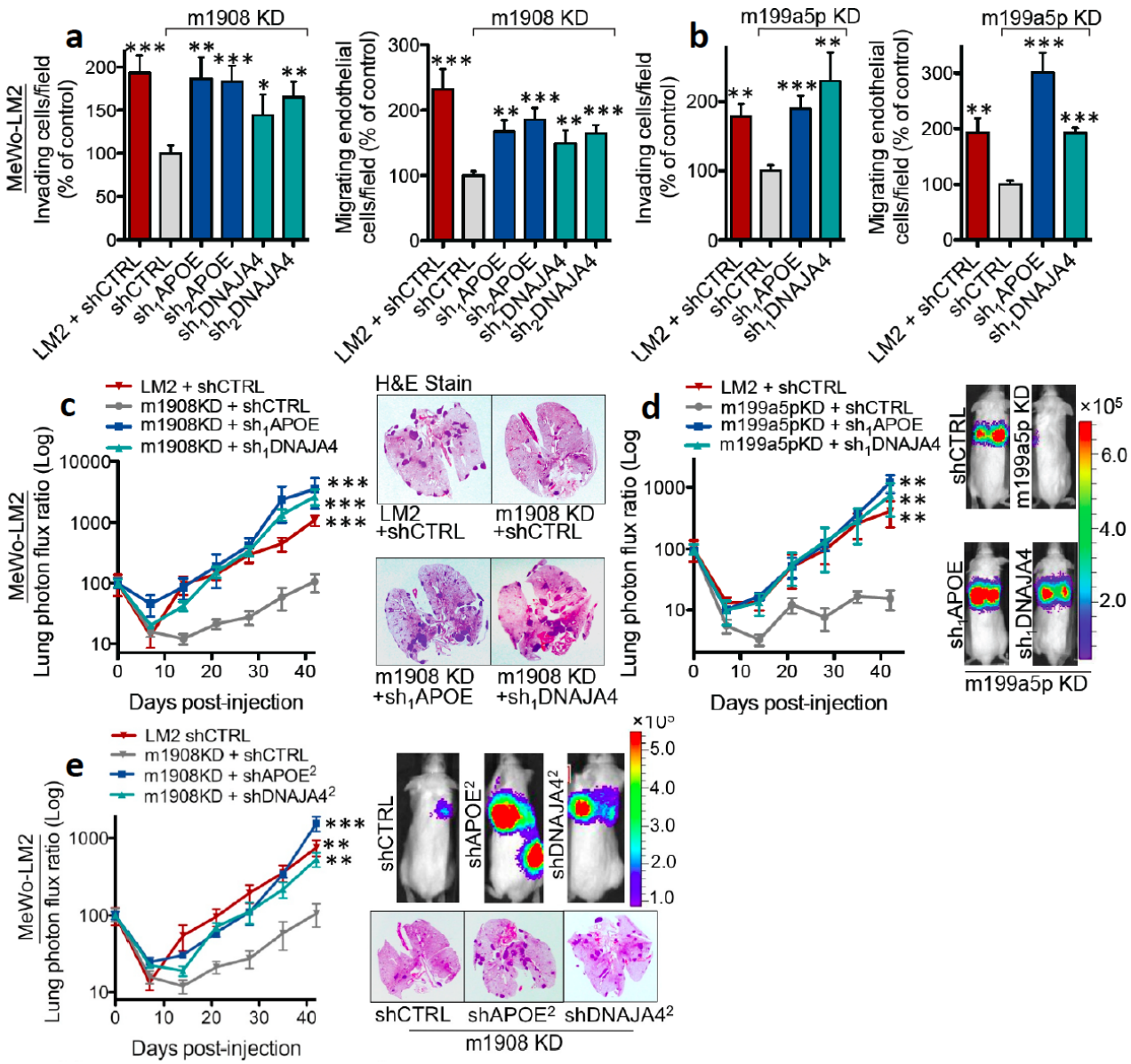

Figure 3.7. Endogenous Epistatic Interactions between miR-199a/miR-1908 and *ApoE* and *DNAJA4*. a-b. Cell invasion and endothelial recruitment by MeWo-LM2 cells transduced with shRNAs targeting *ApoE*, *DNAJA4*, or a control in the setting of miR-1908 silencing (**a**) or miR-199a-5p silencing (**b**). n ≥ 6. **c-e**. Lung metastasis, quantified by bioluminescence imaging, by 1×10^5 MeWo-LM2 cells with shRNA-mediated knockdown of *ApoE* or *DNAJA4* in the setting of miR-1908 (**c, e**) or miR-199a-5p inhibition. n = 5. All data are plotted as mean ± SEM. *p < 0.05, **p < 0.01, ***p < 0.001. p-values based on an unpaired student's t-tests (**a-b**) or Mann-Whitney's t-tests (**c-e**).

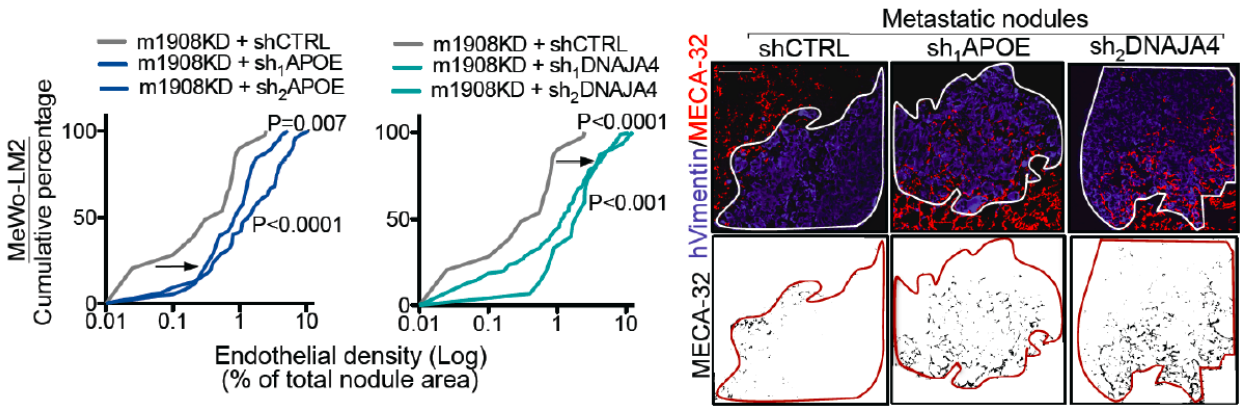

Figure 3.8. Endogenous *ApoE* and *DNAJA4* suppress miRNA-dependent metastatic endothelial recruitment *in vivo*. Cumulative percentage plots depicting the density of endothelial content within metastatic nodules formed by 1×10^5 MeWo-LM2 cells expressing independent shRNAs targeting *ApoE*, *DNAJA4*, or a control sequence in the setting of miR-1908 inhibition. Thresholded images displaying only MECA-32 signal within the demarcated nodule area are shown in the lower panel. $n \geq 19$. Scale bar, 100 μm. p-values based on Kolmogorov-Smirnov tests.

Next, Colin Buss conducted the converse overexpression epistasis experiments where he ectopically expressed the protein-coding regions of *ApoE* or *DNAJA4* in the setting of miRNA overexpression. Given that overexpression of each miR-199a or miR-1908 significantly reduced the levels of both *ApoE* and *DNAJA4*, we wondered whether re-introducing ApoE or DNAJA4 in that setting could occlude the ability of each miRNA to promote melanoma progression phenotypes. Indeed, the miRNA-mediated enhancement effects on cell invasion, endothelial recruitment, and metastatic colonization were inhibited upon concurrent overexpression of ApoE or DNAJA4 (Figure 3.9). Our findings implicate ApoE and DNAJA4 as direct downstream effectors of miRNA-dependent metastatic invasion, colonization, and endothelial recruitment phenotypes in melanoma.

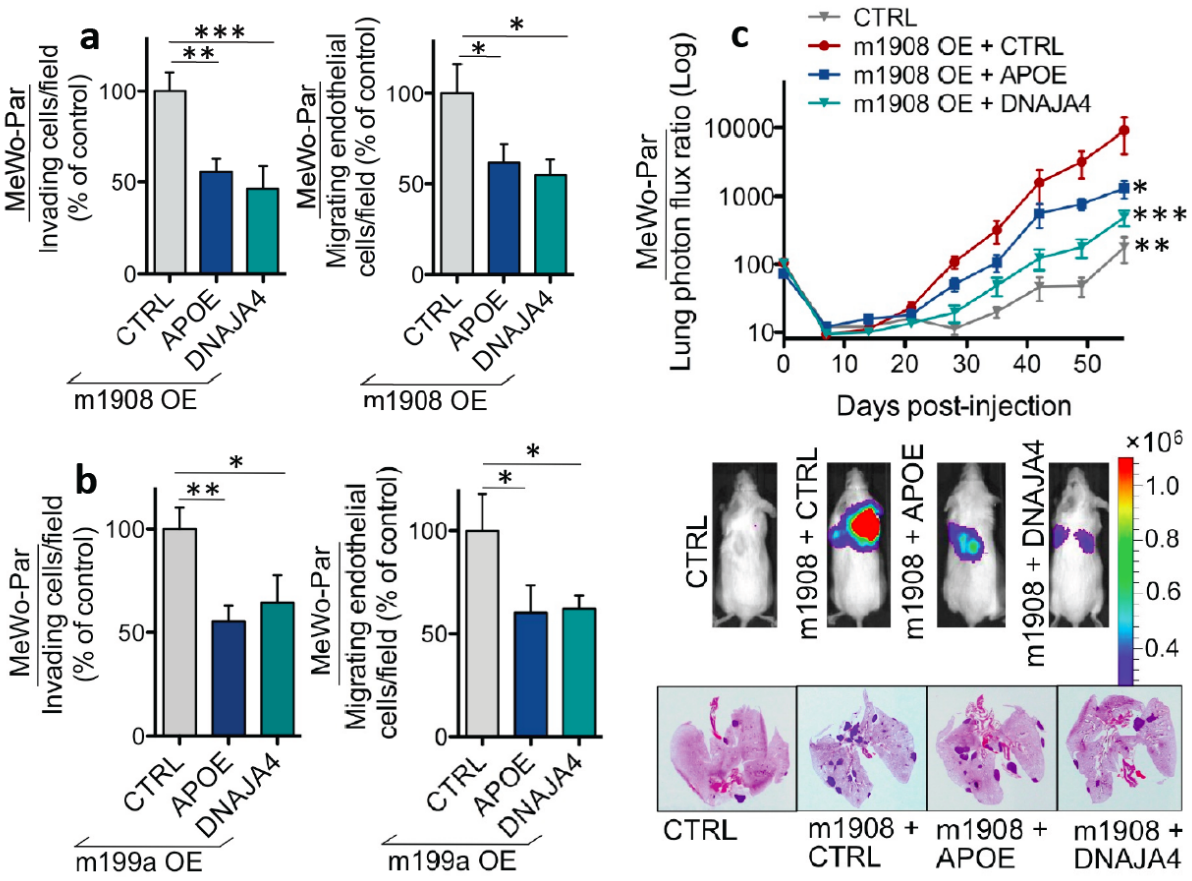

Figure 3.9. miR-199a/miR-1908-Mediated Effects on Melanoma Progression Phenotypes are Occluded by Concurrent Overexpression of ApoE or DNAJA4.

a-b. Matrigel invasion and endothelial recruitment by parental MeWo cells ectopically expressing the protein-coding regions of *ApoE* or *DNAJA4* in the setting of miR-1908 (**a**) or miR-199a (**b**) overexpression. n ≥ 7. **c.** Bioluminescence imaging plot of lung metastasis by 4×10^4 parental MeWo cells overexpressing ApoE or DNAJA4 or expressing a control vector in the setting of miR-1908 overexpression. n ≥ 4. All data are plotted as mean ± SEM. *p < 0.05, **p < 0.01, ***p < 0.001. p-values based on unpaired student's t-tests (**a-b**) and Mann-Whitney's t-test (**c**).

Mechanisms of Action by DNAJA4 in Melanoma

DNAJA4 Positively Regulates ApoE Expression

We next sought to determine the downstream mechanisms by which ApoE and DNAJA4 elicit metastasis suppression. First, we examined how DNAJA4, a poorly characterized heat-shock protein, suppresses melanoma progression phenotypes. Given that DNAJA4 was found to regulate cell-extrinsic endothelial recruitment—a phenotype poised to be mediated by an extracellular factor—we reasoned that the suppressive effects of melanoma cell-expressed DNAJA4 on endothelial migration might arise through the regulation of a downstream molecule secreted by melanoma cells. In light of the known role of ApoE as a secreted factor and our findings that ApoE and DNAJA4 mediate the same set of *in vitro* and *in vivo* melanoma progression phenotypes, we hypothesized that DNAJA4 might positively regulate *ApoE* expression. Consistent with this, I found that depletion of *DNAJA4* in melanoma cells led to a reduction in *ApoE* transcript levels (Figure 3.10a) and also decreased extracellular ApoE protein levels detected in melanoma cell-conditioned media (Figure 3.10b). Additionally, *DNAJA4* knockdown in the setting of miRNA inhibition also inhibited the miRNA-dependent induction in *ApoE* levels (Figure 3.10c). Conversely, overexpression of DNAJA4 robustly upregulated *ApoE* expression (Figure 3.10d). Collectively, these findings provide strong evidence for DNAJA4 acting as a positive regulator of *ApoE* expression in melanoma cells.

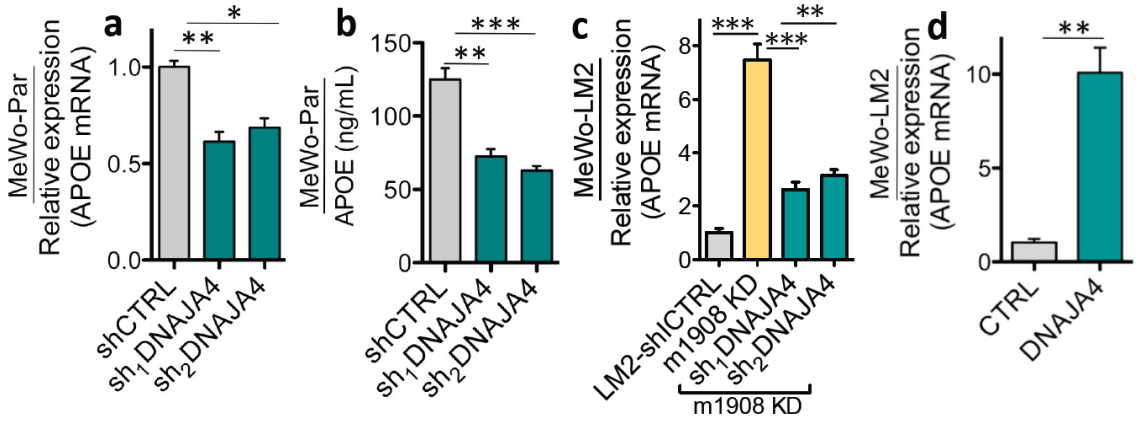

Figure 3.10. Regulation of *ApoE* Expression by DNAJA4. a-c. Effect of shRNA-mediated *DNAJA4* depletion in MeWo cells on *ApoE* transcript levels (**a, c**) and ApoE extracellular protein levels (**b**). n = 3. **d**. *ApoE* transcript levels, determined by qRT-PCR, in response to DNAJA4 overexpression in MeWo-LM2 cells. n = 3. All data are plotted as mean ± SEM. *p < 0.05, **p < 0.01, ***p < 0.001. p-values based on unpaired student's t-tests.

I next examined whether DNAJA4's phenotypic effects on melanoma invasion and endothelia recruitment are mediated through ApoE. Consistent with our previous findings, shRNA-based depletion of *DNAJA4* elevated the invasive capacity of melanoma cells and also increased their ability to recruit endothelial cells (Figures 3.11a-b). We hypothesized that if these effects are mediated through a respective decrease in ApoE expression, then addition of recombinant ApoE protein should prevent the increase in each respective phenotype elicited by *DNAJA4* knockdown. Indeed, addition of ApoE to the cell media decreased both cell invasion and endothelial recruitment in the setting of *DNAJA4* knockdown (Figure 3.11a-b). Conversely, blocking ApoE with a neutralization antibody antagonized the suppression of the two phenotypes seen upon DNAJA4 overexpression in the highly metastatic MeWo-LM2 cells (Figures 3.11c-d). These findings suggest that the effects of DNAJA4 on melanoma progression phenotypes might at least in part be mediated through the downstream induction of *ApoE* expression.

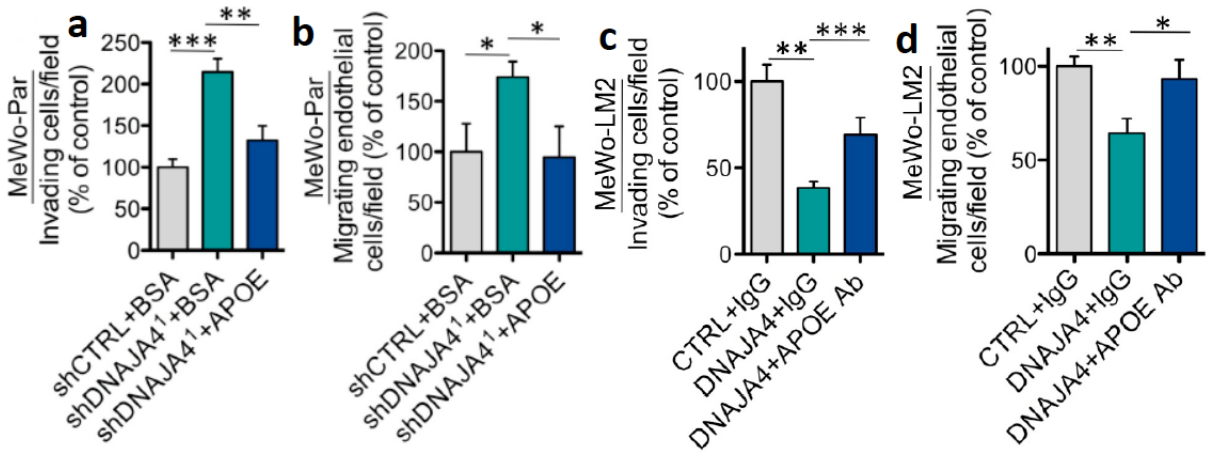

Figure 3.11. DNAJA4-Mediated Metastatic Phenotypes are Dependent on ApoE.

a-d. Matrigel invasion and endothelial recruitment by MeWo parental cells depleted of DNAJA4 and treated with recombinant ApoE or BSA (**a-b**) and MeWo-LM2 cells overexpressing DNAJA4 and treated with an ApoE neutralization antibody or a control IgG antibody (**c-d**). n = 4. All data are plotted as mean ± SEM. *p < 0.05, **p < 0.01, ***p < 0.001. p-values based on unpaired student's t-tests.

Identification of Putative DNAJA4 Binding Partners in Melanoma Cells

Presently, there are three annotated isoforms for the human *DNAJA4* gene (*DNAJA4.1*, *DNAJA4.2*, and *DNAJA4.3*). While the majority of the *DNAJA4* protein-coding region is conserved among the three isoforms, *DNAJA4.1* and *DNAJA4.3* exhibit distinct N-terminal regions of 29 and 17 amino acids in length, respectively, that are absent in *DNAJA4.2* (Figure 3.12a). Interestingly, these isoform-specific structural differences mirror the differential regulation of *DNAJA4.2* versus *DNAJA4.1*/*DNAJA4*.3 transcript levels in highly metastatic melanoma cells. Whereas the expression levels of *DNAJA4.2* remain relatively unchanged, the levels of *DNAJA4.1* and *DNAJA4.3* are more than 25-fold downregulated in the MeWo-LM2 metastatic derivatives relative to their parental cells (Figure 3.12b). Additionally, I further found that the three DNAJA4 isoforms display phenotypic differences in their ability to regulate matrigel invasion by melanoma cells *in*

vitro. Suppression of melanoma cell invasion was observed only in response to DNAJA4.3 overexpression, while DNAJA4.1 or DNAJA4.2 overexpression had no appreciable effects on the ability of melanoma cells to invade through matrigel. These findings suggest that, in addition to differential mRNA expression regulation of the three *DNAJA4* isoforms in highly metastatic melanoma cells, the suppression of melanoma progression phenotypes by DNAJA4 may also be isoform-specific, with DNAJA4.3 being the predominant isoform mediating the invasion-suppressive function of DNAJA4.

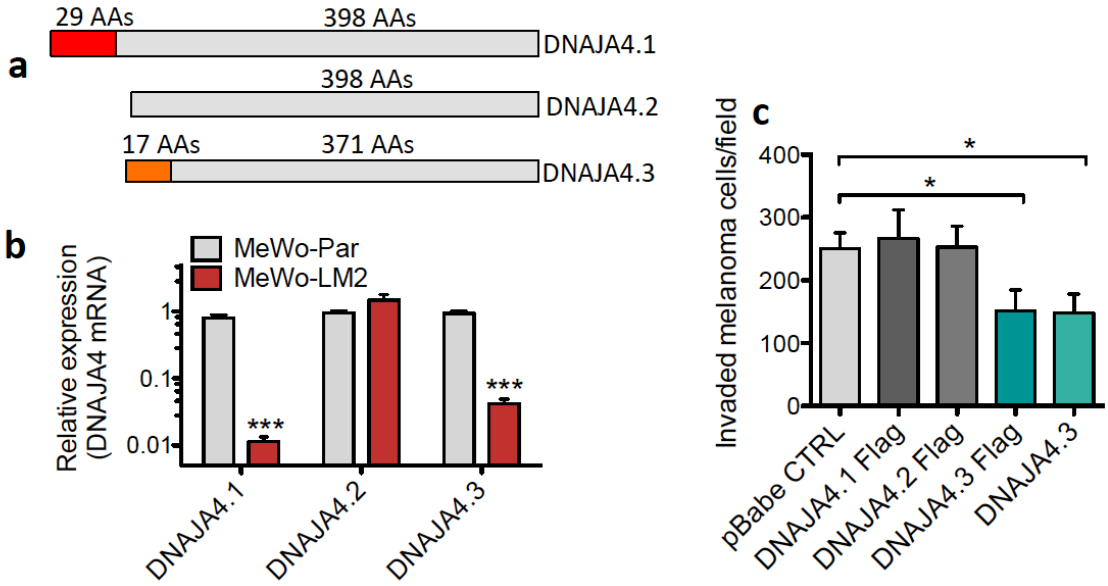

Figure 3.12. Isoform-Specific Regulation of *DNAJA4* Expression in Metastatic Melanoma Cells and Suppression of Melanoma Invasion by DNAJA4.3. a. Schematic representing the CDS structural differences between the three known isoforms of the *DNAJA4* human gene. **b.** Expression levels of *DNAJA4.1*, *DNAJA4.2*, and *DNAJA4.3*, determined by qRT-PCR and using *DNAJA4* isoform-specific primer pairs, in MeWo-LM2 metastatic derivatives and their parental MeWo cells. n = 3. **c.** Matrigel invasion by MeWo parental cells overexpressing the C-terminally flag-tagged coding regions of each *DNAJA4.1*, *DNAJA4.2*, or *DNAJA4.3* or the untagged CDS of *DNAJA4.3*. n ≥ 3. Data are depicted as mean ± SEM. *$p < 0.05$, ***$p < 0.001$. p-values based on unpaired student's t-tests.

We hypothesized that the isoform-specific function of DNAJA4.3 in suppressing melanoma invasion might be due to its distinct N-terminus tail, which might allow for its unique interactions with proteins that regulate melanoma cell invasion. To determine putative proteins specifically bound by DNAJA4.3, but not bound by a DNAJA4 isoform that lacks activity in suppressing cell invasion, I retrovirally expressed C-terminally flagged protein-coding regions encoding full-length DNAJA4.2 or DNAJA4.3 in MeWo parental and MeWo-LM2 melanoma cells. Subsequent flag immunoprecipitation followed by mass spectrometry analyses revealed a large number of common candidate proteins bound by both DNAJA4.2 and DNAJA4.3, as expected from the > 90% homology between the two DNAJA4 isoforms. Interestingly, five proteins (PFKFB3, HNRNPF, PSMD11, FLG, and TPM4) were only detected in the DNAJA4.3-Flag immunoprecipitation product, suggesting that they might represent interacting partners specific to DNAJA4.3 (Figure 3.13).

Further work is needed to i.) validate the DNAJA4.3-specific interactions with each PFKFB3, HNRNPF, PSMD11, FLG, or TPM4, ii.) identify the domain(s) of DNAJA4.3 responsible for these interactions, and iii.) examine whether any of these candidate proteins mediate the DNAJA4-dependent effects on melanoma metastatic phenotypes. Whereas our findings implicate some ApoE dependency of the DNAJA4 effects on melanoma invasion and endothelial recruitment, the incomplete rescue of the DNAJA4-dependent invasion phenotype upon ApoE modulation (Figures 3.11a, c) suggests the existence of additional downstream DNAJA4 mediators independent of ApoE. The functional implications of the interactions of DNAJA4.3 with each of its unique partners for the ApoE-dependent and ApoE-independent effects of DNAJA4 on melanoma suppression will be an interesting question for future work to explore.

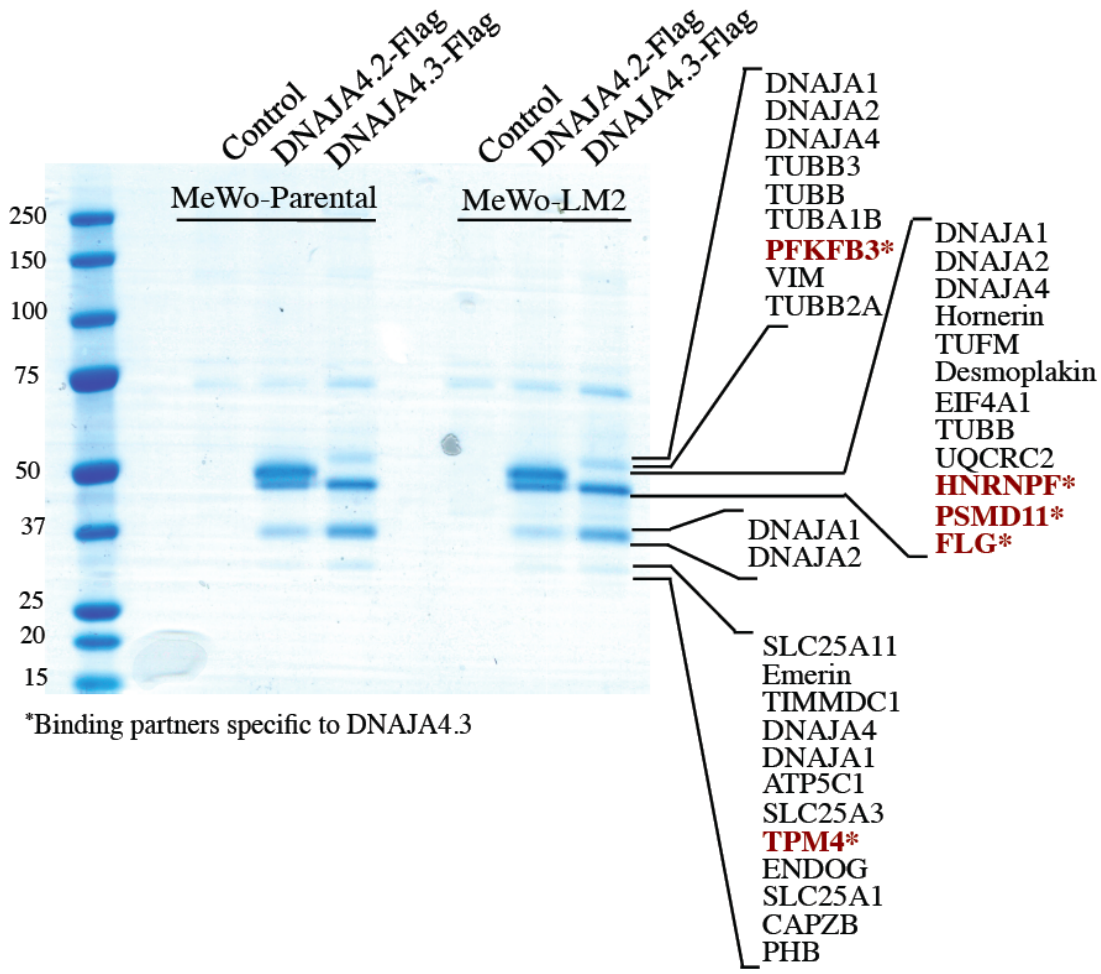

Figure 3.13. Identification of Putative Binding Partners for DNAJA4.2 and DNAJA4.3 in Melanoma Cells. Flag immunoprecipitation (IP) in protein lysates collected from MeWo-parental or MeWo-LM2 cells overexpressing C-terminally flag-tagged DNAJA4.2 or DNAJA4.3 or an empty control vector. The IP product was separated by SDS-PAGE and protein bands of interest (stained in blue) were submitted for mass-spectrometry (MS) analyses. Protein identities shown on the right were ranked based on the number of unique peptides detected by MS for each protein hit. Only proteins for which three or more unique peptides were detected are listed. Candidate interacting protein bound by DNAJA4.3, but not DNAJA4.2, are highlighted in red.

Clinical Association of ApoE and DNAJA4 Expression with Melanoma Progression

In light of the robust metastasis-suppressive roles of ApoE and DNAJA4, we next examined whether the expression levels of these two proteins correlate with human melanoma progression. While DNAJA4 was not a part of a previously published array-based clinical melanoma gene expression dataset (Haqq et al., 2005), we found that the transcript levels of *ApoE* were significantly lower in distal organ metastases relative to primary melanoma and nevi lesions (Figure 3.14a). To further validate the clinical correlation of ApoE expression with melanoma progression in a larger and independent patients' cohort as well as to extend these findings to DNAJA4, we obtained a human melanoma tissue-microarray (TMA) progression panel from the National Institute of Health (NIH). With the help of Colin Buss, we assessed the protein expression of each ApoE and DNAJA4 across the TMA progression set by performing blinded immunohistochemical analyses using a previously validated commercial antibody against ApoE as well as a custom-made antibody that we validated to be specific for isoform 3 of DNAJA4. We found that the protein levels of both ApoE and DNAJA4 were significantly reduced in nodal and distal melanoma metastases relative to primary melanoma skin lesions (Figures 3.14b-c).

Even though the clinical correlation between reduced ApoE and DNAJA4 expression and melanoma progression is consistent with the metastasis-suppressive function exerted by these two proteins, this observation does not address whether ApoE or DNAJA4 at the early stages of melanoma progression could be used as prognostic biomarkers in the clinic to predict which patients will develop metastatic relapse and which ones will remain melanoma-free. Additionally, in light of the significant prognostic capacity displayed by the combined expression of miR-199a-3p, miR-199a-5p, and miR-1908, we hypothesized that their

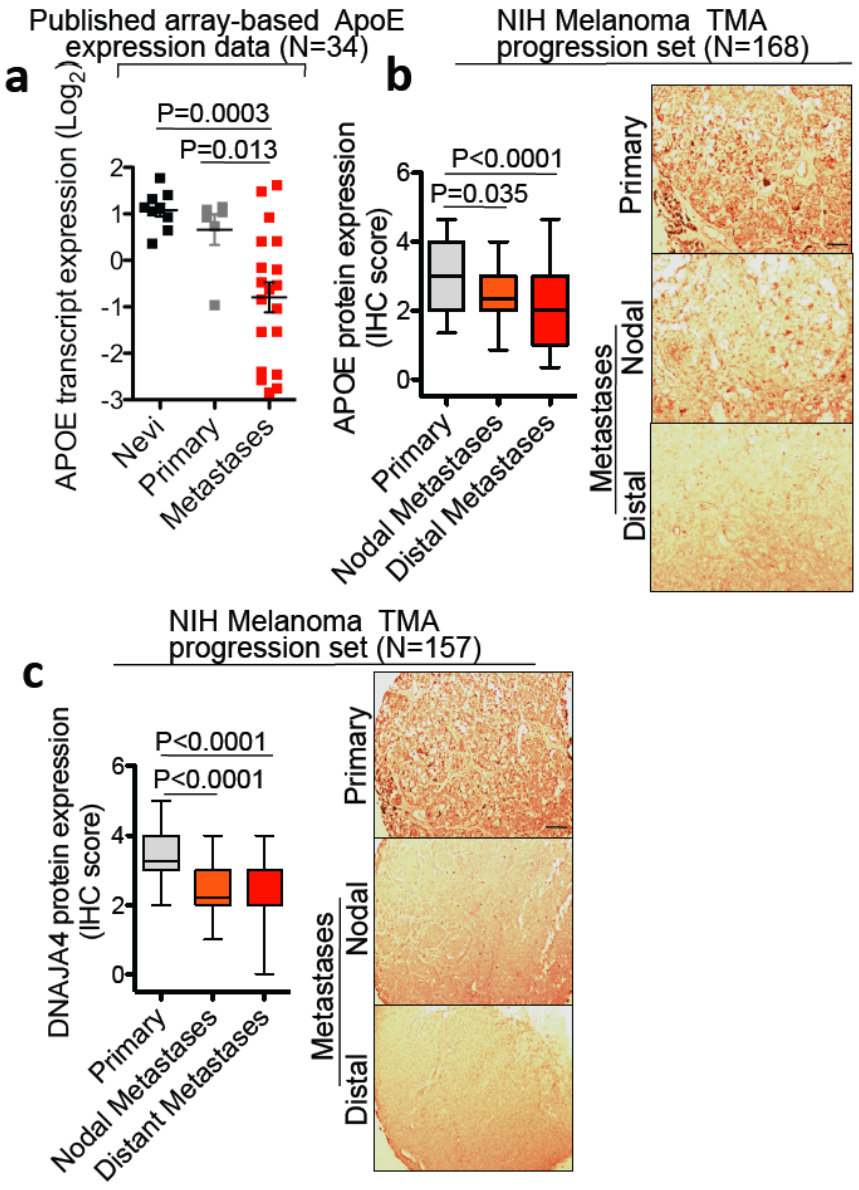

Figure 3.14. Clinical Correlation of ApoE and DNAJA4 Expression with Melanoma Progression Outcomes. a. *ApoE* transcript levels in nevi, primary melanomas, and distal metastases from a previously published array-based melanoma gene expression dataset (Haqq et al., 2005). **b-c.** Box and whisker plots of ApoE (**b**) and DNAJA4 (**c**) protein expression, assessed by double-blinded immunohistochemical analyses, in the NIH melanoma TMA progression sets. Data shown in (**a**) are represented as mean ± SEM. In (**b**) and (**c**): whiskers = 5th-95th population percentile, box extent = 25th-75th percentile. Scale bar, 100 μm. p-values based on unpaired student's t-tests.

convergent targets, *ApoE* and *DNAJA4*, should also exhibit prognostic capacity in metastatic melanoma. To this end, we performed immunohistochemical analyses to assess the protein expression levels of ApoE and DNAJA4 in 71 primary melanoma skin lesions obtained from patients at the MSKCC. We found that primary melanoma tumors with a propensity to metastasize exhibited lower levels on average of each ApoE and DNAJA4 relative to primary melanomas that did not metastasize (Figures 3.15a-b). Importantly, retrospective analyses of the relationship between the expression levels of each ApoE or DNAJA4 and documented history of patients' clinical melanoma outcomes revealed both ApoE and DNAJA4, as single molecular markers, to exhibit significant prognostic power in stratifying patients at high versus low risk of metastatic relapse in that cohort (Figures 3.15c-d).

Finally, we wondered whether the combined expression of ApoE and DNAJA4 might exert additive prognostic effects compared to the expression of each protein alone. Indeed, more than 90% of MSKCC melanoma patients, whose tumors exhibited high levels of both ApoE and DNAJA4, remained melanoma-free at 10 years after diagnosis compared to less than 20% of the patients, whose tumors had low levels of both ApoE and DNAJA4 (Figure 3.16a). Importantly, the prognostic stratification attained by the combined ApoE and DNAJA4 expression signature exceeded that seen with individual ApoE or DNAJA4 expression (Figure 3.15a). Remarkably, adding the three miRNAs' aggregate expression to the combined expression of ApoE and DNAJA4 further improved the signature's prognostic power. Namely, the full fraction (100%) of patients in this cohort, whose tumors exhibited high levels of ApoE and DNAJA4 and low miR-199a-3p/miR-199a-5p/miR-1908 expression, remained melanoma-free at 10 years in comparison to only 13% of patients bearing tumors with low ApoE/DNAJA4 expression and high levels of the three miRNAs (Figure 3.16b).

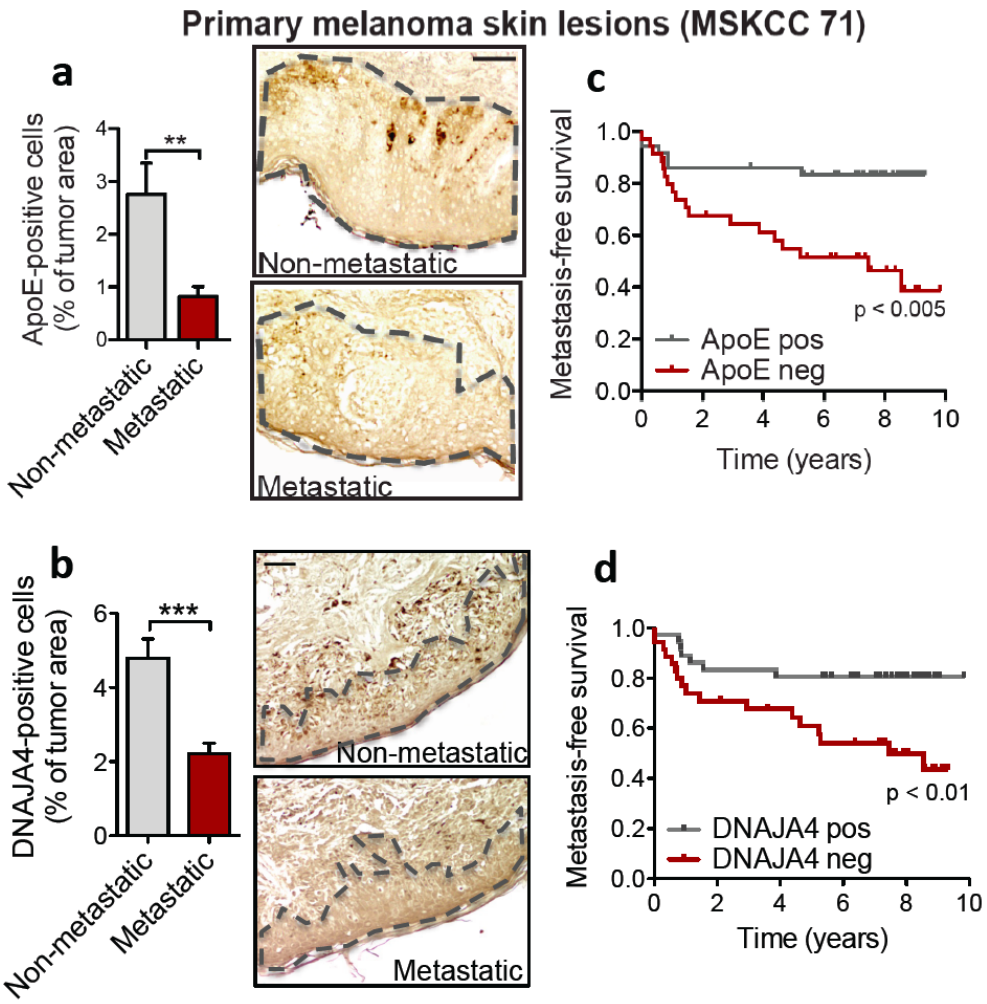

Figure 3.15. Prognostic Capacity of ApoE and DNAJA4 Expression in Metastatic Melanoma. a-b. Protein expression levels, determined by blinded immunohistochemical analyses, for ApoE (**a**) and DNAJA4 (**b**) in non-metastatic (n = 39) and metastatic (n = 34) primary melanoma skin lesions resected from patients at the MSKCC. **c-d.** Kaplan-Meier curves for the MSKCC cohort depicting metastasis-free survival of patients as a function of ApoE (**c**) or DNAJA4 (**d**) protein expression in patients' primary melanoma tumors. Tumors for which ApoE or DNAJA4 expression was above or below the population's median were classified as positive or negative for ApoE or DNAJA4, respectively. Scale bar, 100 μm. For (**a**) and (**b**), data are depicted as mean ± SEM. p-values based on unpaired student's t-tests (**a-b**) or Mantel-Cox (log-rank) tests (**c-d**).

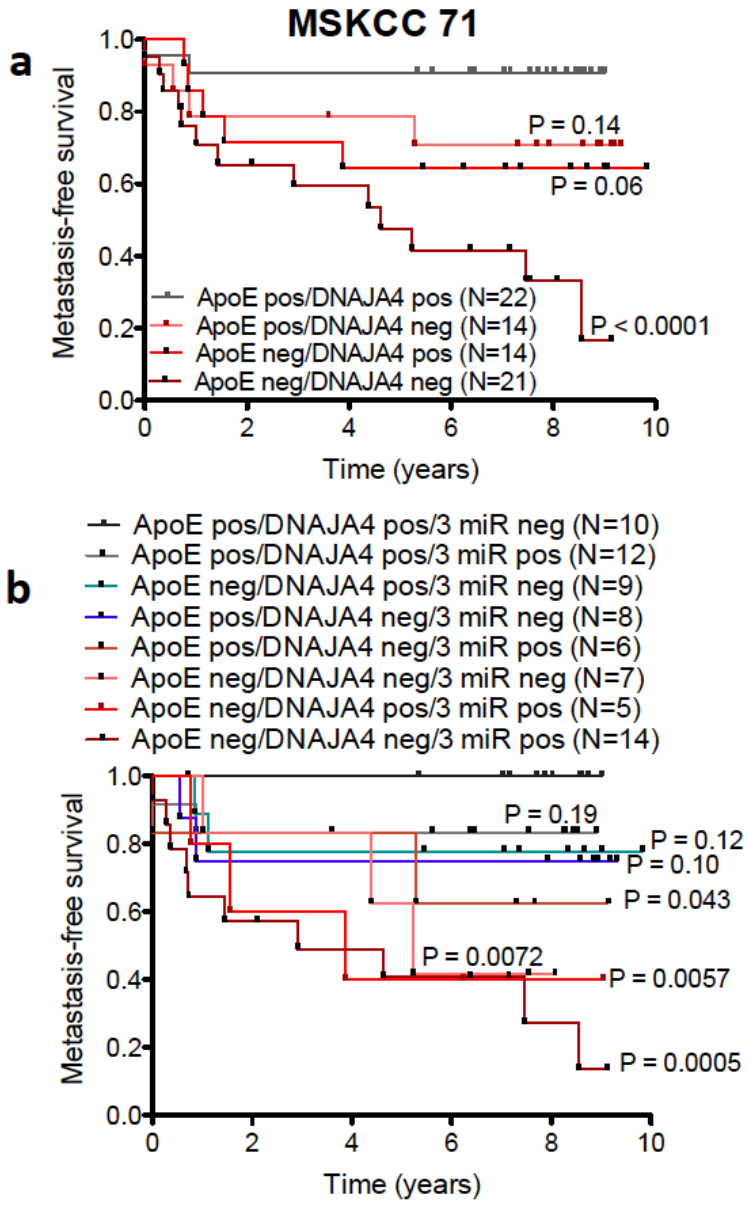

Figure 3.16. Prognostic Capacity of Combined ApoE/DNAJA4 and Combined ApoE/DNAJA4/3 miRNAs Expression Signatures in Melanoma. a-b. Kaplan-Meier curves depicting patients' metastasis-free survival times as a function of the combined expression of ApoE and DNAJA4 (**a**) or ApoE, DNAJA4, and the three miRNAs (miR-199a-3p, miR-199a-5p, and miR-1908) (**b**) in their primary melanoma lesions. Tumors were classified as negative or positive in expression relative to the median expression levels of the population for each marker. p-values were determined using Mantel-Cox tests.

Our findings are consistent with clinical relevance to human melanoma progression and functional robustness of the miR-199a-3p/miR-199a-5p/miR-1908 convergent multi-miRNA regulatory network. Interestingly, the inferior prognostic capacity of ApoE alone compared to that of the combined ApoE and DNAJA4 tumor expression signature suggests that DNAJA4 likely mediates additional downstream targets independent of ApoE that could account for the additive prognostic effects seen. If the full effect of DNAJA4 on melanoma suppression was mediated solely through the induction of ApoE, then one would not expect improved prognostic capacity upon combining ApoE and DNAJA4 expression relative to ApoE expression alone. While the potential use of these molecules as novel prognostic factors in metastatic melanoma is exciting in light of the present lack of reliable molecular biomarkers in the clinic for informing one's likelihood of melanoma metastatic relapse, further studies are needed to validate the prognostic capacity of each ApoE, DNAJA4, miR-199a-3p, miR-199a-5p, and miR-1908 as well as their combined expression signatures across multiple independent melanoma patient cohorts that would together constitute a larger total sample size.

Summary of Findings from Chapter III

In this chapter, I describe the whole-genome transcriptomic-based approach that we used in order to identify transcripts inhibited by each miR-199a-3p, miR-199a-5p, and miR-1908. We found two genes (*ApoE* and *DNAJA4*) that were convergently repressed by the three miRNAs. By performing heterologous reporter assays coupled with mutagenesis studies, I demonstrated that *ApoE* was directly targeted by miR-199a-5p and miR-1908, and *DNAJA4* was directly repressed by all three miR-199a-3p, miR-199a-5p, and miR-1908. In a

series of epistasis experiments, we then showed that the miRNA-based silencing of *ApoE* and *DNAJA4* was necessary for the miRNA-dependent effects on melanoma invasion, endothelial recruitment, and metastasis. These findings reveal *ApoE* and *DNAJA4* as novel suppressors of melanoma metastasis. Interestingly, I also found that DNAJA4 suppressed melanoma progression phenotypes through the positive regulation of *ApoE*. Out of the three *DNAJA4* isoforms expressed by melanoma cells, I found that only overexpression of DNAJA4.3 was sufficient to inhibit melanoma invasion. To this end, we performed immunoprecipitation studies coupled with mass spectrometry analyses, which led to the identification of PFKFB3, HNRNPF, PSMD11, FLG, and TPM4 as candidate interacting partners specific for DNAJA4.3. In the final section of this chapter, I describe our clinical findings that the expression levels of each ApoE and DNAJA4 correlated with melanoma progression stage and were also prognostic of patients' likelihood for metastatic recurrence. Importantly, combining ApoE and DNAJA4 expression as well as ApoE, DNAJA4, and the aggregate expression of the three miRNAs displayed enhanced prognostic capacity relative to each individual signature, suggestive of clinical cooperativity among the miRNAs and their effector genes in predicting metastatic melanoma outcomes in patients.

CHAPTER IV: CELL-AUTONOMOUS AND NON-CELL-AUTONOMOUS REGULATION OF MELANOMA PROGRESSION PHENOTYPES BY EXTRACELLULAR APOE

Extracellular ApoE Suppresses Melanoma Invasion and Endothelial Recruitment

Our findings of regulatory convergence of the metastasis-promoting miRNAs, miR-199a and miR-1908, and the heat-shock factor DNAJA4 onto *ApoE* implicate *ApoE* as the central molecule in this convergent multi-miRNA regulatory network. The functional role of ApoE as a metastasis suppressor was further supported by the significant clinical correlation between reduced ApoE expression and melanoma metastasis outcomes (Chapter III). In light of ApoE's role in suppressing metastatic colonization and angiogenesis as revealed by our experiments, I next sought to identify the downstream molecular mechanisms mediating ApoE's effects on melanoma metastatic phenotypes. Consistent with the known role of ApoE as an extracellular factor, I found that highly metastatic melanoma cells secrete about five times less ApoE compared to their less metastatic parental derivatives (Figure 4.1a). Importantly, extracellular ApoE protein levels were also repressed by endogenous miR-199a and miR-1908 (Figures 4.1b-c).

Our previous findings revealed that molecular depletion of melanoma-cell *ApoE* led to an increase in melanoma invasion and endothelial recruitment (Figure 3.6). We thus wondered whether the ApoE-dependent suppression of these phenotypes could be mediated by melanoma-derived extracellular ApoE. We found that neutralization of extracellular ApoE protein with a blocking antibody elevated the matrigel invasive capacity of melanoma cells and also enhanced *in vitro* endothelial recruitment by melanoma cells (Figures 4.2 a-b),

revealing endogenous melanoma-secreted ApoE as a suppressor of cell-autonomous and non-cell-autonomous melanoma progression phenotypes. Conversely, adding recombinant ApoE to the cell media resulted in the suppression of both matrigel invasion and endothelial recruitment phenotypes displayed by the highly metastatic MeWo-LM2 cells (Figures 4.2c).

I next tested whether the miRNA-dependent effects on melanoma invasion and endothelial recruitment are mediated through extracellular ApoE. Given that miRNA silencing upregulated melanoma cell-secreted ApoE expression, we hypothesized that the effects of miRNA depletion might be antagonized by the blockade of extracellular ApoE. Consistent with this, the suppression of both phenotypes seen with silencing of each mature miRNA was prevented by an antibody-mediated neutralization of extracellular ApoE. These findings reveal melanoma-derived extracellular ApoE as the downstream mediator of miRNA-dependent invasion and endothelial recruitment (Figures 4.2d-e).

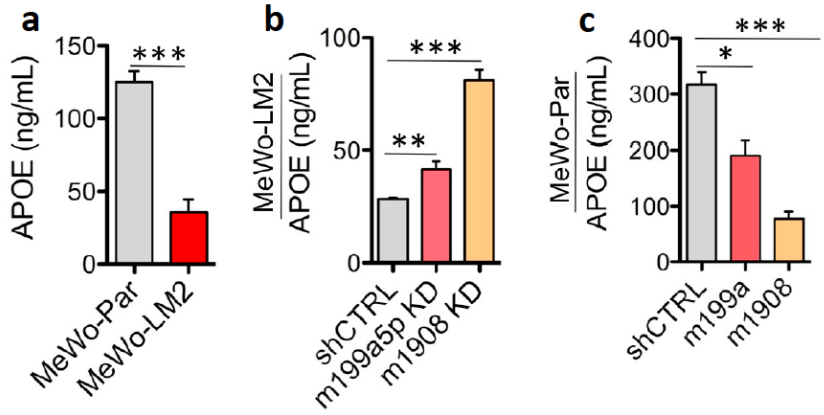

Figure 4.1. Endogenous miR-199a-5p and miR-1908 Repress Extracellular ApoE Levels. a-c. Extracellular ApoE protein levels quantified by ELISA in melanoma cell-conditioned media from MeWo-parental and MeWo-LM2 cells (**a**), MeWo-LM2 cells silenced for each miR-199a-5p, miR-1908, or control (**b**), and parental MeWo cells overexpressing miR-199a, miR-1908, or control (**c**). n = 3. Data are depicted as mean ± SEM. *p < 0.05, **p < 0.01, ***p < 0.001. p-values based on unpaired student's t-tests.

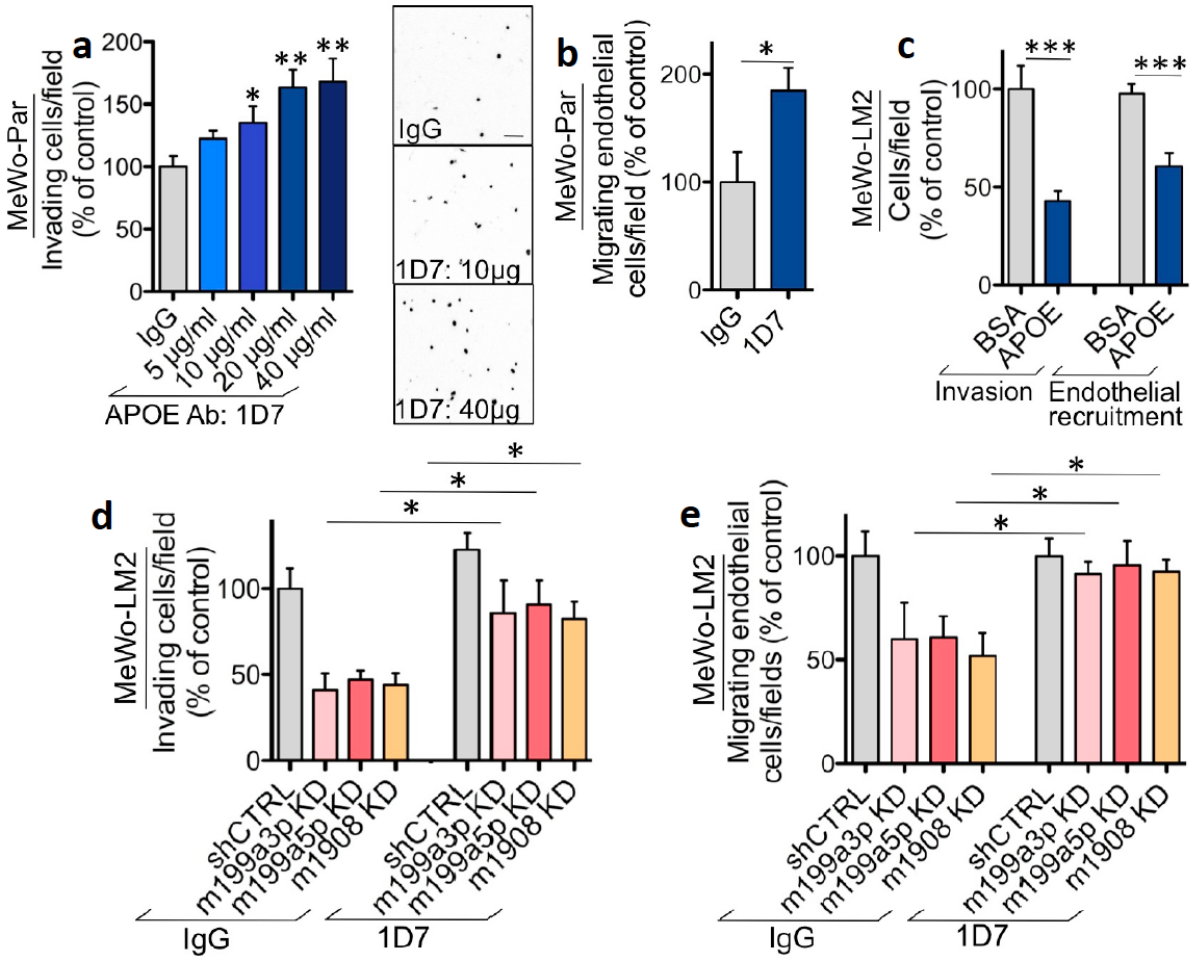

Figure 4.2. Extracellular ApoE Suppresses Melanoma Invasion and Endothelial Recruitment a. Matrigel invasion by parental human melanoma MeWo cells that were incubated with a control IgG antibody or increasing doses of an ApoE neutralization antibody (1D7). n ≥ 4. **b.** Endothelial recruitment capacity by MeWo parental cells in response to a control IgG or an ApoE blocking antibody (1D7) treatment at 40 µg/mL. n = 4. **c.** Matrigel invasion and endothelial recruitment phenotypes displayed by highly metastatic MeWo-LM2 cells in response to addition of bovine serum albumin (BSA) or recombinant ApoE protein to the cell media. n ≥ 7. **d-e.** MeWo-LM2 metastatic derivatives with silenced expression of each miR-199a-3p, miR-199a-5p, or miR-1908 were subjected to matrigel invasion (**d**) and endothelial recruitment (**e**) assays in the presence of IgG or ApoE blocking (1D7) antibodies. n ≥ 5. Scale bar, 100 µm. All data are plotted as mean ± SEM. *p < 0.05, **p < 0.01, ***p < 0.001. p-values based on unpaired student's t-tests.

Enhancement of Extracellular ApoE Levels Robustly Suppresses Melanoma Metastasis

Our findings that the miRNA-dependent effects on the matrigel invasion and endothelial recruitment *in vitro* phenotypes are in large part mediated through extracellular ApoE motivated us to examine whether the modulation of extracellular ApoE levels also regulates *in vivo* metastatic colonization by melanoma cells. We thus tested whether pre-incubation of melanoma cells with recombinant ApoE or bovine serum albumin (BSA) affects their subsequent lung colonization capacity. Remarkably, ApoE pre-treatment robustly suppressed (>300-fold) metastatic colonization by the highly metastatic MeWo-LM2 line, as well as the independent A375-LM3 (145-fold), WM-266-4 (80-fold), HT-144 (119-fold), and A2058 (85-fold) human melanoma lines (Figures 4.3a-e). This dramatic suppression of metastasis by ApoE pre-incubation of multiple human melanoma cell lines indicates that the melanoma cell-autonomous effects of ApoE are essential for metastatic initiation. Treatment of melanoma cells with ApoE did not appreciably affect the proliferation/survival of melanoma cells *in vitro* up to five days after treatment (Figure 4.3f), implying that the suppression of melanoma metastatic colonization in response to the ApoE protein treatment is likely not due to impaired cell proliferation and/or survival disadvantage, but it rather emerges through the inhibition of melanoma cell invasion and endothelial recruitment—phenotypes that can be rate-limiting for metastatic initiation. The strong inhibition of metastasis observed upon ApoE pre-treatment suggests that therapeutic approaches aimed at enhancing extracellular ApoE levels and ApoE signaling in melanoma cells might be therapeutically effective in preventing melanoma metastasis (see Chapter V).

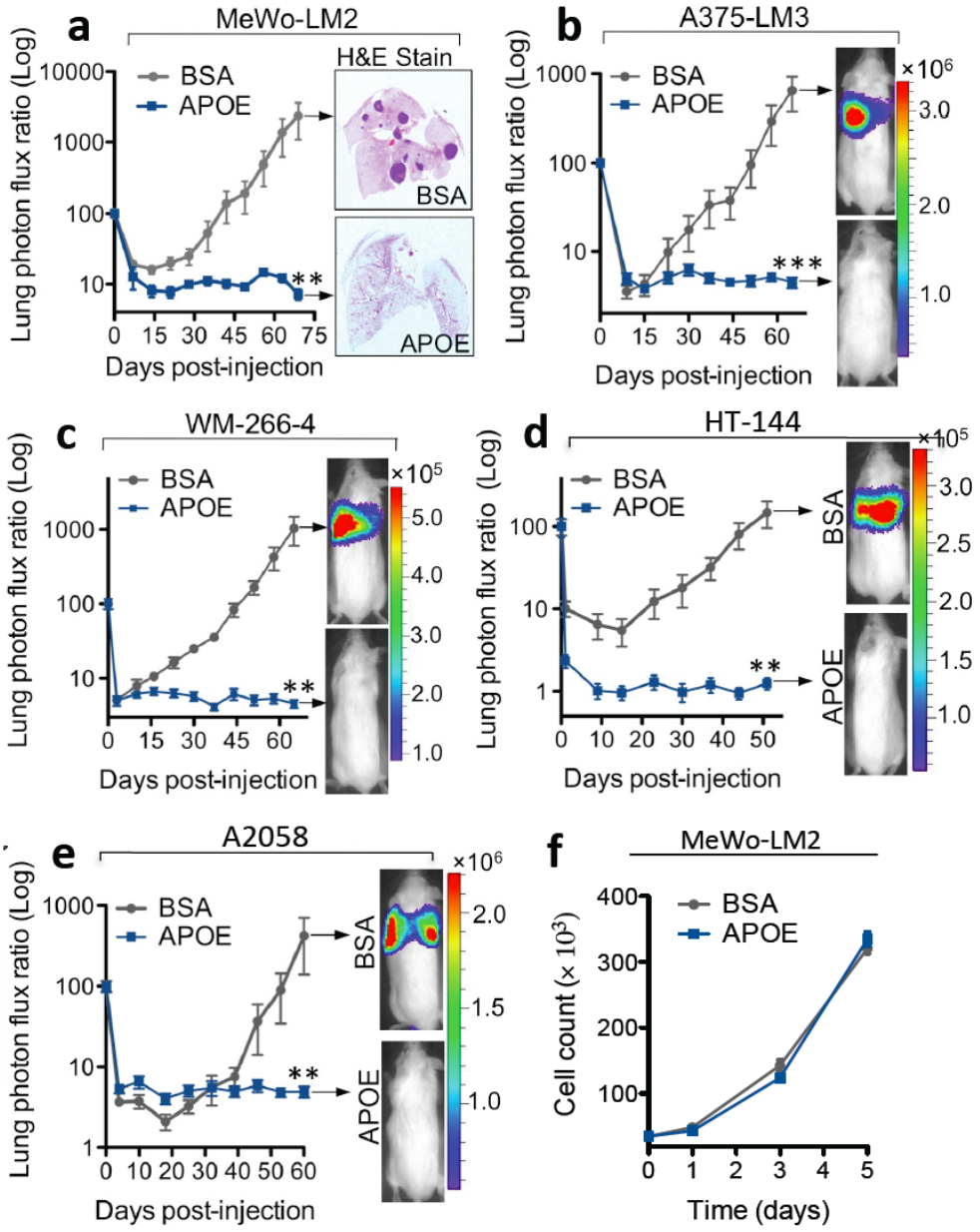

Figure 4.3. ApoE Pre-Treatment Suppresses Metastatic Colonization by Melanoma Cells. a-e. Bioluminescence signal quantification plots corresponding to lung colonization by 4×10^4 MeWo-LM2 (**a**), 2×10^5 A375-LM3 (**b**), 1.5×10^5 WM-266-4 (**c**), 3.5×10^5 HT-144 (**d**), and 2×10^5 A2058 (**e**) human melanoma cells that were pre-treated with BSA or ApoE at 100 µg/mL for 24 hours prior to intravenous injection into immunocompromised mice. $n \geq 5$. **f.** *In vitro* cell proliferation by 3.5×10^4 MeWo-LM2 cells in response to BSA or ApoE treatment at 100 µg/mL. Live cells were counted on days 0, 1, 3, and 5. $n = 3$. All data are displayed as mean ± SEM. $^{**}p < 0.01$, $^{***}p < 0.001$. p-values based Mann-Whitney's t-tests.

In light of our findings that elevating extracellular ApoE levels *in vitro* (by adding ApoE protein to the cell media) subsequently impairs melanoma cells' ability to metastasize, we wondered whether we could model the reverse scenario *in vivo* by removing stromally-derived extracellular ApoE. To this end, we investigated the impact of genetic deletion of stromal *ApoE* on melanoma progression in an immunocompetent mouse model of melanoma metastasis. Consistent with a major suppressive role for extracellular ApoE in metastasis, B16F10 mouse melanoma cells injected into the circulation of syngeneic immunocompetent mice exhibited a 10-fold increase in metastatic colonization in mice genetically inactivated for *ApoE* compared to wild-type mice. Importantly, the metastatic capacity of B16F10 cells was dramatically abrogated by ApoE cell pre-treatment in both wild-type (60-fold inhibition) and ApoE-null (460-fold inhibition) genetic contexts (Figure 4.4).

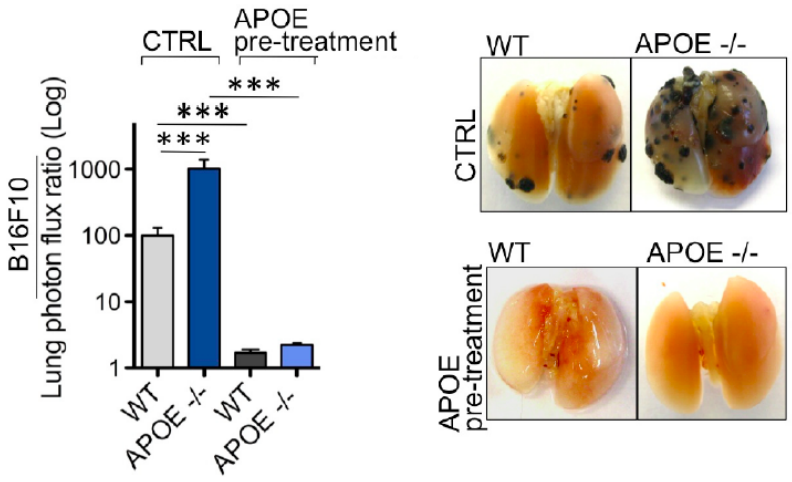

Figure 4.4. Genetic Inactivation of *ApoE* Accelerates Melanoma Lung Colonization. Lung colonization quantified by bioluminescence imaging 19 days following intravenous injection of 5×10^4 mouse melanoma cells into wild-type or *ApoE* genetically null mice. The cells were pre-incubated with ApoE at 100 μg/mL or control for 24 hours and subsequently injected via the tail-vein into C57BL/6 mice. Representative *ex vivo* lung images taken at day 19 post-injection are shown on the right. $n \geq 12$ (control); $n \geq 5$ (ApoE pre-treatment). All data are displayed as mean ± SEM. ***$p < 0.001$, based on Mann-Whitley's t-tests.

The metastasis suppression elicited by exogenously supplied ApoE (Figure 4.3) as well as the increase in metastatic colonization upon removal of endogenous stromal ApoE (Figure 4.4) reveal melanoma cell-extrinsic extracellular ApoE as a robust suppressor of melanoma progression. In addition, our molecular findings of convergent miRNA targeting of *ApoE* in melanoma cells (Chapter III) implicate melanoma cell-intrinsic ApoE as a downstream effector of the miRNA-dependent effects on melanoma progression phenotypes. Taken together, these findings implicate extracellular ApoE, derived either from melanoma cells or supplied from stromal tissues, as a key suppressor of melanoma metastasis. The relative contribution of melanoma versus stromally derived ApoE is discussed in Chapter V.

ApoE Targeting of Melanoma LRP1 Receptors Suppresses Melanoma Cell Invasion

We next examined the molecular mechanisms through which extracellular ApoE inhibits melanoma progression phenotypes. First, I investigated the downstream molecular mediators of ApoE's effects on melanoma cell invasion. Given that there are only four known receptors for ApoE (VLDLR, LRP1, LRP8, and LDLR), I used RNA interference (RNAi) to individually silence the expression of each receptor in melanoma cells by 50% or more, as confirmed by mRNA transcript level analyses. I then examined what happens to the ApoE-induced suppression of invasion upon knocking down each receptor. Interestingly, melanoma cell depletion of *LRP1*, but not any of the other ApoE receptors, specifically prevented the ability of ApoE to inhibit matrigel invasion (Figure 4.5a). Additionally, *LRP1* knockdown in the setting of miRNA silencing rescued the reduced invasive capacity resulting from miRNA inhibition (which leads to de-repression of *ApoE*) and also modestly elevated the baseline invasion phenotype displayed by control MeWo-LM2 melanoma cells

(Figure 4.5b-d). Importantly, *LRP1* depletion in the setting of miRNA silencing also enhanced *in vivo* lung colonization (Figure 4.6). These *in vitro* and *in vivo* findings together implicate melanoma-cell LRP1 as the downstream mediator of the miRNA/ApoE-dependent effects on melanoma cell invasion and metastatic colonization phenotypes.

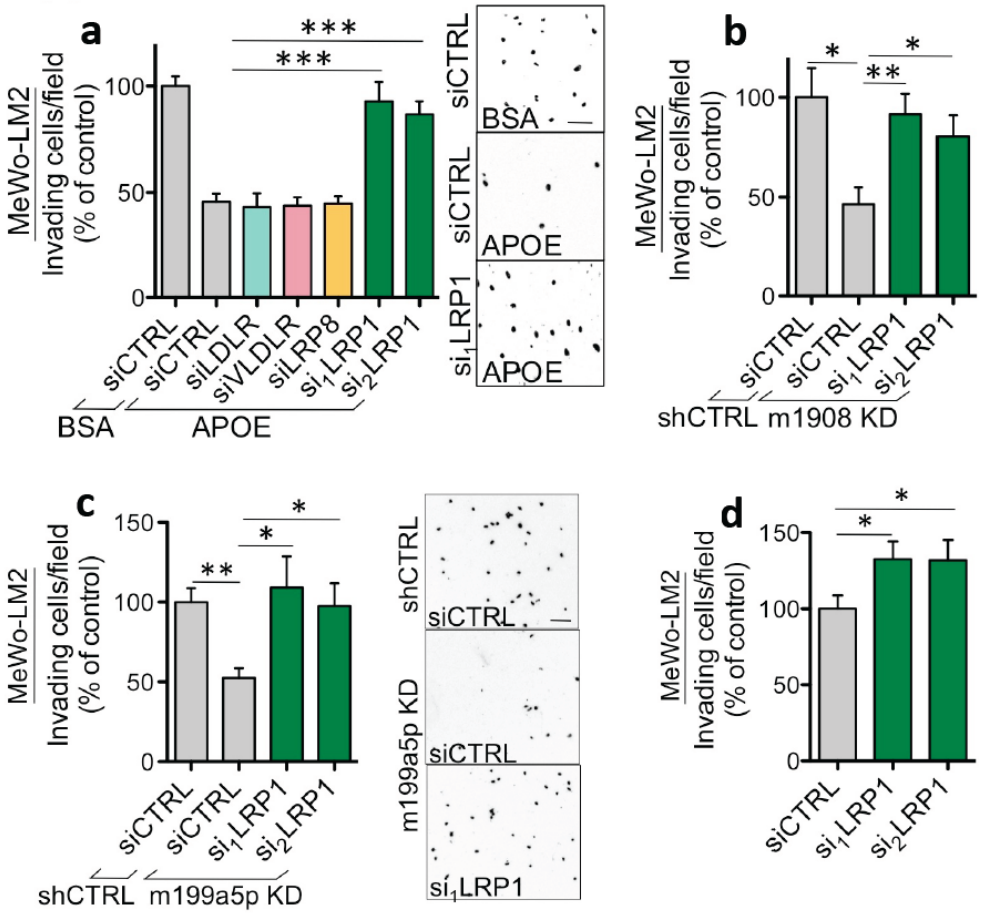

Figure 4.5. Identification of LRP1 as the ApoE Receptor on Melanoma Cells Mediating ApoE's Effects on Invasion Suppression. a. Trans-well matrigel invasion by MeWo-LM2 cells transfected with short interfering RNAs (siRNAs) targeting *LDLR, VLDLR, LRP8, LRP1*, or a control sequence. At the start of they assay, the cells were treated with BSA or ApoE. n ≥ 3. **b-c.** MeWo-LM2 cells, with silenced expression of miR-1908 (**b**) or miR-199a -5p (**c**), were transfected with siRNAs targeting *LRP1* or a control siRNAs and assessed for their matrigel invasion capacity. n = 4. **d.** Matrigel invasion by MeWo-LM2 cells expressing a control siRNA or siRNAs targeting *LRP1*. n ≥ 9. Scale bar, 100 μm. All data are plotted as mean ± SEM. *p<0.05, **p <0.01, ***p<0.001. p-values based on unpaired student's t-test.

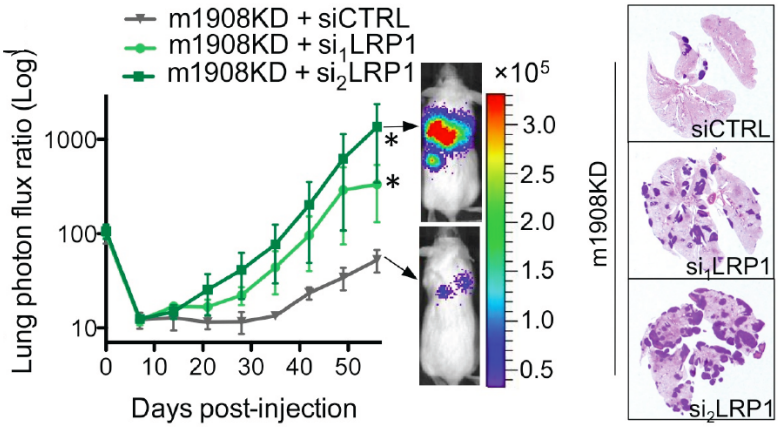

Figure 4.6. Melanoma-Cell LRP1 Mediates miRNA-Dependent Metastatic Colonization. Lung metastasis, quantified by weekly bioluminescence imaging, by 1×10^5 MeWo-LM2 cells with silenced expression of miR-1908 and transfected with siRNAs targeting *LRP1* or a control. Representative H&E-stained lungs extracted at the final day 56 of imaging are shown of the right. $n \geq 4$. Weekly bioluminescence data are shown as mean ± SEM. *$p < 0.05$. p-values based on Mann-Whitney's t-tests.

ApoE Targeting of Endothelial LRP8 Receptors Suppresses Endothelial Cell Migration

The regulation of melanoma cell invasion by the miRNA/ApoE/LRP1 pathway reflects the cell-autonomous effects of melanoma-derived ApoE. The endothelial recruitment phenotype, on the other hand, is suggestive of non-cell autonomous effects of melanoma-expressed and secreted ApoE on endothelial cell migration. Consistent with direct effects of ApoE on endothelial cells, pre-treatment of endothelial cells with ApoE diminished their subsequent ability to migrate towards melanoma cells (Figure 4.7a). To identify the ApoE receptor(s) on endothelial cells that mediate(s) ApoE's effects on endothelial migration, I individually depleted each of the four ApoE receptors in endothelial cells using RNAi and confirmed silencing of each receptor by 50% or greater at the mRNA level. I then tested the ability of endothelial cells to migrate towards melanoma cells with silenced miRNA expression, which results in endogenously elevated extracellular ApoE levels (Figure 4.1) and inhibition of endothelial recruitment (Figure 4.2). Contrary to our identification of LRP1

as the melanoma cell receptor mediating suppression of invasion by ApoE, we observed that, in endothelial cells, knockdown of a different receptor, *LRP8*, specifically blocked the inhibition in endothelial recruitment attained by miRNA silencing (Figure 4.7b-d). These findings reveal LRP8 as the downstream endothelial cell mediator of the miRNA/ApoE-dependent effects on endothelial recruitment.

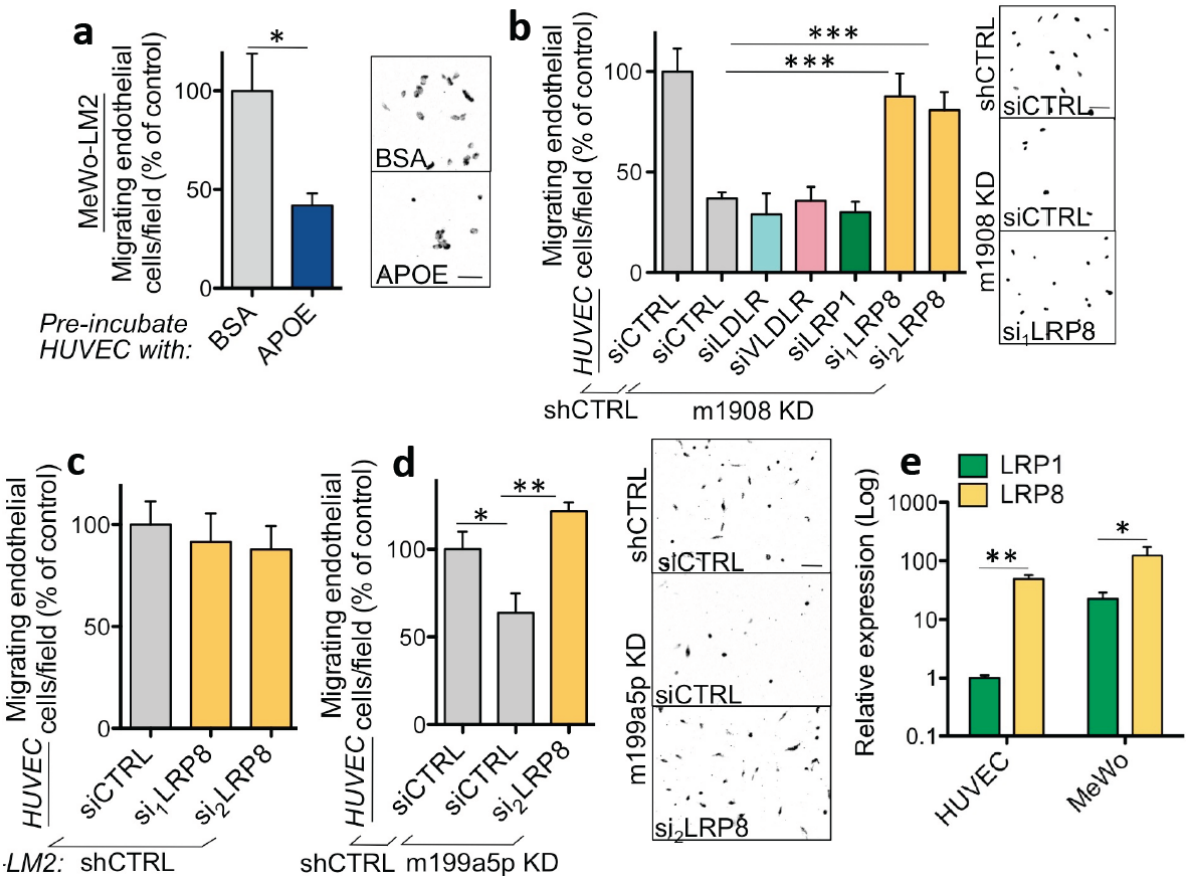

Figure 4.7. Endothelial-Cell LRP8 Mediates miRNA/ApoE-Dependent Endothelial Recruitment. a. Endothelial recruitment by MeWo-LM2 cells following endothelial cell pre-treatment with BSA or ApoE. n ≥ 3. **b-d.** Recruitment of endothelial cells (HUVEC) transfected with siRNAs targeting *LDLR, VLDLR, LRP1, LRP8*, or a control by MeWo-LM2 cells with a silenced expression of miR-1908 (**b**), miR-199a-5p (**d**), or control MeWo-LM2 cells (**c**). n ≥ 4. **e.** Relative expression levels of LRP1 and LRP8, determined by qRT-PCR, in endothelial cells (HUVECs) and MeWo human melanoma cells. n = 3. Scale bar, 100 μm. Error bars =cSEM. *p < 0.05, **p < 0.01, ***p < 0.001. p-values based on student's t-tests.

We found that endothelial cells expressed 50-fold higher levels of *LRP8* relative to *LRP1* (Figure 4.7e), hinting that the greater abundance of endothelial *LRP8* receptors may determine preferential ApoE/LRP8 targeting in endothelial cells. Human melanoma MeWo cells, on the other hand, exhibited higher levels of both *LRP1* and *LRP8* relative to endothelal cells, with melanoma cell *LRP8* levels being 5-fold higher than melanoma cell *LRP1* levels. These expression data suggest that i) the higher *LRP1* levels in melanoma cells compared to endothelial cells could explain why ApoE/LRP1 targeting is more relevant in the melanoma cell type and ii) the choice of melanoma LRP1 receptors as the functional mediator of ApoE-dependent invasion suppression is not solely determined by greater relative abundance of this receptor.

I next examined whether targeting of LRP8 by ApoE might regulate general endothelial cell migration in a cancer cell-free system. Antibody neutralization of extracellular ApoE, which is present in the endothelial cell media, significantly elevated endothelial cell migration (Figure 4.8a). Conversely, addition of recombinant ApoE suppressed endothelial cell migration both in trans-well assays (Figure 4.8b) as well as in gradient-based migration assays (Figure 4.8c). Importantly, the ApoE-mediated suppression of endothelial migration was abolished in response to depletion of *LRP8* in endothelial cells (Figures 4.8b-c).

In light of the robust *in vitro* effects, we investigated whether ApoE could affect endothelial migration *in vivo*. In experiments performed by Colin Buss, we found that addition of ApoE blocked (> 40-fold) VEGF-induced *in vivo* endothelial recruitment into subcutaneously implanted matrigel plugs (Figure 4.9a), suggesting that ApoE acts as a strong repellant that can override the chemotactic positive VEGF signal. Consistent with the robust

suppression of endothelial migration elicited by ApoE, we further found that mice that had been genetically inactivated for *ApoE* exhibited a significant increase in blood vessel density within metastatic nodules formed by B16F10 mouse melanoma cells (Figure 4.9b). These genetic findings implicate stromally supplied ApoE, in addition to melanoma-derived ApoE (Figure 3.8), as a suppressor of metastatic endothelial recruitment.

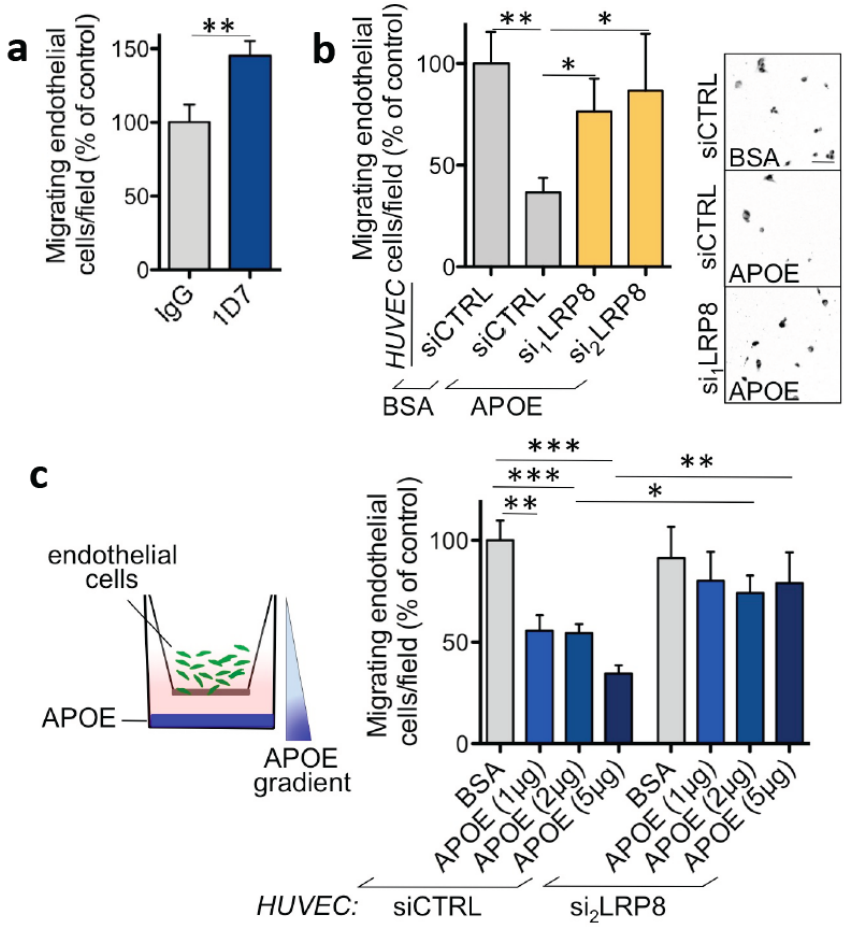

Figure 4.8. ApoE/LRP8 Targeting Suppresses Endothelial Cell Migration in a Cancer Cell-Free System. a. Trans-well endothelial cell migration in the presence of IgG or an ApoE neutralization antibody (1D7). n ≥ 6. **b.** Endothelial cells transfected with a control siRNAs or siRNAs targeting *LRP8* were subjected to a trans-well migration assay in response to BSA or ApoE treatment. n ≥ 6. **c.** Trans-well migration along an ApoE matrigel gradient by endothelial cells transfected with a control siRNA or siRNAs targeting *LRP8*. n ≥ 4. Scale bar, 100 µm. All data are represented as mean ± SEM. *p < 0.05, **p < 0.01, ***p < 0.001. p-values based on unpaired student's t-tests.

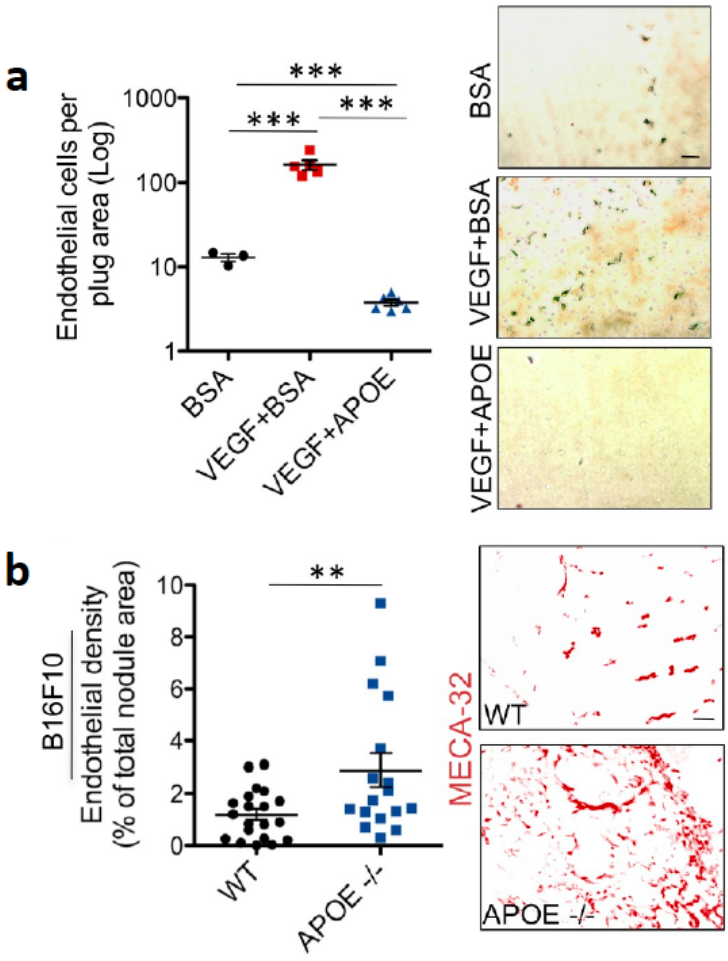

Figure 4.9. ApoE Inhibits *In Vivo* Endothelial Cell Recruitment and Angiogenesis.

a. Endothelial cell recruitment into subcutaneously implanted matrigel plugs containing BSA (10 μg/mL), VEGF (400 ng/mL) + BSA (10 μg/mL), or VEGF (400 ng/mL) + ApoE (10 μg/mL). Endothelial cells were immunohistochemically detected by staining for MECA-32, and the number of endothelial cells migrating into each plug was quantified 3 days post-implantation. $n \geq 3$. **b.** Endothelial cell density within lung metastatic nodules formed by 5×10^4 B16F10 mouse melanoma cells 19 days post-intravenous cell injection into *ApoE* wild-type or *ApoE* genetically null mice. $n \geq 17$. Scale bar, 100 μm. All data are represented as mean ± SEM. $^{**}p < 0.01$, $^{***}p < 0.001$. p-values based on unpaired student's t-tests.

ApoE/LRP8-Dependent Regulation of Endothelial VEGFR2 Activity

The identification of LRP8 as the endothelial cell mediator of extracellular ApoE's effects on angiogenesis raised the question of how LRP8 targeting regulated endothelial cell migration. Recently, an independent group reported that a synthetic dimer-peptide comprised of the ApoE receptor-binding domain inhibited phosphorylation of VEGFR2 (Bhattacharjee et al., 2011), a receptor essential for multiple aspects of endothelial biology including migration and angiogenesis (Olsson et al., 2006; Carmeliet and Jain, 2011). In light of this, I hypothesized that full-length ApoE might modulate VEGFR2 activation in an LRP8-dependent manner. Indeed, I found that addition of recombinant ApoE inhibited the VEGF-induced phosphorylation of endothelial cell VEGFR2, whereas siRNA-mediated depletion of *LRP8* rendered ApoE ineffective in blunting VEGFR2 activation (Figure 4.10a).

These findings prompted us to further examine the role of ApoE/LRP8 signaling as a novel regulator of VEGFR2 activity using a previously described genetic mouse model of *LRP8* inactivation (Trommsdorff et al., 1999). In experiments conducted together with Jessica Posada, a medical student doing a one-year research project in the lab, we isolated primary endothelial cells from the lungs of wild-type, *LRP8* heterozygous, or *LRP8* null mice. Consistent with our findings in human endothelial cells (Figure 4.10a), ApoE addition decreased the VEGF-induced phosphorylation of VEGFR2 in primary mouse lung endothelial cells expressing one or both copies of *LRP8* (Figure 4.10b-c). Importantly, deletion of *LRP8* prevented the inhibitory effect of ApoE on VEGFR2 phosphorylation (Figure 4.10c), providing genetic evidence that LRP8 is the endothelial receptor mediating ApoE's effects on VEGFR2 activation. Interestingly, endothelial cells lacking one copy of

LRP8 exhibited elevated VEGFR2 activation in response to VEGF, suggesting that partial reduction in the levels of LRP8 might enhance ligand-mediated VEGFR2 phosphorylation.

Consistent with ApoE's suppressive effects on VEGFR2 activation, we further found that phosphorylated VEGFR2 levels were elevated in primary tumors formed by melanoma cells over-expressing the metastasis-promoting miR-1908 and miR-199a, each of which directly represses *ApoE* expression (Figure 4.8d). Given that the majority of VEGFR2 expression is restricted to endothelial cells, these findings imply that melanoma-expressed miR-199a and miR-1908 positively regulate endothelial VEGFR2 activation *in vivo*, presumably through their downstream targeting of the ApoE/LRP8 pathway in endothelial cells. Future studies will investigate whether the non-cell-autonomous endothelial recruitment phenotype conferred by miR-199a and miR-1908 is functionally mediated through indirect ApoE-dependent modulation of endothelial VEGFR2 signaling by the miRNAs.

Ongoing work in the lab is currently examining the role of LRP8 in VEGFR2-dependent angiogenesis in the context of genetic inactivation of *LRP8*. Consistent with the enhanced ligand-induced VEGFR2 phosphorylation in endothelial cells lacking one copy of LRP8 (Figure 4.10c), preliminary experiments conducted by Jessica Posada have shown that *LRP8* -/+ heterozygous mice exhibit a roughly 2-fold enhancement in tumor growth and a corresponding increase in tumor angiogenesis relative to wild-type mice (data not shown). Additionally, in aortic ring assays, *LRP8* +/- aortas display an enhanced capacity to form VEGF-induced endothelial cell sprouts relative to wild-type aortas (data not shown), implying that the LRP8-mediated effects on VEGFR2 activation might also be relevant to physiological angiogenesis.

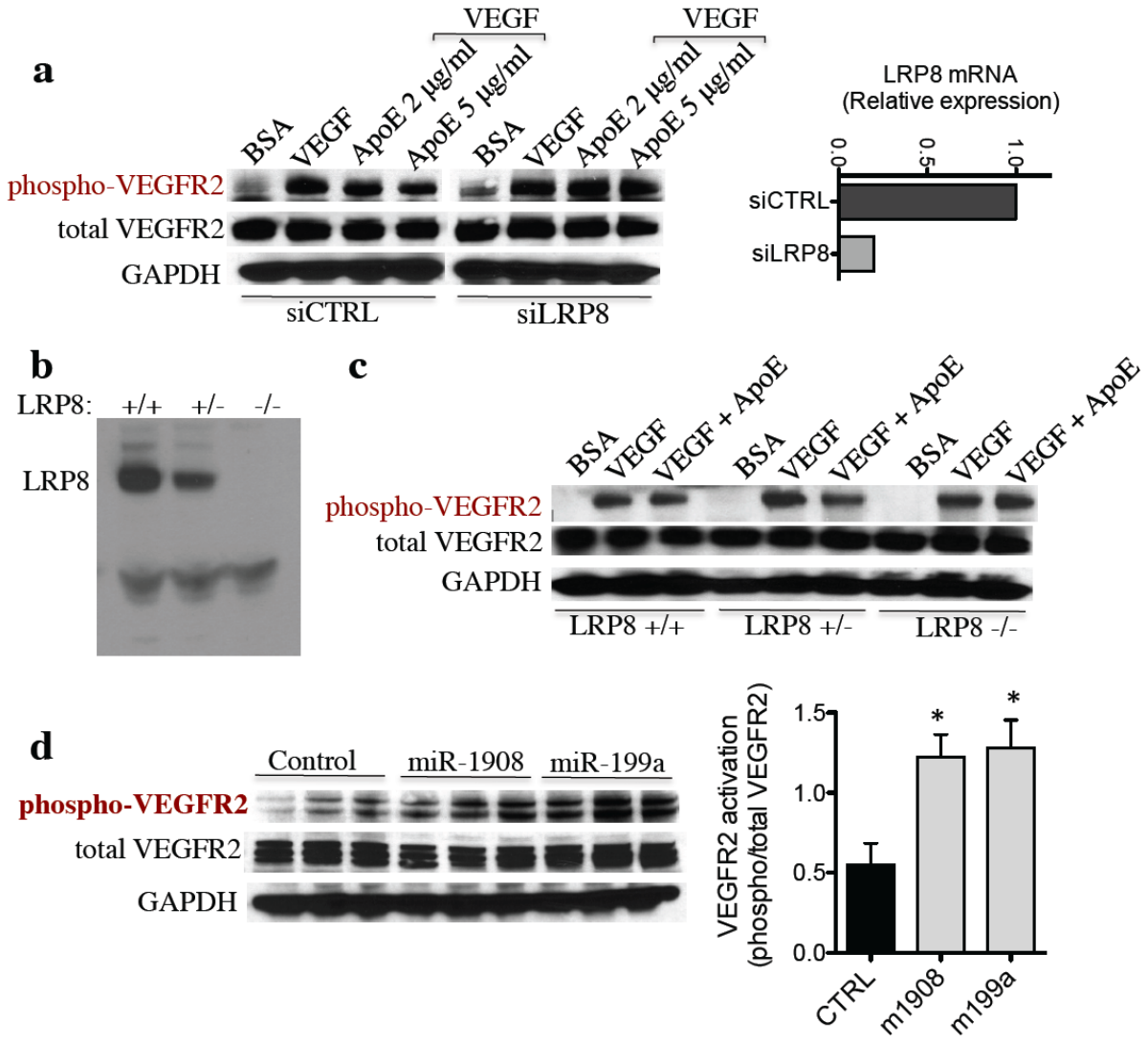

Figure 4.10. ApoE Inhibits VEGFR2 Activation in an LRP8-Dependent Manner.

a. Western blotting for phosphorylated and total VEGFR2 in human umbilical vein endothelial cells (HUVEC) transfected with a control siRNA or an siRNA targeting *LRP8* and treated with BSA, VEGF, or VEGF + ApoE. **b.** Western blotting for LRP8 in endothelial cell lysates from *LRP8* wild-type (+/+), heterozygous (+/-), or null (-/-) mice. **c.** Western blotting for phosphorylated and total VEGFR2 in primary mouse lung endothelial cells isolated from *LRP8* +/+, *LRP8* -/+, and *LRP8* -/- mice and treated with either BSA, VEGF, or VEGF + ApoE. **d.** Phosphorylated and total VEGFR2 levels were assessed in total lysates from subcutaneous tumors formed by MeWo human melanoma cells overexpressing each miR-199a or miR-1908. VEGFR2 activation was quantified as the ratio of phosphorylated over total VEGFR2 expression. n = 3. Error bars = SEM. *$p<0.05$, based on student's t-tests.

Interestingly, however, our preliminary analyses have revealed that the *LRP8* -/- null mutants do not display any appreciable change in ligand-induced VEGFR2 phosphorylation (Figure 4.10c) and do not exhibit any apparent angiogenic or tumor growth aberration compared to their wild-type littermates (data not shown), suggesting that the pro-angiogenic effects are restricted to partial loss of LRP8 expression in the heterozygous genetic context. Future work will examine the molecular and cellular mechanism(s) by which ApoE/LRP8 targeting regulates VEGFR2 activation, which should facilitate our molecular understanding of the non-linear relationship between LRP8 expression and VEGFR2-dependent angiogenesis.

Summary of Findings from Chapter IV

In this chapter, I present our findings that extracellular ApoE, which can be derived either from melanoma cells or supplied stromally, acts as a robust suppressor of melanoma metastasis. This is supported by our observations that i.) neutralization of extracellular melanoma cell-secreted ApoE with an antibody prevented the suppression of invasion and endothelial recruitment phenotypes upon miRNA silencing, ii.) treatment of melanoma cells with ApoE protein impaired their invasive and endothelial recruitment capacities and blocked *in vivo* metastasis, and iii.) genetic inactivation of stromal ApoE accelerated melanoma metastasis. Extracellular ApoE was found to act in a dual cell-autonomous/non-cell-autonomous fashion by divergently targeting distinct receptors on melanoma cells and endothelial cells, respectively. ApoE acting on LRP1 receptors on melanoma cells led to suppression of melanoma invasion and ApoE acting on endothelial LRP8 receptors inhibited endothelial recruitment by melanoma cells as well as endothelial cell migration in a cancer cell-free system. Whereas endothelial cells expressed substantially higher LRP8 than LRP1

levels, melanoma cells were found to display high levels of both LRP1 and LRP8, suggesting that the choice of ApoE receptor is not solely determined by relative target abundance, but receptor specificity, at least in melanoma cells, may rather be conferred by additional molecular coupling mechanisms (See Discussion). Finally, I describe our preliminary work on characterizing some of the endothelial cell biology downstream of LRP8 targeting. We found that ApoE inhibited ligand-induced VEGFR2 phosphorylation in an LRP8-dependent fashion both in primary human endothelial cells as well as primary mouse endothelial cells. We also observed that genetic inactivation of one *LRP8* allele enhanced VEGFR2 activation by VEGF. These findings implicate the ApoE/LRP8 pathway as a potential novel regulator of VEGFR2 activation and VEGFR2-dependent angiogenesis.

CHAPTER V: THERAPEUTIC ACTIVATION OF *APOE* IN METASTATIC MELANOMA THROUGH NUCLEAR HORMONE RECEPTOR TARGETING

Identification of LXRβ as a Novel Therapeutic Target in Melanoma

In light of our findings that extracellular ApoE robustly suppressed melanoma metastatic progression through its inhibitory effects on cell-autonomous invasion and non-cell-autonomous endothelial recruitment, we hypothesized that increasing extracellular ApoE levels may represent a novel therapeutic approach in metastatic melanoma. Since the half-life of naked recombinant proteins in serum is very short in the range of minutes to a few hours (Kontermann, 2011), making exogenous administration of ApoE protein unfeasible as a potential therapeutic approach, we sought to identify an *ApoE* trans-activator that is expressed across melanoma as well as in normal tissues, allowing for global induction of endogenous extracellular ApoE protein. Given the well-known role of ApoE in cholesterol metabolism (Hatters et al., 2006) and previous work showing that nuclear hormone receptors, a well-studied class of transcription factors, can regulate the transcription of multiple downstream target genes involved in cellular homeostasis and metabolism (Calkin and Tontonoz, 2012; Deblois and Giguère, 2013), we wondered whether there was a specific nuclear hormone receptor that i.) exhibits stable expression in melanoma and ii.) regulates downstream ApoE signaling. To this end, I first examined the expression levels of all nuclear hormone receptor family members across the National Cancer Institute (NCI-60) collection of human melanoma cell lines. Consistent with previous analyses of nuclear hormone receptor expression in the NCI-60 series (Holbeck et al., 2010), I found that several receptors

displayed stable expression across multiple melanoma lines (Figure 5.1). Notably, of these stably expressed receptors, the liver X receptors (LXRs) and the retinoid X receptors (RXRs) had previously been shown to activate ApoE transcription in adipocytes and macrophages (Laffitte et al., 2001; Mak et al., 2002). We further validated the stable expression of select LXR and RXR isoforms in seven primary melanoma lines obtained from patients at the MSKCC (Figure 5.1c).

The stable expression of specific LXR and RXR isoforms in melanoma suggested that they could represent druggable targets across diverse melanoma subtypes. In light of the availability of pharmacologic agents to activate LXRs and RXRs and the previously shown role of LXR/RXR heterodimers in activating *ApoE* transcription, we hypothesized that pharmacologic activation of LXR or RXR signaling might inhibit melanoma progression phenotypes through the downstream induction of *ApoE* expression. We first examined the effect of pharmacologic agonism of LXRs or RXRs on melanoma cell invasion and endothelial recruitment—phenotypes that we previously found to be displayed by highly metastatic melanoma cells and also to be robustly suppressed by ApoE. We found that LXR agonist (T0901317 or GW3965) treatment suppressed melanoma invasion and endothelial recruitment by four mutationally diverse melanoma lines: MeWo *(B-Raf*/N-Ras wild-type), HT-144 (*B-Raf* mutant), and SK-Mel-2 (*N-Ras* mutant) established human lines as well as the SK-Mel-334.2 (*B-Raf* mutant) primary human melanoma line (Figure 5.2). In contrast, treatment of melanoma cells with the RXR agonist bexarotene inhibited invasion in two of the four melanoma lines examined, and it was ineffective in suppressing endothelial recruitment by melanoma cells (Figure 5.2).

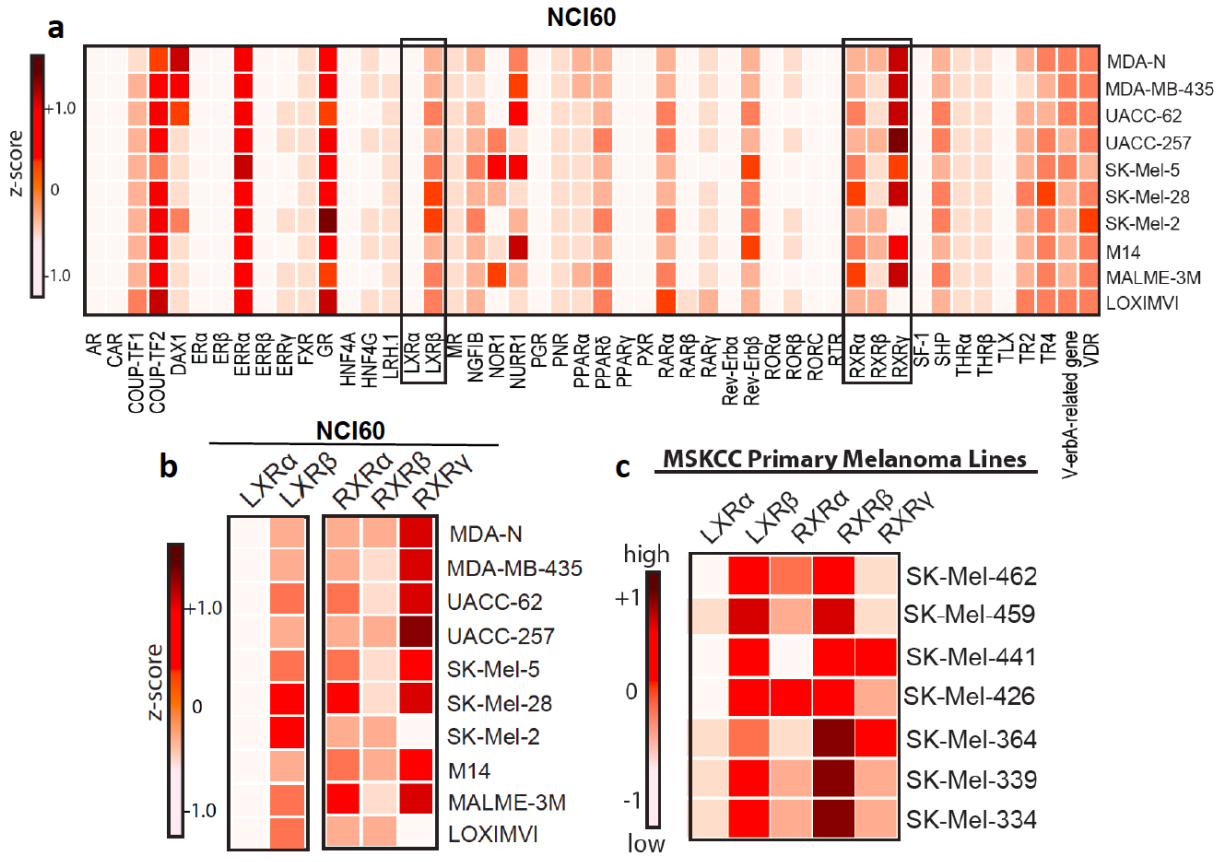

Figure 5.1. Analysis of Nuclear Hormone Receptor Expression in Melanoma.

a-c. Heat-maps showing microarray-based expression levels of all nuclear hormone receptor family members (**a**) or an extracted heat-map of only LXR and RXR isoforms (**b**) across the NCI-60 melanoma line collection. Color-map key indicates the changes in standard deviations (z-score) for the expression value of each receptor relative to the average expression of all profiled genes (> 39,000 transcript variants) in each cell line. **c**. Heat-map of the qRT-PCR-based expression levels of LXR and RXR isoforms in seven primary melanoma lines dissociated from melanoma tumors of patients at the MSKCC. Color-map corresponds to the standard deviations change in the expression of each receptor relative to the average expression value in each melanoma line.

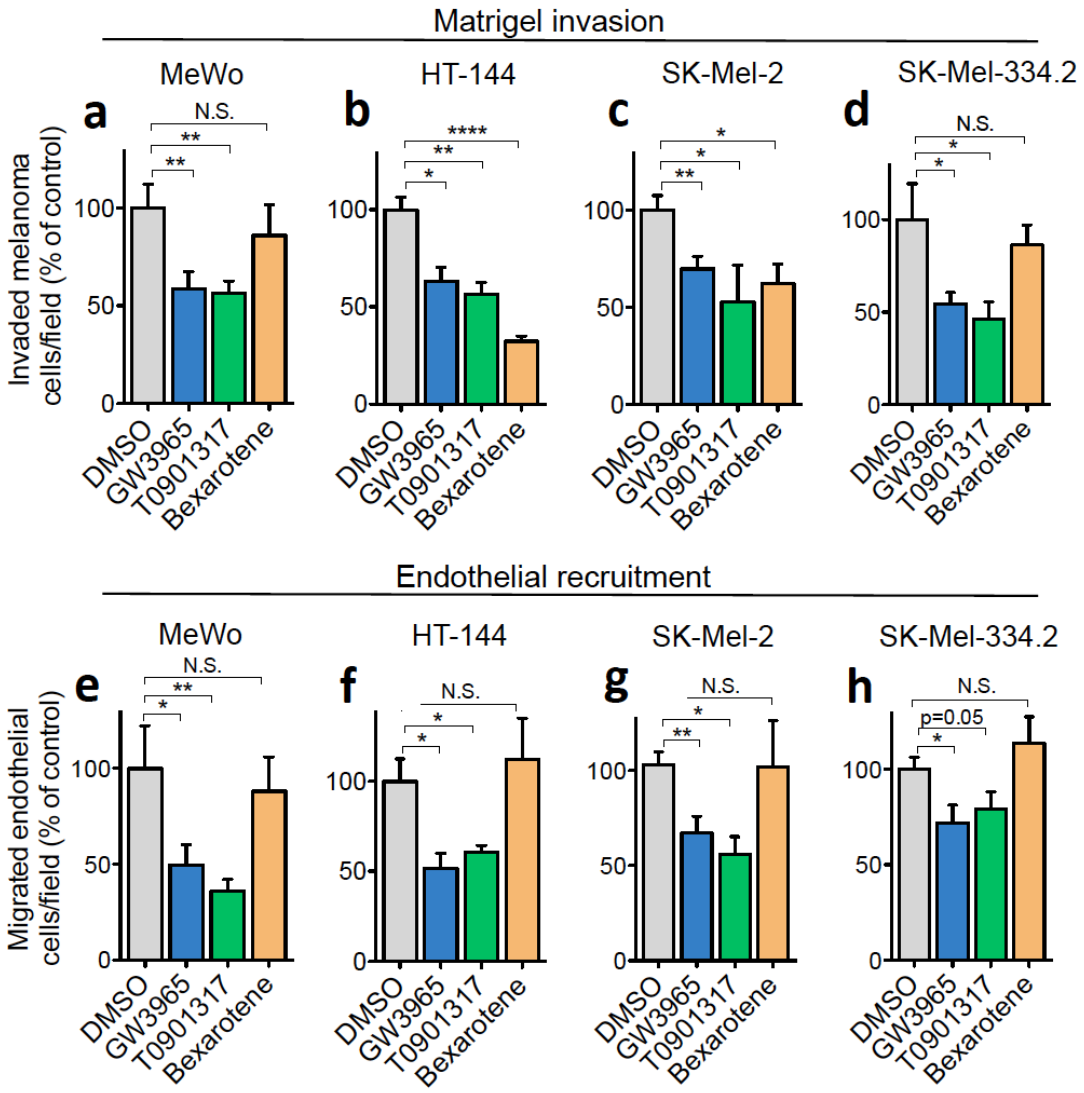

Figure 5.2. Effects of LXR or RXR Agonists on *In Vitro* Melanoma Cell Invasion and Endothelial Recruitment. a-d. Trans-well matrigel invasion by 1×10^5 MeWo (**a**), 5×10^4 HT-144 (**b**), 5×10^4 SK-Mel-2 (**c**), and 5×10^4 SK-Mel-334.2 (**d**) human melanoma cells. Cells were treated with DMSO, GW3965, T0901317, or bexarotene at 1 μM for 72 hours and subjected to trans-well matrigel invasion assays. $n \geq 4$. **e-h.** Trans-well endothelial recruitment by 5×10^4 MeWo (**e**), HT-144 (**f**), SK-Mel-2 (**g**), and SM-Mel-334.2 (**h**) human melanoma cells, following treatment of the melanoma cells with DMSO, GW3965, T0901317, or bexarotene at 1 μM for 72 hours. $n \geq 4$. All data are displayed as mean ± SEM. *$p < 0.05$, **$p < 0.01$, ****$p < 0.0001$. p-values based on unpaired student's t-tests.

Treatment of melanoma cells with the LXR agonists GW3965 or T0901317 or the RXR agonist bexarotene did not affect cell proliferation or survival rates (Figure 5.3), indicating that the suppression in melanoma progression phenotypes (invasion and endothelial recruitment) is not secondary to impaired *in vitro* cell proliferation/survival.

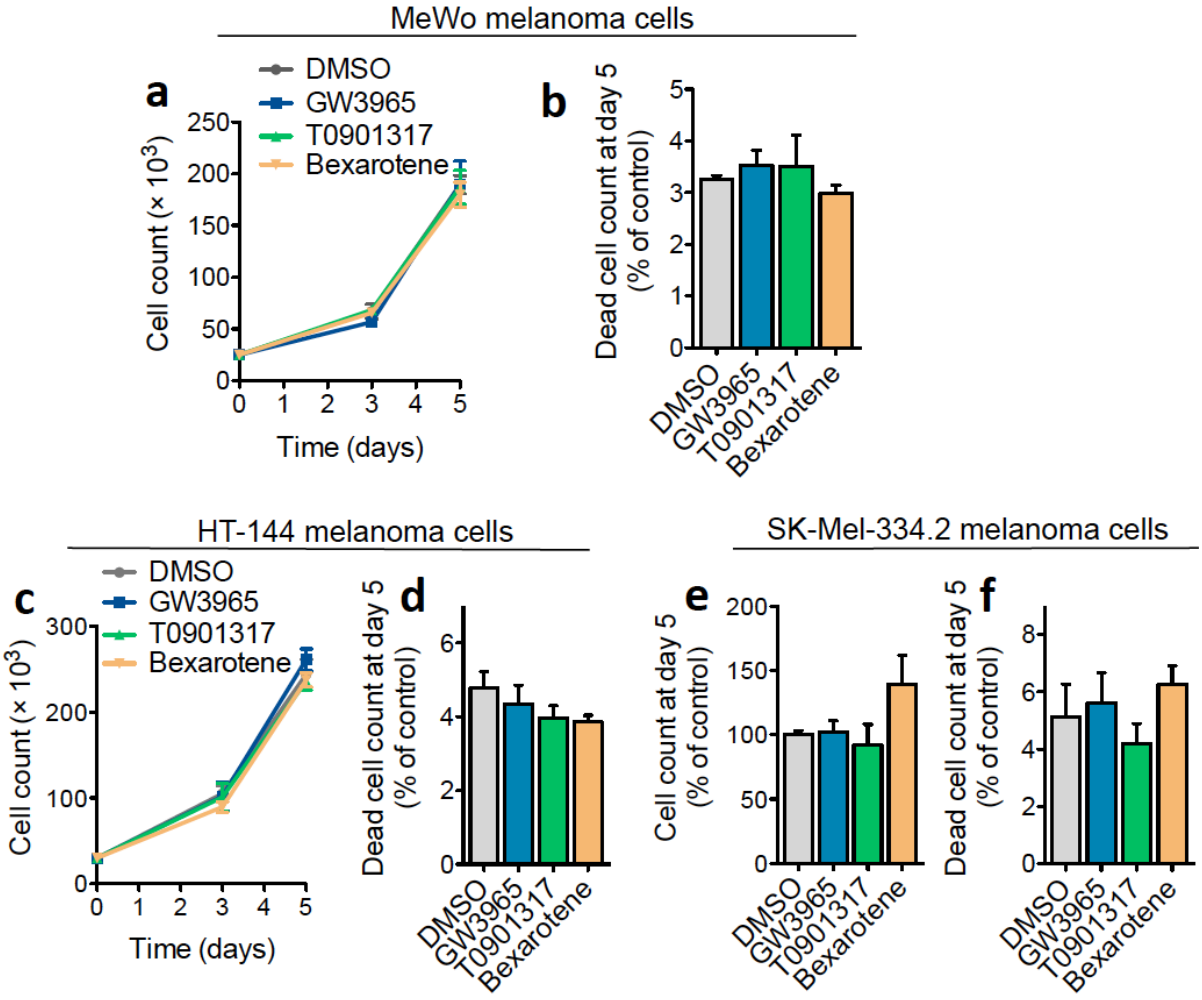

Figure 5.3. Effects of LXR or RXR Agonists on *In Vitro* Melanoma Cell Proliferation and Survival. a-c. 2.5 × 10^4 MeWo (**a-b**), HT-144 (**c-d**), or SK-Mel-334.2 (**e-f**) human melanoma cells were cultured in the presence of DMSO, GW3965, T0901317, or bexarotene at 1 μM. Viable cells were counted on days 0, 3, and 5 post-seeding (**a, c, e**). The number of dead cells was quantified on day 5 post-seeding using the trypan blue dead cell exclusion dye (**b, d, f**). n ≥ 3. Error bars = SEM.

The superiority of LXR activation over RXR agonism in broadly suppressing cell invasion and endothelial recruitment phenotypes prompted us to examine whether LXR signaling in melanoma cells is necessary for the inhibitory effects of GW3965 and T0901317 on this set of *in vitro* phenotypes. To this end, I depleted each of the two *LXR* isoforms in melanoma cells and assessed the phenotypic effects of LXR agonists in the context of *LXRα* or *LXRβ* silencing. Consistent with *LXRβ* being the predominant *LXR* isoform expressed by melanoma cells (Figure 5.1, $P < 0.0001$), I found that knockdown of melanoma-cell *LXRβ*, but not *LXRα*, in two independent melanoma lines prevented the suppression of cell invasion and endothelial recruitment phenotypes incurred by LXR agonist treatment (Figure 5.4). These findings implicate melanoma-cell LXRβ as the primary downstream target and molecular effector of LXR agonists in inhibiting melanoma invasion and endothelial recruitment.

To assess the expression of LXRβ during melanoma progression, we performed double-blinded immunohistochemical analyses for LXRβ protein expression in two independent melanoma tissue-microarray (TMA) progression sets. These experiments, performed and analyzed with the help of Jessica Posada, revealed that LXRβ is ubiquitously expressed in both primary melanoma lesions as well as melanoma metastases (Figure 5.5), consistent with our previous observations of broad LXRβ expression across the NCI-60 series and various primary melanoma cells (Figure 5.1) as well as its previously reported ubiquitous expression in normal tissues (Song et al., 1994). Such pervasive expression of LXRβ during melanoma progression makes this receptor an attractive therapeutic target, as the stable basal presence of LXRβ could allow for a therapeutically broad pharmacologic activation of this target, both in primary tumors as well as in melanoma metastases.

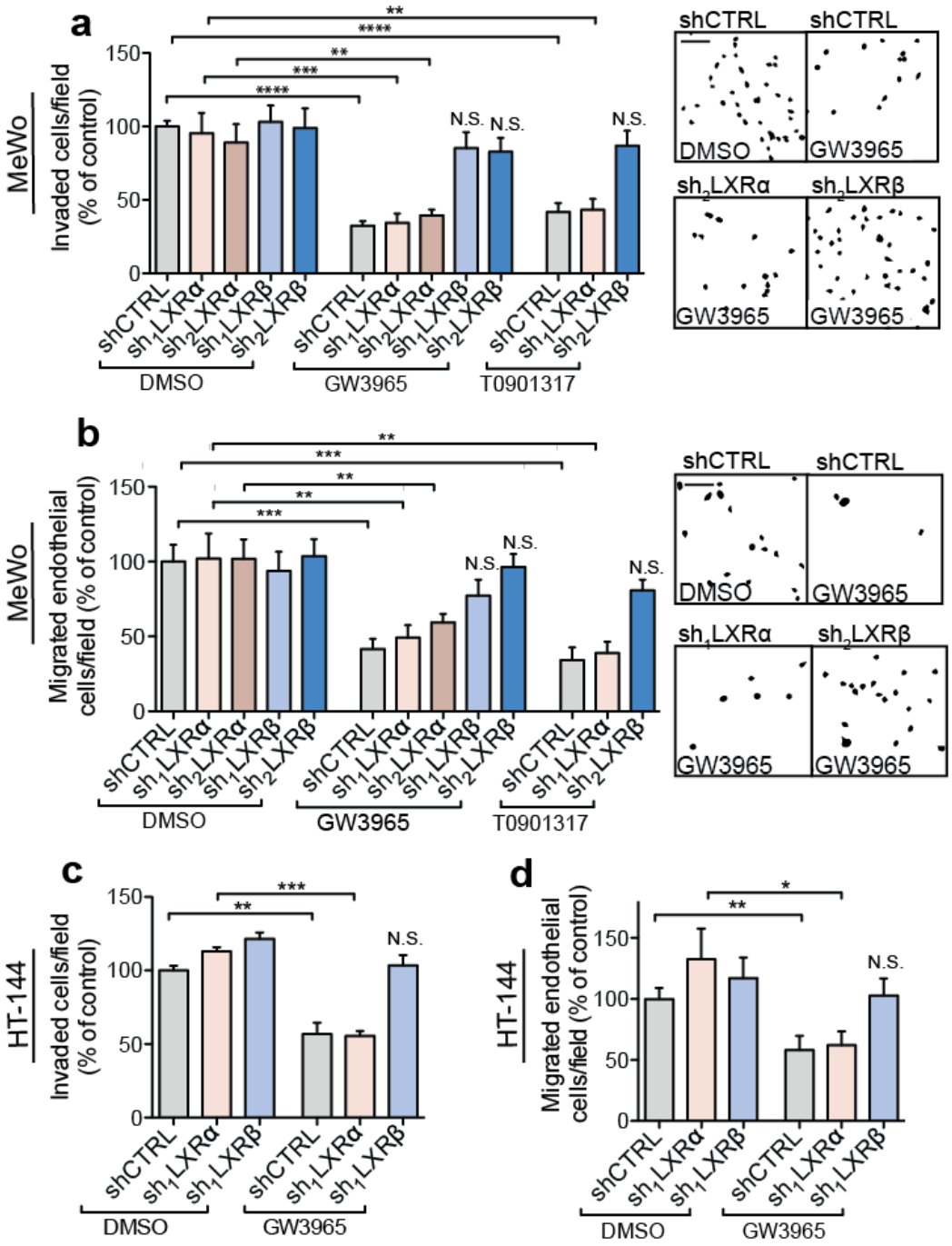

Figure 5.4. LXRβ Mediates Invasion and Endothelial Recruitment Suppression by LXR Agonists. a-d. Matrigel invasion (**a,c**) and endothelial recruitment (**b,d**) by MeWo and HT-144 melanoma cells expressing shRNAs targeting *LXRα* or *LXRβ* or a control shRNA in response to DMSO, GW3965, or T0901317 treatment at 1 μM for 72 hours. n ≥ 4. Scale bar, 50 μm, Error bars = SEM. *p < 0.05, **p < 0.01, ***p < 0.001, ****p < 0.0001. p-values based on unpaired student's t-tests

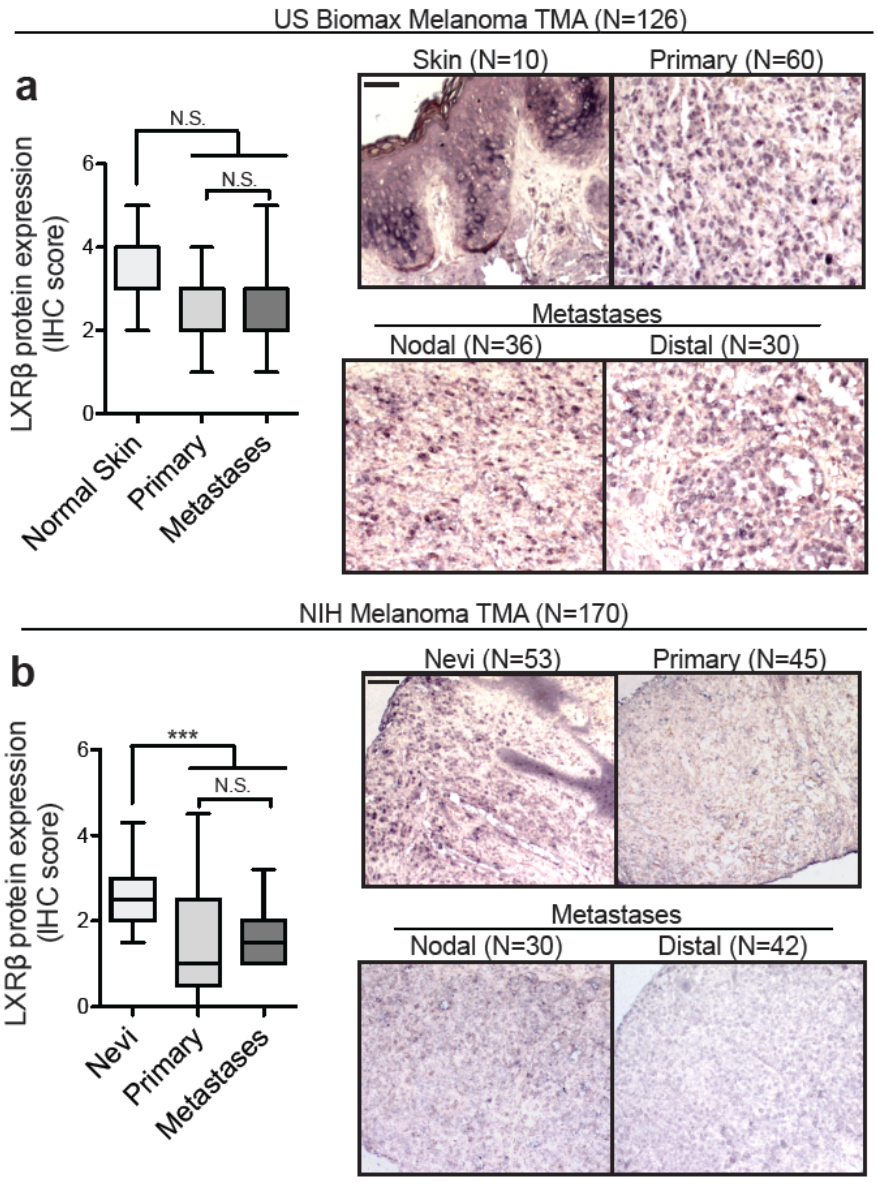

Figure 5.5. Expression of LXRβ during Melanoma Progression. a-b. Box and whisker plots of LXRβ protein expression assessed by double-blinded immunohistochemical analyses of cutaneous melanoma lesions from the US Biomax TMA (**a,** N = 126) and the NIH TMA (**b**, N = 170) melanoma progression sets. Whiskers indicate the 5th to 95th population percentile; box extent corresponds to the 25th-75th population percentile. Scale bars, 50 μm (**a**), 100 μm (**b**). ***p<0.001. p-value based on an unpaired student's t-test.

Oral Delivery of LXR Agonists Inhibits Melanoma Tumor Progression

LXR agonists were originally conceived as orally active drug candidates for the purpose of cholesterol lowering in patients with dyslipidemia (Collins et al., 2002; Joseph and Tontonoz, 2003; Barish and Evans, 2004). However, their clinical development was largely stalled when they were found to lack activity in reducing cholesterol levels in large animal models (Groot et al., 2005). Given the robust activity of LXR agonists in suppressing *in vitro* melanoma progression phenotypes (Figure 5.2), we wondered whether their clinical development could be revived for the management of melanoma progression. To this end, we investigated whether therapeutic delivery of LXR agonists could yield tumor-suppressive activity in various *in vivo* models of melanoma progression. In an extensive series of therapeutic mouse experiments conduced with the help of Colin Buss, we found that orally administering low doses (20 mg/kg) of the independent LXR agonists GW3965 or T0901317, subsequent to tumor formation, suppressed the growth of mouse melanoma tumors in an immunocompetent model by 67% and 61%, respectively (Figures 5.6a-b). Importantly, administering a higher LXR agonist dose (100 mg/kg) reduced tumor growth by 80%, consistent with dose-dependent suppressive effects (Figure 5.6a).

Given the superior potency of GW3965 over T0901317, likely due to the lower EC_{50} of the GW3965 compound for LXRβ (Collins et al., 2002; Schultz et al., 2000), we utilized this LXR agonist for the remainder of our therapeutic experiments. To determine the robustness of LXR agonist treatment in conferring tumor suppression across different melanoma subtypes, we examined its effects on human melanoma progression in multiple mutationally diverse xenograft models. Notably, oral administration of GW3965 substantially suppressed tumor growth by the *B-Raf*/*N-Ras* wild-type MeWo human

melanoma line (70% inhibition, Figure 5.6c) and the *N-Ras* mutant SK-Mel-2 human melanoma cells (49% inhibition, Figure 5.6d), as well as the *B-Raf* mutant SK-Mel-334.2 primary human melanoma line (73% inhibition, Figure 5.6e).

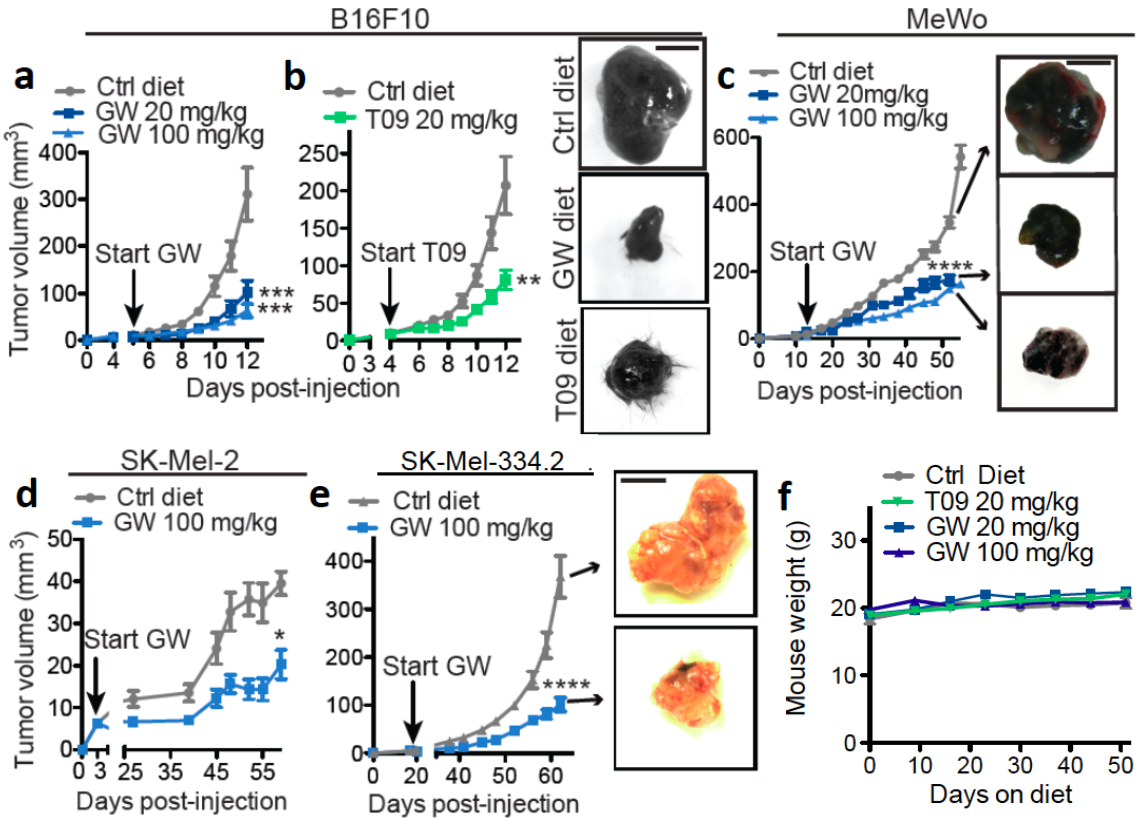

Figure 5.6. Therapeutic Delivery of LXR Agonists Suppresses Melanoma Tumor Growth. a-b. Primary tumor growth by 5×10^4 B16F10 mouse melanoma cells subcutaneously injected into C57BL/6-WT mice. Following tumor growth to 5-10 mm^3 in volume, mice were administered a control chow or a chow supplemented with GW3965 (20 or 100 mg/kg/day) (**a**) or T0901317 (20 mg/kg/day) (**b**). Representative tumor images were taken at the final day 12. n ≥ 10 (**a**); n ≥ 8 (**b**). **c-e.** Primary tumor growth by 1×10^6 MeWo (**c**), 2×10^6 SK-Mel-2 (**d**), and 7.5×10^5 SK-Mel-334.2 (**e**) human melanoma cells grafted onto immunocompromised mice. Following tumor growth to 5-10 mm^3 in volume, mice were randomly assigned to a control diet or a diet supplemented with GW3965. n ≥ 6 (**c**); n = 5 (**d**); n = 8 (**e**). **f**. Weight of mice administered a control diet, T0901317 diet, or GW3965 diet. n ≥ 5. Scale bar, 5 mm. Error bars = SEM. *p < 0.05, **p < 0.01, ***p < 0.001, ****p < 0.0001. p-values based on unpaired student's t-tests.

Importantly, the tumor-suppressive effects of LXR agonists occurred in the absence of any symptomatic animal health deterioration or weight loss in response to the LXR agonist treatment (Figure 5.6f) Our findings of robust melanoma suppression in response to LXR agonist treatment across multiple mutationally diverse human melanoma lines are consistent with broad-spectrum activity of LXR activation therapy in melanoma.

Encouraged by the strong tumor-suppressive impact of LXR agonists on established small tumors (5-10 mm^3) (Figure 5.6), we next investigated whether LXR activation therapy could inhibit the growth of substantially larger (~150 mm^3) melanoma tumors. Notably, oral administration of GW3965 following the formation of tumors measuring at least 150 mm^3 in volume led to a ~50% reduction in B16F10 melanoma tumor growth (Figure 5.7a), suggesting that LXR activation therapy could exhibit activity against more advanced melanoma tumors. We next wondered about the persistence of the LXR agonist-elicited suppression response. To that end, we monitored the long-term progression of GW3965-treated tumors formed by the aggressive MeWo human melanoma line. Even though GW3965 treatment initially delayed tumor growth progression, the tumors resumed to grow at a constant rate for the first seven weeks. Remarkably, upon reaching a critical size of roughly 250 mm^3, the GW3965-treated MeWo tumors exhibited partial regression and their size remained stable beyond 100 days (Figure 5.7b), consistent with long-term effects of the LXR agonist treatment on tumor growth suppression. Importantly, all members of this entire GW-treated cohort remained alive at 120 days (Figure 5.7c). Administration of GW3965 after tumor establishment also prolonged, albeit to a less extent, the overall survival time of immunocompetent mice injected with B16F10 cells as well as immunocompromised mice bearing primary SK-Mel-334.2 human melanoma burden (Figures 5.7d-e).

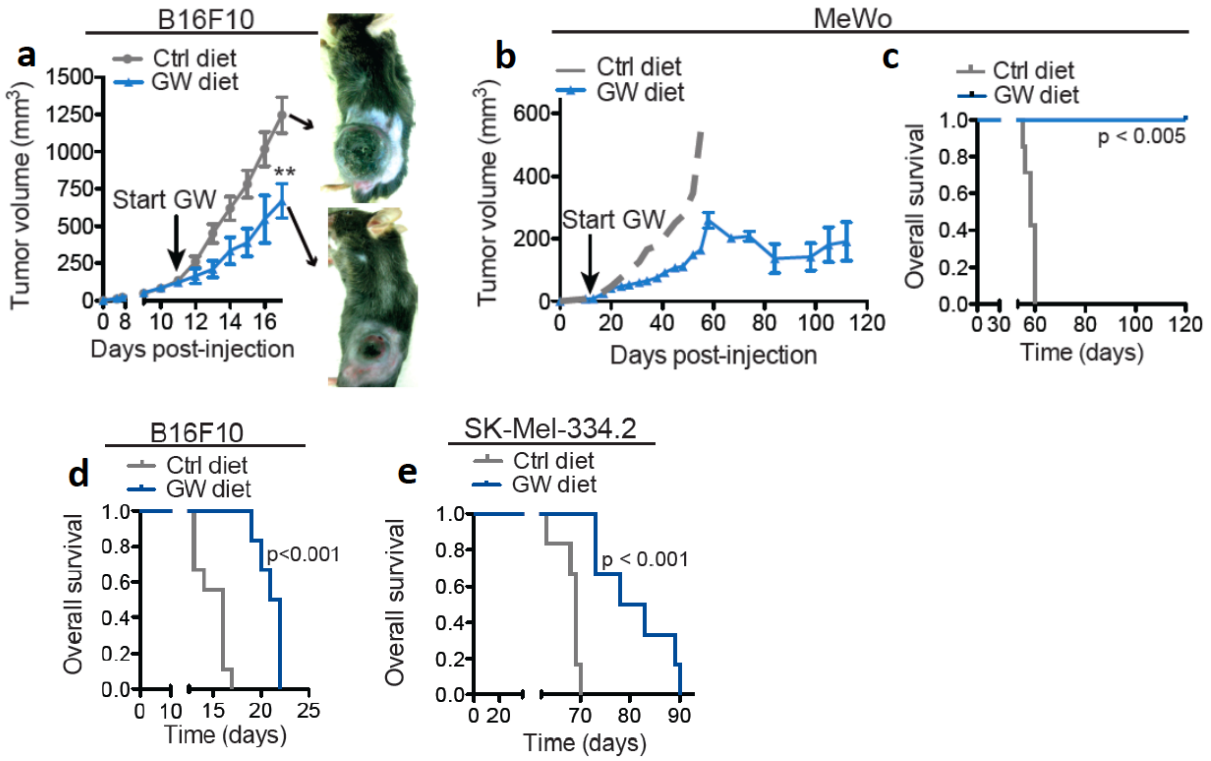

Figure 5.7. Therapeutic Delivery of LXR Agonists Suppresses the Growth of Large Melanoma Tumors, Inhibits Long-Term Tumor Progression, and Extends Animal Survival. a. Tumor growth by 5×10^4 B16F10 cells subcutaneously implanted into C57BL/6-WT mice. Upon tumor growth to 150 mm^3, mice were administered a control chow or a chow containing GW3965 (100 mg/kg). $n \geq 6$. **b.** NOD SCID mice bearing MeWo melanoma tumor burden were monitored for the long-term progression of their GW3965-treated tumors. $n \geq 6$. **c-e.** Overall survival of mice following subcutaneous grafting of 1×10^6 MeWo cells (**c**), 5×10^4 B16F10 cells (**d**), or 7.5×10^5 SK-Mel-334.2 primary melanoma cells (**e**) and treatment of the mice with a control diet or a GW3965-supplemented diet (100 mg/kg) upon formation of tumors measuring 5-10 mm^3 in volume. $n \geq 4$ (**c**), $n \geq 6$ (**d, e**). Error bars = SEM. **$p < 0.01$. p-values based on an unpaired student's t-test (**a**) or Mantel-Cox tests (**c-e**).

We next sought to determine the cellular mechanisms by which LXR agonists suppress tumor growth. Consistent with the suppression of endothelial recruitment upon treatment of melanoma cells with LXR agonists *in vitro*, GW3965 administration substantially reduced the number as well as the size of endothelial vessels present in tumors, as evidenced by staining for two independent endothelial cell markers, CD31 (Figures 5.8a-c) and MECA-32 (Figures 5.8d-f). This was accompanied by a modest decrease (23%) in the number of actively proliferating Ki-67-positive tumor cells *in vivo* (Figure 5.8g) without a change in the number of Caspase-3-positive apoptotic cells (Figure 5.8h). These results suggest that, in addition to reducing melanoma cell invasion, LXR activation suppresses melanoma tumor growth through inhibiting tumor angiogenesis and modestly decreasing *in vivo* tumor cell proliferation.

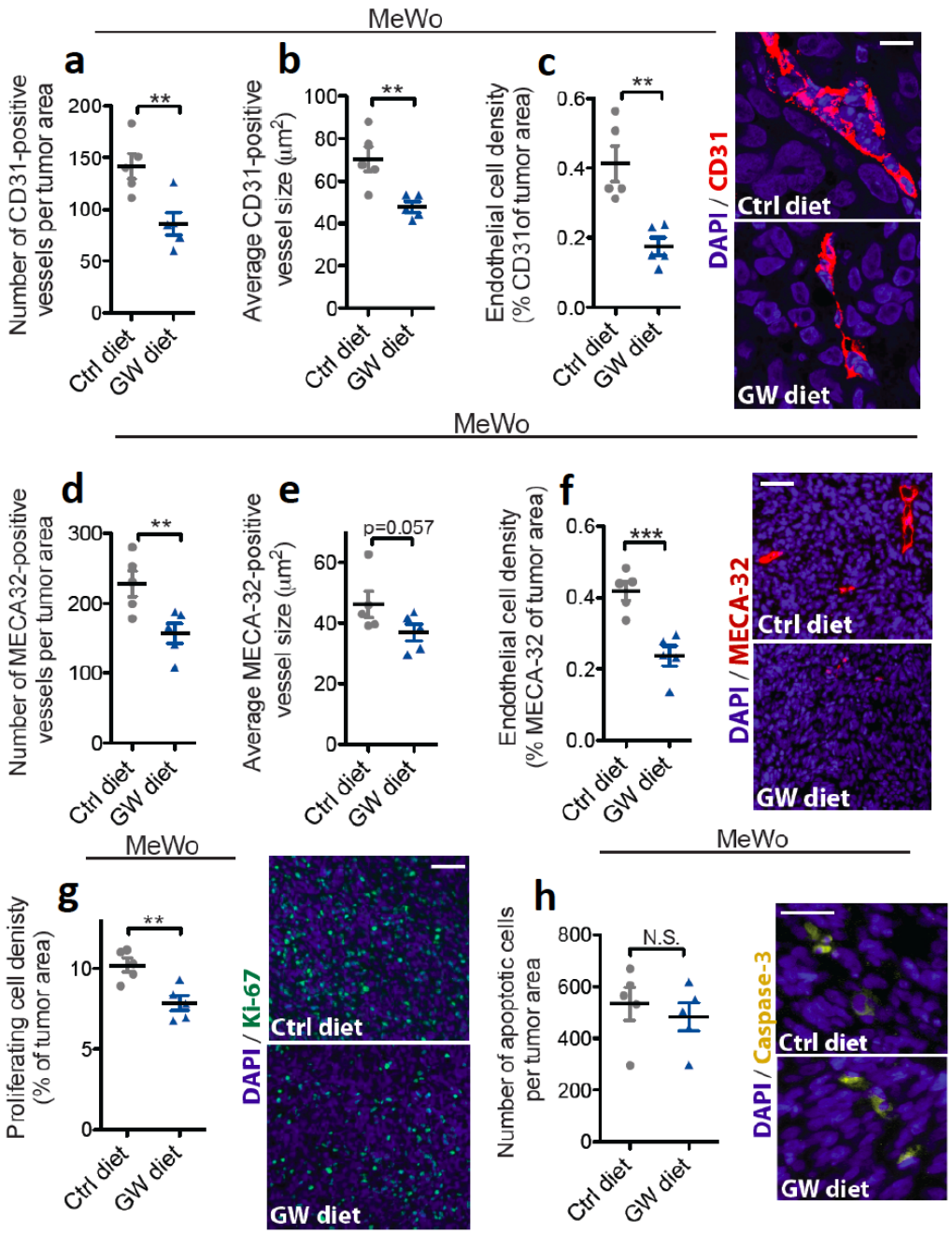

Figure 5.8. LXR Agonist Treatment Suppresses Tumor Angiogenesis. a-f. Average number and size of endothelial vessels and endothelial cell density, as determined by CD31 staining (**a-c**) or MECA-32 staining (**d-f**), in MeWo tumors following mouse treatment with a GW3965-supplemented (20 mg/kg) or control diet for 35 days. n = 5. **g-h**. Number of proliferating (**g**) and apoptotic (**h**) tumor cells, determined by staining for Ki-67 or cleaved caspase-3, respectively, in MeWo tumors in response to GW3965 treatment. n = 5. Error bars = SEM. **p < 0.01, ***p < 0.001. Scale bars, 10 μm (**c**), 50 μm (**f**), 80 μm (**g**), 25 μm (**h**).

LXR Agonist Therapy Suppresses Melanoma Metastatic Progression

In light of the fact that nearly all melanoma patients die due to metastatic spread of their primary tumors and colonization of distal organs such as the lung and the brain (Bhatia et al., 2009), we next examined whether LXR activation could also suppress multi-organ metastatic colonization by melanoma cells. Remarkably, mice that were orally administered GW3965 or T0901317, starting 10 days prior to cancer cells injection, exhibited 31-fold and 23-fold less lung metastatic colonization burden, respectively, from human MeWo cells (Figures 5.9a-b). Treatment with GW3965 also suppressed lung metastatic colonization by the independent HT-144 melanoma line (Figure 5.9c) as well as the SK-Mel-334.2 primary human melanoma line (Figure 5.9d). Importantly, treatment of mice with GW3965 in this 'adjuvant' pre-clinical context significantly prolonged their survival times following metastatic dissemination (Figure 5.9e). These findings from pre-clinical mouse models suggest efficacy of LXR activation therapy for the prevention of melanoma metastasis.

GW3965 is a lipophilic molecule that can efficiently cross the blood-brain barrier and effectively activate LXR signaling in the brain (Jiang et al., 2008). We thus wondered whether LXR agonism could exhibit therapeutic activity for the suppression of melanoma brain metastasis—a devastating outcome affecting ~30% of metastatic melanoma patients, for which there is currently no available targeted therapeutic (Fonkem et al., 2012). Notably, oral administration of GW3965 inhibited both brain metastatic colonization and systemic metastasis following intracardiac injection of brain-metastatic melanoma cells derived by *in vivo* selection of the MeWo parental line (Figure 5.10).

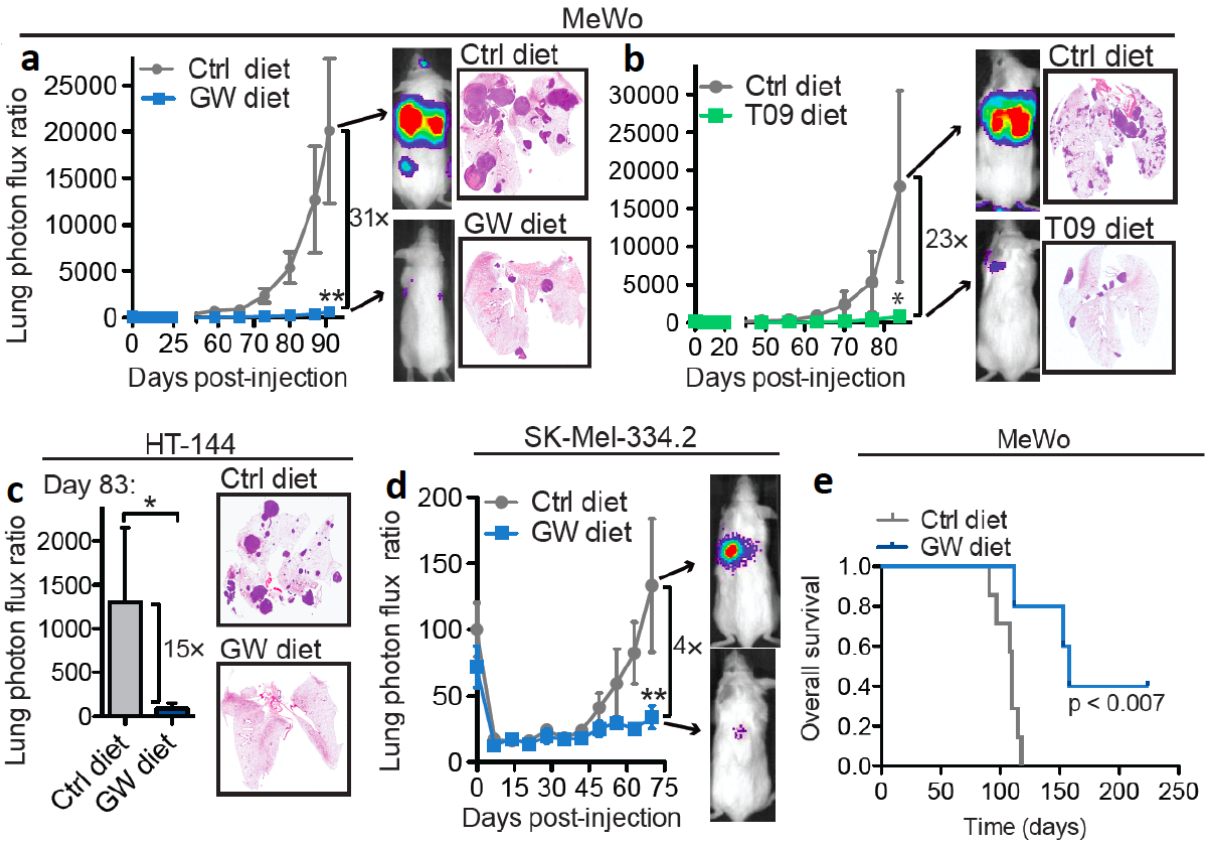

Figure 5.9. Therapeutic LXR Activation Inhibits Lung Metastatic Colonization by Melanoma Cells. a-b. Bioluminescence imaging of lung metastasis by 4×10^4 MeWo cells intravenously injected into NOD SCID mice fed a control chow or a chow containing GW3965 (20 mg/kg) (**a**) or T0901317 (20 mg/kg) (**b**), starting 10 days prior to cancer cell injection. Representative H&E-stained lungs correspond to the final imaging day. $n \geq 5$. **c-d.** Lung metastasis following intravenous injection of 2.5×10^5 HT-144 cells (**c**) and 4×10^4 primary SK-Mel-334.2 melanoma cells (**d**) into NOD SCID mice administered a control chow or a chow supplemented with GW3965 (20 mg/kg), starting 10 days prior to cancer cell injection. $n \geq 5$. **e.** Overall mouse survival following intravenous injection of 4×10^4 MeWo cells into NOD SCID mice that were continuously fed a control chow or a GW3965-supplemented chow (20 mg/kg) starting 10 days prior to cancer cell injection. $n \geq 5$. All data are shown as mean ± SEM. $^*p < 0.05$, $^{**}p < 0.01$. p-values based on Mann-Whitney's t-tests (**a-d**) or Mantel-Cox test (**e**).

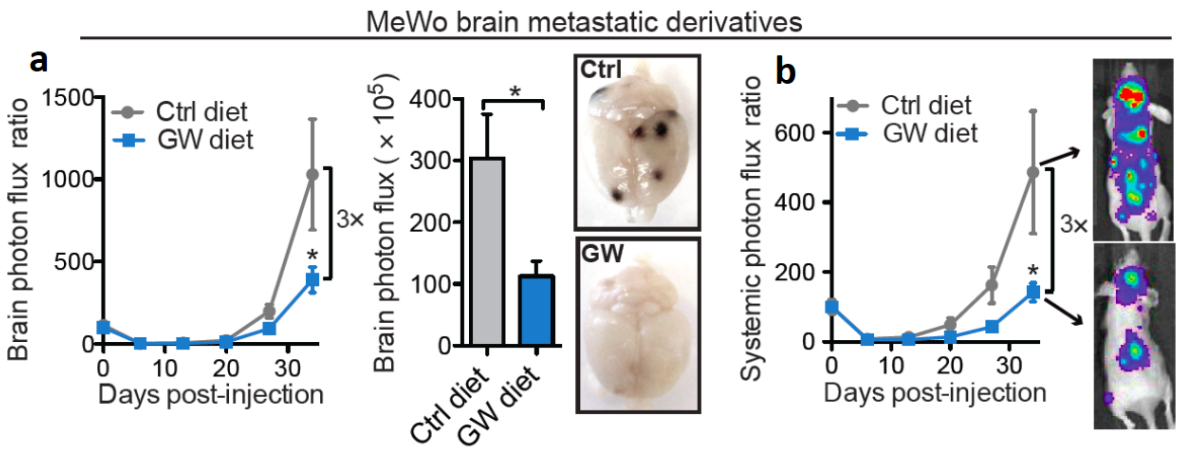

Figure 5.10. LXR Agonist Treatment Suppresses Melanoma Metastasis to the Brain.

a-b. Brain **(a)** and systemic (**b**) photon flux following intracardiac injection of 1×10^5 MeWo brain metastatic derivative cells into athymic nude mice that were fed a control diet or a GW3965-supplemented diet (100 mg/kg) starting on day 0 post-injection. $n \geq 6$. All data are shown as mean ± SEM. *$p < 0.05$, based on Mann-Whitney's t-tests.

Encouraged by the metastasis suppression effects observed in response to LXR agonist treatment initiated 10 days prior to (Figure 5.9) or immediately upon (Figure 5.10) cancer cell injection, we sought to determine whether LXR activation therapy could halt the progression of melanoma cells that had already metastatically disseminated. We first tested the ability of GW3965 to reduce lung colonization by melanoma cells disseminating from an orthotopic site following removal of the primary tumor (Figure 5.11a). Importantly, administration of GW3965 post-tumor resection inhibited lung colonization by 17-fold (Figure 5.11b). We next wondered whether LXR activation therapy could also be effective in inhibiting established melanoma lung metastases. Remarkably, treating mice with GW3965 after incipient metastases had progressed by 8-fold from the baseline at seeding also dramatically suppressed (28-fold) metastatic colonization (Figure 5.11c). Consistent with LXR activation inhibiting metastatic initiation and the frequency of resulting metastatic

events, mice administered the LXR agonist treatment exhibited a reduced number of macroscopic metastatic nodules in the lung (Figures 5.11d).

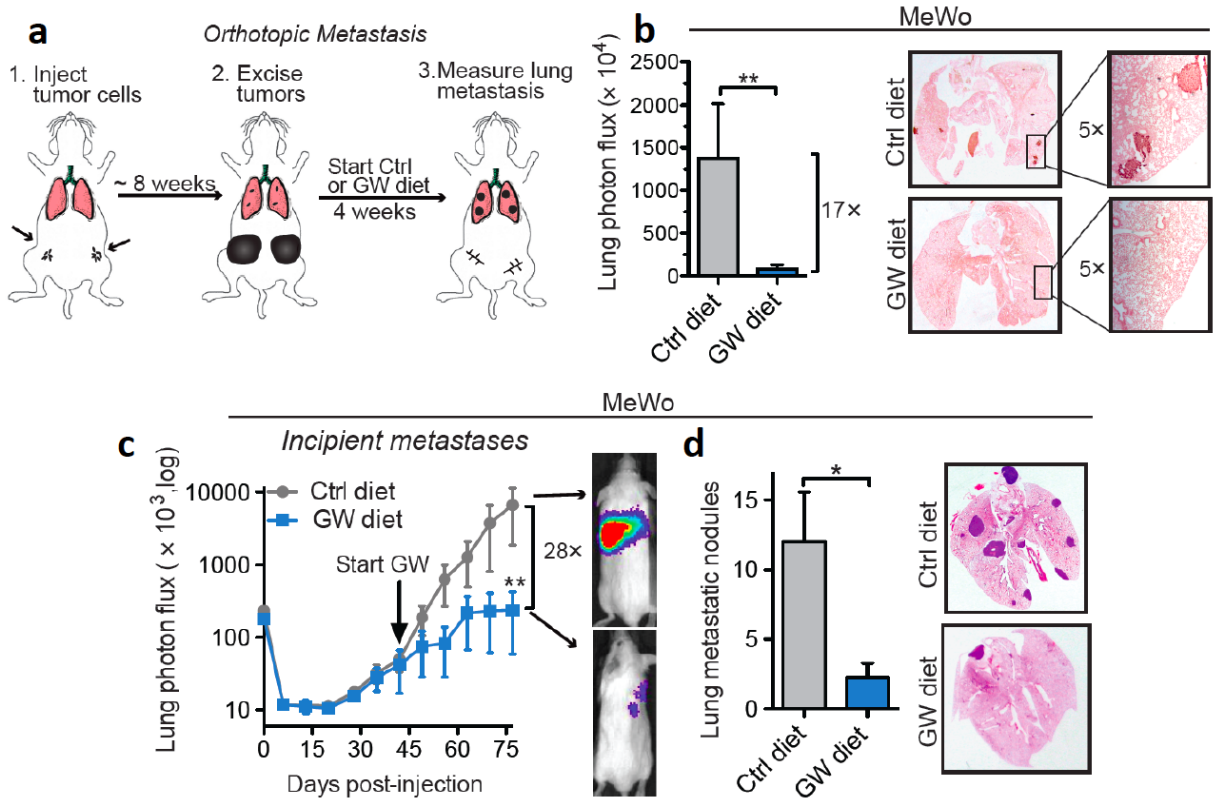

Figure 5.11. LXR Activation Therapy Suppresses Colonization by Disseminated Melanoma Cells and Halts the Progression of Established Metastases. a Schematic of orthotopic metastasis model used to assess the ability of GW3965 treatment to suppress lung metastasis post-tumor excision. **b.** *Ex vivo* lung photon flux, determined by bioluminescence imaging, in NOD SCID mice that were administered a control chow or a chow containing GW3965 (100 mg/kg) for 1 month following the excision of size-matched (~300-mm^3 in volume) subcutaneous tumors formed by 1 × 10^6 MeWo melanoma cells. Representative lung images stained for human vimentin are shown o the right. n ≥ 7. **c**. Lung colonization by 4 × 10^4 MeWo cells intravenously injected into NOD SCID mice. Following formation of metastases, detected by bioluminescence imaging on d42, mice were assigned to a control diet or a GW3965 diet (100 mg/kg). n = 6. **d.** Number of lung macroscopic metastatic nodules quantified at the final day 77 in mice shown in (**c**). n ≥ 4. All data are shown as mean ± SEM. *p<0.05, **p<0.01, based on Mann-Whitney's t-tests (**b, c**) or a student's t-test (**d**).

LXRβ Agonism Suppresses In Vitro Melanoma Progression Phenotypes by Transcriptionally Activating ApoE in Melanoma Cells

We had initially hypothesized that LXRs might inhibit melanoma progression through transcriptionally activating *ApoE*, given that *ApoE* is a known target of LXRs in adipocytes and macrophages (Laffitte et al., 2001). However, whether *ApoE* expression is similarly regulated by LXR signaling in melanoma cells was unknown at the time. Additionally, LXRs can have a wide range of downstream targets, some of which might also be contributing to the suppression of melanoma phenotypes. Therefore, we undertook a systematic approach to determine the downstream molecular target(s) of LXRβ that mediate(s) melanoma suppression. The inhibitory effects of LXR agonists on cell-extrinsic endothelial recruitment by melanoma cells are consistent with the action of a secreted molecule. To identify such factors, we performed whole-genome transcriptomic profiling, which revealed a total of 41 extracellular factors to be significantly induced in human MeWo melanoma cells in response to treatment with the LXR agonist GW3965 (Table 5.1). Out of these, *ApoE* was the top upregulated secreted factor in melanoma cells upon LXR activation. Subsequent validation by qRT-PCR confirmed the upregulation in *ApoE* transcript expression following treatment of multiple melanoma lines with independent LXR agonists (Figure 5.12). GW3965 and T0901317 also enhanced the melanoma cell-driven activity of a luciferase reporter construct containing the *ApoE* promoter fused to either one of two previously characterized LXR-binding multi-enhancer elements (*ME.1* and *ME.2* (Laffitte et al., 2001)), suggestive of direct LXR-mediated transcriptional effects on *ApoE* expression (Figure 5.13a). Consistent with this, chromatin immunoprecipitation (ChIP) analyses confirmed a direct interaction between endogenous LXRβ and the *ApoE* multi-enhancer genomic DNA element in melanoma cells

(Figure 5.13b). Importantly, this transcriptional regulation resulted in elevated levels of both intracellular (Figures 5.13c-e) and secreted ApoE protein (Figures 5.13f-h).

Table 5.1. List of Secreted Factors Significantly Upregulated in MeWo Cells in Response to GW3965 Treatment.

Gene ID	Fold-change*	q-value	Rank	Gene ID	Fold-change*	q-value	Rank
APOE	**4.11**	**1.04E-07**	**1**	IL13RA2	1.30	1.03E-02	22
IGFBP5	2.91	1.15E-13	2	IGFBP7	1.30	2.97E-02	23
TF	2.88	2.37E-12	3	GLIPR1	1.29	2.86E-02	24
FCRLA	2.19	9.13E-09	4	LY96	1.29	2.05E-03	25
ADM	1.88	3.78E-05	5	CBLN3	1.27	1.27E-02	26
CCL2	1.83	1.00E-08	6	SEMA3B	1.26	1.68E-04	27
CEACAM1	1.83	5.58E-06	7	IGFBP3	1.25	3.62E-02	28
SMPDL3A	1.59	2.39E-04	8	CTSK	1.24	2.89E-03	29
APOLD1	1.51	9.50E-05	9	TNFRSF11B	1.24	3.48E-02	30
ERBB3	1.41	3.95E-05	10	CTHRC1	1.23	3.27E-02	31
KIT	1.40	2.31E-04	11	TFPI	1.22	2.83E-02	32
SERPINB2	1.39	2.39E-03	12	PI15	1.20	3.79E-02	33
COL16A1	1.36	1.04E-05	13	UCN2	1.20	9.09E-03	34
HSD17B12	1.36	1.04E-03	14	COL9A3	1.19	4.16E-02	35
EFNA1	1.35	1.14E-02	15	ACTN4	1.18	4.32E-03	36
TNFAIP6	1.35	1.85E-02	16	LTBP3	1.17	4.46E-02	37
DCN	1.35	2.73E-04	17	HSD17B12	1.17	1.59E-02	38
IL7R	1.34	8.62E-04	18	RAGE	1.17	7.09E-03	39
COL1A1	1.34	7.99E-04	19	CYR61	1.16	2.92E-02	40
MMP8	1.33	3.55E-02	20	SEMA6A	1.14	3.89E-02	41
TFF3	1.30	4.51E-03	21				

*Fold-change reflective of fold-upregulation in gene expression in GW3965 versus DMSO cell treatment

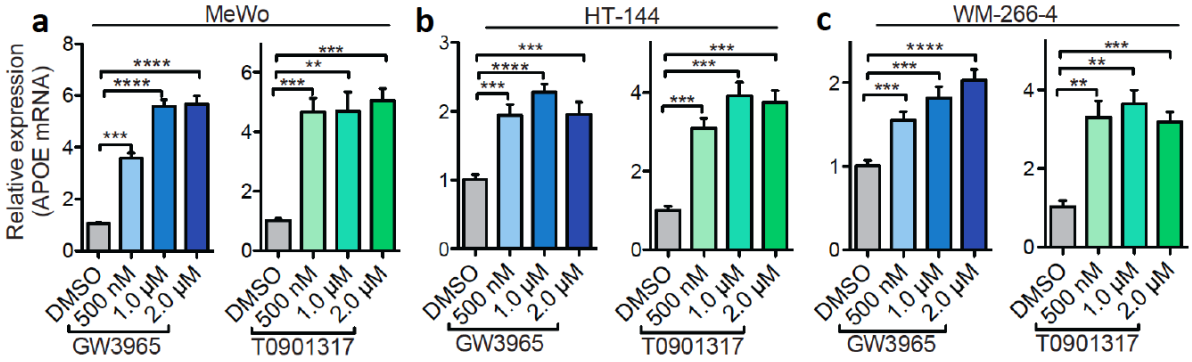

Figure 5.12. Pharmacologic LXR Activation Enhances *ApoE* Transcript Levels.

a-c. MeWo (**a**), HT-144 (**b**), and WM-266-4 (**c**) melanoma cells were treated with GW3965 or T0901317 at the indicated concentrations for 48 hours, and the expression levels of *ApoE* were analyzed by qRT-PCR. n = 3. Error bars = SEM. **p < 0.01, ***p < 0.001, ****p < 0.0001. p-values based on unpaired student's t-tests.

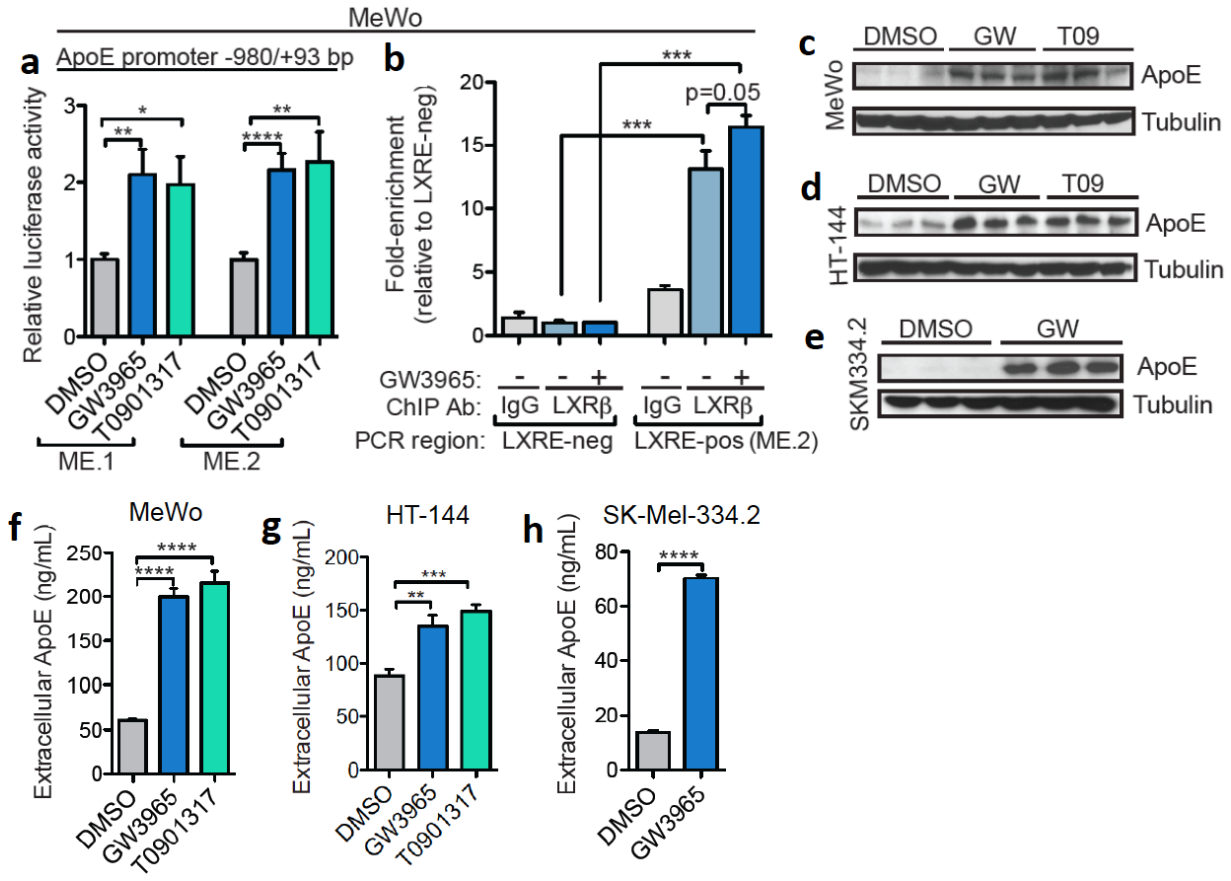

Figure 5.13. LXR Agonism Transcriptionally Activates Melanoma Cell *ApoE* Expression. a. Luciferase activity driven off the *ApoE* promoter fused to multi-enhancer elements ME.1 or ME.2 and transfected into MeWo cells treated with DMSO, GW3965, or T0901317 at 1 μM for 24 hours. n ≥ 4. **b.** ChIP of genomic ME.2 DNA in MeWo cells using an antibody against endogenous LXRβ. The ChIP product was analyzed by qRT-PCR, and data are expressed as the fold-enrichment relative to a genomic region that lacks the LXR binding element (LXRE-neg). MeWo cells were pulsed with DMSO or GW3965 (1 μM) for 8 hours prior to performing ChIP. n=4. **c-e.** Intracellular ApoE protein levels, assessed by western blotting, in MeWo (**c**), HT-144 (**d**), and SK-Mel-334.2 (**e**) human melanoma cells treated with DMSO, GW3965, or T0901317 at 1 μM for 72 hours. Tubulin was used as an endogenous control. n = 3. **f-h.** Extracellular ApoE protein levels were quantified by ELISA in serum-free conditioned media from MeWo (**f**), HT-144 (**g**), or SK-Mel-334.2 (**h**) cells treated with DMSO, GW3965, or T0901317 at 1 μM for 72 hours. n ≥ 3. Error bars = SEM. *p < 0.05, **p < 0.01, ***p < 0.001, ****p < 0.0001, based on unpaired student's t-tests.

In light of the robust transcriptional activation of *ApoE* in melanoma cells upon LXRβ agonism, we next investigated whether ApoE is the functional determinant of the LXRβ -dependent suppression of metastatic phenotypes. We hypothesized that if the suppressive effects of LXR agonists on melanoma invasion and endothelial recruitment are elicited through an increase in ApoE signaling, then blockade of ApoE in the setting of LXR agonism should abrogate these effects. Indeed, we found that neutralization of extracellular ApoE with a blocking antibody (1D7) completely prevented the LXR agonist-mediated suppression of invasion and endothelial recruitment phenotypes across multiple melanoma lines (Figure 5.14), revealing the effects of LXR agonism to be functionally mediated through the downstream induction of extracellular ApoE. Notably, the ApoE antibody treatment further enhanced the melanoma invasion and endothelial recruitment phenotypes relative to the control antibody/DMSO baseline (Figures 5.14), unmasking an important role for endogenous ApoE in suppressing these phenotypes. Consistent with a requirement of endogenous LXRβ for the LXR agonist-dependent ApoE induction, depletion of *LXRβ*, but not *LXRα*, in melanoma cells abrogated the ability of GW3965 and T0901317 to induce *ApoE* transcription and ApoE protein expression (Figure 5.15). Collectively, these findings indicate that pharmacologic activation of LXRβ, the predominant LXR isoform expressed by melanoma cells, suppresses melanoma invasion and endothelial recruitment by melanoma cells through transcriptionally activating *ApoE* expression in melanoma cells.

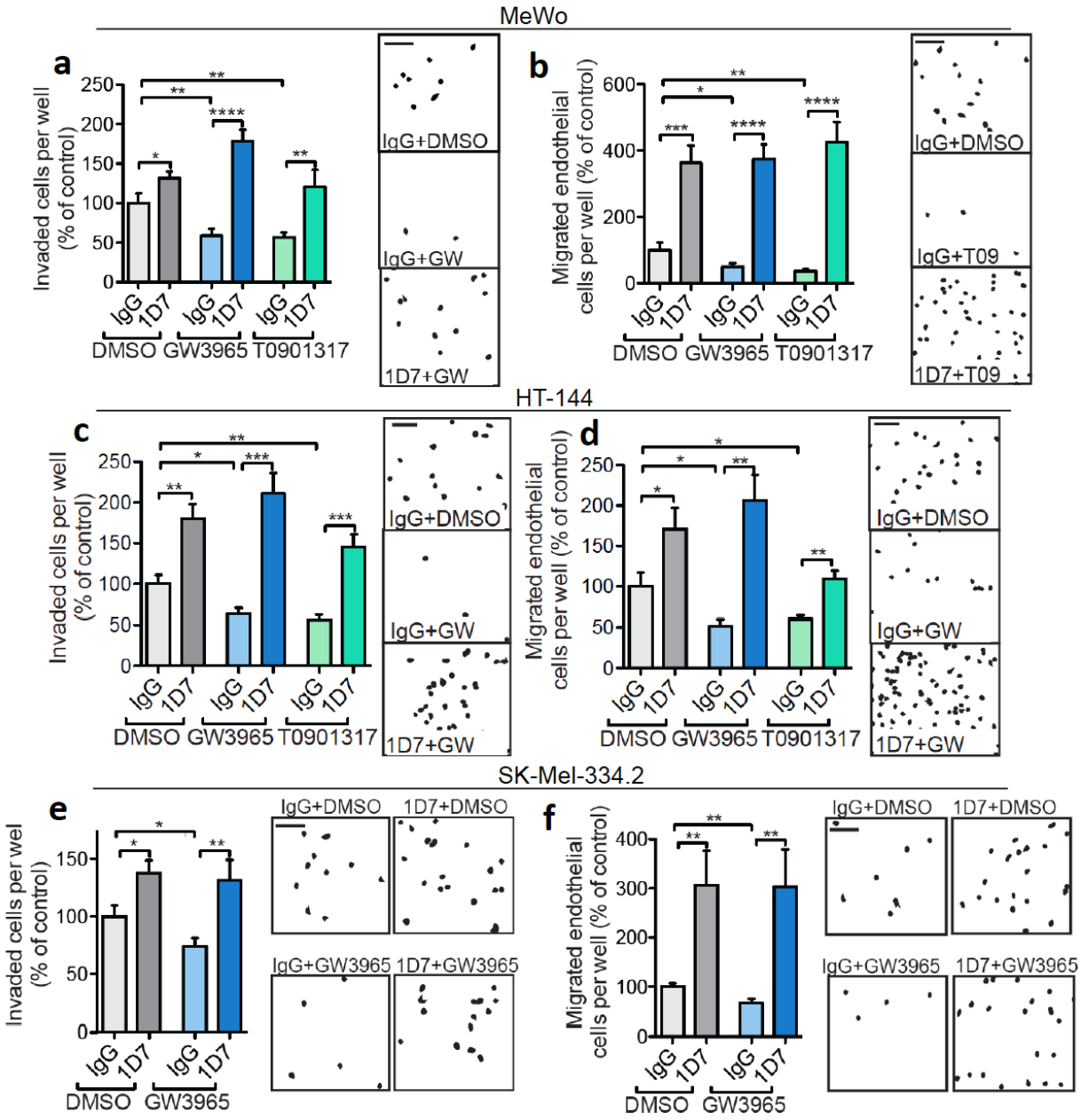

Figure 5.14. ApoE is the Downstream Determinant of LXRβ-Dependent Suppression of Melanoma Invasion and Endothelial Recruitment. a, c, e. Matrigel invasion by 1×10^5 MeWo (**a**), 5×10^4 HT-144 (**c**), and 5×10^4 SK-Mel-334.2 (**e**) melanoma cells, treated with DMSO, GW3965, or T0901317 at 1 μM for 72 hours, in response to 1D7 or IgG antibodies (40 μg/mL). n ≥ 4. **b, d, f.** Endothelial recruitment by 5×10^4 MeWo (**b**), HT-144 (**d**), and SK-Mel-334.2 (**f**) cells, pre-treated with DMSO, GW3965, or T0901317 at 1 μM for 72 hours, in response to 1D7 or IgG antibodies (40 μg/mL). n ≥ 4. Scale bars, 50 μm. Error bars = SEM. *p<0.05, **p<0.01, ***p<0.001, ****p<0.0001, based on unpaired student's t-tests.

Figure 5.15. LXRβ is Required for LXR Agonist-Mediated Transcriptional *ApoE* Induction. Relative expression of *ApoE* mRNA (**a-b**) and extracellular ApoE protein (**c-d**) in MeWo (**a, c**) and HT-144 (**b, d**) melanoma cells transduced with shRNAs targeting *LXRα, LXRβ,* or a control and treated with DMSO, GW3965, or T0901317 at 1 μM for 48 (**a-b**) or 72 (**c-d**) hours. n ≥ 3. **e.** Luciferase-based activity of the *ApoE* promoter fused to ME.1/ME.2 enhancer elements and transfected into MeWo melanoma cells expressing shRNAs against *LXRα, LXRβ*, or a control in the presence of DMSO or GW3965 (1μM) for 24 hours. n ≥ 3. All data are shown as mean ± SEM.*p < 0.05, **p < 0.01, ***p < 0.001, ****p < 0.0001. p-values based on unpaired student's t-tests.

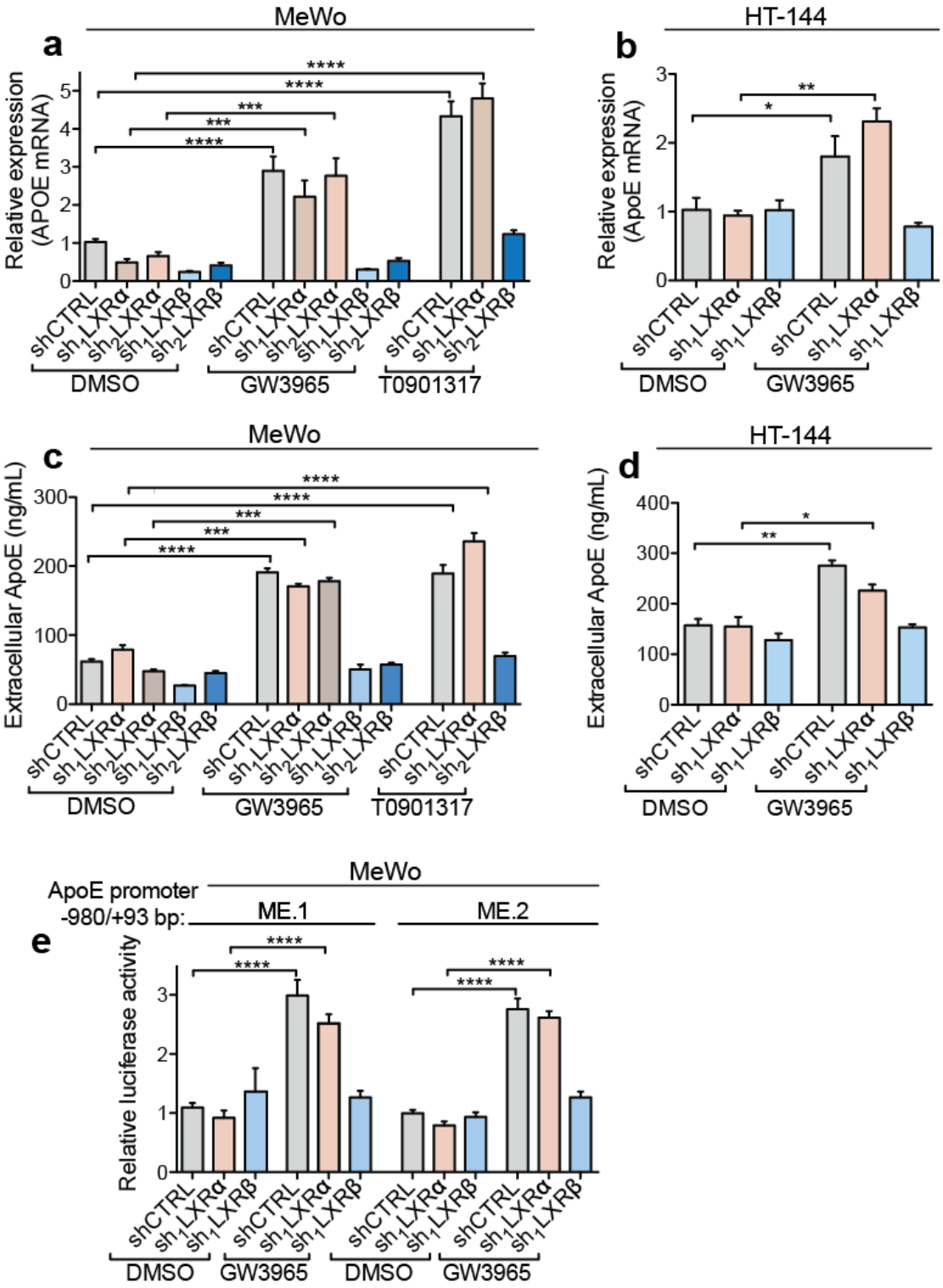

Figure 5.15. LXRβ is Required for LXR Agonist-Mediated Transcriptional *ApoE* Induction.

LXRβ Agonism Suppresses In Vivo Melanoma Progression through the Engagement of both Melanoma-Derived and Stromal ApoE

In the *in vivo* LXR activation therapy experiments, the orally delivered LXR agonists can act systemically, exerting effects on both melanoma cells as well as various stromal tissues, which express LXRβ. Given the observed suppression of key melanoma phenotypes by extracellular ApoE *in vitro,* we hypothesized that the suppressive effects of LXR agonists *in vivo* might be further augmented by the activation of LXRs in peripheral tissues, which could serve as robust sources of extracellular ApoE released into the circulation. We thus investigated whether the suppression in melanoma tumor progression *in vivo*, attained upon LXR agonist treatment, is mediated by ApoE derived from melanoma cells or that derived from stromal tissues. Consistent with LXRβ agonism increasing *ApoE* expression in melanoma cells *in vivo*, *ApoE* transcript levels were upregulated in melanoma primary tumors as well as in melanoma lung and brain metastases dissociated from mice that were fed a diet containing LXR agonists (Figures 5.16a-d). Additionally, treatment of mice with either GW3965 or T0901317 significantly elevated ApoE protein expression in systemic adipose, lung, and brain tissues of mice (Figures 5.16e-f) and also upregulated *ApoE* transcript levels in circulating white blood cells (Figure 5.16g). These results indicate that LXR agonist-based therapy globally activates ApoE expression in both the tumoral and stromal tissue compartment, as indicated by the elevated expression levels of ApoE across melanoma tumors, metastases, as well as various peripheral stromal tissues following *in vivo* LXR agonist treatment of mice.

Figure 5.16. LXR Agonist Therapy Activates Melanoma-Derived and Stromal *ApoE* Expression. a-c. *ApoE* transcript levels in primary tumors (**a**), lung metastases (**b**), and brain metastases (**c**) formed by MeWo human melanoma cells following grafting of the cells onto immunocompromised mice that were administered a control chow or a chow supplemented with GW3965. *ApoE* levels were assessed on day 35 (**a**), day 153 (**b**), or day 34 (**c**) post-injection of the cancer cells, respectively. $n \geq 3$. **d.** *ApoE* expression levels, quantified by qRT-PCR, in subcutaneous tumors formed by B16F10 mouse melanoma cells injected into C57BL/6-WT mice. Upon 5-10 mm^3 tumor formation, mice were fed a control diet or a diet containing GW3965 or T0901317 at 20 mg/kg for 7 days. $n \geq 3$. **e.** Western blot measurements of ApoE protein levels in adipose, lung, and brain tissue lysates extracted from immunocompromised mice that were administered a control chow or a chow supplemented with GW3965 (20 mg/kg) or T0901317 (20 mg/kg) for 10 days. **f.** Quantification of ApoE protein expression based on western blots shown in (**e**)**.** Total tubulin was used as an endogenous control for normalization. $n \geq 3$. **g**, Expression levels of *ApoE*, determined by qRT-PCR, in circulating white blood cells collected from NOD SCID mice that were fed a control diet or a diet supplemented with GW3965 or T0901317 at 20 mg/kg for 10 days. $n \geq 3$. All data are displayed as mean ± SEM. $^*p < 0.05$; $^{**}p < 0.01$; $^{***}p < 0.001$. p-values based on unpaired student's t-tests.

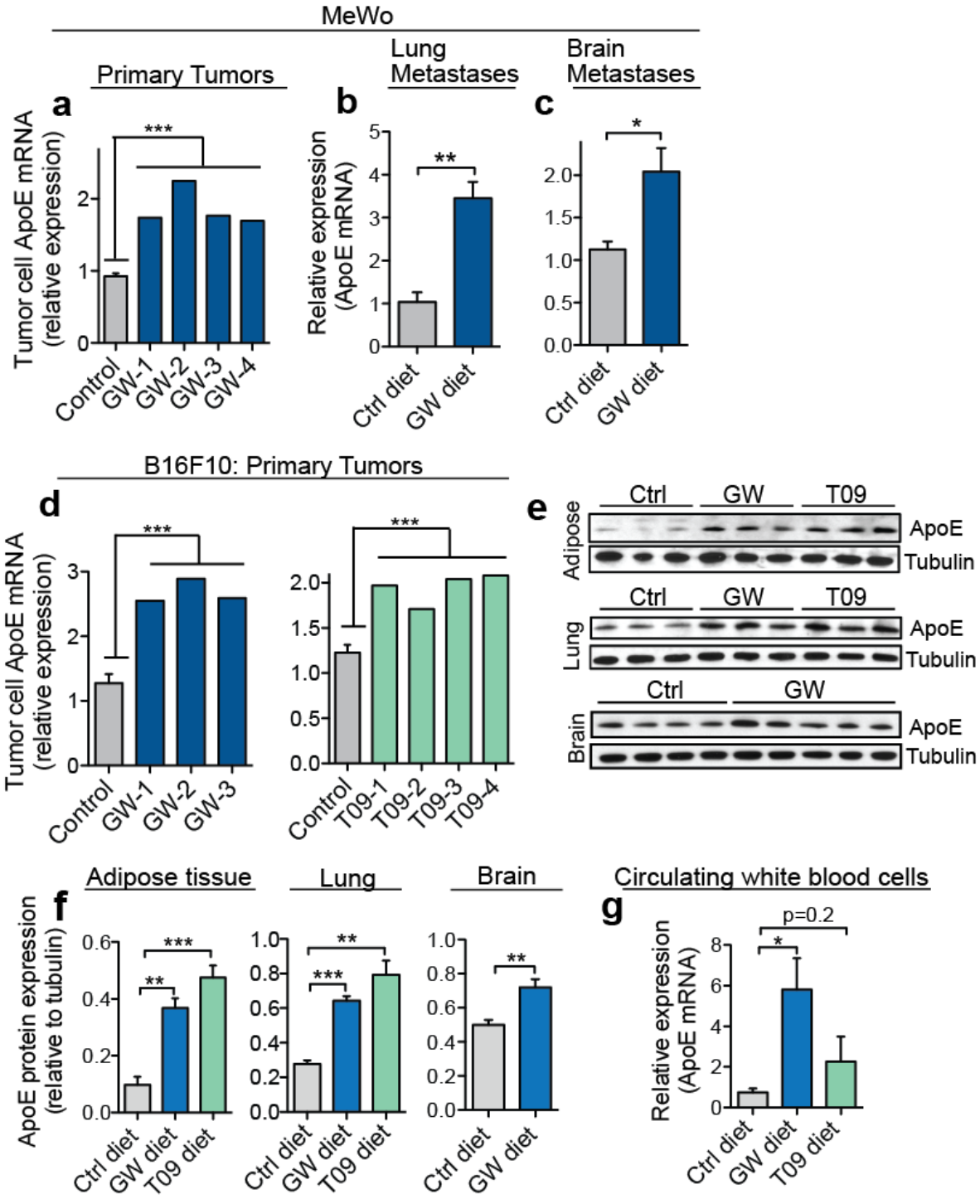

Figure 5.16. LXR Agonist Therapy Activates Melanoma-Derived and Stromal *ApoE* Expression.

We next sough to determine the relative contribution of ApoE produced by melanoma cells versus that of ApoE supplied by stromal tissue compartments to the suppression of melanoma progression upon LXR activation therapy. We first focused on tumor growth. Interestingly, GW3965 fully inhibited the growth of primary tumors formed by *LXRβ*-depleted melanoma cells (Figure 5.17a,d), indicating that loss of melanoma cell *LXRβ* is dispensable for the LXR-mediated growth inhibition and implicating a role for melanoma-extrinsic (stromal) LXR activation in tumor suppression by GW3965. To identify the LXR isoform that mediated this non-tumor autonomous melanoma suppressive effect, we examined the effects of GW3965 on tumors implanted onto *LXRα* or *LXRβ* genetically null mice (Peet et al., 1998). Importantly, genetic inactivation of stromal *LXRβ* rendered GW3965 completely ineffective, while *LXRα* inactivation had no effect on the ability of GW3965 to suppress tumor growth (Figure 5.17d). Consistent with LXRβ being the main molecular target and effector of GW3965 in mediating ApoE-dependent melanoma tumor growth suppression, GW3965 failed to induce *ApoE* expression in circulating white blood cells collected from *LXRβ* null mice, but not from *LXRα* null mice (Figure 5.17b). This LXRβ dependency was not restricted to *ApoE* expression since *ABCA1* (a well-characterized LXR target gene (Laffitte et al., 2001)) showed comparable upregulation in circulating *LXRα* -/- white blood cells, but not in *LXRβ* -/- cells, in response to the GW3965 treatment (Figure 5.17c), consistent with this agonist's 6-fold greater activity towards LXRβ over LXRα.

In agreement with our findings that tumor growth suppression is primarily mediated by stromal LXRβ activation, we observed that genetic inactivation of stromal *ApoE* fully rescued the LXR agonist-based suppression in melanoma tumor growth (Figure 5.17e). Accordingly, depletion of *ApoE* in melanoma cells had no effect on GW3965-induced tumor

growth suppression (Figure 5.17a,e). These findings reveal that the tumor-suppressive effects of GW3965 are primarily mediated through stromal LXRβ activation and the resulting induction of extracellular ApoE derived from various peripheral tissues and supplied to the tumor via the circulation and/or ApoE produced by local stromal cells present in the tumor microenvironment. To this end, we sought to identify specific stromal cell types in the tumor microenvironment that induce ApoE in response to LXRβ activation and may thus contribute to melanoma suppression. In immunohistochemical co-localization experiments conducted by Jessica Posada, we found that GW3965 treatment significantly upregulated ApoE protein expression within tumor-infiltrating macrophages (~2.6-fold) and leukocytes (~2-fold) and modestly increased endothelial cell ApoE expression (~1.2-fold) (Figure 5.18).

In contrast to primary tumor growth regulation, neither knockdown of melanoma cell *ApoE* nor genetic inactivation of stromal *ApoE* completely occluded the effects of GW3965 on metastasis suppression (Figure 5.19a). The metastasis-suppressive activity of the GW3965 treatment was entirely prevented only upon combined silencing of both melanoma-derived and stromal *ApoE* (Figure 5.19a). Based on these findings, we conclude that while tumor growth inhibition is primarily driven by *ApoE* induction in stromal cells, metastasis suppression by GW3965 is elicited through the activation of both stromal and melanoma-derived *ApoE*. Tissue-specific differences in microenvironmental *ApoE* expression levels in the lung relative to the skin could explain the differential contribution of melanoma-derived *ApoE* to tumor growth versus metastasis suppression (Figure 5.19b).

Figure 5.17. Activation of Stromal LXRβ Inhibits Melanoma Tumor Growth through Induction of Stromal *ApoE*. a. Expression of *LXRα*, *LXRβ*, and *ApoE* mRNA in B16F10 cells expressing a control hairpin or an shRNA targeting *LXRα*, *LXRβ*, or ApoE. **b-c.** *ApoE* (**b**) and *ABCA1* (**b**) mRNA levels in circulating white blood cells extracted from *LXRα* -/- or *LXRβ* -/- mice that were administered a control diet or a GW3965 diet (20 mg/kg) for 10 days. $n \geq 3$. **d.** B16F10 control cells or B16F10 cells expressing shRNAs targeting *LXRα* or *LXRβ* were subcutaneously injected into C57BL/6-WT, *LXRα*-/-, or *LXRβ*-/- mice. Once the tumors reached 5-10 mm^3 in volume, mice were fed a control diet or a diet supplemented with GW3965 (20 mg/kg) for 7 days, after which final tumor volume was measured. Representative tumor images extracted at the end point are shown in the right panel. $n \geq 6$. **e.** Subcutaneous tumor growth by 5×10^4 B16F10 control cells or B16F10-sh*ApoE* cells grafted onto C57BL/6-WT or *ApoE*-/- mice. Following the formation of tumors measuring 5-10 mm^3 in volume, mice were fed a control diet or a diet supplemented with GW3965 (20 mg/kg) for 7 days, and final tumor volume was quantified. $n \geq 8$. All data are displayed as mean ± SEM. Scale bar, 5 mm. *$p < 0.05$, **$p < 0.01$, ***$p < 0.001$. p-values based on unpaired student's t-tests.

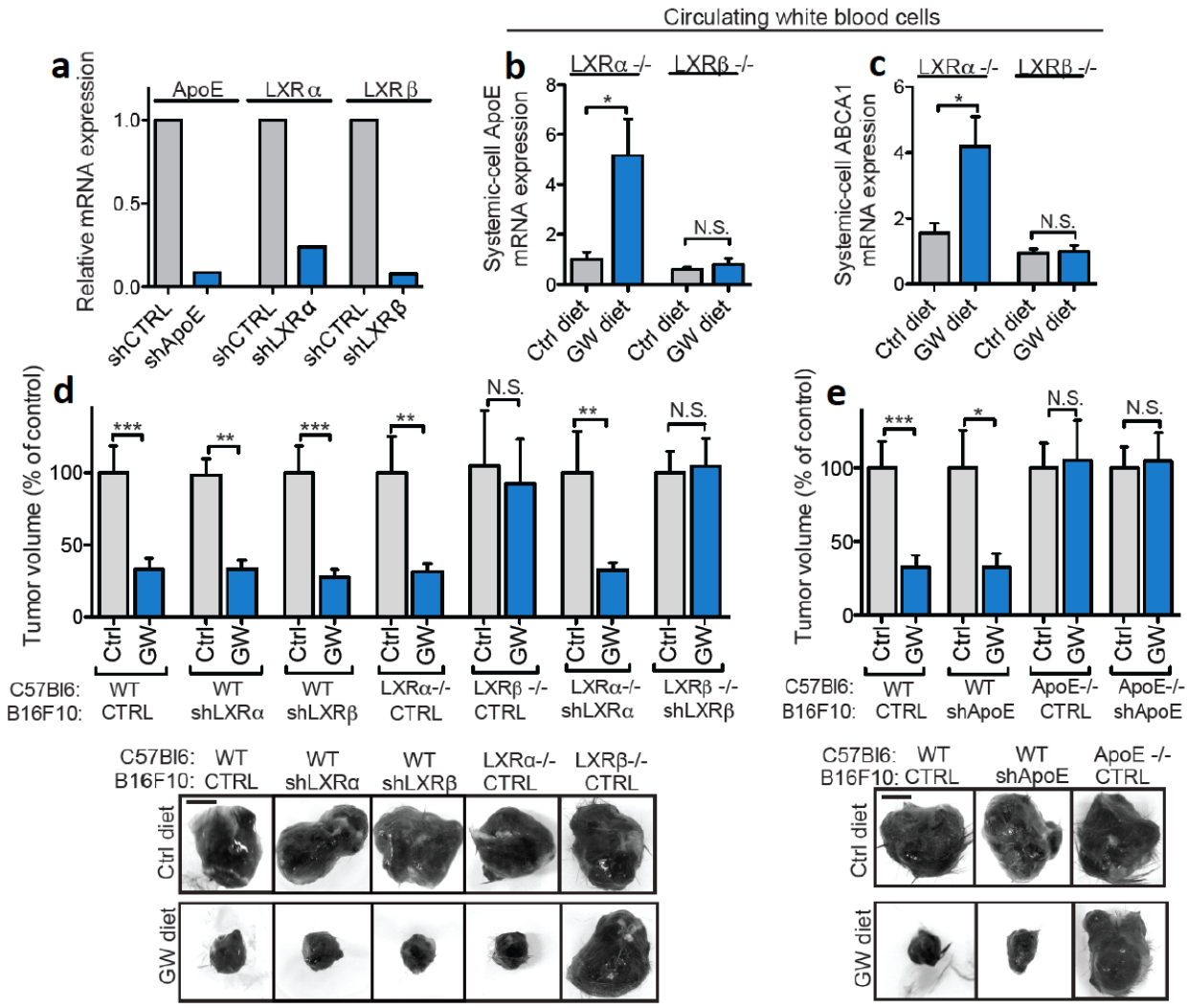

Figure 5.17. Activation of Stromal LXRβ Inhibits Melanoma Tumor Growth through Induction of Stromal *ApoE*.

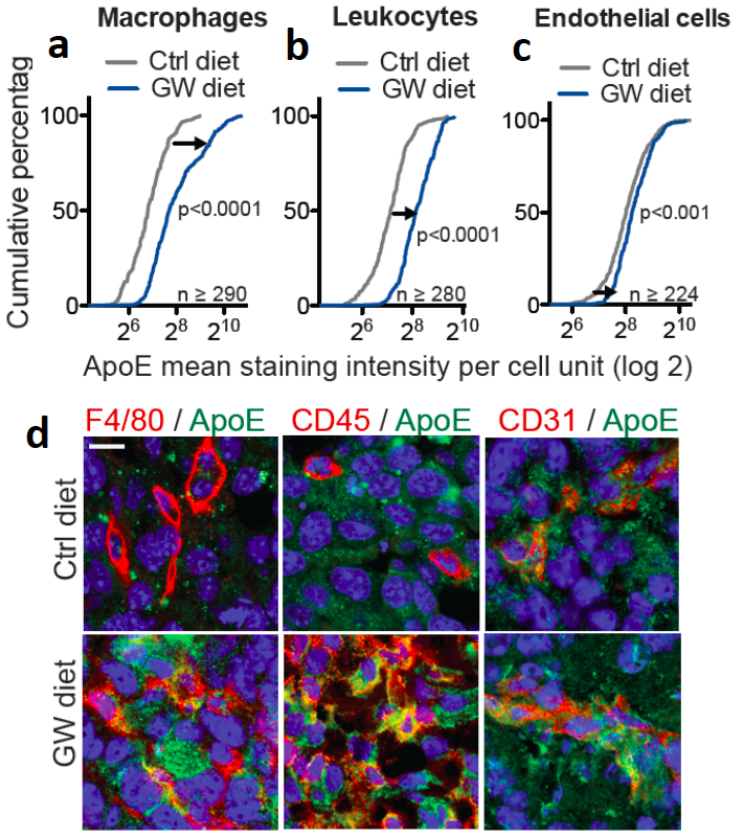

Figure 5.18. Identification of Stromal Cells in the Tumor Microenvironment that Upregulate ApoE upon LXR Agonist Treatment. a-c. Cumulative percentage plots depicting mean ApoE staining intensity per cell unit within F4/80-postivie macrophages (**a**), CD45-positive leukocytes (**b**), and CD31-postivie endothelial cells (**c**) in B16F10 subcutaneous tumors in response to mouse treatment with a control diet or a GW3965 diet. n ≥ 290 cells (**a**), n ≥ 280 cells (**b**), n ≥ 224 cells (**c**). **d.** Representative confocal images showing ApoE co-localization with macrophages (F4/80), leukocytes (CD45), and endothelial cells (CD31). Scale bar, 10 μm. p-values based on Kolmogorov-Smirnov tests.

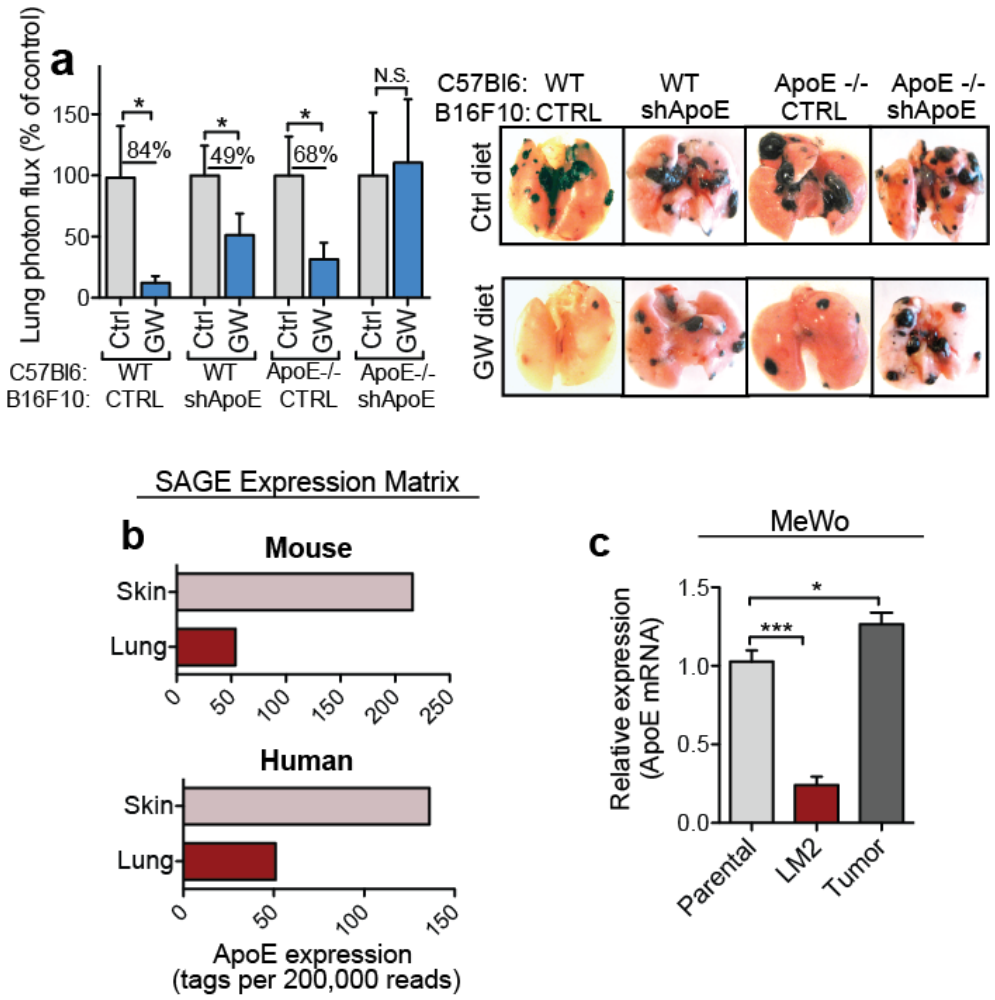

Figure 5.19. LXRβ Therapy Engages both Melanoma-Intrinsic and Stromal *ApoE* in Metastasis Suppression. a. Lung colonization by 5×10^4 B16F10 cells transduced with a control shRNA or sh*ApoE* and intravenously injected into C57BL/6-WT or *ApoE*-/- mice. Ten days prior to cancer cell injection, mice were assigned to a control diet or a GW3965 diet (20 mg/kg) treatment. Representative lungs extracted at the end point (d22) are shown in the right panel. n ≥ 5. **b.** Relative expression of *ApoE* mRNA, expressed as the frequency of SAGE tags, in mouse and human skin and lung tissues was determined using the publicly available mouse and human SAGE Expression Matrix databases accessible through the NCI-funded Cancer Genome Anatomy Project (CGAP). **c.** *ApoE* mRNA expression levels in parental MeWo cells or *in vivo* selected MeWo cells dissociated from lung metastatic nodules (LM2) or primary tumors. n = 3. All data are displayed as mean ± SEM. *$p < 0.05$, ***$p < 0.001$. p-values based on Mann Whitney's t-tests (**a**) or unpaired student's t-tests (**c**).

For instance, a primary melanoma tumor that is exposed to high extracellular levels of stromally supplied ApoE may fail to respond to the relatively weak ApoE signal coming from the tumor itself. In contrast, melanoma metastases at a distal site such as the lung, which has lower relative ApoE tissue abundance, would be expected to be more sensitive to melanoma-secreted ApoE. Consistent with this, the relative levels of *ApoE* in both human and mouse lung are three to four-fold lower than its respective expression in human and mouse skin (Figure 5.19b). Additionally, tumorigenic and metastatic melanoma cells face differential selective pressures for *ApoE* silencing. Whereas *in vivo* selected metastatic melanoma cells dissociated from mouse lung nodules exhibited a 4-fold reduction in *ApoE*, melanoma cells dissociated from primary tumors were not found to downregulate *ApoE* (Figure 5.19c). These findings from *in vivo* selection are consistent with our genetic and molecular findings on *ApoE*'s role in primary tumor growth: with microenvironmental/ stromal *ApoE* exerting a dominant influence on tumor growth suppression. Metastasis contrasts this: we found that *in vivo* selected melanoma metastases were dependent on melanoma cell *ApoE* silencing, and their progression was impaired by melanoma-autonomous re-activation of *ApoE* in addition to stromal induction of extracellular ApoE.

LXRβ Therapy Inhibits Melanoma Progression in a Genetically Initiated Melanoma Model

To further evaluate the robustness of LXRβ activation as a new therapeutic approach in melanoma, we examined the efficacy of LXR agonist therapy in a genetically-initiated mouse model of melanoma progression driven by mutational alterations frequently found in human melanomas—activation of the *B-Raf* oncogene and loss of the *Pten* tumor-suppressor.

Nearly 60% of human melanoma tumors are marked by activating mutations in the *Braf* oncogene, with one single amino acid variant, *B-Raf*^{V600E}, being the predominant mutation found (Davies et al., 2002). Roughly 20-40% of melanomas exhibit activating mutations in *B-Raf* with concurrent silencing of the *Pten* tumor-suppressor, which drives progression to a malignant melanoma state (Hodis et al., 2012). Recently, *Tyrosinase* (*Tyr*)-driven conditional *B-Raf*^{V600E} expression and *Pten* loss were shown to cooperate in driving mouse melanoma progression (Dankort et al., 2009). We thus investigated whether LXR activation could suppress melanoma progression in this genetically initiated melanoma model. Notably, oral administration of GW3965 following melanoma initiation attenuated tumor progression and significantly prolonged the overall survival times of both *Pten* heterozygous *(Pten*$^{lox/+}$*)* and *Pten* null (*Pten*$^{lox/lox}$*) Tyr::CreER; B-Raf*$^{V600E/+;}$ mice (Figure 5.20). Next, we examined the ability of GW3965 to suppress melanoma metastasis in this genetic context. While we did not detect macroscopic metastases in the lungs or brains of *Tyr::CreER; B-Raf*$^{V600E/+;}$ *Pten*$^{lox/lox}$ mice at the late stages of melanoma progression, we consistently observed melanoma metastases to the salivary gland lymph nodes. Importantly, *Tyr::CreER; B-Raf*$^{V600E/+;}$ *Pten*$^{lox/lox}$ mice treated with GW3965 exhibited a significant reduction in the number of lymphatic metastases detected post-mortem (Figure 5.20). These findings indicate that LXR activation inhibits orthotopic metastasis in a genetically driven melanoma model, in addition to its suppressive effects on primary melanoma tumor progression.

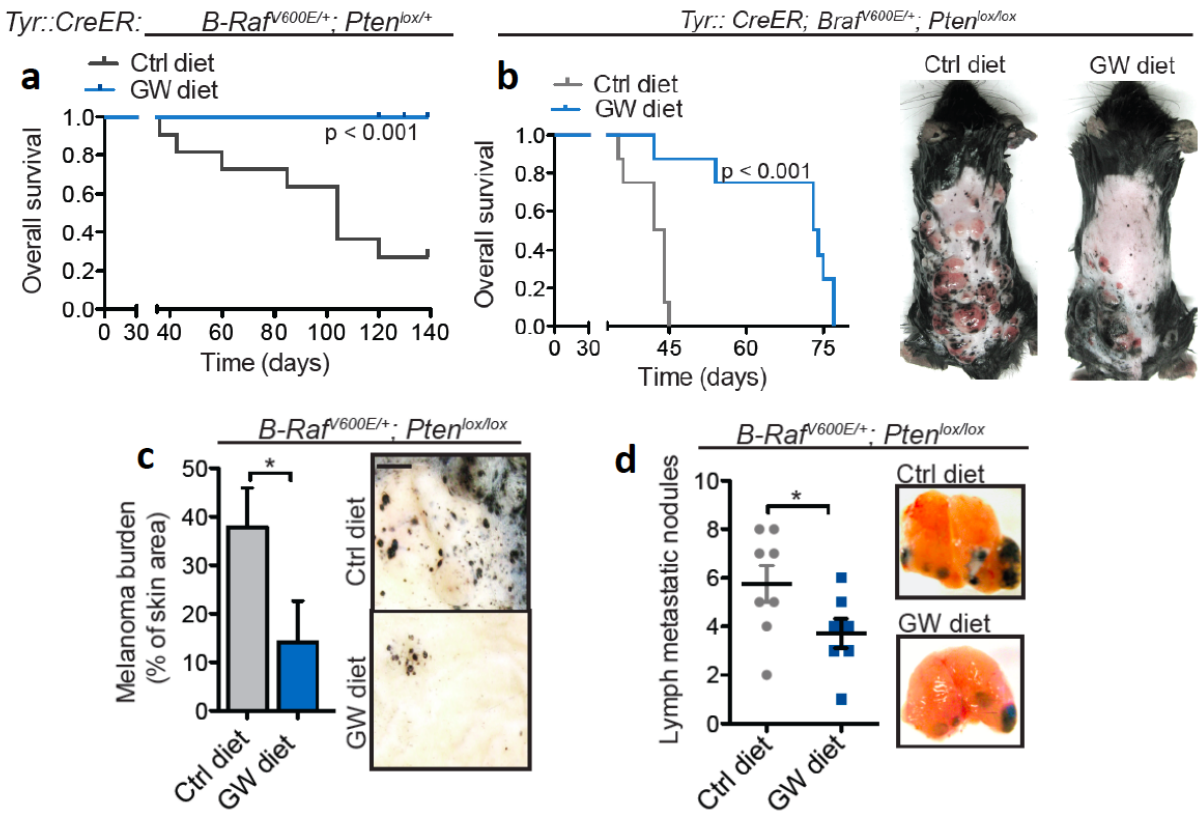

Figure 5.20. LXR Agonist Treatment Inhibits Melanoma Progression in a *B-Raf*^{V600E}/ *Pten*-Null Genetically Driven Model. a-b. Overall survival of *Tyr::CreER; Braf*$^{V600E/+}$; *Pten*$^{lox/+}$ (**a**) and *Tyr::CreER; Braf*$^{V600E/+}$; *Pten*$^{lox/lox}$ (**b**) C57BL/6 mice following general melanoma induction by intraperitoneal administration of 4-hydroxytamoxifen (4-HT) (25 mg/kg) on three consecutive days. After the first 4-HT injection, mice were randomly assigned to a control diet or a diet supplemented with GW3965 (100 mg/kg). n ≥ 10 (**a**), n ≥ 7 (**b**). **c.** Melanoma tumor burden, expressed as the percentage of dorsal skin area, measured on day 35 in *Tyr::CreER; Braf*$^{V600E/+}$; *Pten*$^{lox/lox}$ mice administered a control chow or a chow supplemented with GW3965 (100 mg/kg) upon melanoma induction. n ≥ 4. **d.** Number of macroscopic metastatic nodules in the salivary gland lymph nodes detected post-mortem in *Tyr::CreER; Braf*$^{V600E/+}$; *Pten*$^{lox/lox}$ mice that were fed a control chow or a chow containing GW3965 (100 mg/kg) following global melanoma induction as described in (**a**). n ≥ 7. Error bars = SEM. Scale bar, 2 mm. *p < 0.05. p-values based on Mantel-Cox tests (**a, b**) or unpaired student's t-tests (**c, d**).

The cooperativity between *B-Raf* activation and *Pten* loss in driving melanoma progression can be further enhanced by inactivation of *CDKN2A*, a cell cycle regulator frequently mutated in familial melanomas (Hussussian et al., 1994; Kamb et al., 1994). We thus examined the effect of LXR activation on *B-Raf*$^{V600E/+}$*; Pten*$^{-/-}$*; CDKN2A*$^{-/-}$ melanomas, allowing us to test the therapeutic efficacy of LXR agonism in this more aggressive genetically driven melanoma progression model. Importantly, therapeutic administration of GW3965 robustly inhibited primary tumor progression and lung colonization by *B-Raf*$^{V600E/+}$*; Pten*$^{-/-}$*; CDKN2A*$^{-/-}$ primary mouse melanoma cells injected into syngeneic immunocompetent mice. LXR agonist treatment also extended the survival times of mice bearing *B-Raf*$^{V600E/+}$*; Pten*$^{-/-}$*; CDKN2A*$^{-/-}$ melanoma burden (Figure 5.21).

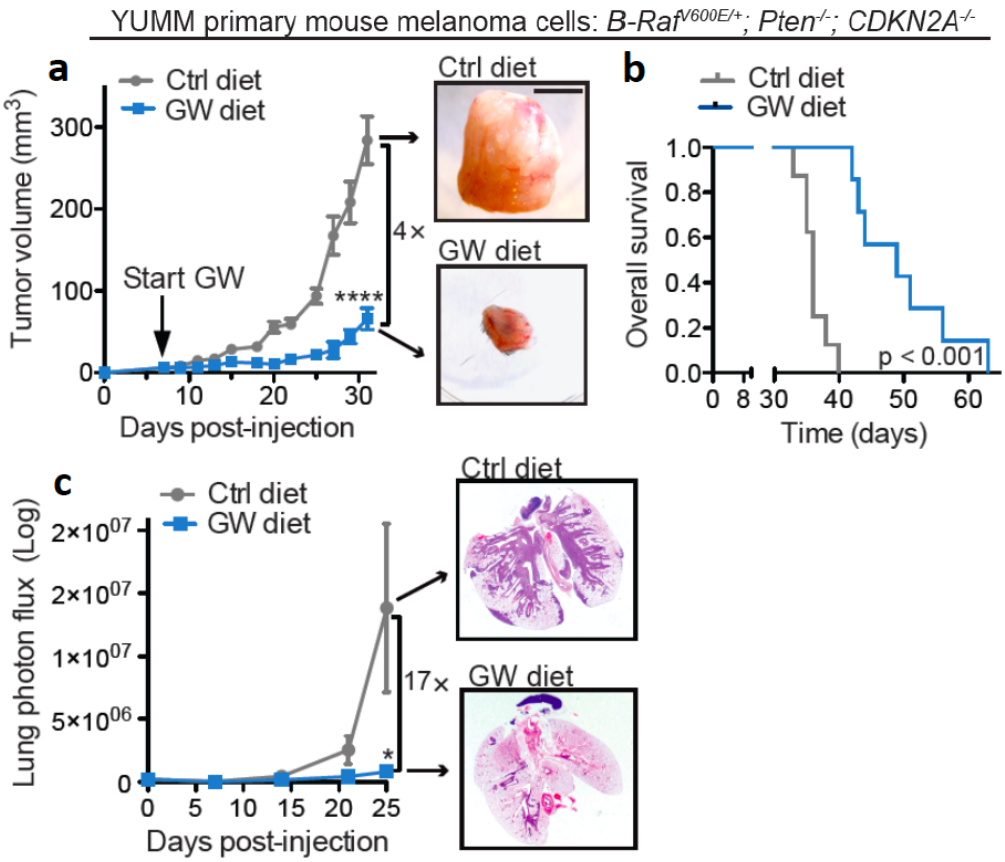

Figure 5.21. LXR Agonist Therapy Suppresses Melanoma Progression in a *B-Raf*^{V600E}/*Pten*-Null/*CDKN2A*-Null Genetic Model. a. Tumor growth by 1×10^5 *Braf*$^{V600E/+}$; *Pten*$^{-/-}$; *CDKN2A*$^{-/-}$ primary melanoma cells (designated as YUMM) subcutaneously injected into syngeneic C57BL/6-WT mice that were treated with a control diet or a GW3965 diet (100 mg/kg). n ≥ 16. **b.** Overall mouse survival following subcutaneous injection of 1×10^5 YUMM cells and mouse treatment with a control diet or a GW3965 diet (100 mg/kg) as indicated. n ≥ 7. **c**. Lung colonization by 1×10^5 YUMM cells intravenously injected into C57BL/6-WT mice. Immediately following cancer cell injection, mice were randomly assigned to a control diet or a GW3965-supplemented diet (100 mg/kg). n ≥ 14. Data are displayed as mean ± SEM. Scale bar, 5 mm. *p < 0.05; ****p < 0.0001. p-values based on an unpaired student's t-test (**a**), Mantel-Cox test (**b**), or Mann-Whitney's t-test (**c**)

ApoE Activation Therapy Inhibits Melanomas Resistant to Mainstay Therapeutics Dacarbazine and Vemurafenib

Dacarbazine (DTIC) and vemurafenib represent two of the modern frontline agents used for the treatment of metastatic melanoma. DTIC is a chemotherapeutic alkylating agent that inhibits tumor growth by incurring DNA damage in tumor cells. It was FDA-approved in the early 1970s based on its demonstrated improvement of overall response rates and, for a long time, DTIC was the only available therapeutic to metastatic melanoma patients. However, large randomized clinical trials have failed to find any significant effects of DTIC on overall patient survival (Chapman et al., 1999; Middleton et al., 2000), as the majority of DTIC-treated melanoma patients quickly develop resistance to this chemotherapeutic. For these reasons, we sought to determine whether melanomas that had acquired resistance to DTIC could still respond to LXRβ activation therapy. We generated B16F10 clones resistant to DTIC by continuously culturing melanoma cells in the presence of DTIC for two months, yielding a sub-line that exhibited a 7-fold increase in survival capacity when cultured in high-dose DTIC *in vitro* (Figure 5.22a). Accordingly, DTIC treatment *in vivo* significantly suppressed tumor growth by the parental line (Figure 5.22b), whereas it had no effect on the growth of the DTIC-resistant sub-line (Figure 5.22c). Importantly, GW3965 administration robustly suppressed tumor growth by the DTIC-resistant sub-line by more than 70% (Figure 5.22c). Additionally, we confirmed the suppressive effect of GW3965 in an independent *in vivo* selected DTIC-resistant human melanoma sub-line, as evidenced by the strong inhibition (~70%) of DTIC-resistant tumors upon oral delivery of GW3965 (Figure 5.22d-e).

We next tested the impact of LXRβ activation therapy on melanoma cells resistant to the recently approved B-Raf kinase inhibitor, vemurafenib—a regimen that shows activity

against *B-Raf*-mutant melanomas on both overall response rates as well as survival outcomes (Chapman et al., 2011; Sosman et al., 2012). However, this targeted therapeutic is notorious for resistance emergence, with more than 90% of treated melanoma tumors acquiring drug resistance after prolonged vemurafenib treatment. To this end, numerous investigators have derived melanoma lines resistant to vemurafenib (Poulikakos et al., 2011; Shi et al., 2012; Das Thakur et al., 2013; Haq et al., 2013). To test whether LXR agonist treatment exhibited activity in vemurafenib-resistant melanomas, we obtained two previously derived independent SK-Mel-239 vemurafenib-resistant clones (C1 and C5), which attain resistance to vemurafenib through distinct molecular mechanisms (Poulikakos et al., 2011). Notably, GW3965 treatment suppressed the growth of tumors formed by both the C1 and C5 clones by 72% and 39%, respectively (Figure 5.23a, c) and significantly prolonged the survival of mice bearing vemurafenib-resistant melanoma burden (Figure 5.23b). Treatment also significantly inhibited tumor growth by the A375 vemurafenib-resistant human melanoma sub-line that we independently generated (Figure 5.23d). Additionally, we generated a vemurafenib-resistant sub-line from *B-Raf*-mutant primary mouse melanoma cells following *in vivo* treatment of tumors with vemurafenib (Figure 5.23e), thereby allowing us to test the effect of LXRβ agonism on vemurafenib-resistant melanoma cells in an immunocompetent syngeneic mouse model. We observed that even though vemurafenib was ineffective in suppressing melanoma progression by the resistant sub-line, GW3965 administration led to a greater than 50% reduction in tumor growth (Figure 5.23f).

These results reveal that LXRβ agonism is effective in suppressing multiple melanoma sub-lines resistant to the widely used B-Raf kinase inhibitor vemurafenib and the sole FDA-approved cytotoxic chemotherapeutic in melanoma, dacarbazine. Our findings

have important clinical implications for melanoma treatment since nearly all stage IV metastatic patients who are treated with dacarbazine and/or vemurafenib ultimately relapse and experience lethal melanoma progression as a direct consequence of resistance emergence to these agents.

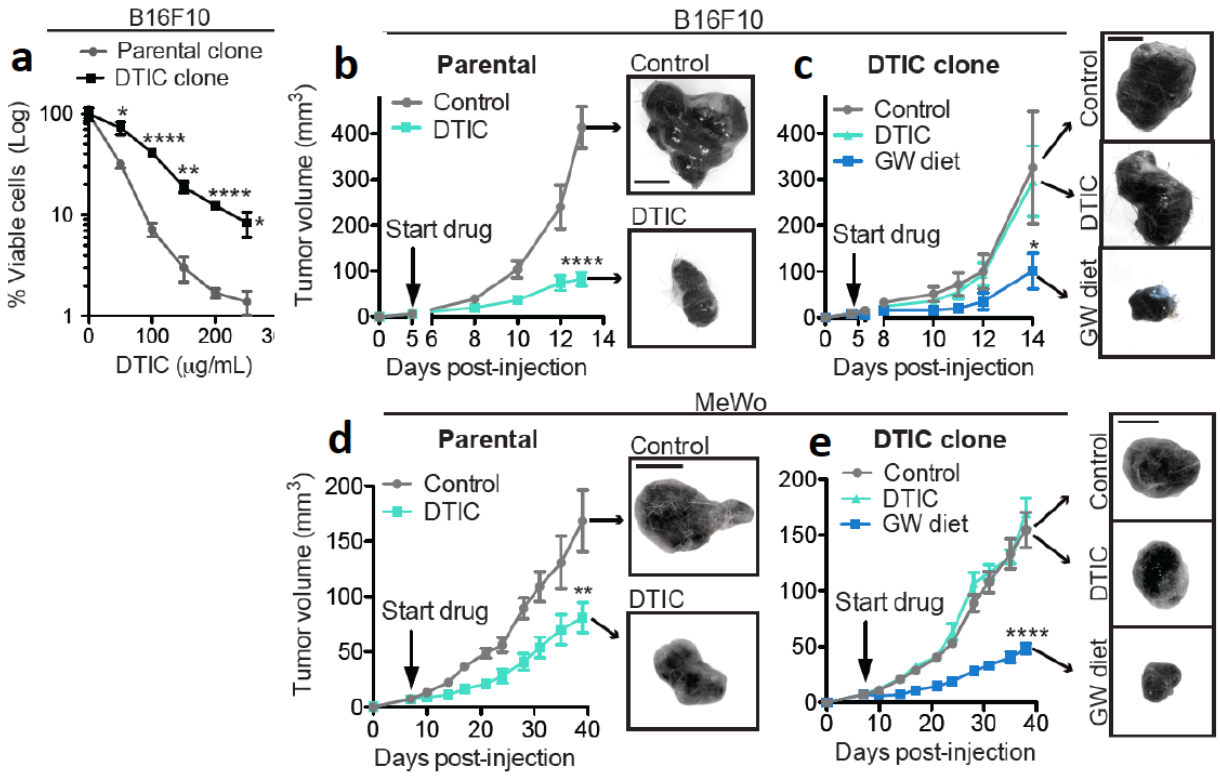

Figure 5.22. LXR Agonist Treatment Suppresses Melanomas Resistant to the Chemotherapeutic Dacarbazine. a. *In vitro* cell growth by 2.5 × 10^4 B16F10 parental and DTIC-resistant cells in response to increasing doses of DTIC added to the cell media for 4 days. n = 3. **b-c.** Tumor growth by 5 × 10^4 B16F10 parental cells (**b**) or 5 × 10^4 DTIC-resistant B16F10 cells (**c**) subcutaneously injected into C57BL/6-WT mice. Following tumor growth to 5-10 mm^3 in volume, mice were treated with a control vehicle, dacarbazine (50 mg/kg, i.p., daily), or GW3965-supplemented diet (100 mg/kg). n ≥ 7. **d-e.** Tumor growth by 5 × 10^5 MeWo parental cells (**d**) and 5 × 10^5 *in vivo*-selected DTIC-resistant MeWo human melanoma cells (**e**) in response to DTIC (50 mg/kg, i.p., daily, 5 days on, 2 days off) or GW3965 (100 mg/kg) treatments. n ≥ 6. All data are represented as mean ± SEM. Scale bars, 5 mm. *p < 0.05; **p < 0.01; ****p < 0.0001. p-values based on unpaired student's t-tests.

Figure 5.23. LXR Agonist Treatment Suppresses Melanomas Resistant to Vemurafenib. **a, c.** Tumor growth by 2×10^6 SK-Mel-239 vemurafenib-resistant sub-lines, clone 1 (C1) (**a**) or clone 5 (C5) (**c**), subcutaneously injected into NOD SCID gamma mice that were assigned to a control diet or a GW3965 diet (100 mg/kg), as indicated. $n \geq 7$ (**a**), $n = 5$ (**c**). **b.** Overall mouse survival post-grafting of 2×10^6 SK-Mel-239 vemurafenib-resistant C1 cells onto mice treated with a control diet or a GW3965 diet. $n = 7$. **d.** Tumor growth by 5×10^5 vemurafenib-resistant A375 melanoma cells upon treatment with a control diet, GW3965 diet (100 mg/kg), or a vemurafenib diet (50 mg/kg), as indicated. $n \geq 6$. **e.** Tumor growth by 1×10^5 vemurafenib-sensitive *B-Raf*-mutant primary mouse YUMM melanoma cells. Cells were subcutaneously implanted onto C57BL/6 mice that were treated with a vemurafenib diet following detection of palpable tumors (5-10 mm^3 in volume). Melanoma cells were dissociated from vemurafenib-resistant tumors that eventually grew in the presence of vemurafenib at day 52, as indicated in the figure. $n \geq 8$. **f.** Tumor growth by 2×10^5 vemurafenib-resistant YUMM cells subcutaneously grafted onto C57BL/6 mice. Following formation of palpable tumors, mice were administered a control diet, vemurafenib diet (50 mg/kg), or a GW3965 diet (100 mg/kg). $n \geq 8$. All data are represented as mean ± SEM. Scale bar, 5 mm. *$p < 0.05$; **$p < 0.01$; ***$p < 0.001$; ****$p < 0.0001$. p-values based on unpaired student's t-tests (**a**, **c**, **d**, **f**) or a Mantel-Cox test (**b**).

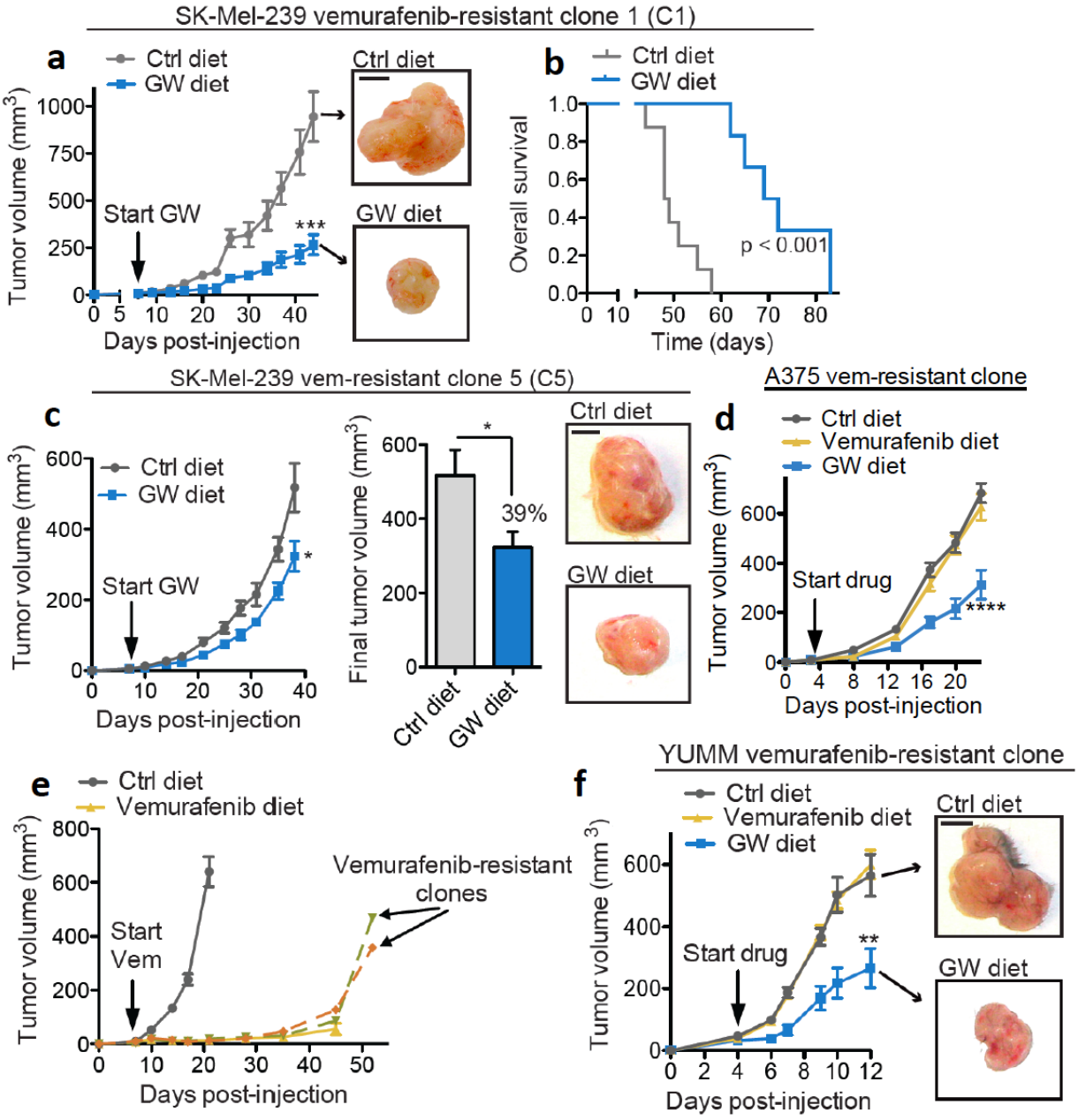

Figure 5.23. LXR Agonist Treatment Suppresses Melanomas Resistant to Vemurafenib.

Cooperativity between LXRβ Activation Therapy and Mainstay Melanoma Therapeutics

Given that the median survival time of advanced melanoma patients rarely exceeds two years even with present FDA-approved therapeutics, owing to limited response rates and/or emergence of resistance to single-agent treatments, we wondered whether combining LXRβ/*ApoE* activation therapy with modern frontline agents could provide further therapeutic benefit. To this end, we examined whether LXR agonist therapy can elicit additive melanoma-suppressive responses when combined with any of the three FDA-approved therapeutics for the treatment of metastatic melanoma: dacarbazine, vemurafenib, and the anti-CTLA-4 antibody (Ab). Remarkably, we found that combining GW3965 treatment with either dacarbazine, vemurafenib, or anti-CTLA-4 Ab led to greater melanoma suppression that each treatment alone (Figures 5.24, 5.25, 5.26).

For instance, while either GW3965 or DTIC treatment alone inhibited B16F10 melanoma growth by 65% and 70%, respectively, combined GW3965 and DTIC therapy led to greater than 90% suppression of tumor growth (Figure 5.24a). We further found that combined GW3965 and vemurafenib treatment suppressed tumor progression by the *B-Raf*-mutant A375 line by 82%, which exceeded the inhibition of tumor growth seen with each drug alone: 44% for GW3965 and 65% for vemurafenib (Figure 5.24b). Additionally, alternating vemurafenib and LXR agonist therapy was more effective (~72% inhibition) in suppressing tumor growth by the independent *B-Raf*-mutant SK-Mel-239 line compared to single-agent GW3965 (56% inhibition) or vemurafenib (50% inhibition) treatment (Figure 5.24d). Importantly, combined GW3965 and vemurafenib therapy also improved survival outcomes in these models relative to each drug alone (Figures 5.24c, e).

Figure 5.24. LXR Agonist Treatment Cooperates with Dacarbazine and Vemurafenib in Suppressing Melanoma Tumor Growth. a. Primary tumor growth by 5×10^4 B16F10 mouse melanoma cells grafted onto C57BL/6-WT mice. Following formation of tumors measuring 5-10 mm^3 in volume, mice were randomly assigned to a control treatment, GW3965 diet (100 mg/kg), DTIC (50 mg/kg, i.p., daily), or combined GW3965 (100 mg/kg) and DTIC (50 mg/kg) treatment. $n \geq 8$. **b.** 8×10^5 *B-Raf*-mutant A375 human melanoma cells were subcutaneously injected into immunocompromised mice, and melanoma tumor progression was monitored in response to a control diet, GW3965 diet (75 mg/kg), vemurafenib diet (50 mg/kg), or a combined GW3965 (75 mg/kg) and vemurafenib (50 mg/kg) diet treatment. $n \geq 8$. **c.** Overall post-tumor survival of mice bearing A375 melanoma tumor burden in response to the various treatments shown in (**b**). $n \geq 4$. **d.** Subcutaneous tumor growth by 1.25×10^6 *B-Raf*-mutant SK-Mel-239 human melanoma cells in response to a control diet, GW3965 diet (75 mg/kg), vemurafenib diet (50 mg/kg), or an alternating vemurafenib/GW3965 diet treatment, as indicated. $n \geq 8$. **e.** Overall post-tumor survival of mice following subcutaneous grafting of SK-Mel-239 melanoma cells in response to the various treatments shown in (**d**). $n \geq 7$. Error bars = SEM. Scale bar, 5 mm. $^*p < 0.05$, $^{**}p < 0.01$, $^{***}p < 0.001$, $^{****}p < 0.0001$. p-value based on unpaired student's t-tests (**a**, **b**, **d**) or Mantel-Cox tests (**c**, **e**).

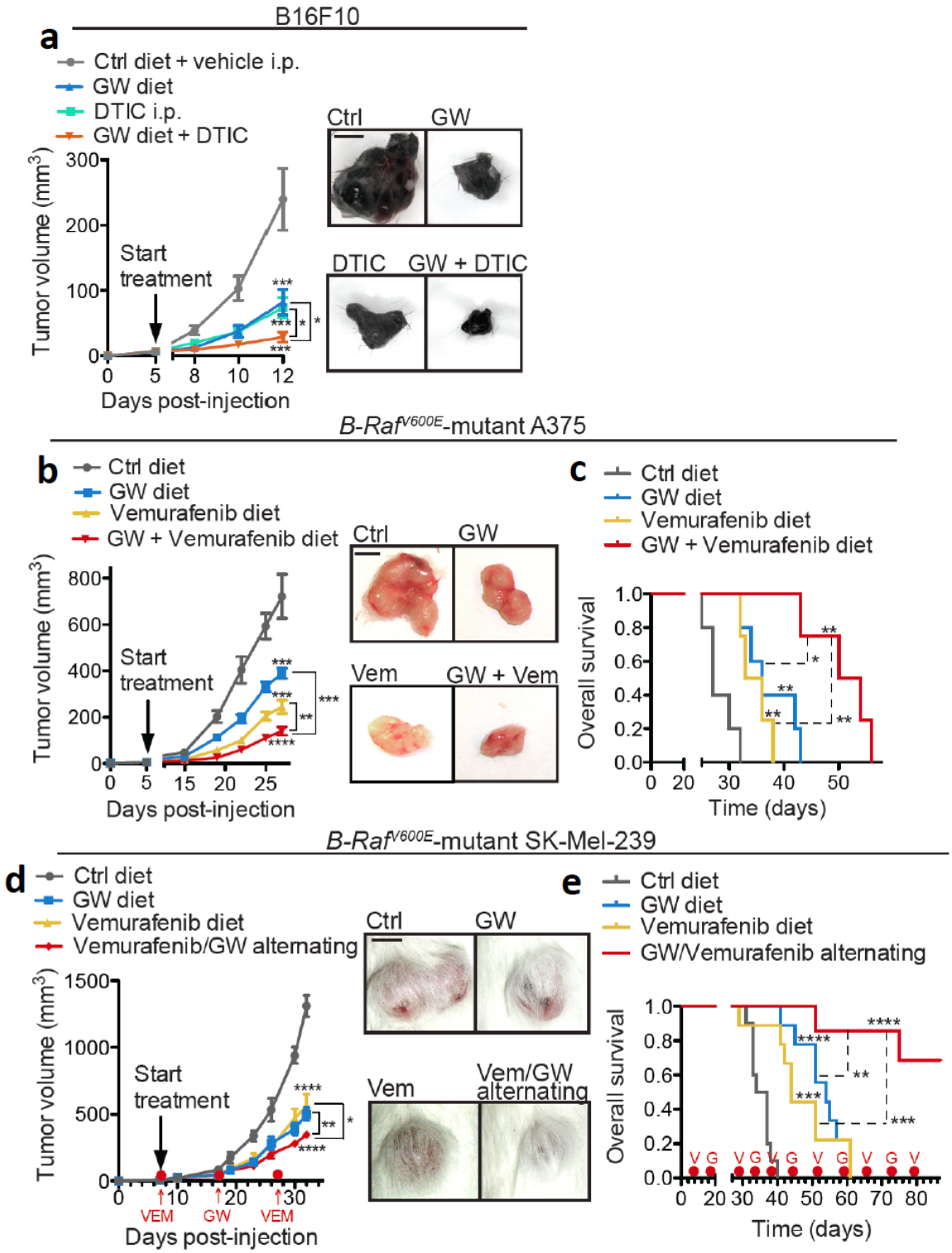

Figure 5.24. LXR Agonist Treatment Cooperates with Dacarbazine and Vemurafenib in Suppressing Melanoma Tumor Growth

The melanoma-suppressive cooperativity between vemurafenib and GW3965 was also seen in lung colonization assays. Whereas vemurafenib and GW3965 each suppressed metastasis of the *B-Raf*-mutant primary SK-Mel-334.2 melanoma line by roughly 50%, combined treatment led to a greater than 85% inhibition (Figure 5.25a). Additionally, GW3965 and vemurafenib each also inhibited lung colonization by the independent *B-Raf*-mutant HT-144 melanoma cells by 84% and 76%, respectively, while the combined therapy elicited nearly 90% suppression in metastasis (Figure 5.25b).

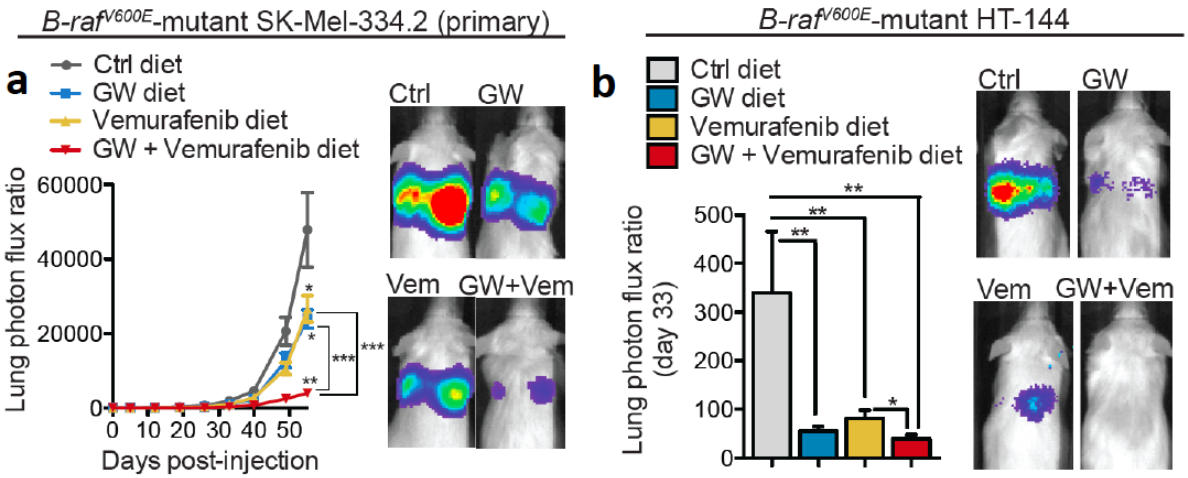

Figure 5.25. Cooperativity between LXRβ Activation and Vemurafenib in Suppressing Melanoma Metastasis. a. Lung colonization by 1×10^5 primary *B-Raf*-mutant SK-Mel-334.2 human melanoma cells in response to a control diet, GW3965 diet (75 mg/kg), vemurafenib diet (50 mg/kg), or a combined GW3965 and vemurafenib diet treatment. Lung colonization was assessed by weekly bioluminescence imaging. Various treatments were initiated 3 days preceding cancer cell injection. $n \geq 5$.**b.** Lung colonization by 7.5×10^4 *B-Raf*-mutant HT-144 human melanoma cells measured by bioluminescence imaging at day 33. Melanoma cells were intravenously injected into immunocompromised mice that were administered a control diet, GW3965 diet (75 mg/kg), vemurafenib diet (50 mg/kg), or a combined GW3965 and vemurafenib diet, starting 3 days prior to cancer cell injection. $n \geq 5$. All data are represented as mean ± SEM. *$p < 0.05$, **$p < 0.01$, ***$p < 0.001$, based on Mann-Whitney's t-tests.

Finally, we examined the impact of combining GW3965 treatment with immunomodulatory anti-CTLA-4 therapy on melanoma progression. Consistent with earlier findings (van Elsas et al., 1999), we observed roughly 20% suppression of tumor growth in response to anti-CTLA-4 Ab monotherapy in the syngeneic immunocompetent B16F10 melanoma murine model (Figure 5.26a). In comparison, GW3965 therapy inhibited B16F10 tumor growth by over 60%. Remarkably, combining the LXR agonist treatment with the anti-CTLA-4 Ab elicited a greater than 80% inhibition in tumor growth, revealing additivity between the effects of GW3965 treatment and anti-CTLA-4 Ab therapy (Figure 5.26a). Importantly, combined GW3965 and anti-CTLA-4 Ab treatment significantly improved survival outcomes relative to each drug alone (Figure 5.26b).

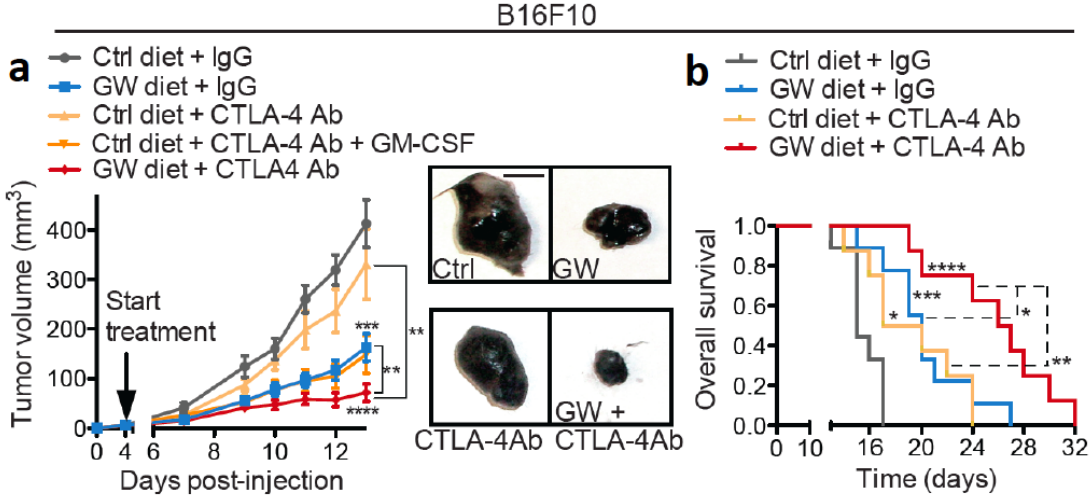

Figure 5.26. Additive Effects of LXRβ Activation and Immunotherapy in Melanoma. **a.** Tumor growth by 5×10^4 B16F10 cells grafted onto C57BL/6-WT mice in response to a control diet/IgG treatment, GW diet/IgG treatment, anti-CTLA-4 Ab monotherapy, anti-CTLA-4 Ab + GM-CSF vaccine treatment, or anti-CTLA-4 Ab + GW3965 combined therapy. $n \geq 8$. **b.** Overall post-tumor survival of mice bearing B16F10 tumors in response to anti-CTLA-4 Ab or GW3965 monotherapy or anti-CTLA-4 Ab + GW3965 combined therapy. $n \geq 8$. Error bars = SEM. *$p < 0.05$, **$p < 0.01$, ***$p < 0.001$, ****$p < 0.0001$. p-values based on student's t-tests (**a**) or Mantel-Cox tests (**b**).

Summary of Findings form Chapter V

This chapter describes our experimental efforts to activate *ApoE* expression as a new therapeutic approach in metastatic melanoma. To this end, we identified a transcriptional activator of *ApoE*, the nuclear hormone receptor LXRβ, as a new therapeutic target that exhibits ubiquitous expression in melanoma tumors. We showed that pharmacologic LXR activation robustly suppressed melanoma progression phenotypes of invasion, endothelial recruitment, tumor growth, and metastasis across multiple pre-clinical melanoma models of diverse mutational backgrounds. LXR activation inhibited melanoma progression in xenograft, immunocompetent, and genetically driven mouse models of melanoma. Through a series of molecular and genetic experiments, we identified LXRβ as the LXR isoform that mediates the effects of LXR agonists on melanoma suppression. Next, we demonstrated that the melanoma-suppressive effects of LXRβ agonism were mediated through the transcriptional activation *ApoE*. We further validated the robustness of LXRβ activation as a new promising therapeutic approach by showing that LXR agonism suppressed melanoma brain metastasis, which presently lacks effective therapies, and also inhibited melanomas resistant to the mainstay melanoma therapeutics dacarbazine and vemurafenib. Finally, we investigated whether LXR activation could elicit additive responses in suppressing melanoma progression upon its combination with present frontline agents used to manage metastatic melanoma. Remarkably, we observed melanoma-suppressive cooperativity upon combining LXRβ therapy with each of the three frontline melanoma regimens—dacarbazine, B-Raf inhibition, and immunotherapy. Our findings implicate LXRβ agonism as a promising therapeutic approach for the treatment of metastatic melanoma.

CHAPTER VI: DISCUSSION

Overview of Major Findings

The complexity and heterogeneity of human cancers necessitate the application of systematic and global analyses addressing multiple aspects of cancer progression. In this thesis, I describe a functionally guided systematic approach that led to the identification of endogenous metastasis regulatory miRNAs and effector genes in human melanoma. We identified three miRNAs (miR-199a-3p, miR-199a-5p, and miR-1908) that displayed broad and robust upregulation across multiple metastatic melanoma sub-lines, which were generated by *in vivo* selection of amelanotic and melanotic melanoma cell populations derived from independent patients. Consistent with their pervasive upregulation in metastatic melanoma cells of diverse mutational backgrounds and pigmentation status, we found that the three miRNAs can act as strong pathologic predictors of human melanoma metastatic recurrence. Importantly, targeting of these miRNAs using therapeutic LNA technology strongly suppressed metastasis in a pre-clinical melanoma model.

By performing global transcriptomic analyses, we uncovered *DNAJA4* and *ApoE*, genes with previously unknown roles in metastasis, as common molecular targets and functional effectors of miR-199a-3p, miR-199a-5p, and miR-1908 in melanoma metastasis. Furthermore, we found that *ApoE* was positively regulated by DNAJA4, revealing an additional level of convergence and highlighting the central role of *ApoE* in this metastasis regulatory pathway (Figure 6.1). Accordingly, we observed reduced ApoE protein expression levels in clinical melanoma metastases relative to primary melanoma lesions, while low ApoE expression in patients' primary tumors significantly correlated with an increased risk of metastatic recurrence. The clinical relevance of ApoE expression to melanoma metastasis

motivated us to examine the mechanistic underpinnings of ApoE's effects in melanoma. We found that extracellular ApoE exerted dual cell autonomous/non-cell-autonomous effects on melanoma progression: ApoE targeting of melanoma cell LRP1 receptors inhibited melanoma invasion, while ApoE targeting of endothelial cell LRP8 receptors suppressed endothelial cell migration/ recruitment (Figure 6.1). The metastasis-suppressive function of *ApoE* was further supported by our findings that genetic inactivation of stromal *ApoE* accelerated melanoma metastasis, indicating that both melanoma-derived and stromally produced extracellular ApoE could contribute to metastasis suppression.

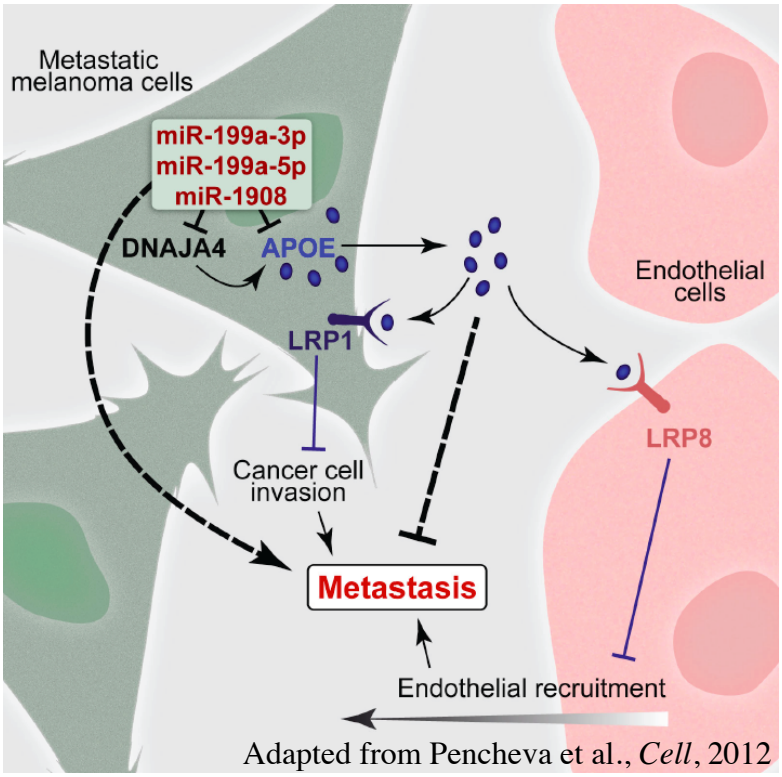

Figure 6.1. Convergent Regulation of Melanoma Metastasis by Multiple miRNAs. Experimentally elucidated model of multi-miRNA targeting of *DNAJA4* and *ApoE* in melanoma metastasis. DNAJA4 was found to induce *ApoE* expression. Melanoma cell-secreted ApoE was shown to exert dual cell-autonomous and non-cell-autonomous effects: ApoE inhibits melanoma invasion by acting on melanoma cell LRP1 receptors, whereas it blocks endothelial recruitment by targeting endothelial cell LRP8 receptors.

In light of the robust suppression exerted by ApoE on melanoma metastasis, we investigated therapeutic approaches to chronically activate *ApoE* expression in melanoma progression. While searching for ubiquitously expressed molecules that could activate *ApoE* expression upon pharmacologic modulation, we identified an *ApoE* transcriptional trans-activator, the nuclear hormone receptor LXRβ, as a novel therapeutic target in metastatic melanoma. We showed that, in addition to its known ubiquitous expression across tissues (Song et al., 1994), LXRβ was also ubiquitously expressed across human melanoma tumors, regardless of their progression stage. Consistent with its stable expression, therapeutic agonism of LXRβ displayed broad-spectrum activity in suppressing melanoma progression across diverse immunocompetent, xenograft, and genetically-driven melanoma models. LXRβ activation also displayed activity in inhibiting melanomas that had acquired resistance to frontline therapeutic agents, dacarbazine and vemurafenib. Importantly, we showed that the melanoma-suppressive activity of LXRβ activation therapy was mediated through the downstream induction of *ApoE*, which was derived from both melanoma (tumor-intrinsic) and stromal (tumor-extrinsic) tissue compartments (Figure 6.2).

Our systematic interrogation of molecular pathways regulating melanoma metastasis has culminated in the discovery of LXRβ activation therapy as a promising new approach for the treatment and prevention of melanoma metastasis. The therapeutic potential of *ApoE* activation therapy in melanoma is further underscored by our observations of strong tumor-suppressive cooperativity upon combining LXR agonist treatment with either of the three mainstay melanoma therapeutics: chemotherapy, B-Raf kinase inhibition, and immunotherapy.

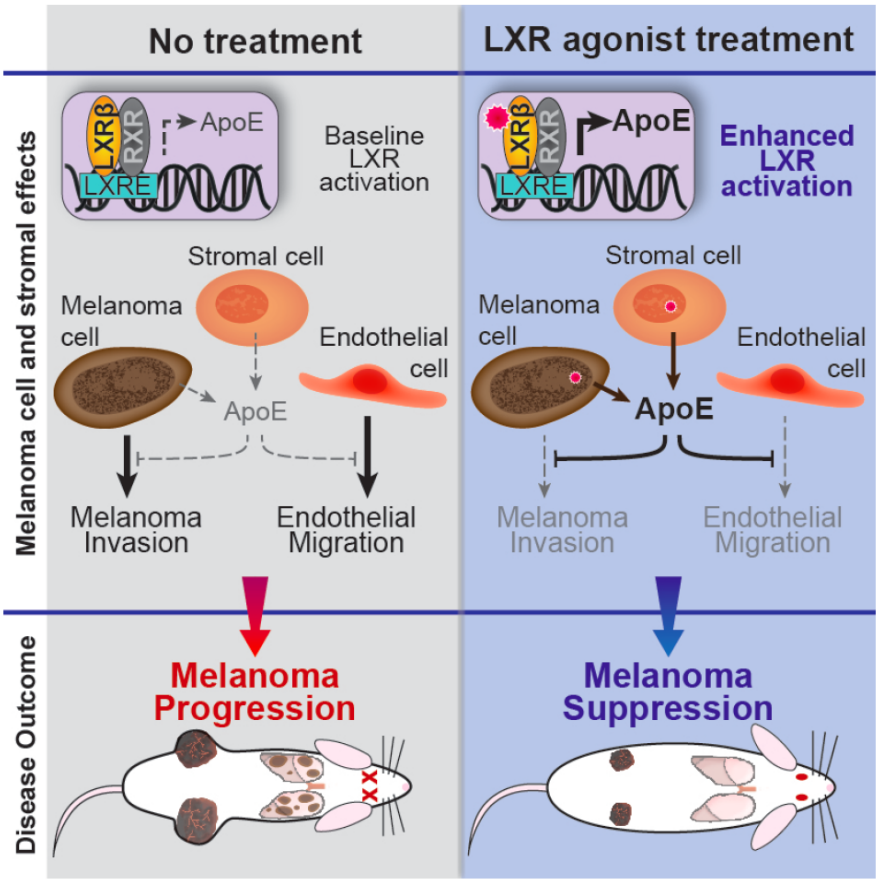

Adapted from Pencheva et al., *Cell*, 2014

Figure 6.2. Suppression of Melanoma Progression by LXR/*ApoE* Activation. Schematic depicting the experimentally derived model of the basis of action of LXRβ activation therapy in melanoma. The LXR agonist treatment activates LXRβ, which in turn induces *ApoE* expression both in melanoma cells as well as in various stromal tissue cells. The LXRβ-dependent augmented expression of extracellular ApoE mediates suppression of melanoma progression phenotypes and extends animal survival times across various pre-clinical models of melanoma progression.

Role of Metastasis Regulatory miRNAs in Development

While there is presently a lack of experimental evidence to support a role for miR-199a-3p/miR-199a-5p/miR-1908 in regulating melanocyte development and differentiation, we speculate that the miRNAs' ability to promote melanoma invasion and metastasis may stem from developmentally conserved programs allowing these miRNAs to regulate melanocyte migration during the course of normal development. Melanoblasts, the precursors for melanocytes, originally arise from the neural crest and are faced with the challenge to migrate over extensive distances in the body as they spread to peripheral skin. Therefore, melanoblasts likely possess intrinsic mechanisms governing their highly migratory nature during development. It is conceivable that the same pathways that regulate melanoblast migration (and are subsequently switched off in differentiated melanocytes) may be hijacked and reactivated by melanoma cells in facilitating their migration and invasion during metastatic dissemination throughout the body. It will be of interest for future studies to determine whether the three miRNAs impact melanocyte migration and examine the dynamics of their expression during melanoblast formation, migration, and subsequent differentiation into melanocytes.

Previous studies have implicated roles for miR-199a-3p and miR-199a-5p in cardiomyocyte development and regeneration. For instance, a recent study demonstrated that miR-199a-3p plays a role in promoting neonatal cardiomyocyte proliferation and neonatal cardiac size, whereas introduction of miR-199a-3p in adult cardiomyocytes triggered cell cycle re-entry and cardiac regeneration following myocardial infraction (Eulalio et al., 2012). Similar to miR-199a-3p, miR-199a-5p has also been implicated in cardiac physiology by studies showing that miR-199a-5p may play a role in increasing cardiac cell size, while the

expression levels of miR-199a-5p were found to be upregulated during cardiac hypertrophy, a condition marked by an increase in heart size (Song et al., 2010). Consistent with a role for miR-199a in heart physiology, we detected high expression levels of mature miR-199a-3p and miR-199a-5p in mouse cardiac tissues (Figure 2.20b). Whereas the mouse homolog for miR-1908 was presently unknown at the time, we also detected expression of miR-1908, using human primers, in mouse heart tissue (Figure 2.20b), suggesting that the mouse miR-1908 sequence is conserved with its human homolog and it is also expressed in the heart. Interestingly, we did not however detect expression of miR-1908 in the liver, implying that its expression may be at least in part restricted to the heart. The high expression of the three miRNAs in cardiac tissue suggests that they may play a prominent role in cardiomyocyte physiology. Given that cardiomyocyte migration has been linked to heart regeneration (Itou et al, 2012), it is possible that miR-199a (and possibly miR-1908) may promote cardiac regeneration through their effects on cardiomyocyte migration.

Finally, while the effects of genetically inactivating miR-199a or miR-1908 on embryonic and/or post-embryonic development are presently unknown, there is some evidence that miR-199a is most highly expressed at mouse embryonic stage E12.5 and its expression is preferentially restricted to the mouse cerebellum, midbrain, nasal processes, and the fore- and hindlimb buds (Lee et al., 2009). Additionally, homozygous deletion of a region on chromosome one, encoding the miR-199a-2 paralog and its polycistronic partner, miR-214, was found to be post-embryonically lethal in the majority of cases, with pups dying within one month after birth. It was observed that pups lacking miR-199a-2/miR-214 exhibited impaired skeletal development, including craniofacial hypoplasia and abnormalities in the dorsal neural arches and vertebrae spine formation (Watanabe et al., 2008). However,

in addition to miR-199a-2 loss, these mice also lacked miR-214, while the other miR-199a paralog, miR-199a-1, was presumably still expressed, confounding any potential interpretation of the specific role that mature miR-199a may play in embryonic and post-embryonic development. In order to get a better understanding of how this multi-miRNA network has evolved to regulate melanoma metastasis, it will be important for future studies to address the functions of these miRNAs and their downstream targets in development and how they become co-opted during melanoma progression.

Convergent versus Divergent Target Regulation by miRNAs

The majority of past work on metastasis regulatory miRNAs has revealed divergent gene targeting to be the pervasive mode of regulation exerted by miRNAs on metastatic progression. This was initially demonstrated for miR-335 (Tavazoie et al., 2008) and subsequently shown to be the preferred mode of action for many other miRNAs in metastasis regulation, such as miR-31 (Valastyan et al., 2009b), miR-126, (Png et al., 2012), let-7 (Yun et al., 2011), and miR-9 (Ma et al., 2010b). In each of these instances, a single miRNA exerted robust metastasis control through the coordinate repression of multiple target genes. Since each of these target genes contributed to the metastasis phenotype, their concurrent silencing by the miRNA inflicted greater metastasis-promoting or metastasis-suppressive effects, respectively, compared to each target alone. This divergent mode of gene targeting by individual miRNAs likely arose through evolution and plays an important role during normal development, allowing certain miRNAs to fine-tune physiological processes through their ability to simultaneously modulate the expression of multiple downstream effector gene. For instance, miR-199a was recently found to be essential for neonatal cardiac cell

proliferation as well as cardiac cell regeneration in adult mice through its additive effects on multiple downstream target genes (Eulalio et al., 2012). Co-option of such divergent miRNA-target gene connectivity in cancer progression likely confers pervasiveness to the post-transcriptional control exerted on gene networks in metastasis, whose complexity requires the concerted action of multiple gene products.

On the contrary, convergent target gene regulation by multiple distinct miRNAs is a molecular phenomenon only recently implicated in cancer progression, and its pervasiveness in the metastasis control of multiple cancer types remains to be seen. In addition to our findings of convergent miRNA regulation as a driving force in melanoma metastasis, recent work described miRNA cooperativity in an *in vitro*-based cell model of T-cell acute lymphoblastic leukemia (T-ALL). Combinatorial silencing of multiple miRNAs cooperatively decreased T-ALL cell proliferation and viability *in vitro* and increased expression of common target genes to an extent greater than that seen with silencing of any individual miRNA (Mavrakis et al., 2011), thereby allowing for a more robust gene expression control than that afforded by each single miRNA. Convergent miRNA regulation is not unique to cancer cells. Similar to divergent miRNA targeting, the need for convergent post-transcriptional gene regulation has presumably emerged developmentally and has been evolutionarily conserved to allow for multi-layered temporal fine-tuning of essential target genes' expression. Consistent with this, examples of multi-miRNA convergence onto a common target gene are seen in neural development (Yoo et al., 2009; Clovis et al., 2012). For instance, convergent repression of *BAF53a,* a subunit of the SWI/SNF chromatin remodeling complex, by miR-24 and miR-9-3p was shown to mediate the key molecular step

in the transition of multipotent neural progenitor cells to post-mitotic neurons that give rise to stable dendritic connections in the developing vertebrate system (Yoo et a., 2009).

Therapeutic Potential of miRNA Targeting

The robust metastasis control afforded by specific miRNAs as well as their ability to act as strong pathologic predictors of human cancer outcomes has triggered extensive clinical interest in therapeutically targeting these small RNAs in metastasis (Ling et al., 2013). Despite the discovery of multiple miRNAs governing various aspects of cancer biology, the clinical translation of miRNA-based therapies has been hindered by two main issues: the limited half-life of systemically administered miRNAs and their insufficient delivery into target tissues. Two recent reports, which described an alternative approach to "naked" nucleic acid delivery through viral-based delivery of miRNAs, have offered renewed promise for the prospect of *in vivo* miRNA-based therapies (Kota et al., 2009; Miyazaki et al., 2012). Using an adeno-associated viral-based approach, therapeutic delivery of the metastasis suppressor miR-26a was found to significantly inhibit the formation and progression of hepatocellular carcinoma (HCC) in a pre-clinical murine model (Kota et al., 2009). In addition to viral-based delivery methods, miRNA mimics can also be formulated in liposome-based nanoparticles, which are coated with tumor specific antibodies, ensuring specific delivery into target tumors (Ling et al., 2013). This approach has yielded the first clinically developed miRNA-based therapeutic, MRX34—a liposome-encapsulated mimetic for miR-34a, a tumor-suppressive miRNA that is transcriptionally induced by p53 (Chang et al., 2007). Pre-clinical findings of reduced tumor growth and enhanced survival in a murine model of hepatocellular carcinoma in response to intravenous administration of MRX34

motivated the evaluation of this miRNA mimetic agent in the clinic (Bader, 2012). Accordingly, MRX34 entered phase I clinical trial testing in the spring of 2013.

The *in vivo* inhibition of miRNAs has also shown great promise in pre-clinical arenas and is actively pursued in clinical studies. The development of locked nucleic acid (LNA) technology for the targeting of specific mature miRNAs has spearheaded the experimental assessment of miRNA inhibition as a potential therapeutic approach across various disease contexts. LNAs are short anti-sense oligonucleotides that display high affinity for single-stranded RNAs, enhanced serum stability owing to their short sequence and "locked" ribose ring, and efficient delivery into target tissues (Obad et al., 2011). In a series of seminal papers, systemic delivery of an LNA targeting the cholesterol regulatory miR-122 was shown to significantly decrease plasma cholesterol levels in non-human primates (Elmén et al., 2008), whereas targeting this same miRNA in a primate model of hepatitis C virus (HCV) replication was found to suppress HCV viremia (Lanford et al., 2010). Based on its pre-clinical promise, an LNA antisense to miR-122, termed miravirsen, was the first miRNA-targeted inhibitor to be clinically developed. Miravirsen was recently evaluated in a phase 2 clinical trial for the treatment of HCV infection and showed promising results in suppressing HCV propagation in patients (Janssen et al., 2013).

Following the initial success in efficiently targeting miR-122 for the *in vivo* inhibition of HCV propagation, therapeutic delivery of LNAs antisense to metastasis-promoting miRNAs was also shown to display metastasis-suppressive activity in pre-clinical models of cancer metastasis (Ling et al., 2013). Proof-of-principle evidence for the feasibility of LNA-based miRNA targeting for the inhibition of cancer metastasis was initially demonstrated for miR-10b, the first metastasis-promoter miRNA to be described (Ma et al., 2007). In that

study, systemic delivery of an LNA targeting miR-10b was found to modestly suppress metastasis in a murine model of breast cancer (Ma et al., 2010a).

The results described in this thesis provide further evidence that LNA-based miRNA targeting displays therapeutic potential for the prevention of human melanoma metastasis, a dreaded and aggressive disease that currently lacks effective preventative and/or curative therapies (Garbe et al., 2011). Remarkably, we found that combinatorial transfection of LNAs targeting miR-199a-3p, miR-199a-5p, and miR-1908 robustly suppressed lung colonization across a multitude of human melanoma cells of diverse mutational backgrounds (Figures 2.16-2.18). Importantly, therapeutically silencing these miRNAs by intravenous administration of a cocktail of such miRNA inhibitors at a low dose dramatically (> 12-fold) suppressed human melanoma metastasis in a mouse model (Figure 2.19). These pre-clinical findings offer promise for the clinical development of combinatorial LNA-based miRNA inhibitors targeting miR-199a-3p, miR-199a-5p, and miR-1908 as potential new agents for the treatment of metastatic melanoma.

Mechanisms Underlying miRNA Deregulation in Metastasis

The emergence of miRNAs as essential regulators of tumor progression and metastasis triggered much interest in the upstream molecular mechanisms that give rise to deregulated expression of these tiny RNAs in human cancers. Multiple studies have shown that miRNA deregulation in cancer can be attained through diverse mechanisms, including genomic copy alterations, epigenetic changes, transcriptional regulation, and post-transcriptional processing aberrations (Ma et al., 2007; Png et al., 2011; Kumar et al., 2007). We herein found that upregulation of miR-199a-3p, miR-199a-5p, and miR-1908 in

metastatic melanoma cells was attained through a combination of transcriptional and post-transcriptional/processing mechanisms. By searching for transcription factor binding sites present in the promoter regions of miR-199a-1, miR-199a-2, and miR-1908, I identified CREB as a putative transcription factor that regulates the expression of miR-199a-3p, miR-199a-5p, and miR-1908 in metastatic melanoma cells (Table 2.1, Figures 2.23-2.24). Consistent with our findings on the three miRNAs, CREB was previously implicated as a promoter of melanoma invasion and metastasis (Aucoin et al., 2004; Dobroff et al., 2009). While further ChIP experiments will be necessary to support a direct transcriptional interaction between CREB and the promoter regions of the three miRNAs in melanoma cells, our findings suggest that at least a part of the pro-invasive effects of CREB in melanoma may be mediated through the transcriptional induction of miR-199a-3p, miR-199a-5p, and miR-1908.

We observed that the levels of phosphorylated CREB were elevated in metastatic melanoma cells, suggesting one possible mechanism through which enhanced CREB activity might contribute to the elevated transcription of miR-199a-3p, miR-199a-5p, and miR-1908 in highly metastatic melanoma cells. From a therapeutic standpoint, it will be of interest to identify the specific kinase that mediates phosphorylation and activation of CREB in metastatic melanoma cells. Small molecule-mediated inhibition of such a kinase could represent a viable therapeutic option in melanoma metastasis. The clinical interest in targeting CREB is further augmented by a recent report showing that elevated CREB activation conferred acquired resistance to the B-Raf kinase inhibitor vemurafenib in a subset of *B-Raf*-mutant melanomas (Johannessen et al., 2013). These findings raise the intriguing question of whether miR-199a-3p, miR-199a-5p, and miR-1908 become induced in

vemurafenib-resistant melanoma tumors following CREB activation and can thus contribute to the progression of vemurafenib-resistant melanomas. If this turns out to be the case, we hypothesize that potential vemurafenib resistance outcomes could be managed by LNA-based combinatorial miRNA inhibition therapy.

In addition to aberrant transcriptional regulation of miR-199a and miR-1908 in a subset of metastatic melanoma derivatives, we uncovered an important role for deregulated miRNA processing in metastatic melanoma. Our findings of increased mature to pri-miRNA expression ratios for miR-199a-3p and miR-199a-5p across all metastatic derivatives that we examined (Figure 2.27) suggest a pervasive deregulation in the processing of miR-199a-3p and miR-199a-5p in melanoma metastasis. In comparison, the mature to pri-miRNA expression ratios for miR-1908 were modestly elevated across the metastatic derivatives of the MeWo line, but not in the A375 metastatic variants, suggesting that overexpression of miR-1908 in the A375 metastatic cells might be primarily mediated transcriptionally. Interestingly, miR-1908 exhibited less pronounced upregulation (up to 5-fold) compared to that displayed by each miR-199a-3p (up to 100-fold) and miR-199a-5p (up to 10,000-fold) in metastatic melanoma cells, suggesting that aberrant miRNA processing may be a determinant of the substantially more dramatic overexpression observed for miR-199a-3p and miR-199a-5p, which arise from the same precursor hairpin and are processed together. It will be of interest for future studies to explore the precise molecular step(s) in the miRNA processing pathway, at which potential deregulation occurs. Namely, a relevant question for future studies to address is whether the alteration happens at the pri-miRNA to pre-miRNA Drosha/DGCR8-mediated conversion, the nuclear to cytoplasmic pre-miRNA trafficking mediated by Exportin-5, or the Dicer/TARBP2-mediated cleavage of the pre-miRNA to

generate the mature miRNA. The fact that the miRNA overexpression observed in highly metastatic melanoma cells was restricted to a subset of four specific miRNAs suggests the effect to be mediated by miRNA-specific processing regulator(s) as opposed to global miRNA processing effectors such as Dicer or Drosha. Systematic computational and biochemical approaches should provide exciting insights into the precise molecular effector(s) responsible for the processing alteration(s) of miR-199a-3p, miR-199a-5p, and miR-1908 in metastatic melanoma cells.

Implications for the ApoE Variants (ApoE2, ApoE3, ApoE4) in Melanoma Progression

Prior to our discovery of ApoE as a metastasis suppressor in melanoma, the biological role of ApoE had been well established in other disease contexts such as cardiovascular and neurodegenerative disorders (Hatters et al., 2006; Corder et al., 1993). *ApoE* exists as a polymorphic molecule with three major variants. Of the three known human *ApoE* alleles (*ApoE2*, *ApoE3*, and *ApoE4*), *ApoE3* exhibits the highest prevalence and is present in ~78% of the population (Hatters et al., 2006). The three isoforms are identical apart from two distinct residues at amino acid positions 112 and 158 in the N-terminal region, which contains the ApoE receptor-binding domain. These structural variations are thought to give rise to distinct functional attributes among the variants. Consistent with this, the three ApoE isoforms differ in their binding affinity for members of the LDL receptor family, lipoprotein-binding preferences, and N-terminus stability. Namely, ApoE2 has 50- to 100-fold attenuated LDL receptor binding ability compared to ApoE3 and ApoE4 (Weisgraber et al., 1982), while ApoE4, unlike the other two variants, preferentially binds to large low-density lipoproteins (Weisgraber et al., 1990) and exhibits the lowest N-terminus stability (Morrow

et al., 2000). These functional differences confer pathophysiological properties to select ApoE isoforms. While *ApoE3* is considered a neutral allele, *ApoE2* is associated with type III hyperlipoprotenemia (Hatters et al., 2006) and *ApoE4* represents the major known genetic risk factor for Alzheimer's disease (Corder et al., 1993) and also correlates with a modestly increased risk of developing cardiovascular disease (Luc et al., 1994). Our findings from melanoma cell lines homozygous for the *ApoE3* allele and observations on recombinant ApoE3's melanoma-suppressive activity are consistent with sufficiency of ApoE3 in suppressing melanoma metastasis.

It will be of interest in the future to determine whether ApoE2 and ApoE4 can suppress pro-metastatic melanoma progression phenotypes to an extent similar to that observed for ApoE3. Additionally, large-scale epidemiologic studies are necessary to establish whether specific *ApoE* genotypes might confer enhanced genetic risk of melanoma development and/or likelihood of metastatic progression. Another outstanding question to address will be whether LXRβ/*ApoE* activation therapy could elicit similar melanoma-suppressive responses in patients harboring the low-prevalence hypomorphic *ApoE2* or *ApoE4* variants, in the case that ApoE2 and ApoE4 are found to display inferior activity in suppressing melanoma progression. Given that the majority of *ApoE2* /*ApoE4*-expressing patients also express an *ApoE3* allele, we speculate that they may at least partially respond to LXR agonist therapy.

LRP1/LRP8 Targeting by Extracellular ApoE

Our findings reveal an essential role for extracellular ApoE in the suppression of melanoma progression phenotypes. ApoE can distribute in the circulatory system both in a lipoprotein-bound and a lipid-free state (Hatters et al., 2006). While we have shown that lipid-free recombinant ApoE was sufficient to suppress melanoma invasion and endothelial migration, it is possible that ApoE contained in lipoprotein particles could also suppress melanoma invasion and endothelial recruitment, especially in light of the fact lipid-associated ApoE exhibits even greater affinity for its receptors compared to lipid-free ApoE (Hatters et al., 2006). The ability of recombinant ApoE to inhibit these pro-metastatic phenotypes as well as the increased melanoma invasion and endothelial recruitment phenotypes seen with antibody-mediated ApoE neutralization suggest that the ApoE molecule itself, rather than any associated lipid particle, is the key mediator of these phenotypes.

Our findings elucidated a dual melanoma cell-autonomous/non-cell-autonomous mode of action for extracellular ApoE. Melanoma-derived ApoE suppressed melanoma cell invasion and cell-extrinsic endothelial recruitment through its divergent targeting of melanoma-cell LRP1 and endothelial-cell LRP8 receptors, respectively. Importantly, the engagement of these two receptors by ApoE in mediating metastasis suppression implicates LRP1 and LRP8 as novel endogenous suppressors of pro-metastatic phenotypes in melanoma. While further work is necessary to examine the molecular pathways downstream of each LRP1 and LRP8 that confer the ApoE-dependent effects on melanoma invasiveness and endothelial migration, the possible implications of ApoE/LRP8 and ApoE/LRP1 targeting to the modulation of each respective phenotype are discussed below.

Implications for LRP8 Receptor Targeting to Tumor Angiogenesis

The identification of LRP8 as the endothelial cell mediator of ApoE's effects on non-cell autonomous endothelial recruitment raises the interesting possibility that ApoE/LRP8 targeting might modulate tumor angiogenesis in additional epithelial cancer types that express ApoE. Therefore, understanding the molecular role of LRP8 in regulating cancer angiogenesis may have mechanistic implications for tumor angiogenesis beyond melanoma. Our preliminary work revealed that ApoE/LRP8 targeting could regulate VEGFR2 activation. Namely, we showed that treatment of human endothelial cells with ApoE blunted ligand-induced VEGFR2 activation in an LRP8-dependent manner (Figure 4.10a). We subsequently validated these results in primary mouse endothelial cells genetically inactivated for one or both copies of *LRP8* (Figures 4.10b-c). Our results are consistent with a requirement for LRP8 in mediating the ApoE-dependent suppression of VEGFR2 activation. Given that the VEGFR2 receptor, an extensively studied determinant of endothelial cell biology, has been shown to play an essential role in mediating endothelial cell migration (Olsson et al., 2006), we speculate that ApoE/LRP8 targeting may suppress endothelial cell migration by decreasing VEGFR2 activation.

Additionally, we also observed that in primary mouse endothelial cells genetically inactivated for only one allele of *LRP8*, ligand-based VEGFR2 activation was increased at baseline relative to wild-type cells, indicative of a role for endogenous LRP8 in inhibiting VEGFR2 activation. Interestingly, this increase in VEGFR2 phosphorylation was not seen upon complete inactivation of LRP8, suggesting that the effect is specific to partial silencing of LRP8 (Figure 4.10c). How could one reconcile these observations? Given the well-known function of LDL receptors in endocytosis and lysosomal trafficking (Hussain et al., 1999) as

well as recent findings that some basal rate of VEGFR2 endocytotic recycling and dynamic turnover is necessary for optimum VEGFR2 receptor activity (Nakayama et al., 2013), we speculate that the inhibitory role of LRP8 in regulating VEGFR2 activation, unmasked upon loss of one *LRP8* allele, may be offset by a potential LRP8-based stabilization of VEGFR2 trafficking that is lost only upon full inactivation of *LRP8*. We hypothesize that LRP8 directly or indirectly associates with VEGFR2 at clathrin-coated pits at the plasma membrane. Upon treatment with ApoE, the LRP8 receptor likely undergoes internalization and recruits VEGFR2, thereby decreasing the effective amount of VEGFR2 present at the plasma membrane that is available for extracellular ligand activation. Ultimately, this is reflected by a decrease in VEGF-induced receptor phosphorylation. Similarly, the partial reduction of LRP8 in *LRP8*-heterozygous endothelial cells might result in less VEGFR2 being internalized, allowing for more receptors present at the plasma membrane to become phosphorylated upon ligand activation. However, full loss of LRP8 contrasts this. We speculate that the disinhibition of VEGFR2 activation seen in the *LRP8* -/+ context is cancelled out by a potential VEGFR2 receptor destabilization, due to impaired receptor endocytotitc trafficking, in the LRP8-/- context, resulting in a net VEGFR2 phosphorylation outcome that resembles the wild-type context. Further experiments are necessary to establish LRP8 as a novel regulator of VEGFR2 and to either support or disprove the experimental hypothesis described above. Given the well-known functions of VEGFR2 during endothelial cell development and endothelial stalk/tip cell fate specification (Olsson et al., 2006), this work will potentially have important implications for both tumor angiogenesis as well as physiological angiogenesis.

Potential Mechanisms Downstream of ApoE/LRP1 Targeting in Melanoma Cells

Unlike the identification of LRP8 as the single endothelial-cell downstream mediator of ApoE, the great molecular heterogeneity displayed by melanoma tumors makes it possible that, besides LRP1, additional melanoma-expressed ApoE receptors could mediate the ApoE response in melanoma cells from diverse patients. Nevertheless, our identification of LRP1 as one such melanoma-expressed receptor that can mediate ApoE's effects on melanoma cell invasiveness raises the interesting question of how LRP1 regulates invasion. Previous work showed that LRP1 associates with the platelet-derived growth factor receptor beta (PDGFRβ) in the endosomal compartments, and depletion of LRP1 enhanced expression and activation of PDGFRβ in mouse fibroblasts and smooth muscle cells (SMCs) (Boucher et al., 2003; Takayama et al., 2005; Muratoglu et al., 2010). Consistent with our findings of ApoE/LRP1-mediated suppression of melanoma invasion (Figure 4.5), ApoE was previously shown to suppress PDGF-induced SMC migration, whereas depletion of LRP1 prevented the inhibitory effect of ApoE on PDGF-dependent SMC migration (Swertfeger et al., 2002). Additionally, independent of mediating ApoE's effects, LRP1 inactivation alone increased SMC migration at baseline and in response to PDGF (Zhou et al., 2009). In light of the known role of the ApoE/LRP1 pathway in suppressing SMC migration, it will be of interest to evaluate the effects of ApoE/LRP1 targeting on melanoma cell migration. Given that cell invasion and migration are two phenotypes that are often coupled in cancer cells since a metastatic cancer cell typically must be able to also migrate as it invades into surrounding tissues (Ma etal., 2007; Huang et al., 2008; Tavazoie et al., 2008; Valastyan et al., 2009b), it is possible that ApoE targeting of LRP1 suppresses melanoma invasion and/or possibly migration by engaging PDGFRβ signaling, as previously described in SMCs. In light of the

reported association of LRP1 with PDGFRβ in endosomes (Muratoglu et a., 2010) and the disinhibition of PDGFRβ expression and signaling seen upon LRP1 inactivation in SMCs (Boucher et al., 2003; Zhou et al., 2009), an interesting emerging hypothesis is that the ApoE-dependent suppression of melanoma cell invasion may arise through an increase in LRP1-induced PDGFRβ endocytotic trafficking with a resulting decrease in cell-surface PDGFRβ activation and signaling.

The potential involvement of PDGFRβ in the ApoE/LRP1-dependent effects on melanoma invasion and metastasis is especially relevant in light of recent findings that PDGFRβ overexpression could determine resistance emergence to B-Raf inhibition therapy in a subset of *B-Raf*-mutated melanoma patients (Nazarian et al., 2010). This raises the interesting possibility that LXRβ/*ApoE* activation therapy may suppress the progression of B-Raf inhibitor-resistant melanomas (Figure 5.23) at least in part through triggering ApoE/LRP1-dependent repression of PDGFRβ signaling.

Besides the well-known role of cell-surface LRP1 in mediating cellular endocytosis, there is some evidence that LRP1 can also play a cell-signaling role through gamma secretase-catalyzed cleavage of its intracellular domain (ICD). Accordingly, gamma secretase was found to inhibit inflammatory signaling in macrophages through the proteolytic generation of an LRP1-ICD fragment, which was found to translocate into the nucleus and indirectly repress the transcription of lipopolysaccharide-inducible genes by transcription factor sequestration and nuclear export (Zurhove et al., 2008). Interestingly, LRP8 can also be proteolytically processed to generate an ICD domain that is then released into the cytoplasm (May et al., 2003). Even though the ability of LRP8-ICD to translocate into the nucleus and regulate gene expression in a manner similar to that described for LRP1-ICD is

presently unknown, these findings suggest a regulatory role for LRP1/LRP8 targeting involving a cell-signaling mechanism alternative to endocytosis. Namely, ApoE/LRP1 and/or ApoE/LRP8 targeting might modulate gene expression programs in melanoma and/or endothelial cells, respectively, through proteolytic LRP1/LRP8 processing and generation of LRP-ICD fragments, which possess transcription regulatory activity.

Metastatic Endothelial Recruitment

Our systematic analyses of pro-metastatic phenotypes displayed by *in vivo*-selected highly metastatic melanoma cells have revealed that, in addition to the well-characterized phenotype of cancer cell invasion, metastatic melanoma cells also acquire an enhanced capacity to recruit endothelial cells both *in vitro* and *in vivo*. Importantly, we identified three metastasis-promoting miRNAs as novel regulators of metastatic endothelial recruitment (MER) in melanoma and showed that their convergent targets, *ApoE* and *DNAJA4*, act as suppressors of MER. Consistent with this, LXR activation therapy, which robustly suppresses melanoma progression by activating *ApoE* expression, was also found to inhibit endothelial recruitment and melanoma tumor angiogenesis, underscoring the importance of endothelial-cancer cell interactions for melanoma metastatic progression.

Even though tumor angiogenesis has long been known to be essntial for tumor progression, MER—the active process of non-cell-autonomous recruitment of endothelial cells by incipient metastases—has only recently emerged as a key cellular phenotype in cancer progression. In addition to melanoma, previous findings from our group have indicated that MER plays a crucial role in breast cancer metastatic initiation as well (Png et al., 2012). Highly metastatic breast cancer cells were found to display an enhanced capacity

to recruit endothelial cells compared to poorly metastatic breast cancer cells. Additionally, the metastasis suppressor miR-126 was found to suppress breast cancer metastatic initiation by targeting a set of cancer cell-expressed genes (*IGFBP2, PITPNC1*, and *MERTK*), each of which was shown to act as a promoter of MER. By silencing miR-126, metastatic breast cancer cells upregulate secretion of IGFBP2 and the MERTK ectodomain, which in turn engage the IGF1 receptor and Gas-6/MERTK receptor signaling pathways on endothelial cells, respectively. Whereas IGFBP2 was found to directly interact with IGF-1 and promote IGF1R-dependent endothelial migration, cancer-derived MERTK was shown to act as a decoy receptor for Gas-6, the ligand for MERTK, and thus repress the endothelial cell MERTK receptor, which is inhibitory to endothelial migration (Png et al., 2012). Our collective findings from breast cancer and melanoma highlight MER as a common key attribute of metastatic cells from two different epithelial cancer types. The importance of endothelial cells for cancer progression phenotypes (Carmeliet and Jain, 2011) complements the diverse roles of these cells in developmental (Lammert et al., 2001) and regenerative biology (Ding et al., 2011; Ding et al., 2010; Kobayashi et al., 2010). In addition to their passive role in supplying oxygen and nutrients to the tumor, it will be of great interest to examine the potential active/signaling role(s) that endothelial cells may play within the tumor microenvironment in dynamically modulating metastatic progression.

Metastasis Suppression by DNAJA4

The identification of DNAJA4 as a novel suppressor of melanoma progression phenotypes raises the interesting question of how DNAJA4 suppresses melanoma metastasis. Our findings revealed that at least a part of the effects of DNAJA4 were mediated through its

positive regulation of the metastasis-suppressive extracellular factor ApoE. Through epistasis experiments, we showed that the DNAJA4-mediated suppression of melanoma invasion and cell-extrinsic endothelial recruitment was dependent on the downstream induction of ApoE expression (Figure 3.11). However, it still remains unclear how DNAJA4 regulates ApoE expression. Additionally, the incomplete rescue of the DNAJA4-dependent invasion phenotype upon modulation of ApoE levels suggests that additional DNAJA4-dependent target genes might be involved in conferring suppression of melanoma invasion by this heat-shock factor in melanoma.

DNAJA4, a poorly characterized heat-shock protein (HSP) that belongs to the Hsp40 family of HSPs, has no previously implicated role in cancer progression. HSPs are normally present at basal levels in the cell and typically become induced in response to heat and/or other environmental stressors. In light of our identification of DNAJA4 as a suppressor of melanoma metastasis, this raises the interesting possibility that DNAJA4 induction upon UV light exposure might act as an endogenous tumor-suppressive mechanism guarding against melanoma development and/or progression. Future studies are needed to address whether DNAJA4 expression in benign melanocytic lesions and/or primary melanoma lesions is affected by UV radiation.

HSPs can have diverse molecular functions such as protein folding and assembly, post-translational protein modification, control of protein aggregation, regulation of protein stability/degradation, intracellular transport, and chaperoning of protein-protein interactions. Even though the name of DNAJA4 suggests potential involvement in DNA binding and transcriptional regulation based on its Hsp40 bacterial homolog, DnaJ, which has known roles in chaperoning DNA-binding of bacterial replication factor RepA and thereby

facilitating bacterial replication (Wickner et al., 1991), the ability of mammalian DNAJA4 to directly and/or indirectly interact with DNA and regulate gene expression is presently unknown. Contrary to a potential transcriptional regulation of *ApoE* by DNAJA4, we did not observe any effect on the activity of an *ApoE* promoter construct by knocking down DNAJA4 (data not shown). Given that DNAJA4 increased both *ApoE*'s transcript and protein levels, our findings are consistent with post-transcriptional modulation of the *ApoE* mRNA stability and/or processing, which is also reflected at the protein levels.

Alternatively, given that *DNAJA4* harbors multiple miRNA binding sites both in its CDS and 3'UTR (Figure 3.4), it is possible that the *DNAJA4* mRNA indirectly induces *ApoE* expression by competing with the *ApoE* transcript for miR-199a-5p and/or miR-1908 binding and sequestering away the miRNAs from acting on *ApoE*. By strongly downregulating *DNAJA4* expression, highly metastatic melanoma cells may ensure *ApoE* silencing through greater occupancy of the *ApoE* transcript by the metastasis-promoting miR-199a-5p and miR-1908. Interestingly, a similar mechanism of action was recently demonstrated for *HMGA2*, one of the target genes of the metastasis suppressor let-7. In addition to its protein-coding function in metastasis, the *HMGA2* transcript was found to indirectly promote lung cancer metastasis in a non-coding manner through its sponge effects on let-7 activity (Kumar et al., 2014).

To gain further mechanistic insight into the biological function of DNAJA4, we performed mass-spectrometric analyses to identify potential interacting partners of DNAJA4 in melanoma. Interestingly, we found a set of five proteins (PFKFB3, HNRNPF, PSMD11, FLG, or TPM4) that specifically associated with the metastasis-regulatory isoform 3 of DNAJA4, but not with isoform 2 that was found to lack activity in suppressing melanoma

invasion (Figures 3.12-3.13). Out of these putative interacting partners, PFKFB3 was recently implicated as an important regulator of vessel sprouting and endothelial tip cell directional migration. PFKFB3, an enzyme catalyzing the rate-limiting step in glycolysis, was found to localize with F-actin and compartmentalize at the leading edge of the cell, where ATP production by PFKFB3-driven glycolysis drives actin remodeling and cell migration (De Bock et al., 2013). Interestingly, this report also showed that, in addition to interacting with F-actin, PFKFB3 also associates with tropomyosin 4 (TPM4), one of the other potential DNAJA4.3-specific interacting partners that we identified independently (Figure 3.13). Based on these findings, we hypothesize that the three proteins, DNAJA4.3, PFKFB3, and TPM4, may associate together in a complex. Given the putative interaction between DNAJA4.3 and PFKFB3/TPM4, the previously implicated role of PFKFB3 in cell migration, and the frequent coupling of cell invasion and migration phenotypes in cancer cells, we speculate that DNAJA4.3 might inhibit melanoma invasion at least in part through interacting with PFKFB3 and/or TPM4 and altering their actin-remodeling activity and/or localization to the leading edge of the cell. Future work will examine whether PFKFB3 and TPM4 regulate invasion and/or migration in melanoma cells and will characterize the biochemical interactions between DNAJA4.3 and these two proteins. Finally, it will be of interest to examine whether any of the potential DNAJA4-interacting partners are also involved in the DNAJA4-dependent regulation of ApoE expression and/or additional secreted factors that could account for DNAJA4's effects on cell-extrinsic endothelial cell recruitment.

The LXRβ Receptor as a Novel Therapeutic Target in Metastatic Melanoma

Our systematic analyses of multiple *in vivo* selected highly metastatic melanoma derivatives led to the discovery of a cooperative multi-miRNA regulatory network that converges onto a single molecule, *ApoE*. In the pathway that we uncovered, three metastasis-promoting miRNAs silenced *ApoE,* whereas the metastasis-suppressor DNAJA4 induced *ApoE*. The tight control exerted on *ApoE* expression in melanoma highlights the importance of this gene as a metastasis suppressor. Indeed, epistasis experiments revealed the miRNA-dependent effects on metastatic colonization to be fully mediated by *ApoE* (Figure 3.7). Based on these findings, we hypothesized that activation of *ApoE* expression might mimic the robust effects of miRNA inhibition and thus have efficacy in suppressing melanoma progression. Consistent with this, we observed that pre-treating melanoma cells from multiple patients with ApoE protein abolished their subsequent metastatic capacity (Figure 4.3). Conversely, genetic inactivation of stromal *ApoE* accelerated lung colonization by melanoma cells (Figure 4.4). Taken together, these findings provide strong evidence that extracellular ApoE, derived either from melanoma cells or the stromal compartments, can act as a strong suppressor of melanoma progression and, as such, may represent an attractive therapeutic target in melanoma.

We reasoned that an ideal therapeutic approach to activate *ApoE* in metastatic melanoma would be to induce circulating extracellular ApoE protein globally by activating ApoE production in both the tumoral and stromal compartments. To that end, we identified the nuclear hormone receptor LXRβ, a previously known transcriptional trans-activator of *ApoE* (Laffitte et al., 2001) that is expressed across most tissues (Song et al., 1994), as a novel therapeutic target, which exhibited ubiquitous expression across melanoma as well

(Figures 5.1 and 5.5). Our findings of broad-spectrum metastasis suppression upon LXRβ activation across multiple xenograft and genetically initiated models highlight the promise of nuclear hormone receptor targeting as a novel therapeutic approach in metastatic melanoma. Nuclear hormone receptors such as the androgen and estrogen receptors have proven to be key therapeutic targets in prostate and breast cancers, whose initiation and progression are intricately linked to the androgen and estrogen sex hormones. Pharmacologic agents targeting the androgen and estrogen receptors, respectively, represent the mainstay of therapy in these two cancers (Scher et al., 2012; Deblois and Giguère, 2013). Our identification of LXRβ as a therapeutic target in melanoma further expands the therapeutic potential displayed by this class of transcription factors by revealing that nuclear hormone receptor targeting could represent a viable therapeutic strategy in epithelial cancers that originate from non-reproductive tissues.

While the ubiquitous basal expression of cellular *LXRβ* in melanoma and other tissue types is likely required for homeostatic metabolic needs, it leaves melanoma cells broadly vulnerable to its modulation for the induction of tumor-suppressive phenotypes. Even though nuclear hormone receptors such as LXRs transcriptionally regulate multiple downstream target genes (Calkin and Tontonoz 2012), our findings reveal that the suppression of melanoma progression in response to LXRβ activation is mediated by the transcriptional induction of a single target gene, *ApoE*. While LXRβ likely retains many additional target genes that may or may not contribute to melanoma progression, our molecular and genetic evidence from *ApoE* silencing experiments indicates that, in the absence of *ApoE*, any melanoma-suppressive effects of LXRβ activation through *ApoE* and/or additional target genes are eliminated. Therefore, even if there were additional LXRβ target genes that

mediate various aspects of melanoma progression, they likely require *ApoE* for their function, as they fail to mediate tumor suppression in the absence of *ApoE*. Thus, we conclude that ApoE is the primary mediator of LXRβ-dependent melanoma suppression.

Presently, there are two known isoforms of the liver-X receptor, *LXRα* and *LXRβ*, which were cloned at roughly the same time by multiple groups (Apfel et al., 1994; Willy et al., 1995; Song et al., 1994; Shinar et al., 1994; Teboul et al., 1995). LXRs belong to a family of nuclear hormone receptors that are endogenously activated by cholesterol and its various oxygenated derivatives known as oxysterols (Janowski et al., 1996). Thus, LXRs serve as intracellular cholesterol-sensors that provide a feedback signal to maintain systemic cholesterol levels. Upon high cholesterol supply, LXR activation mediates transcription of multiple genes involved in cholesterol and fatty acid metabolism (Calkin and Tonotnoz, 2012). In light of our findings on melanoma suppression through pharmacologic LXRβ activation, the ability of cholesterol to activate LXRs may bear interesting implications for the interaction of dietary cholesterol and melanoma progression. Future studies are needed to determine whether high dietary cholesterol levels could sufficiently activate LXRβ to elicit melanoma tumor suppression.

LXRs regulate target gene transcription by forming obligate heterodimers with RXRs (Willy et al., 1995). The LXR/RXR heterodimer resides in an inactive state within the enhancer region of target genes by recognizing and binding to *cis*-acting LXR response elements (LXRE). Structural studies have revealed that allosteric interaction of an LXR agonist with the ligand-binding domain of LXR (LXR-LBD) triggers a conformational change in the protein, resulting in the positioning of C-terminal helix 12 (also known as the activation function 2 (AF-2) domain) right above the ligand-binding pocket. This leads to the

release of any bound co-repressor and the introduction of a co-activator binding site. Co-activator binding ultimately allows for recruitment of the basal transcriptional machinery and activation of target gene transcription (Svensson et al., 2003; Calkin and Tontonoz, 2012). The LXR-LBD possesses a great extent of structural flexibility, allowing it to accommodate various endogenous and synthetic ligands that share very little structural homology, yet are able to trigger receptor activation through a common mechanism affecting the conformation of AF-2 and co-activator recruitment (Färnegårdth et al., 2003).

Even though LXRs typically work in tandem with RXRs, we found that LXR activation exhibited more robust activity than RXR agonism in broadly suppressing melanoma cell invasion, with RXR activation failing to inhibit endothelial recruitment by melanoma cells. Additionally, in contrast to the robust suppression of melanoma metastasis observed upon LXR activation therapy, we found that RXR activation therapy lacks metastasis-suppressive activity *in vivo* and it might even promote melanoma metastasis at early time points (data not shown). Even though both LXRs and RXRs in tandem upregulate *ApoE* transcription, RXRs can retain additional heterodimeric partners such as farnesoid X receptors (FXRs), retinoid acid receptors (RARs), and peroxisome proliferator-activated receptors (PPARs) that activate alternative sets of transcriptional pathways (Barish and Evans, 2004; Calkin and Tontonoz, 2012). Thus, we speculate that the inferior ability of RXR agonism in suppressing melanoma progression phenotypes may stem from its modulation of additional secreted factor(s) that might antagonize ApoE's suppressive effects. Consistent with this, transcriptomic profiling of melanoma cells treated with the RXR agonist bexarotene revealed that, in addition to upregulating *ApoE* expression, RXR activation induced the expression of a number of additional genes (data not shown) previously

implicated to have a pro-tumorigenic and pro-metastatic functions, such as MERTK (Png et al., 2012), and ANGPTL4 (Padua et al., 2008). Importantly, none of these genes were induced by the LXR agonist treatment, suggestive of downstream target decoupling between LXRs and RXRs.

Potential Roles of LXR Targeting in Other Epithelial Cancer Types

Prior to our discovery of LXRβ as a novel broadly expressed therapeutic target in melanoma, LXR signaling was implicated in the progression of several additional epithelial cancer types. Consistent with our findings of LXR-mediated suppressive effects in melanoma, oral administration of GW3965 was recently shown to inhibit tumor growth by glioblastoma cells (Guo et al., 2011). Although this study did not examine any potential effects on metastasis, this work found that GW3965 suppressed the tumor growth by an *EGFR*-mutant glioblastoma line through enhancement of tumor cell apoptosis (Guo et al., 2011). In contrast, we found that LXR activation inhibited melanoma tumor angiogenesis and proliferation without any observed effects on tumor apoptosis, suggesting that the respective reductions of *EGFR*-mutant glioblastoma and melanoma tumor growth by LXR agonists are elicited through disparate mechanisms.

Contrary to our findings of melanoma metastasis suppression upon LXR activation, 27-hydroxycholesterol, an oxysterol that acts as a partial LXR agonist as well as an estrogen receptor agonist, was recently shown to modestly increase metastatic dissemination in an inflammatory model of murine breast cancer (Nelson et al., 2013). The potentially different roles played by LXR agonism in breast versus melanoma metastasis could be attributed to cancer type-specific differences or 27-hydroxycholesterol's partial agonism of LXR

signaling. Further experiments are needed to determine whether LXR agonism actually increases metastatic colonization by breast cancer cells that are more representable of human breast cancer.

Besides its stable expression in melanoma, LXRβ exhibits ubiquitous expression across multiple additional metastatic cancer types, as evidenced by previous analyses of nuclear hormone receptor expression in the NCI60 cancer cell line collection (Holbeck et al., 2010). This suggests that LXRβ could represent a therapeutic target in other metastatic cancers as well. Our findings of a cell-extrinsic function of ApoE in inhibiting melanoma angiogenesis suggest that other angiogenic tumor types may also respond to LXRβ activation therapy in an ApoE-dependent fashion. However, for cancers to sustain the full impact of ApoE's suppressive activity, they would need to also express LRP1 or a related ApoE receptor, which could mediate invasiveness suppression as we found for melanoma cells (Figure 4.5). The comprehensive pre-clinical analyses across multiple melanoma models described in the present thesis work will provide the framework for testing the therapeutic potential of LXRβ across additional cancer types in the future.

Clinical Implications for LXRβ Activation Therapy in Melanoma

The final results chapter of this thesis (Chapter V) describes the scientific basis for testing LXRβ activation therapy in clinical trials by demonstrating its broad-spectrum activity and safety across multiple pre-clinical mouse models of melanoma progression. Importantly, the strong melanoma-suppressive effects of LXR agonists occurred in the absence of any noted potential adverse effects such as weight loss or symptomatic health deterioration. LXR agonists were originally developed and conceived as life-long therapies

for the chronic management of dyslipidemia (Joseph and Tontonoz, 2003). Their clinical application, however, was stalled when they were found to modestly, yet reversibly, elevate LDL-cholesterol levels in primates—an effect stemming from LXRα-modulated induction of cholesteryl ester transfer protein (CETP) (Groot et al., 2005). Their failure to reduce cholesterol levels was a major setback for the clinical development of these agents in cardiovascular disease. However, such modest lipid-profile alterations would not pose an obstacle for the testing of these agents in metastatic melanoma, especially in light of the high mortality rate in melanoma, the accepted toxicities arising from approved melanoma drugs (2-3% mortality rate for anti-CTLA-4 Ab (Hodi et al., 2010); 18-26% risk of cutaneous squamous cell carcinoma for vemurafenib (Chapman et al., 2011)), and the clinically accepted dyslipidemia effects of a number of approved therapeutics such as retinoids and rexinoids (Duvic et al., 2001). Additionally, dyslipidemia can be readily managed by the use of statins (hypercholesterolemia) and fibrates (hypertriglyceridemia). To simulate this in a pre-clinical model, we tested the ability of GW3965 to suppress melanoma progression in the setting of its co-administration with lipitor and gemfibrozil—clinical agents widely used for lowering cholesterol and triglyceride levels, respectively. Importantly, neither of these drugs affected the ability of GW3965 to suppress tumor growth (data not shown), suggesting that any potential adverse effects of LXR agonists on cholesterol and triglyceride levels in humans could be managed by lipitor and/or gemfibrozil treatment, if need be, without compromising the tumor-suppressive activity of LXR agonists.

Based on our findings of broad-spectrum suppression of melanomas of diverse mutational subtypes, we propose that future clinical trials test the activity of LXRβ activation therapy in patients with advanced (stage IV) melanoma bearing *B-Raf* wild-type or *B-Raf*

mutant tumors that are insensitive to approved agents such as dacarbazine, vemurafenib, ipilimumab, or novel experimental agents targeting MEK or PD-1. Importantly, our observations of tumor-suppressive activity of the LXR agonist treatment in melanomas resistant to vemurafenib or dacarbazine motivates the clinical testing of LXR activation therapy in patients, whose melanomas have previously progressed on dacarbazine or vemurafenib. Furthermore, our findings of tumor-suppressive cooperativity between LXR activation and the three present melanoma mainstay therapeutics (dacarbazine, vemurafenib, and the CTLA-4 antibody) calls for the clinical testing of combination therapeutic regimens incorporating LXR agonist treatment (Figures 5.24-5.27). Finally, given the herein demonstrated activity of LXRβ activation therapy in suppressing brain metastatic colonization (Figure 5.10), the trial population should also contain melanoma patients with brain metastasis, who are prevalent (about 30% of all melanoma metastasis outcomes) and for whom there currently exist no approved therapies targeting brain metastasis (Fonkem et al., 2012).

Demonstration of safety and efficacy in such advanced stage melanoma clinical trials will enable the subsequent testing of LXR agonist agents for the prevention of melanoma metastasis in clinical trials with stage II and III patients who are at risk for metastatic relapse. Importantly, the robust prognostic capacity of ApoE expression in stratifying melanoma patients into those at low risk versus high risk for metastatic relapse (Figure 3.15) suggests that expression levels of this gene may be a useful diagnostic for selecting high-risk patients in need of metastasis prevention therapy after resection of their primary tumors.

Potential Solutions to Emergence of Clinical Resistance to LXR Activation Therapy

Despite the unprecedented clinical success of the two recently approved melanoma therapeutics, the B-Raf kinase inhibitor vemurafenib and the anti-CTLA-4 immunomodulatory antibody, the present median survival time of advanced melanoma patients still remains less than two years. This is in large part due to the notorious propensity exhibited by advanced stage metastatic melanomas to develop resistance to single-agent targeted therapies such as the ones presently used in the clinic (Nazarian et al., 2010; Poulikakos et al., 2011; Prahallad et al., 2012). Cancer cells display a great extent of molecular plasticity, which allows them to re-wire and activate multiple compensatory pathways and/or mutate signaling effectors in response to a selection pressure, thereby escaping modulation by targeted therapeutics (Bernards, 2012). In contrast, non-transformed stromal tissues are less prone to re-wiring and the development of resistance to targeted agents. Our observations that the melanoma-suppressive activity of LXR agonists was in large part mediated through the sustained elevation of ApoE in peripheral tissues suggest that resistance to LXRβ activation therapy in melanoma may be less likely to emerge through LXRβ mutational and/or expression alteration mechanisms in stromal tissues, in which LXRβ plays an essential metabolic role and its activity is likely to be tightly maintained. This finding also makes the LXRβ activation therapy described herein unique since this is the first targeted therapy that we know of to work through the activation of a metastasis suppressor gene (*ApoE*) in both the tumoral and stromal compartments. However, if resistance does emerge in the clinic, the development of next-generation LXRβ agonists that are able to bind and activate the mutated/deregulated receptor with greater potency might offer a potential solution to such resistance outcomes, as previously demonstrated by the clinical development

of next generation antiandrogens for the treatment of metastatic prostate cancer (Tran et al., 2009).

Alternatively, potential resistance to *ApoE* activation therapy could also arise through post-transcriptional mechanisms that silence *ApoE*, such as modulation by the three metastasis-promoting miRNAs (miR-199a-3p, miR-199a-5p, and miR-1908), which were found to convergently target *ApoE,* and/or the metastasis-suppressive factor DNAJA4, which was shown to induce *ApoE* expression. We predict that potential resistance to LXRβ-based transcriptional activation of *ApoE* may be overcome, as least in part, by LNA-mediated silencing of miR-199a-3p, miR-199a-5p, and miR-1908. Given that the three miRNAs convergently target and maximally silence the expression of *ApoE* and *DNAJA4*, miRNA inhibition should lift the post-transcriptional brake imposed on *ApoE* expression in metastatic melanoma cells. We thus speculate that combinatorial LNA-based miRNA silencing might represent an effective therapeutic alternative in cases where LXRβ activation therapy fails to induce ApoE and elicit melanoma metastasis suppression. This is supported by our findings of strong metastasis reduction upon LNA-based inhibition of miR-199a-3p, miR-199a-5p, and miR-1908 across multiple melanoma lines (Figure 2.17). Furthermore, it will be of interest to examine potential therapeutic synergy upon combining *ApoE* transcriptional activation (LXRβ therapy) and *ApoE* post-transcriptional de-repression (LNA therapy) in the suppression of melanoma metastasis.

In the case that resistance emerges due to acquired unresponsiveness of melanoma tumors to sustained *ApoE* induction rather than an inability to activate *ApoE* expression, one could perform wide-genome RNAi synthetic lethality screens (Prahallad et al., 2012) to identify additional pathways in melanoma cells, whose concurrent molecular modulation

might confer responsiveness to LXRβ activation therapy. It will be of particular interest to determine whether mutational inactivation and/or expression deregulation of LRP1, the melanoma cell receptor found to mediate ApoE's effects on melanoma invasion, could represent a potential mechanism of acquired resistance to *ApoE* activation therapy. Given ApoE's effects in suppressing metastatic endothelial recruitment, we speculate that even if melanoma tumors lost their responsiveness to ApoE/LRP1 targeting, those tumors could still, at least partially, respond to ApoE activation therapy through ApoE/LRP8-dependent suppression of endothelial recruitment. LRP8's activity in non-transformed endothelial cells is likely to be tightly maintained.

Finally, our findings of melanoma-suppressive cooperativity in response to combining LXRβ activation with each of the three frontline melanoma therapeutics used in the clinic (dacarbazine, vemurafenib, and the CTLA-4 Ab) have important clinical implications and suggest that combination regimens incorporating LXR agonists could negatively impact the likelihood of clinical resistance emergence. Concurrent targeting of multiple pro-tumorigenic and/or pro-metastatic pathways will leave less room for melanoma cells to escape modulation by targeted therapeutics and may ultimately provide greater therapeutic benefit to patients. While the present findings are promising, future work is needed to determine the optimum dosing regimens to attain maximum melanoma suppression response upon combining LXR agonist treatment with either of the current frontline melanoma therapeutics.

Conclusions

This thesis describes the systematic interrogation of molecular pathways regulating melanoma metastasis. The identification of a set of miRNAs with pervasive upregulation across multiple melanoma metastatic derivatives was functionally supported by our findings of robust metastasis control exerted by these miRNAs. We utilized the three miRNAs as unbiased probes into the downstream biology of melanoma metastasis and uncovered a novel molecular pathway that surprisingly converges onto a single target gene, *ApoE*. Through complementary molecular, genetic, and pharmacologic approaches, we found that ApoE acts as a strong suppressor of metastatic progression, while its therapeutic activation represents a promising new approach for the treatment of melanoma metastasis. These findings illustrate the power of functionally guided systematic approaches for the unbiased discovery of novel metastasis regulatory molecules and their rational therapeutic targeting in cancer progression.

MATERIALS AND METHODS

Cell Culture

For a full list of cell lines used in this study, see Appendix A. Established melanoma cell lines were obtained from ATCC and cultured in standard conditions, following recommendations by the supplier. Primary HUVEC cells were obtained from ATCC and cultured in EGM-2 media supplemented with 2% FBS (CC-3162, Lonza). Primary human melanoma lines were generated at MSKCC following dissociation of melanoma cells from the tumors of patients the MSKCC. These primary cells were generously provided by Taha Merghoub (MSKCC). Primary cells were maintained in RPMI medium supplemented with 20% FBS. The SK-Mel-239 parental and vemurafenib-resistant clones (C1 and C5) were a gift from Poulikos Poulikakos (Mount Sinai Medical School), and the *B-Raf$^{V600E/+}$; Pten$^{-/-}$; CDKN2A$^{-/-}$* murine melanoma line (designated at YUMM) was generously provided by Marcus Rosenberg (Yale University).

Mouse Experiments

All mouse experiments were conducted in agreement with a protocol approved by the Institutional Animal Care and Use Committee (IACUC) at the Rockefeller University. NOD SCID, NOD SCID gamma, athymic nu/nu, and C57BL/6 (WT; *Tyr::CreER, B-Raf$^{V600E/+}$, Pten$^{lox/+}$; LXRa* -/-; *LXRβ* -/-) mice were obtained from the Jackson Laboratory. ApoE -/- mice were generously provided by Jan Breslow (Rockefeller University). All mouse genotyping was performed using standard PCR conditions and genotyping primers, as recommended by the Jackson Laboratory.

In Vivo Selection for Highly Metastatic Melanoma Derivatives

To generate multiple metastatic derivatives from the MeWo and A375 human melanoma cell lines, *in vivo* selection was performed as previously described (Minn et al., 2005; Pollack and Fidler, 1982). In brief, 1×10^6 MeWo or A375 melanoma parental cells were resuspended in 0.1 mL of PBS and intravenously injected into 6-8-week old immunocompromised NOD SCID mice. Following lung metastatic nodule formation, nodules were dissociated and cells were propagated *in vitro*, giving rise to first generation of lung metastatic derivatives (LM1). The LM1 cells were then subjected to another round of *in vivo* selection by injecting 2×10^5 LM1 cells into NOD SCID mice, giving rise to metastatic nodules, whose subsequent dissociation yielded a second generation of lung metastatic derivatives (LM2). For the A375 cell line, a third round of *in vivo* selection was performed, yielding the highly metastatic A375-LM3 derivatives. Cell dissociation of *in vivo* selected metastatic melanoma cells was performed by dissecting individual lung nodules, cutting them into small pieces, and dissociating individual cells by incubating the nodule pieces in 0.125% Collagenase Type I (XOM12195, Worthington Biochemical) and 0.1% Hyalouronidase (P1B12524, Worthington Biochemical) serum-free DMEM-based solutions for 3 hours at 37°C shaking and in 0.25 % Trypsin-EDTA (25200-056, Invitrogen) solution for 10 minutes at 37°C shaking. Trypsin digestion was neutralized in 10% FBS DMEM-based cell media. Following DNAse I (51M13032, Worthington Biochemical) treatment (20 000 unitl/L in 25 mM HEPES DMEM-based solution supplemented with 1 mg/mL BSA) for 10 min at 37°C shaking, single cells were filtered though a 70-μm cell strainer.

In vivo selection of the primary SK-Mel-334 and SK-Mel-462 cell lines was performed as described above. 1×10^6 parental SK-Mel-334 or SK-Mel-462 cells were

intravenously injected into NOD SCID gamma mice. Following formation of lung metastatic nodules, melanoma cells were dissociated, and expanded *in vitro*. 5×10^5 cells were then re-injected into NOD SCID mice for a second round of *in vivo* selection. For the generation of HT-144 and WM-266-4 metastatic derivatives, we injected 1.5×10^5 and 2×10^5 WM-266-4 or HT-144 parental cells, respectively, into NOD SCID mice in the first round of selection, and 1.5×10^5 and 2×10^5 WM-266-4 or HT-144 LM1 derivatives were re-injected for a second round of *in vivo* selection.

The MeWo brain-metastatic derivatives were generated by performing two successive rounds of *in vivo* selection with the MeWo parental cells. First, 5×10^5 parental MeWo cells resuspended in 0.1 mL of PBS were intracardially injected into athymic nu/nu mice. Upon formation of brain metastatic nodules, cells were dissociated, expanded *in vitro*, and re-injected intracardially at 2×10^5 cells/ 0.1 mL PBS per mouse. Cells dissociated from brain metastatic nodules ultimately yielded a second-generation of brain-metastatic MeWo cell line derivatives that were used in this study to test the efficacy of orally delivered GW3965 in suppressing brain metastatic colonization.

Experimental Metastasis Assays

In order to monitor metastasis *in vivo* through bioluminescence imaging, cancer cells were transduced with a retroviral construct expressing a luciferase reporter (Ponomarev et al., 2004). The indicated numbers of cancer cells were resuspended in 0.1 mL of PBS and administered via the lateral tail-vein or through an intracardiac injection, as indicated. For all metastasis experiments, lung, systemic, or brain colonization was monitored over time and quantified through non-invasive weekly bioluminescence imaging, as described previously (Minn et al., 2005). In all metastasis bioluminescence imaging experiments, photon flux was

normalized relative to the signal measured at day 0 immediately post-injection. Various numbers of cancer cells were injected in different experiments, as described below.

In Vivo Selection Validation

To determine whether *in vivo* selection for melanoma cells enriched in metastatic capacity had been achieved, 4×10^4 MeWo parental or MeWo-LM2 cells and 1×10^5 A375 parental or A375-LM3 cells were injected via the lateral tail vein into 6-8-week old NOD SCID mice.

Functional Testing of Metastasis Promoter miRNAs

For experimental metastasis assays testing the effects of putative promoter miRNAs on lung colonization, 4×10^4 MeWo parental cells overexpressing miR-199a, miR-1908, miR-214, or a control hairpin, 4×10^4 MeWo-LM2 cells with miR-Zip-based silenced expression of miR-199a-3p, miR-199a-5p, miR-1908, or a control sequence, and 2×10^5 A375-LM3 cells inhibited for miR-199a-3p, miR-199a-5p, miR-1908, or a control sequence were resuspended in 0.1 mL of PBS and tail-vein injected into NOD SCID mice.

LNA Pre-Treatment Experiments

To determine the effect of pre-treating melanoma cells with specific LNAs targeting miR-199a-3p, miR-199a-5p, or miR-1908 on metastasis, melanoma cells were transfected with LNAs targeting each miRNAs individually (50 nM), a cocktail of LNAs targeting all three regulatory miRNAs (50 nM), or a control LNA (50 nM) (426917, LNA-miR-199a-3p; 426918, LNA-miR-199a-5p; 426878, LNA-miR-1908; 199005, LNA-control; Exiqon). After 48 hours, 1×10^5 MeWo-LM2 cells (NOD SCID), 2×10^5 A375-LM3 cells (NOD SCID), 5×10^5 SK-Mel-2 cells (NOD SCID gamma), 5×10^5 WM-266-4 cells (NOD SCID),

5×10^5 HT-144 cells (NOD SCID), 5×10^5 A2058 cells (NOD SCID), and 5×10^5 SK-Mel-28 cells (NOD SCID gamma) were injected intravenously into NOD SCID or NOD SCID gamma mice, as indicated after each cell line. For systemic metastasis assays, 1×10^5 MeWo-LM2 cells, pre-treated with LNA-CTRL or LNA-3 miRNAs for 48 hours, were intracardially injected into athymic nu/nu mice.

In Vivo LNA Therapy

In the LNA therapy experiment, mice were tail-vein injected with 4×10^4 MeWo-LM2 cells and treated intravenously twice a week for four weeks and then once weekly with a cocktail of *in vivo*-optimized LNAs (Exiqon) antisense to mature miR-199a-3p, miR-199a-5p, and miR-1908 at a total dose of 12.5 mg/kg. The LNAs were delivered in 0.2 mL of PBS via the lateral tail vein. 0.2 mL of PBS was administered as a control mock treatment.

Epistasis Experiments

For miRNA loss-of-function experiments, 1×10^5 MeWo-LM2 cells expressing an shRNA targeting *ApoE*, *DNAJA4*, or a control sequence or siRNAs inhibiting *LRP1* or a control siRNA in the setting of miR-199a-5p or miR-1908 inhibition were intravenously injected into NOD SCID mice. For miRNA gain-of-function experiments, 4×10^4 MeWo parental cells overexpressing ApoE, DNAJA4, or an empty vector in the setting of miR-1908 overexpression were intravenously injected into NOD SCID mice.

ApoE Pre-Treatment Experiments

For ApoE pre-treatment experiments, melanoma cells were incubated in the presence of recombinant human ApoE3 (4696, BioVision) or BSA (A2153, Sigma-Aldrich) at 100 μg/mL at 37°C. After 24 hours, 4×10^4 MeWo-LM2 cells, 2×10^5 A375-LM3 cells, 1.5×10^5

WM-266-4 cells, 3.5×10^5 HT-144 cells, and 2×10^5 A2058 cells were injected via the tail-vein into NOD SCID mice. To determine the effect of genetic deletion of *ApoE* on metastasis, C57BL/6-WT or C57BL/6-*ApoE*-/- mice were intravenously injected with 5×10^4 B16F10 melanoma cells pre-treated with human recombinant ApoE3 (100 μg/mL) for 24 hours or control untreated B16F10 cells.

Effect of LXR Agonists on Metastasis

The LXR agonists GW3965 (Sigma-Aldrich, AdooQ Bioscience) and T0901317 (Tocris Bioscience) were formulated into mouse chow diet at the indicated doses (20, 75, or 100 mg/kg/day) by Research Diets, Inc. To test the effect of LXR agonist treatment on melanoma metastasis prevention, the following numbers of melanoma cells, resuspended in 0.1 mL of PBS, were injected intravenously via the tail-vein: 4×10^4 MeWo cells, 2.5×10^5 HT-144 cells, 4×10^4 SK-Mel-334.2 cells, 5×10^4 B16F10 cells, or 1×10^5 YUMM cells. The MeWo, HT-144, and SK-Mel-334.2 cells were injected into 6-8 week-old sex-matched NOD SCID mice, while the B16F10 and YUMM cells were injected into 6-8 week-old sex-matched C57BL/6-WT mice. In all experiments testing the effects of GW3965 on metastasis prevention, mice were pre-treated on a control regular chow diet, a GW3965-supplemented diet (20 mg/kg), or T0901317-supplemented diet (20 mg/kg) for 10 days prior to cancer cell injection and kept on each respective diet for the remainder of the experiment. In the experiment testing GW3965 effects on metastatic colonization by primary mouse YUMM melanoma cells, the mice were assigned to a GW3965 diet treatment (100 mg/kg) immediately after injection. To assess the effect of GW3965 treatment on brain metastasis, 1×10^5 MeWo brain-metastatic derivatives were injected intracardially into athymic nu/nu mice. Immediately following injection, mice were randomly assigned to a control diet or a

GW3965-supplemented diet (100 mg/kg). To determine whether oral delivery of GW3965 can inhibit the progression of incipient metastasis, NOD SCID mice were intravenously injected with 4×10^4 MeWo cells, and the cells were allowed to colonize the lungs for 42 days (at which point lung colonization had progressed by 8-fold relative to the baseline at seeding), after which mice were blindedly assigned to a control diet or a GW3965-supplemented diet (100 mg/kg) treatment. To test the effect of combined GW3965/ vemurafenib treatment on lung colonization, 1×10^5 SK-Mel-334.2 cells and 7.5×10^4 HT-144 cells were intravenously injected into 6-8 week-old sex-matched NOD SCID gamma mice. In these experiments, mice were pre-treated on a control diet, GW3965 diet (75 mg/kg), vemurafenib (Genentech) diet (50 mg/kg), or a combined GW3965 (75 mg/kg) and vemurafenib diet (50 mg/kg) starting three days prior to cancer cell injection. GW3965 and vemurafenib were formulated in the rodent chow by Research Diets, Inc.

Orthotopic Metastasis Assay

To determine the effect of GW3965 treatment on lung colonization by melanoma cells dissociated from an orthotopic site, 1×10^6 MeWo cells expressing a luciferase reporter were subcutaneously injected into both lower flanks of NOD SCID mice. Upon formation of tumors measuring ~300 mm^3 in volume, the tumors were excised and the mice were randomly assigned to a control diet or a GW3965-supplemented diet (100 mg/kg). One month after tumor resection, the lungs were extracted and lung colonization was measured by *ex vivo* bioluminescence imaging. To histologically confirm the extent of melanoma lung colonization, lungs were then fixed in 4% PFA overnight, paraffin-embedded, sectioned into 5-μm thick increments and stained for human vimentin (VP-V684, Vector Laboratories).

Primary Tumor Growth Assays

Effects of miR-199a and miR-1908 on Tumor Growth

1×10^6 parental MeWo cells overexpressing miR-199a, miR-1908, or a control hairpin were mixed 1:1 with matrigel (356231, BD Biosciences) and subcutaneously injected into the lower right flank of NOD SCID mice. Animals were palpated weekly for tumor formation, after which sizeable tumors were measured twice a week. Tumor dimensions were measured using digital calipers, and tumor volume was calculated as (small diameter)^2 × (large diameter)/2.

Effects of LXR Agonist Therapy on Tumor Growth

To determine the effect of LXR agonists on *in vivo* subcutaneous tumor growth, we injected the following numbers of melanoma cells: 5×10^4 B16F10 cells, 1×10^6 MeWo cells, 7.5×10^5 SK-Mel-334.2 cells, 2×10^6 SK-Mel-2 cells, 2×10^6 SK-Mel-239 vemurafenib-resistant C1 or C5 cells, 1×10^5 YUMM parental cells, and 2×10^5 vemurafenib-resistant YUMM cells. For all tumor growth experiments, cells (suspension in 50 μL of PBS) were mixed 1:1 with matrigel and subcutaneously injected into the lower flank of 6-8 week-old sex-matched C57BL/6 (B16F10, YUMM), NOD SCID (MeWo and SK-Mel-334.2), athymic nu/nu (SK-Mel-2), and NOD SCID gamma (SK-Mel-239) mice. Animals were palpated every two days for tumor formation. Upon detection of tumors measuring 5-10 mm^3 in volume, mice were randomly assigned to a control diet treatment, a GW3965-supplemented diet (20 mg/kg/day or 100 mg/kg/day), or a T0901317-supplemented diet (20 mg/kg/day) treatment, as indicated in each figure. To assess the effect of GW3965 on the growth of large established tumors, B16F10-tumors were allowed to reach 150 mm^3 in volume, and mice were randomly assigned to a control chow or a chow supplemented with GW3965 (100

mg/kg). To test the effect of combined GW3965/DTIC, GW3965/vemurafenib, or GW3965/anti-CTLA-4 Ab therapeutic regimens on tumor growth, the following numbers of cells were injected: 5×10^4 B16F10 cells, 8×10^5 A375 cells, and 1.25×10^6 SK-Mel-239 cells. B16F10 cells were implanted onto C57BL/6-WT mice, whereas A375 and SK-Mel-239 human cells were grafted onto NOD SCID gamma mice. Following formation of palpable 5-10 mm^3 tumors, mice were assigned to the following treatment groups, as described below. GW3965 + DTIC Therapy: i) control diet + vehicle, i.p. (citric acid, 50 mg/kg); ii) GW3965 diet (100 mg/kg) + vehicle, i.p.; iii) control diet + DTIC (Sigma-Aldrich), i.p. (50 mg/kg); iv) GW3965 diet (100 mg/kg) + DTIC, i.p. (50 mg/kg). DTIC was co-dissolved with citric acid (1:1 by weight) in dH_2O and administered daily by intraperitoneal injection. GW3965 + Vemurafenib Therapy: i.) control diet; ii.) GW3965 diet (75 mg/kg); iii) vemurafenib diet (50 mg/kg); iv) GW3965 (75 mg/kg) + vemurafenib (50 mg/kg) combined diet or vemurafenib diet (50 mg/kg) alternated with GW3965 diet (75 mg/kg), as indicated. GW3965 + anti-CTLA-4 Ab Therapy: i) control diet + IgG; ii) GW3965 diet (100 mg/kg) + IgG; iii) control diet + anti-CTLA-4 Ab; iv) control diet + anti-CTLA-4 Ab + B16F10-GM-CSF vaccine; v) GW3965 diet (100 mg/kg) + anti-CTLA-4 Ab. IgG Ab or anti-CTLA-4 Ab (BioXcell) was administered on day 4 post-injection at a dose of 100 μg/mouse followed by two successive 50 μg/mouse doses every 3 days by i.p injection. The antibodies were administered in PBS for a total injection volume of 200 μL per mouse. The B16F10 GM-CSF vaccine, comprised of 1×10^6 irradiated (16,000 Rads, 1 hour prior to treatment) B16F10-GM-CSF cells, was administered at the same time as the antibody treatment by subcutaneous injection into the lower back area, as previously described (van Elsas et al., 1999). B16F10 cells were engineered to overexpress GM-CSF by transfection of 2 μg of

pCMV6-GM-CSF vector (MC208342, OriGene) into B16F10 cells 48 hours prior to injection. GM-CSF overexpression was confirmed by ELISA (88-7334-22, Affymetrix eBioscience) analyses of conditioned cell media collected 48 hours post-transfection. Typical extracellular GM-CSF levels detected were in the range of 20-40 ng of GM-CSF per 1 million cells.

Tumor dimensions were measured using digital calipers, and tumor volume was calculated as (small diameter)^2 × (large diameter)/2. For survival analyses, mice were euthanized when total tumor burden exceeded 1500 mm^3 in volume. All drug-formulated diets were prepared by Research Diets, Inc.

Genetically Initiated Model of Melanoma Progression

The *Tyr::CreER; B-Raf$^{V600E/+}$; Pten$^{lox/+}$ / Tyr::CreER; B-Raf$^{V600E/+}$; Pten$^{lox/lox}$* conditional model of melanoma progression was previously established and characterized by Dankort et al. (2009). Briefly, melanoma in these mice was induced at 6 weeks of age by intraperitoneally injecting 4-HT (H6278, 70% isomer, Sigma-Aldrich) at a dose of 25 mg/kg. The 4-HT stock solution was prepared by dissolving it in 100% EtOH at 50 mg/mL by heating at 45°C for 5 min and mixing. Once dissolved, the stock 4-HT solution was then diluted 10-fold in peanut oil, yielding a 5 mg/mL 4-HT working solution that was then injected into mice on three consecutive days. After the first 4-HT injection, mice were blindedly assigned to receive either a control diet or a diet supplemented with GW3965 (100 mg/kg). Mice were examined three times a week for the presence and progression of melanoma lesions. At day 35, dorsal skin samples were harvested from control-treated and GW3965-treated *Tyr::CreER; B-Raf$^{V600E/+}$; Pten$^{lox/lox}$* mice, washed in PBS, fixed in 4% PFA, and photographed at 10X. The percentage of pigmented melanoma lesion area out of the total

dorsal skin area was quantified using ImageJ. For survival analyses, mice were monitored daily for melanoma progression and euthanized according to a standard body condition score, taking into account initial signs of moribund state and discomfort associated with the progression of melanoma burden. Post-mortem, the lungs, brains, and salivary glands were harvested and examined for the presence of macroscopic melanoma lesions.

Generation of DTIC-Resistant Melanoma Cells

DTIC-resistant B16F10 mouse melanoma cells were generated by continuously culturing the cells in the presence of DTIC (D2390, Sigma-Aldrich). First, the cells were treated with 500 μg/mL DTIC for one week. Following this initial DTIC treatment, the remaining (~10%) viable cells were allowed to recover for one week, after which 750 μg/mL of DTIC was added to the cell media for 5 days. Subsequent to this high-dose treatment, the cells were allowed to recover in the presence of low-dose DTIC (100 μg/mL) for one week. The cells were then continuously cultured in media containing 200 μg/mL DTIC for two months prior to grafting the cells onto mice. DTIC was added to fresh cancer cell media every 3 days. For tumor growth experiments, 5×10^4 B16F10 parental and DTIC-resistant cells were subcutaneously injected into the lower flank of 7-week-old C57BL/6 mice. Following formation of small tumors measuring 5-10 mm^3 in volume, the mice were randomly assigned to the following treatment groups: (1) control diet + vehicle, i.p. (citric acid, 50 mg/kg); (2) control diet + DTIC i.p. (50 mg/kg); (3) GW3965-supplemented diet (100 mg/kg) + vehicle i.p. . DTIC was co-dissolved with citric acid (1:1 by weight) in dH_2O and administered daily by intraperitoneal injection.

The DTIC-resistant MeWo human melanoma sub-line was generated following DTIC treatment of mice bearing MeWo tumors measuring 600-800 mm^3 in volume. After initial

tumor shrinkage in response to daily DTIC dosing (50 mg/kg, i.p.), the tumors eventually developed DTIC resistance and resumed growth, at which point tumor cells were dissociated, propagated *in vitro*, and the DTIC-resistant MeWo cell line was established. The cells were expanded *in vitro* in the presence of DTIC (200 μg/mL) for one week, after which 5×10^5 DTIC-resistant MeWo cells were subcutaneously implanted onto 8-week old NOD SCID gamma mice. Following the growth of tumors to 5-10 mm^3 in volume, mice were blindedly assigned to the following treatment groups: (1) control diet; (2) control diet + DTIC (50 mg/kg); (3) GW3965-supplemented diet (100 mg/kg). To determine the effect of DTIC on tumor growth by parental unselected MeWo cells, 5×10^5 MeWo cells were subcutaneously injected into NOD SCID gamma mice, and the mice were treated with a control vehicle or DTIC (50 mg/kg) following the formation of tumors measuring 5-10 mm^3 in volume. DTIC was administered as described above in cycles consisting of five consecutive daily treatments interspersed by two-day off-treatment intervals. Tumor growth was measured twice a week.

Generation of Vemurafenib-Resistant Melanoma Cells

For generation of vemurafenib-resistant primary mouse melanoma YUMM cells, 1×10^5 cells were subcutaneously injected bilaterally into the lower flank of C57BL/6 mice. Following formation of tumors measuring ~10 mm^3 in volume, the mice were randomly assigned to a control diet or a vemurafenib-supplemented diet (100 mg/kg), prepared by Research Diets, Inc. After initial inhibition of tumor growth in response to vemurafenib, tumor growth in the presence of the drug eventually resumed, and resistant clones were isolated from a subset of vemurafenib-resistant tumors (~400 mm^3) harvested at day 52. The resistant sub-lines were propagated in the presence of vemurafenib (2 μM) continuously added to the cell media. The A375 vemurafenib-resistant cells were similarly generated

following the *in vivo* vemurafenib treatment of A375 melanoma tumors grafted onto NOD SCID gamma mice. Following tumor relapse, melanoma cells were dissociated and expanded *in vitro* as described above.

miRNA Microarray Hybridization

For identification of miRNAs showing deregulated expression across highly metastatic melanoma cell line derivatives, total RNA from multiple independent metastatic derivatives and their respective parental MeWo and A375 cell populations was used to enrich for small RNAs, which were then labeled and hybridized onto microfluidic custom microarray platforms by LC Sciences. The arrays were designed to detect 894 mature miRNAs corresponding to the miRNA transcripts listed in the Sanger miRBase Release 13.0. Out of all the probes analyzed, those corresponding to 169 miRNAs yielded signal above a background threshold across the multiple cell lines tested. The raw signal intensities, corresponding to probe hybridization, were median-normalized for each cell line. We used a threshold of 2-fold or higher up-regulation of median-normalized expression values in order to identify miRNAs commonly induced in multiple metastatic derivatives for two independent human melanoma cell lines.

Microarray-Based Target Gene Prediction for miR-199a and miR-1908

In order to identify potential genes targeted by miR-199a-3p, miR-199a-5p, and miR-1908, total RNA was extracted from MeWo cell lines with loss- or gain-of-function of each miRNA and submitted to the genomics core facility at The Rockefeller University for hybridization onto Illumina HT-12 v3 Expression BeadChip microarrays. The raw signal

intensities, corresponding to probe hybridization, were then median-normalized for each cell line sample. We generated three sets of microarray profile comparisons: (1) MeWo control cells relative to MeWo cells over-expressing miR-199a or miR-1908, (2) MeWo-LM2 control cells relative to MeWo-LM2 cells expressing a short hairpin (miR-Zip) targeting miR-199a-3p, miR-199a-5p, or miR-1908, and (3) MeWo parental cells relative to MeWo-LM2 cells. Based on the median-normalized expression values from these arrays, we used the following criteria to arrive at possible target genes common to miR-199a and miR-1908: (1) genes downregulated by more than 1.5-fold upon individual overexpression of each miR-199a and miR-1908, (2) genes upregulated by more than 1.5-fold upon inhibition of either both miR-199a-3p and miR-1908 or both miR-199a-5p and miR-1908, and (3) genes downregulated by more than 1.5-fold in LM2 cells, which express physiologically higher levels of the three miRNAs, relative to MeWo parental cells.

Analysis of miRNA and mRNA Expression in Cell Lines

Total RNA was extracted from various cell lines using the miRvana kit (AM1560, Applied Biosystems). The expression levels of mature miRNAs were quantified by a stem-loop qRT-PCR method, starting with 100 ng of total RNA and using the TaqMan miRNA expression assay (4427975, Life Technologies) and the TaqMan universal master mix (4440040, Life Technologies), as per the supplier's recommendation. RNU44 was used as an endogenous control for normalization. For mRNA transcript expression analyses, 600 ng of total RNA was reverse transcribed using the cDNA First-Strand Synthesis Kit (18080-051, Invitrogen), and roughly 200 ng of the resulting cDNA was then mixed with SYBR® green PCR Master Mix (4309155, Applied Biosystems) and the appropriate primers. Each reaction

was performed in quadruplicate, and mRNA expression was quantified by performing real-time PCR amplification using an ABI Prism 7900HT Real-Time PCR System (Applied Biosystems). GAPDH was used as an endogenous control for normalization. For pri-miRNA transcript expression analyses, 600 ng of total RNA were converted to cDNA as described above and analyzed using the TaqMan pri-miRNA assay (4427013, Life Technologies) and the GusB TaqMan gene expression assay (4333767T, Life Technologies), which was used as an endogenous control. For experiments testing the effect of LXR agonist treatment on melanoma cell ApoE mRNA expression, roughly 7×10^5 melanoma cells were treated with DMSO, GW3965, or T0901317 at 1 μM for 48 hours, after which the transcript levels of ApoE were analyzed as described above. All primers used for qRT-PCR analyses are listed in Appendix B.

Analysis of miRNA Copy Number

To determine the relative genomic copy number of miR-199a-1, miR-199a-2, and miR-1908, genomic DNA was extracted from melanoma parental cells and their metastatic derivatives, and the genomic regions spanning each miRNA sequence were amplified and quantified by qRT-PCR using two independent primer sets corresponding to each genomic miRNA region (See Appendix B). The expression of each miRNA was normalized to let-7c.

Analysis of Nuclear Hormone Receptor Expression in the NCI60 Series

The heat-map displaying the relative expression of all nuclear hormone receptors in the NCI-60 melanoma cell line collection was constructed using the publicly available RNA: Affy HG-U133 (A, B) NCI-60 microarray dataset (PMID: 17339364) downloaded from the

CellMiner™ Database Version 1.4 (http:// discover.nci.nih.gov/cellminer/loadDownload.do). To determine the relative expression of each nuclear hormone receptor, we calculated the change in standard deviations (z-score) for the expression value of each receptor relative to the average expression value of all genes (>39,000 transcripts) detected in each melanoma cell line.

Analysis of LXR and RXR Isoform Expression in Primary Human Melanoma Lines

Whole-cell total RNA was extracted from primary melanoma cells using the Total RNA Purification Kit (17200, Norgen, Thorold, Canada) and 600 ng of total RNA was reverse transcribed into cDNA using the cDNA First-Strand Synthesis Kit (18080-051, Invitrogen, Carlsbad, CA). The heatmap depicting the relative expression of *LXRα, LXRβ, RXRα, RXRβ*, and *RXRγ* in primary human melanoma lines was constructed using expression levels determined by qRT-PCR amplification using an ABI Prism 7900HT Real-Time PCR System (Applied Biosystems) and normalized as previously described (Fu et al., 2005). In brief, the PCR efficiency (E) for each primer pair used to specifically amplify each nuclear hormone receptor was calculated based on the slope of a standard curve generated from known quantities of cDNA, using the following formula:

$$E=10^{-1/slope}$$

The determined efficiencies for each primer set were then used to convert logarithmic cycle times (Ct) raw amplification values into linear units, and the relative expression of each receptor was obtained by normalization to an internal positive control (GAPDH) for each sample based on the following formula:

$$(E^{-Ct})_{\text{LXR or RXR isoform}} / (E^{-Ct})_{\text{GAPDH}}$$

Transcriptomic Analysis of Secreted Gene Products in Melanoma Cells Treated with GW3965

In order to identify secreted factors transcriptionally upregulated by activation of LXR signaling in melanoma cells, MeWo cells were treated with DMSO or GW3965 at 1 μM for 48 hours, after which total RNA was extracted, biotin-labeled using the TargetAmp-Nano Labeling Kit for Illumina Expression BeadChip (TAN091096, Epicentre), and submitted to the genomics core facility at the Rockefeller University for hybridization onto Illumina HumanHT-12 V4.0 expression beadchip. The raw signal intensities, corresponding to probe hybridization, were quantile-normalized and processed using the lumi package. For statistical comparisons, q-values < 0.05 were deemed statistically significant. Out of the 365 genes that were significantly upregulated in the GW3965 treatment group relative to the DMSO group, we identified 41 factors that were previously annotated on the NCBI server as extracellular components.

Lentiviral miRNA Inhibition and mRNA Knockdown Studies

293T cells were seeded in a 10-cm plate and allowed to reach 60% confluency. Prior to transfection, the cell media was replaced with fresh antibiotic-free DMEM media supplemented with 10% FBS. 6 μg of vector A, 12 μg of vector K, and 12 μg of the appropriate miR-Zip (System Biosciences, Mountain View, CA) or shRNA plasmid construct (MSKCC HTS Core Facility or Sigma-Aldrich) were co-transfected using 60 μL of TransIT-293 transfection reagent (MIR 2700, Mirus Bio LLC). The cells were incubated at 37°C for 48 hours, and the virus was harvested by spinning the cell media for 10 minutes at 2000 g followed by virus filtration through a 0.45-μm filter. Subsequently, 1×10^5 cancer cells were

transduced with 2 mL of the appropriate virus in the presence of 10 μg/mL of polybrene (TR-1003-G, Millipore) for 6 hours. After 48 hours, 2 μg/mL of puromycin (P8833, Sigma-Aldrich) was added to the cell media for lentiviral selection. The cells were kept in puromycin selection for 72 hours. The miR-Zip or shRNA sequences used for knocking down each respective miRNA or mRNA are listed in Appendix C.

Retroviral miRNA and Protein Overexpression Studies

6 μg of vector VSVG, 12 μg of vector Gag-Pol, and 12 μg of pBabe plasmid containing the coding sequences of human ApoE, DNAJA4, or an empty vector or 12 μg of miR-Vec containing the precursor sequence of miR-199a, miR-214, miR-1908, or a control hairpin were co-transfected into 60%-confluent 293T cells using 60 μL of TransIT-293 transfection reagent. The cells were incubated at 37°C for 48 hours, after which the virus was harvested and transduced into cancer cells in the presence of 10 μg/mL of polybrene for 6 hours. After 48 hours, 2 μg/mL of puromycin or 10 μg/mL of blasticidin (15205, Sigma-Aldrich) were added to the cell media for retroviral selection. The cells were kept in puromycin selection for 72 hours or in blasticidin selection for 7 days. The cloning primers used for overexpression of the coding sequences of ApoE and DNAJA4 are listed in Appendix B.

siRNA-Based Gene Knockdown

To determine whether transient knockdown of CREB regulates miR-199a-3p, miR-199a-5p, or miR-1908, MeWo-LM2 cells were transferected with siRNAs targeting *CREB1* or a control siRNA at a final siRNA concentration of 100 nM and using lipofectamine™

2000 transfection reagent (11668-09, Invitrogen). The transfection cell media was replaced with fresh media 5 hours post-transfection. The levels of the mature and pri-miRNAs were quantified 48 hours post-transfection by qRT-PCR. To identify the ApoE receptors on melanoma cells and endothelial cells mediating ApoE's effects, siRNAs targeting *LRP1*, *LRP8*, *VLDLR*, *LDLR*, or a control sequence were transfected into cancer cells or HUVEC cells at a final concentration of 100 nM using lipofectamine™ 2000 transfection reagent. After 5 hours, the transfection media was replaced with fresh media. The cells were subjected to matrigel invasion or endothelial recruitment assays 72-96 hours post-transfection. Cells transduced with siRNAs targeting LRP1 or a control sequence in the setting of miR-1908 inhibition were tail-vein injected into NOD SCID mice for lung colonization assays 72 hours post-transfection. Individual targeting siRNAs and control non-targeting siRNAs were obtained from Dharmacon (Thermo Fisher Scientific).

LNA-Based miRNA Inhibition

LNAs complementary to mature miR-199a-3p, miR-199a-5p, miR-1908, or a control sequence were transfected at a final concentration of 50 nM into 50-70% confluent cancer cells cultured in antibiotics-free media using lipofectamine™ 2000 transfection reagent. After 8 hours, the transfection media was replaced with fresh media. After 48 hours, the cells were intravenously injected into immunocompromised mice for lung colonization assays.

Therapeutic LNA-Based In Vivo Targeting of miRNAs

To determine whether intravenously administered *in vivo* optimized LNAs antisense to miR-199a-3p, miR-199a-5p, and miR-1908 get delivered into metastatic nodules and

inhibit expression of these miRNAs, mice were injected with 4×10^4 MeWo-LM2 cells. Following lung metastatic nodule formation, mice were treated with LNA-3 miRNAs (at a total dose of 12.5 mg/kg per each treatment) or a control mock PBS treatment three times with a three-day interval between each treatment. MeWo-LM2 cells were dissociated from lung nodules 24 hours after the last LNA treatment, as described above, and propagated in culture for 48 hours prior to RNA extraction using the miRvana total RNA extraction kit. Expression levels of miR-199a-3p, miR-199a-5p, and miR-1908 in MeWo-LM2 cells dissociated from lung nodules of LNA-3 miRNAs or PBS-treated mice were quantified by qRT-PCR using the TaqMan miRNA expression assays and starting with 100 ng of total RNA, as described above. RNU44 was used as an endogenous control. To determine whether the *in vivo* administered LNAs also target the mouse homologs of the three miRNAs, 24 hours after the last LNA treatment, mouse cardiac and liver tissues were harvested, and total RNA was extracted. The expression levels of miR-199a-3p, miR-199a-5p, and miR-1908 in mouse cardiac and liver tissues were assessed by qRT-PCR using the TaqMan miRNA expression assays and starting with 100 ng of total RNA. Mouse U6 snRNA was used as an endogenous control for normalization.

Luciferase Reporter Assays

Validation of Direct miRNA Target Genes

Heterologous luciferase reporter assays were performed as previously described (Tavazoie et al., 2008). In brief, the full-length 3'UTR's of ApoE and DNAJA4 were cloned downstream of a renilla luciferase reporter into the psiCheck2 dual luciferase reporter vector (C8021, Promega), while the full-length CDS's (minus the start codon) of ApoE and

DNAJA4 were chimerically fused to the C-terminus of the renilla luciferase reporter in the psiCheck2 vector by removing the luciferase stop codon and inserting a 6 amino acid-long linker connecting the CDS of luciferase to the CDS of each ApoE or DNAJA4. 4×10^4 parental MeWo cells, MeWo-LM2 cells, MeWo cells overexpressing miR-199a, miR-1908, or a control hairpin, and MeWo-LM2 cells expressing a miR-Zip hairpin targeting miR-199a-3p, miR-199a-5p, miR-1908, or a control sequence were transfected with 100 ng of the respective specific reporter constructs using the TransIT-293 transfection reagent. After 48 hours, the cells were lysed, and the ratio of renilla to firefly luciferase expression was determined using the dual luciferase assay (E1910, Promega). Putative miRNA binding sites in each target construct were identified by alignment to the complementary miRNA seed sequences (miR-199a-3p: 5'-CAGUAGUC-3'; miR-199a-5p: 5'-CCAGUGUU-3'; miR-1908: 5'-GGCGGGGA-3'). The miRNA complementary sites on each target construct were mutated using the QuickChange Multi Site-Directed Mutagenesis Kit (200514, Agilent Technologies). Based on miRNA seed sequence complementarity analysis, the CDS of ApoE was mutated by introducing silent mutations at amino acid positions: 45 (GAA to GAG), 46 (CTG to CTT), 47 (GCA to GCT), 48 (CTG to CTT), 95 (GAA to GAG), 96 (CTG to CTT), 277 (GCC to GCT), and 278 (CGC to CGA). The CDS of DNAJA4 was mutated by introducing silent mutations at amino acid positions: 124 (TGC to TGT), 125 (CCG to CCA), and 306 (CAC to CAT). The 3'UTR of ApoE was mutated at nucleotide positions: 83-85 (GCC to ATA) and 98-100 (CTG to ACA). The 3'UTR of DNAJA4 was mutated at nucleotide positions: 576-578 (CTG to ACA), 1096-1098 (CTG to TCT), 1396-1398 (CGC to TGT), and 1596-1598 (CTG to TGT). All cloning and mutagenesis primers used are listed in Appendix B.

ApoE Promoter Activity Assay

The *ApoE* promoter, consisting of a sequence spanning 980 base pairs upstream and 93 base pairs downstream of the *ApoE* gene, was cloned into a pGL3-Basic vector (E1751, Promega) upstream of the firefly luciferase gene using NheI and XhoI restriction enzymes. Then, multi-enhancer elements 1 (*ME.1*) or 2 (*ME.2*) were cloned directly upstream of the *ApoE* promoter using MluI and NheI restriction enzymes. To assess *ApoE* promoter- and *ME.1*/*ME.2*-driven transcriptional activation by LXR agonists, 5×10^4 MeWo cells were seeded into a 24-well plate. The following day, 100 ng of pGL3-ME.1/ME.2-*ApoE* promoter construct and 2 ng of pRL-CMV renilla luciferase construct (E2261, Promega) were co-transfected into cells in the presence of DMSO, GW3965, or T0901317 at 1 μM, each condition in quadruplicates. To assess transcriptional activation by LXRα or LXRβ, 5×10^4 MeWo cells expressing a control shRNA or an shRNA targeting *LXRα* or *LXRβ* were seeded into a 24-well plate. The following day, 200 ng of pGL3-*ME.1*/*ME.2*-*ApoE* promoter construct and 2 ng of pRL-CMV renilla luciferase were co-transfected into cells in the presence of DMSO, GW3965, or T0901317 at 1μM, each condition in quadruplicates. After 24 hours, cells were lysed, and cell lysates were analyzed for firefly and renilla luciferase activity using the Dual Luciferase Assay System (E1960, Promega) and a Bio-Tek Synergy NEO Microplate Reader. Firefly luciferase signal was normalized to renilla luciferase signal, and all data are expressed relative to the luciferase activity ratio measured in the DMSO-treated control cells. The cloning primers used to generate the reporter constructs are listed in Appendix B.

Western Blotting

Total and phosphorylated CREB levels were assessed in parental MeWo and MeWo-LM2 cells by lysis of the cells in RIPA buffer (Sigma-Aldrich), SDS-PAGE separation of total protein lysates (15 μg), transfer to a PVDF membrane, and blotting with antibodies against total CREB (48H2, Cell Signaling), phospho-CREB (87G3, Cell Signaling), or GAPDH (G9545, Sigma-Aldrich).

To determine the effect of ApoE/LRP8 targeting on endothelial VEGFR2 activation, HUVEC or primary mouse lung endothelial cells (MLECs) were incubated in the presence of recombinant ApoE3 for 1 hour at 2 μg/mL or 5 μg/mL (HUVEC) or 10 μg/mL (MLECs). Subsequently, endothelial cells were pulsed with either human VEGF (12 ng/mL) or mouse VEGF (30 ng/mL), respectively, for 15 min. After that, cells were lysed in RIPA buffer on ice, and protein was extracted. Total protein lysates (20 μg) were separated by SDS-PAGE and transferred to a PVDF membrane that was then blotted with antibodies against total VEGFR2 (2472, Cell Signaling), phospho-VEGFR2 (2478, Cell Signaling), or GAPDH (G9545, Sigma-Aldrich). For analysis of VEGFR2 expression and activation in primary melanoma tumors, subcutaneous tumors formed by MeWo cells overexpressing miR-199a or miR-1908 or a control were extracted and homogenized on ice in RIPA buffer. The expression of total and phopsho-VEGFR2 was assessed as described above. The LRP8 protein expression levels in MLECs dissociated from *LRP8* wild-type, *LRP8* heterozygous, or *LRP8* null mice were analyzed in 40 μg of total protein lysate by SDS-PAGE and blotting with an antibody specific for LRP8 (NB100-2216, Novus Biologicals).

For analysis of ApoE protein expression in stromal tissues upon LXR agonist treatment, mouse lung, adipose, and brain tissues were extracted from mice treated with a

control diet or an LXR-agonist supplemented diet (20 mg/kg) for 10 days. Lung and brain tissues were homogenized on ice in RIPA buffer (Sigma-Aldrich). Mouse adipose tissue was homogenized in TNET buffer (1.5 mM Tris pH 7.5, 150 mM NaCl, 2mM EDTA, 1% triton, protease inhibitors). For analysis of ApoE protein expression in human melanoma cells treated with DMSO, GW3965, or T0901317 at 1 μM for 72 hours, cells were lysed in RIPA buffer. Total protein lysates (2 μg for tissue lysates; 40 μg for melanoma cell lysates) were separated by SDS-PAGE, transferred to a PVDF membrane, and blotted with antibodies against mouse ApoE (ab20874, Abcam), human ApoE (ab1906, Abcam), and tubulin (2148, Cell Signaling).

ApoE ELISA

Extracellular ApoE levels in serum-free conditioned media collected from melanoma cells were quantified using the human ApoE ELISA kit (Innovative Research), following the manufacturer's protocol. Conditioned cancer cell media was prepared by culturing 70%-80%-confluent cells in 02% FBS media for 24-36 hours.

DNAJA4 Immunoprecipitation and MS-Based Analysis of Interacting Partners

To identify putative interacting partners of DNAJA4, total protein was extracted from melanoma cells overexpressing flag-tagged DNAJA4.2 or DNAJA4.3 or melanoma cells expressing an empty control vector. The cells were lysed in a buffer comprised of 50 mM Tris (pH 7.5), 150 mM NaCl, 1 mM EDTA, 1% triton, and protease/phosphatase inhibitors. Flag-tagged DNAJA4.2 and DNAJA4.3 were immunoprecipitated from MeWo parental or MeWo-LM2 cells using magnetic beads coated with an anti-flag antibody and rotating at 4°C

for four hours. The beads were consecutively washed in wash buffer 1 (50 mM Tris (pH 7.5), 300 mM NaCl, 1% triton) and wash buffer 2 (50 mM Tris (pH 7.5), 150 mM NaCl) and the immunoprecipitated product was eluted using a flag peptide (50 mM Tris (pH 7.5), 150 mM NaCl, 10% 3X Flag Peptide). The eluted product was then mixed with 5X sample buffer and separated by SDS-PAGE on a 4-12% Bis-Tris Gel. Proteins that ran on the gel were coomassie stained, and bands of interest were submitted for mass spectrometry (MS) analysis at the Proteomics Core Facility at the Rockefeller University. Identified protein candidates were ranked by the number of unique peptides detected by MS. Hits with three or more unique peptides present were prioritized. The MS results only list proteins that were detected in either the DNAJA4.2 or DNAJA4.3 flag immunoprecipitation product, but not in the empty control pull down.

LXRβ ChIP

To determine a potential interaction of endogenous LXRβ with the ApoE multi-enhancer element in human melanoma cells, the ChIP-IT® High Sensitivity kit (53040, Active Motif) along with an LXRβ antibody previously optimized for ChIP (61177, Active Motif) were used. The ChIP experiment was carried out by following the precise recommendations of the kit's manufacturer. In brief, chromatin was extracted from ~5×10^6 MeWo cells treated with DMSO or GW3965 (1 μM) for 8 hours and cross-linked in formaldehyde-based cell fixation solution. Chromatin was sonicated on ice using a micotrip system (Branson Sonifier, model SSE-1, Danbury, CT) and the following sonication regime: 25% amplitude, 30 seconds on and 30 seconds off for a total "on" sonication time of 10 minutes. Chromatin shearing efficiency was confirmed by running 500 ng of reversely cross-

linked sheared chromatin on an agarose gel. ChIP reactions were set-up by mixing 18 μg of sheared chromatin with anti-LXRβ (10 μL per reaction) or IgG antibody and ChIP buffer, containing protease inhibitions. The ChIP reactions were incubated on an end-to-end rotator for 16 hours at 4 °C. The ChIP product was then filtered and bound to a column, eluted, reverse cross-linked, protein-digested, and DNA was purified. Purified DNA product was analyzed by qRT-PCR. Standard curves for each primer set were generated using dilution series from known amounts of input chromatin and used to extrapolate the amount of PCR product in each ChIP reaction. Appendix B lists the qRT-PCR primers used to detect a region on chromosome 19 containing the ME.2 LXRβ-binding motif (LXRE-pos) and a negative control genomic region on chromosome 1 devoid of LXRβ-binding sites (LXRE-neg).

Phenotypic Assays

In Vitro Cell Proliferation Assay

To determine the effects of miR-199a or miR-1908 overexpression and combinatorial LNA-based miRNA inhibition on cell proliferation, 2.5×10^4 cells were seeded in triplicate in, and viable cells were counted after 3 or 5 days. To test the effect of recombinant ApoE on in vitro melanoma cell proliferation, 3×10^4 MeWo-LM2 cells were seeded in triplicates and incubated in the presence of BSA or recombinant ApoE (100 μg/mL), and viable cells were quantified at days 1, 3, and 5 post-treatment. To determine the effects of GW3965, T0901317, and bexarotene on *in vitro* cell proliferation, 2.5×10^4 melanoma cells were seeded in triplicate and cultured in the presence of DMSO, GW3965, T0901317, or bexarotene at 1 μM each. After 3 or 5 days, the number of viable and dead cells was counted using the trypan blue dye (72-57-1, Sigma-Aldrich), which selectively labels dead cells.

Endothelial Adhesion Assay

1×10^5 HUVEC were seeded in 6-well plates and allowed to form monolayers. Cancer cells were serum starved in 0.2% FBS DMEM-based media for 30 minutes and pulsed with Cell Tracker Green CMFDA dye (C7025, Invitrogen) for 45 minutes. 2×10^5 cancer cells, resuspended in 0.5 mL starvation media, were seeded onto each endothelial monolayer. The cancer cells were allowed to adhere to the HUVEC monolayers for 30 minutes at 37°C. The endothelial monolayers were then washed gently with PBS and fixed with 4% paraformaldehyde for 15 minutes. Each well was then coated with PBS, and 8 images were taken for each endothelial monolayer using an inverted Fluorescence microscope (Zeiss Axiovert 40 CFL) at 10X magnification. The number of cancer cells adhering to HUVEC was quantified using ImageJ.

Colony Formation Assay

Fifty MeWo parental cells overexpressing miR-199a, miR-1908, or a control hairpin were seeded in quadruplicate into 6-cm plates. After two weeks, the cells were washed with PBS, fixed with 6% glutaraldehyde (G5882, Sigma-Aldrich), and stained with 0.5% crystal violet (HT90132, Sigma-Aldrich). The number of positive-staining colonies was counted.

Serum Starvation Assay

To determine the effects of miR-199a and miR-1908 on melanoma cell serum starvation capacity, 1×10^5 MeWo parental cells overexpressing miR-199a, miR-1908, or a control hairpin were seeded in quadruplicate and incubated in 0.2% FBS starvation DMEM-based media for 48 hours, after which the number of viable cells was counted using trypan blue.

Anoikis Assay

1×10^6 MeWo cells overexpressing miR-199a, miR-1908, or a control hairpin were seeded in low adherent plates containing cell media supplemented with 0.2% methylcellulose (M7140, Sigma-Aldrich). Following 48 hours in suspension, the numbers of dead and viable cells were counted using trypan blue (T8154, Sigma-Aldrich).

Matrigel Invasion Assay

Cancer cells were serum-starved in 0.2% FBS DMEM-based media for 12-16 hours. Trans-well invasion chambers (354480, BD Biosciences) were pre-equilibrated prior to beginning the assay by adding 0.5 mL of starvation media to the top and bottom chambers. After 30 minutes, the media in the top chamber was removed, and 0.5 mL of media containing melanoma cells (1×10^5 for the MeWo line; 5×10^4 for the A375, HT-144, SK-Mel-2, or SK-Mel-334.2 lines), was added into each matrigel-coated trans-well insert and incubated at 37°C for 24 hours. For neutralization antibody and/or recombinant protein experiments, antibody/recombinant protein was added to each trans-well at the start of the assay at the following concentrations: 40 μg/mL anti-ApoE 1D7 (Heart Institute, University of Ottawa) or anti-IgG (AB-108-C, R&D Systems) and 3.44 μg/mL recombinant human ApoE3 or BSA. For experiments testing the effects of LXR or RXR agonists on cell invasion, various melanoma cells were cultured in the presence of DMSO, GW3965, T0901317, or bexarotene at 1 μM for 56 hours, after which melanoma cells were switched to starvation media (0.2% FBS) for 16 hours in the presence of each drug. Following starvation, cells were seeded into matrigel-coated trans-well inserts, and the invasion assay was allowed to proceed for 24 hours at 37°C. Upon completion of the assay, matrigel-coated inserts were washed with PBS, the cells at the top side of each insert were scraped off, and the inserts

were fixed in 4% paraformaldehyde for 15 minutes. The inserts were then cut out and mounted onto slides using VectaShield mounting medium containing DAPI (H-1000, Vector Laboratories). The basal side of each insert was imaged using an inverted fluorescence microscope (Zeiss Axiovert 40 CFL) at 5X magnification, taking three representative images for each insert. The number of invaded cells was quantified using ImageJ (NIH).

Endothelial Recruitment Assay

5×10^4 melanoma cells were seeded into 24-well plates approximately 24 hours prior to the start of the assay. HUVEC were grown to 80% confluency in EGM-2 media supplemented with 2% FBS and subsequently serum starved in EGM-2 media supplemented with 0.2% FBS for 16 hours. HUVEC were then pulsed with Cell Tracker Red CMTPX dye (C34552, Invitrogen) for 45 minutes. Meanwhile, cancer cells were washed with PBS, 0.5 mL of 0.2% FBS EGM-2 media was added to each well, and a 3.0 μm HTS Fluoroblock insert (351151, BD Falcon) was placed into each well. 1×10^5 HUVEC, resuspended in 0.5 mL of starvation media, were seeded into each trans-well insert, and the recruitment assay was allowed to proceed for 16-20 hours at 37°C. For neutralization antibody and/or recombinant protein experiments, antibody/recombinant protein was added at the start of the assay to each bottom well containing the melanoma cells at the following concentrations: 40 μg/mL anti-ApoE 1D7 or anti-IgG and 3.44 μg/mL recombinant human ApoE3 or BSA. To test the effect of LXR or RXR agonists on endothelial recruitment, melanoma cells were treated with DMSO, GW3965, T0901317, or bexarotene at 1 μM for 56 hours, after which 5×10^4 cells were seeded in a 24-well plate in the presence of each drug and allowed to attach for 16 hours prior to starting the endothelial recruitment assay. Upon completion of the assay, the inserts were processed and analyzed as described for the matrigel invasion assay above.

Endothelial Migration Assay

Serum-starved HUVEC cells were pulsed with Cell Tracker Red CMTPX dye for 45 minutes and seeded into HTS Fluoroblock trans-well inserts at a concentration of 1×10^5 HUVEC in 0.5 mL starvation media per each insert. The assay was allowed to proceed for 16-18 hours at 37°C, and the inserts were processed and analyzed as described above (See Matrigel Invasion Assay).

ApoE Gradient Migration Assay

HUVEC transduced with a control siRNA or an siRNA targeting LRP8 were serum-starved in 0.2% FBS EGM-2 media for 16 hours and labeled with Cell Tracker Red CMTPX dye for 45 minutes. Meanwhile, the indicated amounts (1, 2, or 5 μg) of recombinant human ApoE3 or BSA were mixed with 250 μL of matrigel and allowed to solidify at the bottom of a 24-well plate for 30 min. 250 μL of HUVEC EGM-2 media containing 0.2% FBS was then added to each matrigel-coated well, and 3.0 μM HTS Fluoroblock inserts were fitted into each well. 1×10^5 HUVEC, resuspended in 0.5 mL of starvation (0.2% FBS) EGM-2 media, were seeded into each insert and allowed to migrate along the matrigel gradient for 16-18 hours at 37°C. Upon completion of the assay, the inserts were mounted on slides and analyzed as described above (See Matrigel Invasion Assay).

In Vivo Matrigel Plug Assay

10 μg/mL recombinant human ApoE3, 10 μg/mL BSA, or 400 ng/ml VEGF (01-185, Millipore) were mixed with matrigel as indicated in Figure 4.9a. 400 μL of matrigel containing the indicated recombinant proteins were injected subcutaneously just above the lower ventral flank of 6-week old immunocompromised NOD SCID mice. Plugs were extracted on day 3 post-injection and fixed in 4% paraformaldehyde for 48 hours. Plugs were

then paraffin-embedded and sectioned at 5-μm thick increments. Plug sections were immunohistochemically stained using a primary antibody against the mouse endothelial antigen MECA-32, detected by peroxidase-conjugated secondary antibody (BA-4000, Vector Laboratories), and subsequently visualized by DAB oxidation. To quantify the extent of endothelial cell recruitment into each matrigel plug, the number of endothelial cells was counted in 4-5 random fields for each plug, and the average number of endothelial cells per given plug area was calculated.

Histochemistry

Macroscopic Lung Nodule Visualization

Animals were perfused with PBS followed by fixation with 4% paraformaldehyde infused via intracardiac and subsequent intratracheal injections. The lungs were sectioned out, incubated in 4% paraformaldehyde at 4°C overnight, washed in PBS, 50% EtOH, and 70% EtOH. Tissues were stored in 70% EtOH and were then embedded in paraffin, and sliced into 5-μm thick increments. For gross macroscopic metastatic nodule visualization, lung sections were H&E stained.

Endothelial Cell Content Analysis

For endothelial content analysis in metastatic nodules formed by human melanoma MeWo cells in mice, paraffin-embedded lung sections were double-stained with primary antibodies against MECA-32 (Developmental Studies Hybridoma Bank, The University of Iowa), which labels mouse endothelial cells, and human vimentin (VP-V684, Vector Laboratories), which labels human melanoma cells. Various Alexa Flour dye-conjugated secondary antibodies were used to detect primary antibodies. To determine the endothelial

density within metastatic nodules, fluorescence was measured using a Zeiss laser scanning confocal microscope (LSM 510), and the MECA-32 signal within each metastatic nodule, outlined based on co-staining with human vimentin, was quantified in a blinded fashion using ImageJ (NIH). For endothelial content analysis in metastatic nodules formed by mouse B16F10 mouse melanoma cells in wild type and ApoE genetically null mice, representative lung sections were stained for MECA-32, and the MECA-32 signal within each nodule, demarcated based on cell pigmentation, was quantified in a blinded fashion. The collective endothelial cell area, given as the percentage area covered by endothelial cells relative to the total area of each metastatic nodule, was obtained by background subtraction (rolling ball radius of 1 pixel) and use of a pre-determined threshold as a cut-off. A metastatic nodule was defined as any region of greater than 2000 μm^2 total area. For large nodules, minimum of four representative images were obtained, and their average blood vessel density was calculated.

Metastatic Nodule Angiogenic Perfusion Analysis

For analysis of metastatic nodule perfusion, mice were intravenously injected with 2 mg of biotinylated dextran (10,000 MW, D1956, Invitrogen) resuspended in 0.2 mL of PBS. Dextran was allowed to circulate through the mouse vasculature for 10 minutes, after which the animals were anesthetized, and lungs were extracted and processed as described above. Dextran perfusion within metastatic nodules was detected by performing co-immunostaining for biotin and human vimentin. The extent of metastatic nodule perfusion was determined in a blinded manner by quantifying the dextran signal within each metastatic nodule using ImageJ and the same approach as described for the MECA-32 signal quantification above.

Histochemical Analyses of LXR Agonist-Treated Tumors

Tumors were excised from mice and fixed in 4% paraformaldehyde at 4°C for 48 hours. Tumors were washed in 50% and 70% EtOH and were subsequently paraffin-embedded and sectioned into 5-μm thick increments. For endothelial cell content analysis in tumors, tumor sections were stained with a primary antibody against the mouse endothelial cell marker MECA-32 (Developmental Studies Hybridoma Bank, The University of Iowa) or CD31 (DIA-310, Dianova) and counterstained with DAPI nuclear stain. To determine tumor cell proliferation and apoptosis, tumor sections were stained with antibodies against the proliferative marker Ki-67 (ab15580, Abcam) and the apoptotic marker cleaved caspase-3 (9661, Cell Signaling), respectively. Various Alexa Flour dye-conjugated secondary antibodies were used to detect primary antibodies. Fluorescence was measured using inverted fluorescence microscope (Zeiss Axiovert 40 CFL) at 5X magnification for MECA-32 and Ki-67 staining and 10X magnification for cleaved caspase-3 staining. Endothelial cell content density and tumor proliferative cell density were quantified by calculating the average percentage of MECA-32 or Ki-67 positively-staining area out of the total tumor area, respectively. Tumor apoptosis rate was measured by counting the number of cleaved caspase-3 expressing cells per given tumor area.

For co-localization analyses of ApoE protein expression within tumor-infiltrating macrophages and leukocytes, anesthetized mice were perfused with PBS followed by 4% paraformaldehyde via intracardiac injection. The tumors were excised and fixed in 4% paraformaldehyde overnight and incubated in a series of sucrose gradients for cryopreservation, (4 hours in 15% sucrose in PBS followed by 30% sucrose in PBS overnight at 4°C). Fixed tumors were embedded in Tissue-Tek O.C.T cryosectioning compound (4383,

Sakura Finetek), and tissue blocks were cut into 10-μm thick sections. For co-localization of ApoE with macrophages, formalin fixed and glycine quenched cross sections of tumors were double-stained with primary antibodies against ApoE (1:1000, sc-6384, Santa Cruz Biotechnology) and F4/80 (1:500, MCA497, Abd Serotec) overnight at 4°C. Co-localization of ApoE with leukocytes was performed using an anti-CD45 antibody (1:250, 550539, BD Biosciences). For co-localization of ApoE with endothelial cells, fresh-frozen sections (no fixation) were stained with an anti-ApoE primary antibody (1:1000, sc-6384, Santa Cruz Biotechnology) and an anti-CD31 primary antibody (1:50, 550274, BD Biosciences). Various alexa Fluor dye-conjugated secondary antibodies were used to detect primary antibodies. Sections were counterstained with DAPI and mounted with ProLong Gold antifade reagent (P36930, Invitrogen). ApoE immunostaining abundance was determined by measuring fluorescence using laser scanning confocal microscope (TCS SP5, Leica Microsystems). ApoE mean signal intensity was then analyzed using FiJi software (NIH) and quantified within F4/80-positive macrophages, CD45-positive leukocytes or CD31-positive endothelial cell present in the tumor microenvironment.

Analysis of miRNA Expression in Primary Melanoma Skin Lesions

All human clinical samples used in this study were obtained, processed, and analyzed in accordance with institutional IRB guidelines. Paraffin-embedded cross-sections of primary melanoma skin lesions from 71 human patients were obtained from the MSKCC. The samples were de-paraffinized by five consecutive xylene washes (5 minutes each). Following de-paraffinization, the malignancy-containing region was identified by H&E staining, dissected, and total RNA was extracted from it using the RecoverAll Total Nucleic Acid

Isolation Kit (AM1975, Applied Biosystems). The expression levels of mature miR-199a-3p, miR-199a-5p, and miR-1908 in each sample were quantified in a blinded fashion using the Taqman miRNA assay and starting with 10 ng of total RNA. RNU44 was used as an endogenous control for normalization. The expression levels of each miRNA were compared between primary melanomas with propensity to metastasize and primary melanomas that did not metastasize. Using the GraphPad Prism software, Kaplan-Meier curves were generated by plotting metastasis-free survival data of patients as a function of the expression levels for each miRNA in each patient's tumor. The aggregate expression of the three miRNAs was determined as the sum of the expression values of each individual miRNA. Patients whose primary melanomas had miRNA levels greater than the median of the population were classified as miRNA positive, while those whose primary tumors had miRNA levels below the median were classified as miRNA negative. Metastatic recurrence to such sites as lung, brain, bone, soft tissue, skin, and subcutaneous tissues were previously documented and allowed for a retrospective analysis of the relationship between the expression levels of the identified miRNAs and metastatic recurrence.

Analysis of ApoE and DNAJA4 Protein Levels in Primary Melanoma Skin Lesions

Human primary melanoma skin samples were resected from melanoma patients at the MSKCC, formalin-fixed, embedded in paraffin, and sectioned into 5-μm thick increments. To determine ApoE and DNAJA4 protein expression, the samples were first de-paraffinized by two consecutive xylene washes (5 minutes each), and rehydrated in a series of ethanol washes (100%, 95%, 80%, and 70% EtOH). Antigen retrieval was performed by incubating the samples in the presence of proteinase K (5 μg/mL) for 20 minutes at room temperature.

To quench endogenous peroxidase activity, the slides were incubated in 3% H_2O_2 solution. The slides were then blocked in three consecutive Avidin, Biotin, and horse serum block solutions for 15 min each at room temperature (SP-2001, Vector Laboratories). ApoE and DNAJA4 were detected by staining with the D6E10 anti-ApoE antibody (1:100, ab1908, Abcam) or a custom-made antibody against DNAJA4.3 (1:100, Yenzyme) at 4°C overnight. The primary antibodies were then recognized by incubating the slides in the presence of a peroxidase-conjugated secondary antibodies (PK-4002, Vector Laboratories) and exposed by DAB (SK-4105, Vector Laboratories) oxidation reaction. The slides were imaged at 10X magnification and analyzed in a double-blinded manner. Expression of each ApoE and DNAJA4 was measured by quantifying the percentage area of DAB-positive staining out of the total melanoma lesion's area, determined based on matched H&E-stained sections for each sample. Kaplan-Meier curves depicting patients' metastasis-free and overall survival times were generated by plotting each patient's relapse-free and overall survival data as a function of ApoE or DNAJA4 expression in that patient's primary melanoma lesion. Patients whose tumors had ApoE or DNAJA4 levels lower than the median ApoE or DNAJA4 expression of the population were classified as ApoE or DNAJA4 negative, whereas patients whose melanomas expressed ApoE or DNAJA4 above the median were classified as ApoE or DNAJA4 positive, respectively.

Analysis of ApoE, DNAJA4, and LXRβ Protein Expression in TMA Melanoma Progression Sets

For analysis of ApoE and DNAJA4 protein expression in the NIH melanoma TMA progression set, TMA slides were de-paraffinized by two xylene washes (5 min each), and

rehydrated in a series of ethanol washes (100%, 95%, 80%, and 70% EtOH). Antigen retrieval was performed by applying a proteinase K solution (5 μg/mL) to tissues for 20 min at room temperature. ApoE expression was detected using a primary antibody against ApoE (1:100, ab1906, Abcam) or DNAJA4.3 (1:100, custom-made by Yenzyme) at 4°C overnight followed by a peroxidase-conjugated secondary antibody (PK-4002, Vector Labs) and visualized by DAB (SK-4105, Vector Labs) oxidation.

To determine the expression of LXRβ in the NIH melanoma TMA and the US Biomax melanoma TMA (ME2082b, Rockville, MD) progression sets, TMA slides were de-paraffinized by three xylene washes (5 min each). For antigen retrieval, slides were placed in 1X antigen unmasking solution (H3300, Vector labs) and steamed in a pressure cooker for 20 min. After slides cooled to room temperature, the tissue was permeabilized in 0.1% Triton-X-100 in PBS for 2 min and blocked in horse serum for 30 min. Samples were stained at 4°C overnight with a primary antibody against LXRβ (1:100, AB24361, Abcam) that was then detected by an alkaline phosphatase-conjugated secondary antibody (1:250, SC2949, Santa Cruz Biotechnology) and visualized by NBT/BCIP (Roche) hydrolysis.

ApoE, DNAJA4, and LXRβ expression across the different melanoma lesions included in the TMA set was quantified in a blinded manner by adopting a scoring system reflective of the different levels of protein staining intensity: 0 = no positive cells detectable; 1 = very few positive cells (< 5%) showing weak light-brown staining; 2 = a few positive cells (< 10%) showing weak to medium brown staining; 3 = a few positive cells (< 10%) showing medium to dark brown staining; 4 = large number of positive cells (> 10%) showing medium to dark brown staining; 5 = large number of positive cells (> 20%) exhibiting medium to dark brown staining.

Statistical Analyses

To determine significance of bioluminescence metastasis measurements, which exhibited non-Gaussian distribution, the non-parametric Mann-Whitney t-test was used. To statistically assess the prognostic power of the expression of the three miRNAs, ApoE, DNAJA4, or their combined expression signatures in predicting metastasis-free survival, the Mantel-Cox log-rank test was employed. For survival analyses testing the effect of LXR agonist treatment or combination regimens on extending post-tumor mouse survival, survival times of control-treated and drug-treated animals were statistically compared using the Mantel-Cox log-rank test. To compare cumulative distributions of endothelial cell density and dextran perfusion density within metastatic nodules formed by either control melanoma cells or cells with knockdown of each miRNA and/or ApoE/DNAJA4, the Kolmogorov-Smirnov test was utilized. Similarly, the Kolmogorov-Smirnov test was used in comparing the ApoE staining cumulative distributions in ApoE co-localization experiments with tumor-infiltrating leukocytes, macrophages, or endothelial cells in GW3965- or control-treated melanoma tumors. All other statistical comparisons were performed using the Student's t-tests: one-tailed in cases with an expected direction of the predicted change based on previous experimental findings or two-tailed in cases without an a priori expectation. All statistical analyses were performed using the GraphPad Prism Software 5.0, except for the Kolmogorov-Smirnov test, which was carried out using a web-based analysis tool available through the Physics Department at the College of Saint Benedict and Saint John's University (http:/www.physics.csbsju.edu/stats/ KS-test.html). Statistical significance was concluded for $p < 0.05$. The following statistical designations apply to all figures: *$p < 0.05$, **$p < 0.01$, ***$p < 0.001$, ****$p < 0.0001$.

APPENDIX A—LIST OF CELL LINES

Cell Line	*Institution Source*	*Type*	*Tissue Source*	*Patient Age*	*Gender*	*Harbored Mutations*	*Notes*
MeWo	ATCC	human MM	lymph node	78 years	male	*p53, CDKN2A, NF1*	*B-Raf/N-Ras* wild-type
A375	ATCC	human MM	skin	54 years	female	*B-Raf, CDKN2A*	
HT-144	ATCC	human MM	subcutaneous tissue	29 years	male	*B-Raf, PTEN*	
WM-266-4	ATCC	human MM	skin	58 years	female	*B-Raf, PTEN*	
A2058	ATCC	human MM	lymph node	43 years	male	*B-Raf, PTEN*	
SK-Mel-2	ATCC	human MM	skin	60 years	male	*N-Ras, PAK1*	
SK-Mel-28	ATCC	human MM	skin	51 years	male	*B-Raf, CDK4*	
SK-Mel-239	Mount Sinai	human MM	n/a	n/a	n/a	*B-Raf*	
SK-Mel-334	MSKCC	human MM	thigh soft tissue	n/a	n/a	*B-Raf*	*primary line*
SK-Mel-462	MSKCC	human MM	n/a	n/a	n/a	n/a	*primary line*
SK-Mel-459	MSKCC	human MM	n/a	n/a	n/a	n/a	*primary line*
SK-Mel-441	MSKCC	human MM	n/a	n/a	n/a	n/a	*primary line*
SK-Mel-426	MSKCC	human MM	n/a	n/a	n/a	n/a	*primary line*
SK-Mel-364	MSKCC	human MM	n/a	n/a	n/a	n/a	*primary line*
SK-Mel-339	MSKCC	human MM	n/a	n/a	n/a	n/a	*primary line*
YUMM*	Yale University	mouse MM	skin	n/a	n/a	*B-Raf, PTEN, CDKN2A*	*primary line*
B16F10*	Internal	mouse MM	skin	n/a	n/a	*CDKN2A*	*B-Raf/N-Ras* wild-type
HUVEC	ATCC	human endothelial cells	umbilical vein				*primary line*

MM = malignant melaoma

* syngeneic to C57BL/6 mouse strain

APPENDIX B—LIST OF PRIMER SEQUENCES

qRT-PCR primers

Gene/Amplicon ID	*Primer Sequence*
ApoE (human)	Fwd: TGGGTCGCTTTTGGGATTAC
	Rev: TTCAACTCCTTCATGGTCTCG
DNAJA4 (human)	Fwd: CCAGCTTCTCTTCACCCATG
	Rev: CCAGCTTCTCTTCACCCATG
GAPDH (human)	Fwd: AGCCACATCGCTCAGACAC
	Rev: GCCCAATACGACCAAATCC
LRP1 (human)	Fwd: TTTAACAGCACCGAGTACCAG
	Rev: CAGGCAGATGTCAGAGCAG
LRP8 (human)	Fwd: GCTACCCTGGCTACGAGATG
	Rev: GATTAGGGATGGGCTCTTGC
LXRα (human)	Fwd: GTTATAACCGGGAAGACTTTGC
	Rev: AAACTCGGCATCATTGAGTTG
LXRβ (human)	Fwd: TTTGAGGGTATTTGAGTAGCGG
	Rev: CTCTCGCGGAGTGAACTAC
RXRα (human)	Fwd: GCAGATGGACAAGACGGAG
	Rev: TCTGGGTACTTGTGCTTGC
RXRβ (human)	Fwd: GAGTAGGAGCCATCTTTGATCG
	Rev: TCACTAGGGTTGGAGAGGC
RXRγ (human)	Fwd: CTACACCAAGCAGAAGTATCCG
	Rev: ATGAGGAAGGTGTCAATGGG
ApoE (mouse)	Fwd: GACCCTGGAGGCTAAGGACT
	Rev: AGAGCCTTCATCTTCGCAAT
GAPDH (mouse)	Fwd: GCACAGTCAAGGCCGAGAAT
	Rev: GCCTTCTCCATGGTGGTGAA
LXRα (mouse)	Fwd: GCGCTCAGCTCTTGTCACT
	Rev: CTCCAGCCACAAGGACATCT
LXRβ (mouse)	Fwd: GCTCTGCCTACATCGTGGTC
	Rev: CTCATGGCCCAGCATCTT
ABCA1 (mouse)	Fwd: ATGGAGCAGGGAAGACCAC
	Rev: GTAGGCCGTGCCAGAAGTT
miR-199a-1-CN_A	Fwd: CCACCTTTCGGGGAAGAGTTT
	Rev: TGATATGATAGGGTCAGGGCAG
miR-199a-1-CN_B	Fwd: TCTCGGGAAGAGTGGTGGTTT
	Rev: GGCTATCCATCCTGCAGAAC
miR-199a-2-CN_A	Fwd: GTTTCCAAATGAGCTCTGCCTTC
	Rev: CAAATTTACTGTCTGACCCAGGC
miR-199a-2-CN_B	Fwd: GAAATCACAGCCCTTGAGTGTG
	Rev: CTTAAAATCCTCTCCCGGTCCTC
miR-1908-CN_A	Fwd: GTCAACCAGAGTGACCACT
	Rev: AATCACACTGCGGGAAGCTC
miR-1908-CN_B	Fwd: CTAAGACAATAAAAGCTGGCCAC
	Rev: ATGAGCAGCAGCAAGGTTTAG
LXRE-pos	Fwd: CACAAGGCCAGCCGAACTAG
	Rev: GCTTCCCACCATCACCAC
LXRE-neg	Fwd: GTTTCCAAATGAGCTCTGCCTTC
	Rev: CAAATTTACTGTCTGACCCAGGC

CN = copy number

APPENDIX B—LIST OF PRIMER SEQUENCES

Cloning Primers

Construct Name	***Primer Sequence***
ApoE CDS	Fwd: TCATGAGGATCCATGAAGGTTCTGTGGGCT
	Rev: TAGCAGAATTCTCAGTGATTGTCGCTGGG
DNAJA4.3 CDS	Fwd: ATCCCTGGATCCATGTGGGAAAGCCTGACCC
	Rev: TACCATGTCGACTCATGCCGTCTGGCACTGC
*ApoE CDS**	Fwd: TAATATCTCGAGAAGGTTCTGTGGGCTGCGTTG
	Rev: AAGTACTCGAGTCAGTGATTGTCGCTGGGCAC
*DNAJA4.3 CDS**	Fwd: TAATATCTCGAGTGGGAAAGCCTGACCCTGG
	Rev: CAATTGCGGCCGCTCATGCCGTCTGGCACTGC
*ApoE 3'UTR**	Fwd: TTAGCCTCGAGACGCCGAAGCCTGCAGCCA
	Rev: TTACTGCGGCCGCTGCGTGAAACTTGGTGAATCTT
*DNAJA4 3'UTR**	Fwd: TAATATCTCGAGCGTGGTGCGGGGCAGCGT
	Rev: CAATTGCGGCCGCTTATCTCTCATACCAGCTCAAT
ApoE promoter	Fwd: TCATAGCTAGCGCAGAGCCAGGATTCACGCCCTG
	Rev: TGGTCCTCGAGGAACCTTCATCTTCCTGCCTGTGA
ME.1	Fwd: TAGTTACGCGTAGTAGCCCCCATCTTTGCC
	Rev: AATCAGCTAGCCCCTCAGCTGCAAAGCTC
ME.2	Fwd: TAGTTACGCGTAGTAGCCCCCTCTTTGCC
	Rev: AATCAGCTAGCCCTTCAGCTGCAAAGCTCTG
DNAJA4.1 Flag	Fwd: ATTCAAGGATCCATGGCCCGGGGCGGCAGTCAGAG
	Rev: CTTAACGTCGACTCACTTATCATCGTCATCTTTATAAT
	CTGCCGTCTGGCACTGCACTCCAG
DNAJA4.2 Flag	Fwd: CCAATAGGATCCATGGTGAAGGAGACCCAGTAC
	Rev: CTTAACGTCGACTCACTTATCATCGTCATCTTTATAAT
	CTGCCGTCTGGCACTGCACTCCAG
DNAJA4.3 Flag	Fwd: TTACAAGGATCCATGTGGGAAAGCCTGACCCTG
	Rev: CTTAACGTCGACTCACTTATCATCGTCATCTTTATAAT
	CTGCCGTCTGGCACTGCACTCCAG

** Luciferase Reporter Assays*

Mutagenesis Primers*

Construct Name	***Primer Sequence***
ApoE CDS mut 1	GCCAGCGCTGGGAACTGGCTCTTGGTCGCTTTTGGGATTACCT
ApoE CDS mut 2	CAGAGCGGCCAGCGCTGGGAGCTTGCACTGGGTCGCTTTTGGG
ApoE CDS mut 3	GTTGAAGGCCTACAAATCGGAGCTTGAGGAACAACTGACCCCG
ApoE CDS mut 4	CAGGCCGAGGCCTTCCAGGCTCGACTCAAGAGCTGGTTCGAGCC
DNAJA4 CDS mut 1	GGGATCGGTGGAGAAGTGTCCACTGTGCAAGGGGCGGGGGAT
DNAJA4 CDS mut 2	GTAATCTTTCCTGAAAAACATTGGCTTTCTCTGGAAAAGCTTC
ApoE 3'UTR mut 1	CAGCGGGAGACCCTGTCCCCATACCAGCCGTCCTCCTGGGGTG
ApoE 3'UTR mut 2	TCCCCGCCCCAGCCGTCCTCACAGGGTGGACCCTAGTTTAATA
DNAJA4 3'UTR mut 1	CAGGGCCAACTTAGTTCCTAACATTCTGTGCCCTTCAGTGGAT
DNAJA4 3'UTR mut 2	ACAGTTTGTATGGACTACTATCTTAAATTATAGCTTGTTTGGA
DNAJA4 3'UTR mut 3	TAATTATTGCTAAAGAACTATGTTTTAGTTGGTAATGGTGTAA
DNAJA4 3'UTR mut 4	CAGCTGCACGGACCAGGTTCCATAAAAACATTGCCAGCTAGTGAG

** Luciferase Reporter Assays*

APPENDIX C—LIST OF MIR-ZIP AND SHRNA SEQUENCES

miR-Zip Sequences

Target	***miR-Zip Sequence***
miR-199a-3p	GATCCGACAGTAGCCTGCACATTAGTCACTTCCTGTCAGTAACCAATGT GCAGACTACTGTTTTTTGAATT
miR-199a-5p	GATCCGCCCAGTGCTCAGACTACCCGTGCCTTCCTGTCAGGAACAGGT AGTCTGAACACTGGGTTTTTGAATT
miR-1908	GATCCGCGGCGGGAACGGCGATCGGCCCTTCCTGTCAGGACCAATCGC CGTCCCCGCCGTTTTTGAATT

shRNA Sequences

Target	***shRNA Sequence***
ApoE (human)	shRNA-1: CCGGGAAGGAGTTGAAGGCCTACAACTCGAGTTGTAGGCCTTCAACTCCTTCTTTTT
	shRNA-2: CCGGGCAGACACTGTCTGAGCAGGTCTCGAGACCTGCTCAGACAGTGTCTGCTTTTT
DNAJA4 (human)	shRNA-1: CCGGGCGAGAAGTTTAAACTCATATCTCGAGATATGAGTTTAAACTTCTCGCTTTTT
	shRNA-2: CCGGCCTCGACAGAAAGTGAGGATTCTCGAGAATCCTCACTTTCTGTCGAGGTTTTT
LXRα (human)	shRNA-1: CCGGCCGACTGATGTTCCCACGGATCTCGAGATCCGTGGGAACATCAGTCGGTTTTT
	shRNA-2: CCGGGCAACTCAATGATGCCGAGTTCTCGAGAACTCGGCATCATTGAGTTGCTTTTT
LXRβ (human)	shRNA-1: CCGGAGAGTGTATCACCTTCTTGAACTCGAGTTCAAGAAGGTGATACACTCTTTTTT
	shRNA-2: CCGGGAAGGCATCCACTATCGAGATCTCGAGATCTCGATAGTGGATGCCTTCTTTTT
ApoE (mouse)	shRNA-1: CCGGGAGGACACTATGACGGAAGTACTCGAGTACTTCCGTCATAGTGTCCTCTTTTT
LXRα (mouse)	shRNA-1: CCGGGCAACTCAATGATGCTGAGTTCTCGAGAACTCAGCATCATTGAGTTGCTTTTT
LXRβ (mouse)	shRNA-2: CCGGTGAGATCATGTTGCTAGAAACCTCGAGGTTTCTAGCAACATGATCTCATTTTTG

siRNA Sequences

Target	***Target Sequence***
LRP1 (human)	siRNA-1: CGAGGACGAUGACUGCUUA
	siRNA-2: GCUAUGAGUUUAAGAAGUU
LRP8 (human)	siRNA-1: CGAGGACGAUGACUGCUUA
	siRNA-2: GAACUAUUCACGCCUCAUC

PUBLICATIONS

Pencheva, N., Buss, C.G., Posada, J., Merghoub, T., Tavazoie, S.F. (2014). Broad-Spectrum Therapeutic Suppression of Metastatic Melanoma through Nuclear Hormone Receptor Activation. Cell, *156*, 986-1001.

Pencheva, N., Tavazoie, S.F. (2013). Control of Metastatic Progression by MicroRNA Regulatory Networks. Nat Cell Biol *15,* 546-554.

Pencheva, N., Tran, H., Buss, C., Huh, D., Drobnjak, M., Busam, K., and Tavazoie, S.F. (2012). Convergent Multi-miRNA Targeting of ApoE Drives LRP1/LRP8-Dependent Melanoma Metastasis and Angiogenesis. Cell *151*, 1068-1082.

BIBLIOGRAPHY

Apfel, R., Benbrook, D., Lernhardt, E., Ortiz, M.A., Salbert, G., and Pfahl, M. (1994). A novel orphan receptor specific for a subset of thyroid hormone-responsive elements and its interaction with the retinoid/thyroid hormone receptor subfamily. Mol Cell Biol *14*, 7025-7035.

Aucoin, R., Reiland, J., Roy, M., and Marchetti, D. (2004). Dominant-negative CREB inhibits heparanase functionality and melanoma cell invasion. J Cell Biochem *93*, 215-223.

Bader, A.G. (2012). miR-34 - a microRNA replacement therapy is headed to the clinic. Front Genet *3*, 120.

Barish, G.D., and Evans, R.M. (2004). PPARs and LXRs: atherosclerosis goes nuclear. Trends Endocrinol Metab *15*, 158-165.

Bartel, D.P. (2004). MicroRNAs: genomics, biogenesis, mechanism, and function. Cell *116*, 281-297.

Bhatia, S., Tykodi, S.S., and Thompson, J.A. (2009). Treatment of metastatic melanoma: an overview. Oncology (Williston Park) *23*, 488-496.

Bhattacharjee, P.S., Huq, T.S., Mandal, T.K., Graves, R.A., Muniruzzaman, S., Clement, C., McFerrin, H.E., and Hill, J.M. (2011). A novel peptide derived from human apolipoprotein E is an inhibitor of tumor growth and ocular angiogenesis. PLoS One *6*, e15905.

Bernards, R. (2012). A missing link in genotype-directed cancer therapy. Cell *151*, 465-468.

Bernstein, E., Caudy, A.A., Hammond, S.M., and Hannon, G.J. (2001). Role for a bidentate ribonuclease in the initiation step of RNA interference. Nature *409*, 363-366.

Bollag, G., Hirth, P., Tsai, J., Zhang, J., Ibrahim, P.N., Cho, H., Spevak, W., Zhang, C., Zhang, Y., Habets, G., *et al*. (2010). Clinical efficacy of a RAF inhibitor needs broad target blockade in BRAF-mutant melanoma. Nature *467*, 596-599.

Boucher, P., Gotthardt, M., Li, W.P., Anderson, R.G., and Herz, J. (2003). LRP: role in vascular wall integrity and protection from atherosclerosis. Science *300*, 329-332.

Burk, U., Schubert, J., Wellner, U., Schmalhofer, O., Vincan, E., Spaderna, S., and Brabletz, T. (2008). A reciprocal repression between ZEB1 and members of the miR-200 family promotes EMT and invasion in cancer cells. EMBO Rep *9*, 582-589.

Calin, G.A., and Croce, C.M. (2006). MicroRNA signatures in human cancers. Nat Rev Cancer *6*, 857-866.

Calin, G.A., Dumitru, C.D., Shimizu, M., Bichi, R., Zupo, S., Noch, E., Aldler, H., Rattan, S., Keating, M., Rai, K., *et al*. (2002). Frequent deletions and down-regulation of micro-RNA genes miR15 and miR16 at 13q14 in chronic lymphocytic leukemia. Proc Natl Acad Sci U S A *99*, 15524-15529.

Calin, G.A., Liu, C.G., Sevignani, C., Ferracin, M., Felli, N., Dumitru, C.D., Shimizu, M., Cimmino, A., Zupo, S., Dono, M., *et al*. (2004). MicroRNA profiling reveals distinct signatures in B cell chronic lymphocytic leukemias. Proc Natl Acad Sci U S A *101*, 11755-11760.

Calkin, A.C., and Tontonoz, P. (2012). Transcriptional integration of metabolism by the nuclear sterol-activated receptors LXR and FXR. Nat Rev Mol Cell Biol *13*, 213-224.

Cao, J., Wan, L., Hacker, E., Dai, X., Lenna, S., Jimenez-Cervantes, C., Wang, Y., Leslie, N.R., Xu, G.X., Widlund, H.R., *et al*. (2013). MC1R is a potent regulator of PTEN after UV exposure in melanocytes. Mol Cell *51*, 409-422.

Caramuta, S., Egyházi, S., Rodolfo, M., Witten, D., Hansson, J., Larsson, C., and Lui, W.O. (2010). MicroRNA expression profiles associated with mutational status and survival in malignant melanoma. J Invest Dermatol *130*, 2062-2070.

Carmeliet, P., and Jain, R.K. (2011). Molecular mechanisms and clinical applications of angiogenesis. Nature *473*, 298-307.

Chang, T.C., Wentzel, E.A., Kent, O.A., Ramachandran, K., Mullendore, M., Lee, K.H., Feldmann, G., Yamakuchi, M., Ferlito, M., Lowenstein, C.J., *et al*. (2007). Transactivation of miR-34a by p53 broadly influences gene expression and promotes apoptosis. Mol Cell *26*, 745-752.

Chapman, P.B., Einhorn, L.H., Meyers, M.L., Saxman, S., Destro, A.N., Panageas, K.S., Begg, C.B., Agarwala, S.S., Schuchter, L.M., Ernstoff, M.S., *et al*. (1999). Phase III multicenter randomized trial of the Dartmouth regimen versus dacarbazine in patients with metastatic melanoma. J Clin Oncol *17*, 2745-2751.

Chapman, P.B., Hauschild, A., Robert, C., Haanen, J.B., Ascierto, P., Larkin, J., Dummer, R., Garbe, C., Testori, A., Maio, M., *et al*. (2011). Improved survival with vemurafenib in melanoma with BRAF V600E mutation. N Engl J Med *364*, 2507-2516.

Chen, D., Sun, Y., Wei, Y., Zhang, P., Rezaeian, A.H., Teruya-Feldstein, J., Gupta, S., Liang, H., Lin, H.K., Hung, M.C., *et al*. (2012). LIFR is a breast cancer metastasis suppressor upstream of the Hippo-YAP pathway and a prognostic marker. Nat Med *18*, 1511-1517.

Chin, L., Garraway, L.A., and Fisher, D.E. (2006). Malignant melanoma: genetics and therapeutics in the genomic era. Genes Dev *20*, 2149-2182.

Clovis, Y.M., Enard, W., Marinaro, F., Huttner, W.B., and De Pietri Tonelli, D. (2012). Convergent repression of Foxp2 3'UTR by miR-9 and miR-132 in embryonic mouse neocortex: implications for radial migration of neurons. Development *139*, 3332-3342.

Collins, J.L., Fivush, A.M., Watson, M.A., Galardi, C.M., Lewis, M.C., Moore, L.B., Parks, D.J., Wilson, J.G., Tippin, T.K., Binz, J.G., *et al*. (2002). Identification of a nonsteroidal liver X receptor agonist through parallel array synthesis of tertiary amines. J Med Chem *45*, 1963-1966.

Corder, E.H., Saunders, A.M., Strittmatter, W.J., Schmechel, D.E., Gaskell, P.C., Small, G.W., Roses, A.D., Haines, J.L., and Pericak-Vance, M.A. (1993). Gene dose of apolipoprotein E type 4 allele and the risk of Alzheimer's disease in late onset families. Science *261*, 921-923.

Creighton, C.J., Fountain, M.D., Yu, Z., Nagaraja, A.K., Zhu, H., Khan, M., Olokpa, E., Zariff, A., Gunaratne, P.H., Matzuk, M.M., *et al*. (2010). Molecular profiling uncovers a p53-associated role for microRNA-31 in inhibiting the proliferation of serous ovarian carcinomas and other cancers. Cancer Res *70*, 1906-1915.

Czech, B., and Hannon, G.J. (2011). Small RNA sorting: matchmaking for Argonautes. Nat Rev Genet *12*, 19-31.

Dangi-Garimella, S., Yun, J., Eves, E.M., Newman, M., Erkeland, S.J., Hammond, S.M., Minn, A.J., and Rosner, M.R. (2009). Raf kinase inhibitory protein suppresses a metastasis signalling cascade involving LIN28 and let-7. EMBO J *28*, 347-358.

Dankort, D., Curley, D.P., Cartlidge, R.A., Nelson, B., Karnezis, A.N., Damsky, W.E., You, M.J., DePinho, R.A., McMahon, M., and Bosenberg, M. (2009). Braf(V600E) cooperates with Pten loss to induce metastatic melanoma. Nat Genet *41*, 544-552.

Das Thakur, M., Salangsang, F., Landman, A.S., Sellers, W.R., Pryer, N.K., Levesque, M.P., Dummer, R., McMahon, M., and Stuart, D.D. (2013). Modelling vemurafenib resistance in melanoma reveals a strategy to forestall drug resistance. Nature *494*, 251-255.

Davies, H., Bignell, G.R., Cox, C., Stephens, P., Edkins, S., Clegg, S., Teague, J., Woffendin, H., Garnett, M.J., Bottomley, W., *et al*. (2002). Mutations of the BRAF gene in human cancer. Nature *417*, 949-954.

Deblois, G., and Giguère, V. (2013). Oestrogen-related receptors in breast cancer: control of cellular metabolism and beyond. Nat Rev Cancer *13*, 27-36.

Demunter, A., Stas, M., Degreef, H., De Wolf-Peeters, C., and van den Oord, J.J. (2001). Analysis of N- and K-ras mutations in the distinctive tumor progression phases of melanoma. J Invest Dermatol *117*, 1483-1489.

Ding, L., and Han, M. (2007). GW182 family proteins are crucial for microRNA-mediated gene silencing. Trends Cell Biol *17*, 411-416.

Ding, B.S., Nolan, D.J., Butler, J.M., James, D., Babazadeh, A.O., Rosenwaks, Z., Mittal, V., Kobayashi, H., Shido, K., Lyden, D., *et al*. (2010). Inductive angiocrine signals from sinusoidal endothelium are required for liver regeneration. Nature *468*, 310-315.

Ding, B.S., Nolan, D.J., Guo, P., Babazadeh, A.O., Cao, Z., Rosenwaks, Z., Crystal, R.G., Simons, M., Sato, T.N., Worgall, S., *et al*. (2011). Endothelial-derived angiocrine signals induce and sustain regenerative lung alveolarization. Cell *147*, 539-553.

Dobroff, A.S., Wang, H., Melnikova, V.O., Villares, G.J., Zigler, M., Huang, L., and Bar-Eli, M. (2009). Silencing cAMP-response element-binding protein (CREB) identifies CYR61 as a tumor suppressor gene in melanoma. J Biol Chem *284*, 26194-26206.

Dohi, O., Yasui, K., Gen, Y., Takada, H., Endo, M., Tsuji, K., Konishi, C., Yamada, N., Mitsuyoshi, H., Yagi, N., *et al*. (2013). Epigenetic silencing of miR-335 and its host gene MEST in hepatocellular carcinoma. Int J Oncol *42*, 411-418.

Dong, H., Strome, S.E., Salomao, D.R., Tamura, H., Hirano, F., Flies, D.B., Roche, P.C., Lu, J., Zhu, G., Tamada, K., *et al*. (2002). Tumor-associated B7-H1 promotes T-cell apoptosis: a potential mechanism of immune evasion. Nat Med *8*, 793-800.

Donnem, T., Lonvik, K., Eklo, K., Berg, T., Sorbye, S.W., Al-Shibli, K., Al-Saad, S., Andersen, S., Stenvold, H., Bremnes, R.M., *et al*. (2011). Independent and tissue-specific prognostic impact of miR-126 in nonsmall cell lung cancer: coexpression with vascular endothelial growth factor-A predicts poor survival. Cancer *117*, 3193-3200.

Duursma, A.M., Kedde, M., Schrier, M., le Sage, C., and Agami, R. (2008). miR-148 targets human DNMT3b protein coding region. RNA *14*, 872-877.

Duvic, M., Hymes, K., Heald, P., Breneman, D., Martin, A.G., Myskowski, P., Crowley, C., Yocum, R.C., and Group, B.W.S. (2001). Bexarotene is effective and safe for treatment of refractory advanced-stage cutaneous T-cell lymphoma: multinational phase II-III trial results. J Clin Oncol *19*, 2456-2471.

Eis, P.S., Tam, W., Sun, L., Chadburn, A., Li, Z., Gomez, M.F., Lund, E., and Dahlberg, J.E. (2005). Accumulation of miR-155 and BIC RNA in human B cell lymphomas. Proc Natl Acad Sci U S A *102*, 3627-3632.

Elmén, J., Lindow, M., Schütz, S., Lawrence, M., Petri, A., Obad, S., Lindholm, M., Hedtjärn, M., Hansen, H.F., Berger, U., *et al*. (2008). LNA-mediated microRNA silencing in non-human primates. Nature *452*, 896-899.

Eulalio, A., Mano, M., Dal Ferro, M., Zentilin, L., Sinagra, G., Zacchigna, S., and Giacca, M. (2012). Functional screening identifies miRNAs inducing cardiac regeneration. Nature *492*, 376-381.

Färnegårdh, M., Bonn, T., Sun, S., Ljunggren, J., Ahola, H., Wilhelmsson, A., Gustafsson, J.A., and Carlquist, M. (2003). The three-dimensional structure of the liver X receptor beta reveals a flexible ligand-binding pocket that can accommodate fundamentally different ligands. J Biol Chem *278*, 38821-38828.

Fidler, I.J. (2003). The pathogenesis of cancer metastasis: the 'seed and soil' hypothesis revisited. Nat Rev Cancer *3*, 453-458.

Filipowicz, W., Bhattacharyya, S.N., and Sonenberg, N. (2008). Mechanisms of post-transcriptional regulation by microRNAs: are the answers in sight? Nat Rev Genet *9*, 102-114.

Fonkem, E., Uhlmann, E.J., Floyd, S.R., Mahadevan, A., Kasper, E., Eton, O., and Wong, E.T. (2012). Melanoma brain metastasis: overview of current management and emerging targeted therapies. Expert Rev Neurother *12*, 1207-1215.

Ford, D., Bliss, J.M., Swerdlow, A.J., Armstrong, B.K., Franceschi, S., Green, A., Holly, E.A., Mack, T., MacKie, R.M., and Osterlind, A. (1995). Risk of cutaneous melanoma associated with a family history of the disease. The International Melanoma Analysis Group (IMAGE). Int J Cancer *62*, 377-381.

Forman, J.J., Legesse-Miller, A., and Coller, H.A. (2008). A search for conserved sequences in coding regions reveals that the let-7 microRNA targets Dicer within its coding sequence. Proc Natl Acad Sci U S A *105*, 14879-14884.

Freeman, G.J., Long, A.J., Iwai, Y., Bourque, K., Chernova, T., Nishimura, H., Fitz, L.J., Malenkovich, N., Okazaki, T., Byrne, M.C.*, et al*. (2000). Engagement of the PD-1 immunoinhibitory receptor by a novel B7 family member leads to negative regulation of lymphocyte activation. J Exp Med *192*, 1027-1034.

Fu, M., Sun, T., Bookout, A.L., Downes, M., Yu, R.T., Evans, R.M., and Mangelsdorf, D.J. (2005). A Nuclear Receptor Atlas: 3T3-L1 adipogenesis. Mol Endocrinol *19*, 2437-2450.

Gandini, S., Sera, F., Cattaruzza, M.S., *et al*. (2005). Meta-analysis of risk factors for cutaneous melanoma: III. Familial history, actinic damage and phenotypic factors. Eur J Cancer *41*, 2040-2059.

Garbe, C., Eigentler, T.K., Keilholz, U., Hauschild, A., and Kirkwood, J.M. (2011). Systematic review of medical treatment in melanoma: current status and future prospects. Oncologist *16*, 5-24.

Garbe, C., Leter, U. (2009) Melanoma epidemiology and trends. Clin Dermat *27*, 3-9.

Garzon, R., Calin, G.A., and Croce, C.M. (2009). MicroRNAs in Cancer. Annu Rev Med *60*, 167-179.

Gao, H., Chakraborty, G., Lee-Lim, A.P., Mo, Q., Decker, M., Vonica, A., Shen, R., Brogi, E., Brivanlou, A.H., and Giancotti, F.G. (2012). The BMP inhibitor Coco reactivates breast cancer cells at lung metastatic sites. Cell *150*, 764-779.

Gaziel-Sovran, A., Segura, M.F., Di Micco, R., Collins, M.K., Hanniford, D., Vega-Saenz de Miera, E., Rakus, J.F., Dankert, J.F., Shang, S., Kerbel, R.S., *et al*. (2011). miR-30b/30d regulation of GalNAc transferases enhances invasion and immunosuppression during metastasis. Cancer Cell *20*, 104-118.

Giancotti, F.G. (2013). Mechanisms governing metastatic dormancy and reactivation. Cell *155*, 750-764.

Gibbons, D.L., Lin, W., Creighton, C.J., Rizvi, Z.H., Gregory, P.A., Goodall, G.J., Thilaganathan, N., Du, L., Zhang, Y., Pertsemlidis, A., *et al*. (2009). Contextual extracellular cues promote tumor cell EMT and metastasis by regulating miR-200 family expression. Genes Dev *23*, 2140-2151.

Glitchrest, B.A., Eller, M.S., Geller, A.C., Yaar, M. (1999). The pathogenesis of melanoma induced by ultraviolet radiation. N Eng J Med *340*, 1341-1348.

Goel, V.K., Lazar, A.J., Warneke, C.L., Redston, M.S., and Haluska, F.G. (2006). Examination of mutations in BRAF, NRAS, and PTEN in primary cutaneous melanoma. J Invest Dermatol *126*, 154-160.

Gregory, P.A., Bert, A.G., Paterson, E.L., Barry, S.C., Tsykin, A., Farshid, G., Vadas, M.A., Khew-Goodall, Y., and Goodall, G.J. (2008). The miR-200 family and miR-205 regulate epithelial to mesenchymal transition by targeting ZEB1 and SIP1. Nat Cell Biol *10*, 593-601.

Gregory, R.I., Chendrimada, T.P., Cooch, N., and Shiekhattar, R. (2005). Human RISC couples microRNA biogenesis and posttranscriptional gene silencing. Cell *123*, 631-640.

Groot, P.H., Pearce, N.J., Yates, J.W., Stocker, C., Sauermelch, C., Doe, C.P., Willette, R.N., Olzinski, A., Peters, T., d'Epagnier, D., *et al*. (2005). Synthetic LXR agonists increase LxDL in CETP species. J Lipid Res *46*, 2182-2191.

Guo, D., Reinitz, F., Youssef, M., Hong, C., Nathanson, D., Akhavan, D., Kuga, D., Amzajerdi, A.N., Soto, H., Zhu, S., *et al*. (2011). An LXR agonist promotes glioblastoma cell death through inhibition of an EGFR/AKT/SREBP-1/LDLR-dependent pathway. Cancer Discov *1*, 442-456.

Guo, H., Ingolia, N.T., Weissman, J.S., and Bartel, D.P. (2010). Mammalian microRNAs predominantly act to decrease target mRNA levels. Nature *466*, 835-840.

Gupta, G.P., and Massagué, J. (2006). Cancer metastasis: building a framework. Cell *127*, 679-695.

Hakem, A., Sanchez-Sweatman, O., You-Ten, A., Duncan, G., Wakeham, A., Khokha, R., and Mak, T.W. (2005). RhoC is dispensable for embryogenesis and tumor initiation but essential for metastasis. Genes Dev *19*, 1974-1979.

Halder, R.M., and Bang, K.M. (1988). Skin cancer in blacks in the United States. Dermatol Clin *6*, 397-405.

Hanahan, D., and Weinberg, R.A. (2011). Hallmarks of cancer: the next generation. Cell *144*, 646-674.

Haq, R., Yokoyama, S., Hawryluk, E.B., Jönsson, G.B., Frederick, D.T., McHenry, K., Porter, D., Tran, T.N., Love, K.T., Langer, R., *et al*. (2013). BCL2A1 is a lineage-specific antiapoptotic melanoma oncogene that confers resistance to BRAF inhibition. Proc Natl Acad Sci U S A *110*, 4321-4326.

Haqq, C., Nosrati, M., Sudilovsky, D., Crothers, J., Khodabakhsh, D., Pulliam, B.L., Federman, S., Miller, J.R., Allen, R.E., Singer, M.I., *et al*. (2005). The gene expression signatures of melanoma progression. Proc Natl Acad Sci U S A *102*, 6092-6097.

Hatters, D.M., Peters-Libeu, C.A., and Weisgraber, K.H. (2006). Apolipoprotein E structure: insights into function. Trends Biochem Sci *31*, 445-454.

Hayashita, Y., Osada, H., Tatematsu, Y., Yamada, H., Yanagisawa, K., Tomida, S., Yatabe, Y., Kawahara, K., Sekido, Y., and Takahashi, T. (2005). A polycistronic microRNA cluster, miR-17-92, is overexpressed in human lung cancers and enhances cell proliferation. Cancer Res *65*, 9628-9632.

He, L., and Hannon, G.J. (2004). MicroRNAs: small RNAs with a big role in gene regulation. Nat Rev Genet *5*, 522-531.

Hodi, F.S., O'Day, S.J., McDermott, D.F., Weber, R.W., Sosman, J.A., Haanen, J.B., Gonzalez, R., Robert, C., Schadendorf, D., Hassel, J.C., *et al*. (2010). Improved survival with ipilimumab in patients with metastatic melanoma. N Engl J Med *363*, 711-723.

Hodis, E., Watson, I.R., Kryukov, G.V., Arold, S.T., Imielinski, M., Theurillat, J.P., Nickerson, E., Auclair, D., Li, L., Place, C., *et al*. (2012). A landscape of driver mutations in melanoma. Cell *150*, 251-263.

Holbeck, S., Chang, J., Best, A.M., Bookout, A.L., Mangelsdorf, D.J., and Martinez, E.D. (2010). Expression profiling of nuclear receptors in the NCI60 cancer cell panel reveals receptor-drug and receptor-gene interactions. Mol Endocrinol *24*, 1287-1296.

Hollstein, M., Sidransky, D., Vogelstein, B., and Harris, C.C. (1991). p53 mutations in human cancers. Science *253*, 49-53.

Huang, Q., Gumireddy, K., Schrier, M., le Sage, C., Nagel, R., Nair, S., Egan, D.A., Li, A., Huang, G., Klein-Szanto, A.J., *et al*. (2008). The microRNAs miR-373 and miR-520c promote tumour invasion and metastasis. Nat Cell Biol *10*, 202-210.

Hussain, M.M., Strickland, D.K., and Bakillah, A. (1999). The mammalian low-density lipoprotein receptor family. Annu Rev Nutr *19*, 141-172.

Hussussian, C.J., Struewing, J.P., Goldstein, A.M., Higgins, P.A., Ally, D.S., Sheahan, M.D., Clark, W.H., Tucker, M.A., and Dracopoli, N.C. (1994). Germline p16 mutations in familial melanoma. Nat Genet *8*, 15-21.

Iorio, M.V., Ferracin, M., Liu, C.G., Veronese, A., Spizzo, R., Sabbioni, S., Magri, E., Pedriali, M., Fabbri, M., Campiglio, M.*, et al*. (2005). MicroRNA gene expression deregulation in human breast cancer. Cancer Res *65*, 7065-7070.

Janowski, B.A., Willy, P.J., Devi, T.R., Falck, J.R., and Mangelsdorf, D.J. (1996). An oxysterol signalling pathway mediated by the nuclear receptor LXR alpha. Nature *383*, 728-731.

Janssen, H.L., Reesink, H.W., Lawitz, E.J., Zeuzem, S., Rodriguez-Torres, M., Patel, K., van der Meer, A.J., Patick, A.K., Chen, A., Zhou, Y.*, et al*. (2013). Treatment of HCV infection by targeting microRNA. N Engl J Med *368*, 1685-1694.

Jemal, A., Siegel, R., Xu, J., and Ward, E. (2010). Cancer statistics, 2010. CA Cancer J Clin *60*, 277-300.

Jiang, Q., Lee, C.Y., Mandrekar, S., Wilkinson, B., Cramer, P., Zelcer, N., Mann, K., Lamb, B., Willson, T.M., Collins, J.L.*, et al*. (2008). ApoE promotes the proteolytic degradation of Abeta. Neuron *58*, 681-693.

Johannessen, C.M., Johnson, L.A., Piccioni, F., Townes, A., Frederick, D.T., Donahue, M.K., Narayan, R., Flaherty, K.T., Wargo, J.A., Root, D.E.*, et al*. (2013). A melanocyte lineage program confers resistance to MAP kinase pathway inhibition. Nature *504*, 138-142.

Joseph, S.B., and Tontonoz, P. (2003). LXRs: new therapeutic targets in atherosclerosis? Curr Opin Pharmacol *3*, 192-197.

Itou, J., Oishi, I., Kawakami, H., Glass, T.J., Richter, J., Johnson, A., Lund, T.C., and Kawakami, Y. (2012). Migration of cardiomyocytes is essential for heart regeneration in zebrafish. Development *139*, 4133-4142.

Kamb, A., Shattuck-Eidens, D., Eeles, R., Liu, Q., Gruis, N.A., Ding, W., Hussey, C., Tran, T., Miki, Y., and Weaver-Feldhaus, J. (1994). Analysis of the p16 gene (CDKN2) as a candidate for the chromosome 9p melanoma susceptibility locus. Nat Genet *8*, 23-26.

Kang, Y., Siegel, P.M., Shu, W., Drobnjak, M., Kakonen, S.M., Cordón-Cardo, C., Guise, T.A., and Massagué, J. (2003). A multigenic program mediating breast cancer metastasis to bone. Cancer Cell *3*, 537-549.

Kim, K.B., Kefford, R., Pavlick, A.C., Infante, J.R., Ribas, A., Sosman, J.A., Fecher, L.A., Millward, M., McArthur, G.A., Hwu, P., *et al*. (2013). Phase II study of the MEK1/MEK2 inhibitor Trametinib in patients with metastatic BRAF-mutant cutaneous melanoma previously treated with or without a BRAF inhibitor. J Clin Oncol *31*, 482-489.

Kim, V.N. (2005). MicroRNA biogenesis: coordinated cropping and dicing. Nat Rev Mol Cell Biol *6*, 376-385.

Kluiver, J., Poppema, S., de Jong, D., Blokzijl, T., Harms, G., Jacobs, S., Kroesen, B.J., and van den Berg, A. (2005). BIC and miR-155 are highly expressed in Hodgkin, primary mediastinal and diffuse large B cell lymphomas. J Pathol *207*, 243-249.

Kobayashi, H., Butler, J.M., O'Donnell, R., Kobayashi, M., Ding, B.S., Bonner, B., Chiu, V.K., Nolan, D.J., Shido, K., Benjamin, L., *et al*. (2010). Angiocrine factors from Akt-activated endothelial cells balance self-renewal and differentiation of haematopoietic stem cells. Nat Cell Biol *12*, 1046-1056.

Kobayashi, N., Nakagawa, A., Muramatsu, T., Yamashina, Y., Shirai, T., Hashimoto, M.W., Ishigaki, Y., Ohnishi, T., and Mori, T. (1998). Supranuclear melanin caps reduce ultraviolet induced DNA photoproducts in human epidermis. J Invest Dermatol *110*, 806-810.

Kontermann, R.E. (2011). Strategies for extended serum half-life of protein therapeutics. Curr Opin Biotechnol *22*, 868-876.

Korpal, M., Ell, B.J., Buffa, F.M., Ibrahim, T., Blanco, M.A., Celià-Terrassa, T., Mercatali, L., Khan, Z., Goodarzi, H., Hua, Y., *et al*. (2011). Direct targeting of Sec23a by miR-200s influences cancer cell secretome and promotes metastatic colonization. Nat Med *17*, 1101-1108.

Korpal, M., Lee, E.S., Hu, G., and Kang, Y. (2008). The miR-200 family inhibits epithelial-mesenchymal transition and cancer cell migration by direct targeting of E-cadherin transcriptional repressors ZEB1 and ZEB2. J Biol Chem *283*, 14910-14914.

Kota, J., Chivukula, R.R., O'Donnell, K.A., Wentzel, E.A., Montgomery, C.L., Hwang, H.W., Chang, T.C., Vivekanandan, P., Torbenson, M., Clark, K.R., *et al*. (2009). Therapeutic microRNA delivery suppresses tumorigenesis in a murine liver cancer model. Cell *137*, 1005-1017.

Kumar, M.S., Armenteros-Monterroso, E., East, P., Chakravorty, P., Matthews, N., Winslow, M.M., and Downward, J. (2014). HMGA2 functions as a competing endogenous RNA to promote lung cancer progression. Nature *505*, 212-217.

Kumar, M.S., Lu, J., Mercer, K.L., Golub, T.R., and Jacks, T. (2007). Impaired microRNA processing enhances cellular transformation and tumorigenesis. Nat Genet *39*, 673-677.

Laffitte, B.A., Repa, J.J., Joseph, S.B., Wilpitz, D.C., Kast, H.R., Mangelsdorf, D.J., and Tontonoz, P. (2001). LXRs control lipid-inducible expression of the apolipoprotein E gene in macrophages and adipocytes. Proc Natl Acad Sci U S A *98*, 507-512.

Lammert, E., Cleaver, O., and Melton, D. (2001). Induction of pancreatic differentiation by signals from blood vessels. Science *294*, 564-567.

Lanford, R.E., Hildebrandt-Eriksen, E.S., Petri, A., Persson, R., Lindow, M., Munk, M.E., Kauppinen, S., and Ørum, H. (2010). Therapeutic silencing of microRNA-122 in primates with chronic hepatitis C virus infection. Science *327*, 198-201.

Lee, Y.B., Bantounas, I., Lee, D.Y., Phylactou, L., Caldwell, M.A., and Uney, J.B. (2009). Twist-1 regulates the miR-199a/214 cluster during development. Nucleic Acids Res *37*, 123-128.

Lee, R.C., Feinbaum, R.L., and Ambros, V. (1993). The C. elegans heterochronic gene lin-4 encodes small RNAs with antisense complementarity to lin-14. Cell *75*, 843-854.

Lee, Y., Ahn, C., Han, J., Choi, H., Kim, J., Yim, J., Lee, J., Provost, P., Rådmark, O., Kim, S.*, et al*. (2003). The nuclear RNase III Drosha initiates microRNA processing. Nature *425*, 415-419.

Ling, H., Fabbri, M., and Calin, G.A. (2013). MicroRNAs and other non-coding RNAs as targets for anticancer drug development. Nat Rev Drug Discov *12*, 847-865.

Liu, J., Carmell, M.A., Rivas, F.V., Marsden, C.G., Thomson, J.M., Song, J.J., Hammond, S.M., Joshua-Tor, L., and Hannon, G.J. (2004). Argonaute2 is the catalytic engine of mammalian RNAi. Science *305*, 1437-1441.

Lu, J., Getz, G., Miska, E.A., Alvarez-Saavedra, E., Lamb, J., Peck, D., Sweet-Cordero, A., Ebert, B.L., Mak, R.H., Ferrando, A.A.*, et al*. (2005). MicroRNA expression profiles classify human cancers. Nature *435*, 834-838.

Luc, G., Bard, J.M., Arveiler, D., Evans, A., Cambou, J.P., Bingham, A., Amouyel, P., Schaffer, P., Ruidavets, J.B., and Cambien, F. (1994). Impact of apolipoprotein E polymorphism on lipoproteins and risk of myocardial infarction. The ECTIM Study. Arterioscler Thromb *14*, 1412-1419.

Lucas, R., McMichael, T., Wayne, S., Armstrong, B. (2006). Solar ultraviolet radiation: global burden of disease from solar ultraviolet radiation. Environmental Burden of Disease Series. *13*. World Health Organization.

Lujambio, A., and Lowe, S.W. (2012). The microcosmos of cancer. Nature *482*, 347-355.

Ma, L., Teruya-Feldstein, J., and Weinberg, R.A. (2007). Tumour invasion and metastasis initiated by microRNA-10b in breast cancer. Nature *449*, 682-688.

Ma, L., Reinhardt, F., Pan, E., Soutschek, J., Bhat, B., Marcusson, E.G., Teruya-Feldstein, J., Bell, G.W., and Weinberg, R.A. (2010a). Therapeutic silencing of miR-10b inhibits metastasis in a mouse mammary tumor model. Nat Biotechnol *28*, 341-347.

Ma, L., Young, J., Prabhala, H., Pan, E., Mestdagh, P., Muth, D., Teruya-Feldstein, J., Reinhardt, F., Onder, T.T., Valastyan, S., *et al*. (2010b). miR-9, a MYC/MYCN-activated microRNA, regulates E-cadherin and cancer metastasis. Nat Cell Biol *12*, 247-256.

Mak, P.A., Laffitte, B.A., Desrumaux, C., Joseph, S.B., Curtiss, L.K., Mangelsdorf, D.J., Tontonoz, P., and Edwards, P.A. (2002). Regulated expression of the apolipoprotein E/C-I/C-IV/C-II gene cluster in murine and human macrophages. A critical role for nuclear liver X receptors alpha and beta. J Biol Chem *277*, 31900-31908.

Mavrakis, K.J., Van Der Meulen, J., Wolfe, A.L., Liu, X., Mets, E., Taghon, T., Khan, A.A., Setty, M., Setti, M., Rondou, P., *et al*. (2011). A cooperative microRNA-tumor suppressor gene network in acute T-cell lymphoblastic leukemia (T-ALL). Nat Genet *43*, 673-678.

May, P., Bock, H.H., Nimpf, J., and Herz, J. (2003). Differential glycosylation regulates processing of lipoprotein receptors by gamma-secretase. J Biol Chem *278*, 37386-37392.

Meister, G., Landthaler, M., Patkaniowska, A., Dorsett, Y., Teng, G., and Tuschl, T. (2004). Human Argonaute2 mediates RNA cleavage targeted by miRNAs and siRNAs. Mol Cell *15*, 185-197.

Michael, M.Z., O' Connor, S.M., van Holst Pellekaan, N.G., Young, G.P., and James, R.J. (2003). Reduced accumulation of specific microRNAs in colorectal neoplasia. Mol Cancer Res *1*, 882-891.

Middleton, M.R., Grob, J.J., Aaronson, N., Fierlbeck, G., Tilgen, W., Seiter, S., Gore, M., Aamdal, S., Cebon, J., Coates, A., *et al*. (2000). Randomized phase III study of temozolomide versus dacarbazine in the treatment of patients with advanced metastatic malignant melanoma. J Clin Oncol *18*, 158-166.

Minn, A.J., Gupta, G.P., Siegel, P.M., Bos, P.D., Shu, W., Giri, D.D., Viale, A., Olshen, A.B., Gerald, W.L., and Massagué, J. (2005). Genes that mediate breast cancer metastasis to lung. Nature *436*, 518-524.

Missiaglia, E., Shepherd, C.J., Patel, S., Thway, K., Pierron, G., Pritchard-Jones, K., Renard, M., Sciot, R., Rao, P., Oberlin, O., *et al*. (2010). MicroRNA-206 expression levels correlate with clinical behaviour of rhabdomyosarcomas. Br J Cancer *102*, 1769-1777.

Miyazaki, Y., Adachi, H., Katsuno, M., Minamiyama, M., Jiang, Y.M., Huang, Z., Doi, H., Matsumoto, S., Kondo, N., Iida, M., *et al*. (2012). Viral delivery of miR-196a ameliorates the SBMA phenotype via the silencing of CELF2. Nat Med *18*, 1136-1141.

Muratoglu, S.C., Mikhailenko, I., Newton, C., Migliorini, M., and Strickland, D.K. (2010). Low density lipoprotein receptor-related protein 1 (LRP1) forms a signaling complex with platelet-derived growth factor receptor-beta in endosomes and regulates activation of the MAPK pathway. J Biol Chem *285*, 14308-14317.

Nakayama, M., Nakayama, A., van Lessen, M., Yamamoto, H., Hoffmann, S., Drexler, H.C., Itoh, N., Hirose, T., Breier, G., Vestweber, D., *et al*. (2013). Spatial regulation of VEGF receptor endocytosis in angiogenesis. Nat Cell Biol *15*, 249-260.

Nazarian, R., Shi, H., Wang, Q., Kong, X., Koya, R.C., Lee, H., Chen, Z., Lee, M.K., Attar, N., Sazegar, H., *et al*. (2010). Melanomas acquire resistance to B-RAF(V600E) inhibition by RTK or N-RAS upregulation. Nature *468*, 973-977.

Nelson, E.R., Wardell, S.E., Jasper, J.S., Park, S., Suchindran, S., Howe, M.K., Carver, N.J., Pillai, R.V., Sullivan, P.M., Sondhi, V., *et al*. (2013). 27-Hydroxycholesterol links hypercholesterolemia and breast cancer pathophysiology. Science *342*, 1094-1098.

Obad, S., dos Santos, C.O., Petri, A., Heidenblad, M., Broom, O., Ruse, C., Fu, C., Lindow, M., Stenvang, J., Straarup, E.M., *et al*. (2011). Silencing of microRNA families by seed-targeting tiny LNAs. Nat Genet *43*, 371-378.

Olsson, A.K., Dimberg, A., Kreuger, J., and Claesson-Welsh, L. (2006). VEGF receptor signalling - in control of vascular function. Nat Rev Mol Cell Biol *7*, 359-371.

Page, D.B., Postow, M.A., Callahan, M.K., Allison, J.P., and Wolchok, J.D. (2013). Immune Modulation in Cancer with Antibodies. Annu Rev Med.

Park, S.M., Gaur, A.B., Lengyel, E., and Peter, M.E. (2008). The miR-200 family determines the epithelial phenotype of cancer cells by targeting the E-cadherin repressors ZEB1 and ZEB2. Genes Dev *22*, 894-907.

Pasquinelli, A.E., Reinhart, B.J., Slack, F., Martindale, M.Q., Kuroda, M.I., Maller, B., Hayward, D.C., Ball, E.E., Degnan, B., Müller, P., *et al*. (2000). Conservation of the sequence and temporal expression of let-7 heterochronic regulatory RNA. Nature *408*, 86-89.

Peet, D.J., Turley, S.D., Ma, W., Janowski, B.A., Lobaccaro, J.M., Hammer, R.E., and Mangelsdorf, D.J. (1998). Cholesterol and bile acid metabolism are impaired in mice lacking the nuclear oxysterol receptor LXR alpha. Cell *93*, 693-704.

Penna, E., Orso, F., Cimino, D., Tenaglia, E., Lembo, A., Quaglino, E., Poliseno, L., Haimovic, A., Osella-Abate, S., De Pittà, C., *et al*. (2011). microRNA-214 contributes to melanoma tumour progression through suppression of TFAP2C. EMBO J *30*, 1990-2007.

Pleasance E.D, Cheetham R.K., Stephens P.J., *et al*. (2009). A comprehensive catalogue of somatic mutations from a human cancer genome. Nature *463*, 191-196.

Png, K.J., Halberg, N., Yoshida, M., and Tavazoie, S.F. (2012). A microRNA regulon that mediates endothelial recruitment and metastasis by cancer cells. Nature *481*, 190-194.

Png, K.J., Yoshida, M., Zhang, X.H., Shu, W., Lee, H., Rimner, A., Chan, T.A., Comen, E., Andrade, V.P., Kim, S.W., *et al*. (2011). MicroRNA-335 inhibits tumor reinitiation and is silenced through genetic and epigenetic mechanisms in human breast cancer. Genes Dev *25*, 226-231.

Pollack, V.A., and Fidler, I.J. (1982). Use of young nude mice for selection of subpopulations of cells with increased metastatic potential from nonsyngeneic neoplasms. J Natl Cancer Inst *69*, 137-141.

Ponomarev, V., Doubrovin, M., Serganova, I., Vider, J., Shavrin, A., Beresten, T., Ivanova, A., Ageyeva, L., Tourkova, V., Balatoni, J., et al. (2004). A novel triple-modality reporter gene for whole-body fluorescent, bioluminescent, and nuclear noninvasive imaging. Eur. J. Nucl. Med. Mol. Imaging *31*, 740-751.

Poulikakos, P.I., Persaud, Y., Janakiraman, M., Kong, X., Ng, C., Moriceau, G., Shi, H., Atefi, M., Titz, B., Gabay, M.T., *et al*. (2011). RAF inhibitor resistance is mediated by dimerization of aberrantly spliced BRAF(V600E). Nature *480*, 387-390.

Prahallad, A., Sun, C., Huang, S., Di Nicolantonio, F., Salazar, R., Zecchin, D., Beijersbergen, R.L., Bardelli, A., and Bernards, R. (2012). Unresponsiveness of colon cancer to BRAF(V600E) inhibition through feedback activation of EGFR. Nature *483*, 100-103.

Reinhart, B.J., Slack, F.J., Basson, M., Pasquinelli, A.E., Bettinger, J.C., Rougvie, A.E., Horvitz, H.R., and Ruvkun, G. (2000). The 21-nucleotide let-7 RNA regulates developmental timing in Caenorhabditis elegans. Nature *403*, 901-906.

Roldo, C., Missiaglia, E., Hagan, J.P., Falconi, M., Capelli, P., Bersani, S., Calin, G.A., Volinia, S., Liu, C.G., Scarpa, A., *et al*. (2006). MicroRNA expression abnormalities in pancreatic endocrine and acinar tumors are associated with distinctive pathologic features and clinical behavior. J Clin Oncol *24*, 4677-4684.

Schaefer, A., Jung, M., Mollenkopf, H.J., Wagner, I., Stephan, C., Jentzmik, F., Miller, K., Lein, M., Kristiansen, G., and Jung, K. (2010). Diagnostic and prognostic implications of microRNA profiling in prostate carcinoma. Int J Cancer *126*, 1166-1176.

Scher, H.I., Fizazi, K., Saad, F., Taplin, M.E., Sternberg, C.N., Miller, K., de Wit, R., Mulders, P., Chi, K.N., Shore, N.D., *et al*. (2012). Increased survival with enzalutamide in prostate cancer after chemotherapy. N Engl J Med *367*, 1187-1197.

Schmitz, K.J., Helwig, J., Bertram, S., Sheu, S.Y., Suttorp, A.C., Seggewiss, J., Willscher, E., Walz, M.K., Worm, K., and Schmid, K.W. (2011). Differential expression of microRNA-675, microRNA-139-3p and microRNA-335 in benign and malignant adrenocortical tumours. J Clin Pathol *64*, 529-535.

Schultz, J.R., Tu, H., Luk, A., Repa, J.J., Medina, J.C., Li, L., Schwendner, S., Wang, S., Thoolen, M., Mangelsdorf, D.J., *et al*. (2000). Role of LXRs in control of lipogenesis. Genes Dev *14*, 2831-2838.

Segura, M.F., Hanniford, D., Menendez, S., Reavie, L., Zou, X., Alvarez-Diaz, S., Zakrzewski, J., Blochin, E., Rose, A., Bogunovic, D., *et al*. (2009). Aberrant miR-182 expression promotes melanoma metastasis by repressing FOXO3 and microphthalmia-associated transcription factor. Proc Natl Acad Sci U S A *106*, 1814-1819.

Shi, H., Moriceau, G., Kong, X., Lee, M.K., Lee, H., Koya, R.C., Ng, C., Chodon, T., Scolyer, R.A., Dahlman, K.B., *et al*. (2012). Melanoma whole-exome sequencing identifies (V600E)B-RAF amplification-mediated acquired B-RAF inhibitor resistance. Nat Commun *3*, 724.

Shinar, D.M., Endo, N., Rutledge, S.J., Vogel, R., Rodan, G.A., and Schmidt, A. (1994). NER, a new member of the gene family encoding the human steroid hormone nuclear receptor. Gene *147*, 273-276.

Singh, P.K., Wen, Y., Swanson, B.J., Shanmugam, K., Kazlauskas, A., Cerny, R.L., Gendler, S.J., and Hollingsworth, M.A. (2007). Platelet-derived growth factor receptor beta-mediated phosphorylation of MUC1 enhances invasiveness in pancreatic adenocarcinoma cells. Cancer Res *67*, 5201-5210.

Song, C., Kokontis, J.M., Hiipakka, R.A., and Liao, S. (1994). Ubiquitous receptor: a receptor that modulates gene activation by retinoic acid and thyroid hormone receptors. Proc Natl Acad Sci U S A *91*, 10809-10813.

Song, X.W., Li, Q., Lin, L., Wang, X.C., Li, D.F., Wang, G.K., Ren, A.J., Wang, Y.R., Qin, Y.W., Yuan, W.J., *et al*. (2010). MicroRNAs are dynamically regulated in hypertrophic hearts, and miR-199a is essential for the maintenance of cell size in cardiomyocytes. J Cell Physiol *225*, 437-443.

Sosman, J.A., Kim, K.B., Schuchter, L., Gonzalez, R., Pavlick, A.C., Weber, J.S., McArthur, G.A., Hutson, T.E., Moschos, S.J., Flaherty, K.T., *et al*. (2012). Survival in BRAF V600-mutant advanced melanoma treated with vemurafenib. N Engl J Med *366*, 707-714.

Svensson, S., Ostberg, T., Jacobsson, M., Norström, C., Stefansson, K., Hallén, D., Johansson, I.C., Zachrisson, K., Ogg, D., and Jendeberg, L. (2003). Crystal structure of the heterodimeric complex of LXRalpha and RXRbeta ligand-binding domains in a fully agonistic conformation. EMBO J *22*, 4625-4633.

Swertfeger, D.K., Bu, G., and Hui, D.Y. (2002). Low density lipoprotein receptor-related protein mediates apolipoprotein E inhibition of smooth muscle cell migration. J Biol Chem *277*, 4141-4146.

Talmadge, J.E., and Fidler, I.J. (2010). AACR centennial series: the biology of cancer metastasis: historical perspective. Cancer Res *70*, 5649-5669.

Takamizawa, J., Konishi, H., Yanagisawa, K., Tomida, S., Osada, H., Endoh, H., Harano, T., Yatabe, Y., Nagino, M., Nimura, Y., *et al*. (2004). Reduced expression of the let-7 microRNAs in human lung cancers in association with shortened postoperative survival. Cancer Res *64*, 3753-3756.

Takayama, Y., May, P., Anderson, R.G., and Herz, J. (2005). Low density lipoprotein receptor-related protein 1 (LRP1) controls endocytosis and c-CBL-mediated ubiquitination of the platelet-derived growth factor receptor beta (PDGFR beta). J Biol Chem *280*, 18504-18510.

Taulli, R., Bersani, F., Foglizzo, V., Linari, A., Vigna, E., Ladanyi, M., Tuschl, T., and Ponzetto, C. (2009). The muscle-specific microRNA miR-206 blocks human rhabdomyosarcoma growth in xenotransplanted mice by promoting myogenic differentiation. J Clin Invest *119*, 2366-2378.

Tavazoie, S.F., Alarcón, C., Oskarsson, T., Padua, D., Wang, Q., Bos, P.D., Gerald, W.L., and Massagué, J. (2008). Endogenous human microRNAs that suppress breast cancer metastasis. Nature *451*, 147-152.

Teboul, M., Enmark, E., Li, Q., Wikström, A.C., Pelto-Huikko, M., and Gustafsson, J.A. (1995). OR-1, a member of the nuclear receptor superfamily that interacts with the 9-cis-retinoic acid receptor. Proc Natl Acad Sci U S A *92*, 2096-2100.

Topalian, S.L., Hodi, F.S., Brahmer, J.R., Gettinger, S.N., Smith, D.C., McDermott, D.F., Powderly, J.D., Carvajal, R.D., Sosman, J.A., Atkins, M.B., *et al*. (2012). Safety, activity, and immune correlates of anti-PD-1 antibody in cancer. N Engl J Med *366*, 2443-2454.

Tran, C., Ouk, S., Clegg, N.J., Chen, Y., Watson, P.A., Arora, V., Wongvipat, J., Smith-Jones, P.M., Yoo, D., Kwon, A., *et al*. (2009). Development of a second-generation antiandrogen for treatment of advanced prostate cancer. Science *324*, 787-790.

Trommsdorff, M., Gotthardt, M., Hiesberger, T., Shelton, J., Stockinger, W., Nimpf, J., Hammer, R.E., Richardson, J.A., and Herz, J. (1999). Reeler/Disabled-like disruption of neuronal migration in knockout mice lacking the VLDL receptor and ApoE receptor 2. Cell *97*, 689-701.

Ul Hussain, M. (2012). Micro-RNAs (miRNAs): genomic organisation, biogenesis and mode of action. Cell Tissue Res *349*, 405-413.

Valastyan, S., Benaich, N., Chang, A., Reinhardt, F., and Weinberg, R.A. (2009a). Concomitant suppression of three target genes can explain the impact of a microRNA on metastasis. Genes Dev *23*, 2592-2597.

Valastyan, S., Reinhardt, F., Benaich, N., Calogrias, D., Szász, A.M., Wang, Z.C., Brock, J.E., Richardson, A.L., and Weinberg, R.A. (2009b). A pleiotropically acting microRNA, miR-31, inhibits breast cancer metastasis. Cell *137*, 1032-1046.

van Elsas, A., Hurwitz, A.A., and Allison, J.P. (1999). Combination immunotherapy of B16 melanoma using anti-cytotoxic T lymphocyte-associated antigen 4 (CTLA-4) and granulocyte/macrophage colony-stimulating factor (GM-CSF)-producing vaccines induces rejection of subcutaneous and metastatic tumors accompanied by autoimmune depigmentation. J Exp Med *190*, 355-366.

Wang, Y., Klijn, J.G., Zhang, Y., Sieuwerts, A.M., Look, M.P., Yang, F., Talantov, D., Timmermans, M., Meijer-van Gelder, M.E., Yu, J., *et al*. (2005). Gene-expression profiles to predict distant metastasis of lymph-node-negative primary breast cancer. Lancet *365*, 671-679.

Watanabe, T., Sato, T., Amano, T., Kawamura, Y., Kawamura, N., Kawaguchi, H., Yamashita, N., Kurihara, H., and Nakaoka, T. (2008). Dnm3os, a non-coding RNA, is required for normal growth and skeletal development in mice. Dev Dyn *237*, 3738-3748.

Weisgraber, K.H. (1990). Apolipoprotein E distribution among human plasma lipoproteins: role of the cysteine-arginine interchange at residue 112. J Lipid Res *31*, 1503-1511.

Weisgraber, K.H., Innerarity, T.L., and Mahley, R.W. (1982). Abnormal lipoprotein receptor-binding activity of the human E apoprotein due to cysteine-arginine interchange at a single site. J Biol Chem *257*, 2518-2521.

White, N.M., Bao, T.T., Grigull, J., Youssef, Y.M., Girgis, A., Diamandis, M., Fatoohi, E., Metias, M., Honey, R.J., Stewart, R., *et al*. (2011). miRNA profiling for clear cell renal cell carcinoma: biomarker discovery and identification of potential controls and consequences of miRNA dysregulation. J Urol *186*, 1077-1083.

Wickner, S., Hoskins, J., and McKenney, K. (1991). Function of DnaJ and DnaK as chaperones in origin-specific DNA binding by RepA. Nature *350*, 165-167.

Wightman, B., Ha, I., and Ruvkun, G. (1993). Posttranscriptional regulation of the heterochronic gene lin-14 by lin-4 mediates temporal pattern formation in C. elegans. Cell *75*, 855-862.

Willy, P.J., Umesono, K., Ong, E.S., Evans, R.M., Heyman, R.A., and Mangelsdorf, D.J. (1995). LXR, a nuclear receptor that defines a distinct retinoid response pathway. Genes Dev *9*, 1033-1045.

Winter, J., Jung, S., Keller, S., Gregory, R.I., and Diederichs, S. (2009). Many roads to maturity: microRNA biogenesis pathways and their regulation. Nat Cell Biol *11*, 228-234.

Wolchok, J.D., Kluger, H., Callahan, M.K., Postow, M.A., Rizvi, N.A., Lesokhin, A.M., Segal, N.H., Ariyan, C.E., Gordon, R.A., Reed, K., *et al*. (2013). Nivolumab plus ipilimumab in advanced melanoma. N Engl J Med *369*, 122-133.

Worley, L.A., Long, M.D., Onken, M.D., and Harbour, J.W. (2008). Micro-RNAs associated with metastasis in uveal melanoma identified by multiplexed microarray profiling. Melanoma Res *18*, 184-190.

Wszolek, M.F., Rieger-Christ, K.M., Kenney, P.A., Gould, J.J., Silva Neto, B., Lavoie, A.K., Logvinenko, T., Libertino, J.A., and Summerhayes, I.C. (2011). A MicroRNA expression profile defining the invasive bladder tumor phenotype. Urol Oncol *29*, 794-801.e791.

Xu, Y., Zhao, F., Wang, Z., Song, Y., Luo, Y., Zhang, X., Jiang, L., Sun, Z., Miao, Z., and Xu, H. (2012). MicroRNA-335 acts as a metastasis suppressor in gastric cancer by targeting Bcl-w and specificity protein 1. Oncogene *31*, 1398-1407.

Yan, M., Huang, H.Y., Wang, T., Wan, Y., Cui, S.D., Liu, Z.Z., and Fan, Q.X. (2012). Dysregulated expression of dicer and drosha in breast cancer. Pathol Oncol Res *18*, 343-348.

Yanaihara, N., Caplen, N., Bowman, E., Seike, M., Kumamoto, K., Yi, M., Stephens, R.M., Okamoto, A., Yokota, J., Tanaka, T., *et al*. (2006). Unique microRNA molecular profiles in lung cancer diagnosis and prognosis. Cancer Cell *9*, 189-198.

Yang, H., Higgins, B., Kolinsky, K., Packman, K., Go, Z., Iyer, R., Kolis, S., Zhao, S., Lee, R., Grippo, J.F., *et al*. (2010a). RG7204 (PLX4032), a selective BRAFV600E inhibitor, displays potent antitumor activity in preclinical melanoma models. Cancer Res *70*, 5518-5527.

Yoo, A.S., Staahl, B.T., Chen, L., and Crabtree, G.R. (2009). MicroRNA-mediated switching of chromatin-remodelling complexes in neural development. Nature *460*, 642-646.

Yu, M., Bardia, A., Wittner, B.S., Stott, S.L., Smas, M.E., Ting, D.T., Isakoff, S.J., Ciciliano, J.C., Wells, M.N., Shah, A.M., *et al*. (2013). Circulating breast tumor cells exhibit dynamic changes in epithelial and mesenchymal composition. Science *339*, 580-584.

Yu, F., Yao, H., Zhu, P., Zhang, X., Pan, Q., Gong, C., Huang, Y., Hu, X., Su, F., Lieberman, J., *et al*. (2007). let-7 regulates self renewal and tumorigenicity of breast cancer cells. Cell *131*, 1109-1123.

Yun, J., Frankenberger, C.A., Kuo, W.L., Boelens, M.C., Eves, E.M., Cheng, N., Liang, H., Li, W.H., Ishwaran, H., Minn, A.J., *et al*. (2011). Signalling pathway for RKIP and Let-7 regulates and predicts metastatic breast cancer. EMBO J *30*, 4500-4514.

Zhang, X.H., Wang, Q., Gerald, W., Hudis, C.A., Norton, L., Smid, M., Foekens, J.A., and Massagué, J. (2009). Latent bone metastasis in breast cancer tied to Src-dependent survival signals. Cancer Cell *16*, 67-78.

Zhang, Y., Guo, J., Li, D., Xiao, B., Miao, Y., Jiang, Z., and Zhuo, H. (2010). Down-regulation of miR-31 expression in gastric cancer tissues and its clinical significance. Med Oncol *27*, 685-689.

Zhou, L., Takayama, Y., Boucher, P., Tallquist, M.D., and Herz, J. (2009). LRP1 regulates architecture of the vascular wall by controlling PDGFRbeta-dependent phosphatidylinositol 3-kinase activation. PLoS One *4*, e6922.

Zhuang, G., Wu, X., Jiang, Z., Kasman, I., Yao, J., Guan, Y., Oeh, J., Modrusan, Z., Bais, C., Sampath, D., *et al*. (2012). Tumour-secreted miR-9 promotes endothelial cell migration and angiogenesis by activating the JAK-STAT pathway. EMBO J *31*, 3513-3523.

Zurhove, K., Nakajima, C., Herz, J., Bock, H.H., and May, P. (2008). Gamma-secretase limits the inflammatory response through the processing of LRP1. Sci Signal *1*, ra15.